Greenhouse Gas Emissions from Northern Wetlands and Lakes: Circumpolar and Local Perspectives

by

McKenzie Ann Kuhn

A thesis submitted in partial fulfillment of the requirements for the degree of

Doctor of Philosophy

in

Water and Land Resources

Department of Renewable Resources
University of Alberta

Abstract

Methane (CH_4) emissions from Boreal-Arctic wetlands and lakes are likely to increase in a warming climate, and thus add to the atmospheric burden of greenhouse gases (GHG). However, there are large uncertainties in current estimates of CH_4 emissions from northern ecosystems, and I have a limited understanding of the sensitivity of northern lake CH_4 and carbon dioxide (CO_2) emissions to warming and the thawing of perennially frozen ground (i.e. permafrost)- a critical gap in our ability to predict the future global atmospheric GHG budget. To address these knowledge gaps, I integrated meta-data analysis of CH_4 fluxes from wetlands and lakes across the northern study domain with intensive, multi-year (2017-2019) field studies of lake biogeochemistry and GHG exchange across a 1600 km transect of western Canada.

First, I compiled a comprehensive dataset of small-scale, ground-based CH_4 flux data from 540 terrestrial sites (wetland and non-wetland) and 1247 aquatic sites (i.e. lakes), from 189 studies (Chapter 2). The dataset was built in parallel with a novel, CH_4-specific land cover dataset for the circumpolar north- the Boreal-Arctic Wetland and Lake Dataset (BAWLD), allowing for flux observations and spatial distribution of land cover features to be classified under the same criteria for the first time at a Boreal-Arctic scale. Most of the observed CH_4 flux variability from terrestrial and aquatic ecosystems could be explained by a land cover classification system focused on splits in permafrost presence and hydrology in wetlands and lake size and genesis in lakes. Using land cover class as the main predictor variable, I arrive at a new estimate of annual CH_4 emissions from the Boreal-Arctic region of ~36.5 Tg CH_4 yr^{-1}. This estimate is on the low end, but within similar ranges of annual emissions reported from other bottom-up studies and is closer to the total emission estimated by inverse models- suggesting

distinguishing between land cover class is an important step towards reconciling circumpolar emission estimates.

To further constrain current estimates of CH_4 from northern lakes and assess potential changes in lake CH_4 and CO_2 emissions with warming and permafrost thaw, I measured seasonal GHG emissions from 20 peatland lakes across a climate and permafrost gradient in western Canada (Chapter 3). Both CO_2 and CH_4 emissions followed opposing trends across the gradient and were associated with different drivers. Less permafrost in the south was associated with greater hydrological connectivity, nutrient availability, and thus increased primary productivity and uptake of CO_2. Conversely, positive trends in CH_4 emissions were driven by higher temperatures towards the south and augmented by shifts in microbial communities. Using a space-for-time approach, the results show that net radiative forcing from altered GHG emissions of boreal peatland lakes this century will be dominated by increasing CH_4 emissions and only partially offset by reduced CO_2 emissions. The influence of permafrost thaw on lake productivity and reduced CO_2 emissions, and the high-temperature sensitivity of CH_4 emissions, are likely associated with characteristics of peatland lakes and the hydrology/landscape history of their surrounding landscape.

Finally, I examined the direct effects of permafrost thaw on CH_4 and CO_2 emissions from one peatland thaw lake in northern Alberta (Chapter 4). There was large spatial variation in CH_4 emissions across the lake with the highest ebullitive emissions from the thaw edge and the highest diffusive emissions from the thaw edge and stable edge. Ebullitive CH_4 and CO_2 from the thaw edge were older than the stable edge and lake center, signifying GHG's from the thaw edge may be sourced from recently thawed permafrost carbon. While the age of CH_4 emitted from the thaw edge is similar to other peatland thaw lakes, ebullitive CH_4 emissions were an

order of magnitude higher than other lakes. This suggests not all peatland lakes have similar responses in GHG emissions to permafrost thaw and that other factors including local peat history/quantity and lake morphology must be considered.

Together, the results of this thesis suggest that future research, including GHG emission models, should consider wetland and lake classes and regional variability when estimating current emissions and projecting changes in future emissions with warming.

Preface

Contributions of authors

All co-authored work presented in this dissertation follows the author order convention of first author is lead author, followed by authors in order of contribution, with the last author as the Principal Investigator. Each chapter in this thesis represents a collaborative, scientific effort resulting in manuscript publication or preparation for submission to peer-reviewed journals, as detailed below. For all chapters, M.A.K. designed the study with input from D.O. and co-authors; M.A.K. led field and laboratory work, data analysis, and manuscript writing; before publication, all co-authors contributed, or will contribute, to writing.

Chapter 2: Kuhn, M.A., Varner, R.K., Bastivken, D., Crill, P., MacIntrye, S., Turetsky, M., Anthony, K.W., McGuire, A.D. and Olefeldt, D. BAWLD-CH_4: A comprehensive dataset of methane fluxes from Boreal and Arctic ecosystems. A version of this paper has been submitted to *Earth System Science Data*.

Chapter 3: Kuhn, M.A., Thompson, L.M., Winder, J., Braga, L., Tanentzap, A., Bastviken, D., Olefeldt, D. Permafrost and climate strongly influence CH_4 and CO_2 emissions from peatland lakes. A version of this paper has been submitted to *Nature Climate Change*.

Chapter 4: Kuhn, M.A., Schmidt, M., Heffernan, L., Knorr, K.H, Estop-Aragonés, C., Moguel, R., Douglas, P., Olefeldt, D. High methane emissions from a peatland thermokarst lake edge driven by millennial-aged peat and released through ebulltion. In preparation for submission to *Journal of Geophysical Research: Biogeosciences*.

Related Research and Contributions:

The following preprint reference is related to the work I did for Chapter 2 of this thesis and detailes the associated land cover model for the Boreal and Arctic Wetlands and Lakes Dataset. The land cover classifications and associated definitions as I describe in Chapter 2 of this thesis are incorporated into this work, but are considered the original product of this thesis.

Olefeldt, D., Hovemyr, M., **Kuhn, M. A.,** Bastviken, D., Bohn, T. J., Connolly, J., Crill, P., Euskirchen, E. S., Finkelstein, S. A., Genet, H., Grosse, G., Harris, L. I., Heffernan, L., Helbig, M., Hugelius, G., Hutchins, R., Juutinen, S., Lara, M. J., Malhotra, A., Manies, K., McGuire, A. D., Natali, S. M., O'Donnell, J. A., Parmentier, F.-J. W., Räsänen, A., Schädel, C., Sonnentag, O., Strack, M., Tank, S., Treat, C., Varner, R. K., Virtanen, T., Warren, R. K., and Watts, J. D.: The Boreal-Arctic Wetland and Lake Dataset (BAWLD), Earth Syst. Sci. Data Discuss. [preprint], https://doi.org/10.5194/essd-2021-140, in review, 2021.

Even things which seem separate

and finished

are infinitely connected

and will infinitely connect

-Ali Smith

Acknowledgements

Firstly, thank you to the funding sources which have made this research possible: the NSERC Discovery Grant and Northern Supplement programs, the Natural Sciences and Engineering Research Council, Campus Alberta Innovates Program, the NWT Cumulative Impact Monitoring Program, the Northern Scientific Training Program, and UAlberta North. Personal funding was provided through Vanier Canada, Michael Smith Foreign Study Supplements, and the W. Garfield Weston Foundation.

I would like to thank my Ph.D. supervisor, Dr. David Olefeldt, for his support throughout my graduate program. I came to David with an idea to research CH_4 emissions from lakes in the Taiga Plains and David helped me foster and grow that idea into this thesis through his enthusiasm for science, his holistic understanding of the Boreal-Arctic region, and his focus on telling clear and powerful stories. I would also like to thank the Polaris Project family and my late mentor, Dr. John Schade, with whom I began my tenure as a northern research scientist. John's kindness, curiosity, and never-ending support made me fall in love with research as a process and inspired me to choose research and mentorship as a career path.

I would also like to thank my supervisor committee, Dr. Suzanne Tank and Dr. Vincent St. Louis, for sharing their time and expertise in northern biogeochemistry. I also thank Dr. Cristian Estop-Aragonés, Dr. Andrew Tanentzap, and Dr. Klaus-Holger Knorr for inspiring conversations about biogeochemistry and advice on study design. Thank you to Kevin Devito and Emily Pugh for providing input on site selection at the Utikima Research Study Area and Carolynn Forsyth for camp facilities at the ArtisInn.

No Ph.D. would be possible without a support group and I am incredibly grateful to my lab mates who have provided the utmost support over the last five years. Thank you, Dr. Liam Heffernan, Katheryn Burd, Jocelyn Egan, Emily Pugh, Lauren Thompson, Rebecca Frei, Megan Schmidt, Christopher Schulze, Maya Frederickson, Trisha Elliot, Johanna Winder, Julia Orlova, Dr. Ryan Hutchins, and Dr. Lorna Harris for the hours of conversations in the field truck, for the feedback on figures, for the much-needed coffee and lunch breaks, and all the laughs in between. Thank you to the 2019 transect crew for making my last field season so special and memorable. The field days were long, but you all made me wish they would never end. Finally, thank you to

my first CAWS field partner turned best friend, Dr. Carolyn Gibson, whose friendship, unwavering support, and kindness helped me make it to the finish line.

To my family, Eric, Sue, Carl, Anna, and Hallie- thank you for your support and encouragement all of these years and for making finishing a Ph.D. during a global pandemic possible. You're my inspiration and my number one fans and I couldn't have done this without you. And to Arlo and Etta, my favourites, thank you for teaching me the true meaning of "work-life balance."

Table of Contents

Abstract ii

Preface v

Contributions of authors v

Acknowledgements viii

Table of Contents x

List of Tables xiii

List of Figures xvii

1. General Introduction 1

1.1 Boreal-Arctic methane emissions 1

1.2 Methane cycling in natural systems and dominant CH_4-emitting characteristics 2

1.3 The influence of climate warming and permafrost thaw on lake GHG emissions 3

1.3.1 Permafrost thaw across the landscape 4

1.3.2 Localized effects of permafrost thaw on lake GHG emissions 5

1.4 The Boreal and Taiga Plains of western Canada 6

1.5 Objectives 8

2. BAWLD-CH_4: A comprehensive dataset of methane fluxes from Boreal and Arctic ecosystems 10

2.2.1.0 Land cover classes in the Boreal Arctic Wetland and Lake Dataset 16

2.2.1.1 Wetland classes 17

2.2.1.2 Upland and other classes 21

2.2.1.3 Aquatic classes 22

2.2.2 Terrestrial methane flux dataset 24

2.2.3 Aquatic methane flux dataset 30

2.2.4 Statistics 35

2.2.5 Scaling 36

2.2.6 Limitations 38

2.3.0 Results 38

2.3.1 Summary statistics 38

2.3.2 Correlations with terrestrial methane fluxes 40

2.3.3 Correlations with aquatic methane fluxes 45
2.3.4 Joint analysis of terrestrial and aquatic fluxes 50
2.3.5 Upscaled methane fluxes 50
2.4.0 Discussion 52
2.4.1 Flux variation largely explained by land cover classes 52
2.4.2 Annual estimates of methane from northern wetland and aquatic ecosystems 54
2.4.3 Directions for future research 56
2.5.0 Conclusions 61
3. Permafrost and climate strongly influence CH_4 and CO_2 emissions from peatland lakes 62
3.1 Introduction 63
3.2 Lake greenhouse gas emissions across a permafrost transect 64
3.3 Connectivity, primary productivity, and CO_2 emissions 67
3.4 Temperature sensitivity, microbial ecology, and CH_4 emissions 70
3.5 Future peatland lake GHG emissions and net radiative forcing 74
3.6 Methods 76
3.6.1 Sampling sites 76
3.6.2 Water sampling 77
3.6.3 Microbial sampling 78
3.6.4 Greenhouse gas fluxes 78
3.6.5 Upscaling 80
3.6.6 Radiative forcing 81
3.6.7 Statistical analysis 81
4. Extreme methane emissions from a peatland thermokarst lake edge driven by millennial-aged peat and released through ebullition 84
4.1 Introduction 85
4.2 Methods 88
4.2.1 Site Description 88
4.2.2 Flux measurement timeframe 89
4.2.3 Ebullitive fluxes 90
4.2.4 Net CH_4 fluxes and diffusive fluxes 91
4.2.5 Water chemistry and meteorological measurements 92

4.2.6 Sediment porewater CH_4 concentrations 94
4.2.7 Radiocarbon analysis 95
4.2.8 Lake peat sediment cores and macrofossil analysis 95
4.2.9 Surface sediment cores and incubations 96
4.2.10 Statistical analysis 97
4.3 Results 98
4.3.1 Sediment and water chemistry characteristics 98
4.3.2 Methane fluxes 99
4.3.3 Carbon dioxide fluxes 104
4.3.4 Flux correlations with environmental variables 106
4.3.5 Porewater concentrations 108
4.3.6 Potential production rates from incubations 109
4.3.7 Radiocarbon 110
4.4 Discussion 112
4.4.1 Spatial variability of methane fluxes 112
4.4.2 Sources of methane production 113
4.4.3 Old carbon from lake thaw edge 114
4.4.4 Influence of local and regional characteristics on lake CH_4 fluxes 116
5. Summary, conclusions, and directions for future research 120
5.1 Summary of findings 120
5.2 Future research directions 122
Bibliography 126
Appendices 148

List of Tables

Table 2.1. Attribute information for the terrestrial flux dataset. 26

Table 2.2. Attribute details for the aquatic fluxes dataset. 32

Table 2.3. Characteristics of BAWLD terrestrial classes based on environmental variables. The number of sites (site years) and contributing studies are shown for each class. Also shown are the mean, median, and quartiles for site average CH_4 flux, water table, soil temperature between 5 and 25 cm (TSoilB), sedge cover, pH, ecosystem respiration (ER), and gross primary productivity (GPP). *In some cases one study contributed flux data for multiple classes. 43

Table 2.4. Characteristics of the BAWLD aquatic classes based on CH_4 and environmental variables. The number of sites and contributing studies are shown for each class and flux pathway. Also shown are the mean, median, and quartiles for site average diffusive and ebullitive CH_4 flux, waterbody surface area, water body depth, and dissolved organic carbon concentrations (DOC). *In some cases one study contributed flux data for multiple classes and pathway types. One ebullition outlier point (flux = 1815 mg CH_4 m^2 d^{-1}) was excluded from the Midsize Glacial class as it was influenced by beaver activity (Sepulveda-Jauregui et al. 2015). 48

Table 2.5. Winter fluxes, including storage, ice bubble storage (IBS), and winter ebullition for each class type. Annual estimates of ice-free diffusion and ebullition are included for comparison. ** Winter ebullition from constant seeps not included in sum winter/ice-out emissions. 49

Table 2.6. Annual CH_4 emission estimates from Boreal-Arctic wetland and aquatic ecosystems. 51

Table 4.1. Average (± one standard deviation) surface water characteristics (2017-2019) from the center of the lake. 99

Table 4.2. **Summary results (± one standard deviation) for GHG fluxes at each lake location.** E_flux = ebullitive flux. D_flux = diffusive flux. [CH_4] = dissolved CH_4 concentration. 100

Table A.2. 1. Temperature sensitivities of CH_4 fluxes (Q_{10} values) across terrestrial and aquatic ecosystem classes. Individual classes without Q_{10} values did not have significant relationships with temperature when analyzed on their own or did not have a large enough sample size (minimum n = 15). 156

Table A.2. 2. Model selection for terrestrial CH_4 emissions. "Site" represents the best model using site level predictor variables (biophysical variables measured directly by the authors). "Region" represents the best model using predictor variables that can be attributed across larger spatial scales and extracted from gridded or mapped products. Tests with "site and region" represent the model models that include both site level and regional level predictors. The null model includes only the random effect of SiteID. The best models for each test represented here were picked through forward model selection. K = number of fixed terms the model, AICc = size-corrected Akaike information criterion, DeltaAICc = change in AICc between a given model and the best model, AICcwt = AICc weights indicating the probability a given model is the most parsimonious model in the group of models tested, R^2m = marginal R^2 for the fixed terms for mixed models. R^2c = conditional R^2 for fixed and random terms for mixed effects models. See main text for explanation of fixed effects short names. Non-significant fixed terms that were tested include: MAAT, MAP, Permafrost Zone, Permafrost Presence or Absence, and Biome. TsoilB = soil temperature at 5-25 cm. WTAv – average water table position. Sedge = graminoid cover. 157

Table A.2. 3. Model selection for aquatic diffusive CH_4 emissions. "Site" represents the best model using site level predictor variables (biophysical variables measured directly by the authors). "Region" represents the best model using predictor variables that can be attributed across larger spatial scales and extracted from gridded or mapped products. Tests with "site and region" represent the model models that include both site level and regional level predictors. The null model was ran as follows lm(log.CH4.flux) ~1. The best models for each test represented here were picked through forward model selection. K = number of fixed terms the model, AICc = size-corrected Akaike information criterion, DeltaAICc = change in AICc between a given model and the best model, AICcwt = AICc weights indicating the probability a given model is the most parsimonious model in the group of models tested, R^2m = marginal R^2 for the fixed terms for mixed models. R^2c = conditional R^2 for fixed and random terms for mixed effects models. See main text for explanation of predictor variable short names. Non-significant predictor terms that were tested include: MAP, Permafrost Zone, DOC, Biome, waterbody depth, and Class). SA = waterbody surface area. TYPE = overarching lake type by lake genesis. TEMP = measured water temperature. GRID_T = gridded mean annual temperature. LAT = latitude. 158

Table A.2. 4. Joint analysis of terrestrial and aquatic warm-season/ice-free emissions. The best models for each test represented here were picked through forward model selection. K =

number of fixed terms the model, AICc = size-corrected Akaike information criterion, DeltaAICc = change in AICc between a given model and the best model, AICcwt = AICc weights indicating the probability a given model is the most parsimonious model in the group of models tested, R^2m = marginal R^2 for the fixed terms for mixed models. GRID_P = gridded mean annual precipitation. GRID_T = gridded mean annual temperature. 159

Table A.3. 1. Climatic and peat characteristics of each study site in the study region. 166

Table A.3. 2. Differences in daytime emissions between the four permafrost zones using mixed model ANOVAs..... 167

Table A.3. 3. Non-parametric post-hoc test for seasonal differences in CH_4 and CO_2 emissions. E = early season (May or early June). M = mid-season (June-early August). L = Late august through September..... 168

Table A.3. 4. Physical and chemical characteristics averaged over the entire sampling period for each lake. F = Fort Simpson. W = Wrigley. L = Lutose. U = Ursa. C = Continuous. D = Discontinuous. S = Sporadic/isolated. N = no permafrost. Depth = max lake depth. Area = lake surface area. CH_4_eb = daytime CH_4 ebullition flux. CH4_dif = daytime diffusive CH_4 flux. CO2_flux = daytime diffusive carbon dioxide flux. Negative values represent uptake. [Fe] = dissolved iron in the lake surface waters. mrcA abund = a) methyl coenzyme A reductase abundance and methanotrophy marker. pmoA = particulate methane monooxygenase. mmoX abund = methane monooxygenase subunit-A. 169

Table A.4. 1. Sampling timeframe. TE= Thaw Edge, M = Intermediate, C = Center, SE = Stable Edge. Note- in 2017 only Cl^- and SO_4^{2-} were measured. 174

Table A.4. 2. Radiocarbon analysis of sediment CH_4 and CO_2 bubbles. TE = Thaw edge. SE = Stable edge. C = Center. 175

Table A.4. 3. Linear mixed model output for CH_4 fluxes as a factor of lake location. Levels with different letters indicate significant differences among the lake locations. 176

Table A.4. 4. Linear mixed model output for CH_4 fluxes and bubble concentrations across the entire lake extent as a factor of sampling month. Levels with different letters indicate significant differences in fluxes between months. 177

Table A.4. 5. Linear mixed model output for CH_4 fluxes within each lake location as a factor of sampling month. Levels with different letters indicate significant differences in fluxes between months. 178

Table A.4. 6. Linear mixed model output for ebullitive CO_2 fluxes and bubble concentrations across the entire lake extent as a factor of lake location and sampling month. Levels with different letters indicate significant differences in fluxes between locations and months. 179

Table A.4. 7. Output from the Kendall's correlation tests. Correlations were classified as weak (± 0.1-0.30), moderate (± 0.3-0.5), or strong (± > 0.5). See text for shortname definitions. 180

Table A.4. 8. Comparison of average water chemistry characteristics across peatland ponds and lakes. DOC = dissolved organic carbon. Cond = conductivity. 181

Table A.4. 9. 2018 and 2019 diffusive CO_2 fluxes and associated water chemistry variables. CO_2_D_flux = diffusive CO_2 flux. Water Temp = Water Temperature. DOC = Dissolved Organic Carbon. TN = Dissolved Total Nitrogen. Cond = Conductivity. 182

List of Figures

Figure 1.1. Northern circumpolar map including peatland and permafrost cover. The black outlines represent the Taiga (upper outline) and Boreal Plains ecozones. The yellow dots represent the study locations for Chapters 3 and 4. Peatlands include bogs, fens, and permafrost bogs extracted from Olefeldt, Hovemyr, Kuhn et al. 2021. Permafrost distribution is from Brown et al. 2002. 8

Figure 2.1. Maps of the individual sites (orange circles) incorporated in BAWLD-CH_4. a) Sites included in the terrestrial flux dataset. b) Sites included in the aquatic flux dataset. The number of "sites" in the terrestrial data set represents site-years, which in some cases represent multiple years of data from one site or data from the same site reported by different studies. "Sites" in the aquatic dataset represent the reported average fluxes for one or multiple lakes. In some cases, studies reported one mean value for multiple lakes, therefore the number of lakes and the number of sites are not the same. *Boreal-Arctic Region boundary from Olson et al. 2001. Permafrost zones are from Brown et al. 2002. Continental shoreline base layers are from Wessel et al. 1996. 16

Figure 2.2. Conceptual diagram of the terrestrial land cover classes and their CH_4-emitting characteristics including permafrost conditions, hydrology, organic layer depth, and associated nutrient and vegetation characteristics. Numbers within the brackets represent the interquartile (IQR) flux ranges. Arrows are scaled based on mean flux values. See Sect. 2.3.2 for a detailed breakdown of terrestrial fluxes. 18

Figure 2.3. Definitions of the five wetland classes in BAWLD along axes of moisture regime and nutrient regime. 19

Figure 2.4. Conceptual diagram of the aquatic land cover classes. Key differences between the three overarching lake genesis "types" and their CH_4-emitting characteristics are shown, including sediment type, permafrost conditions, and water column depth. Fluxes (interquartile ranges-IQR) for each class size within the overarching types are shown above the lakes for both diffusive and ebullitive transport pathways. Arrows are scaled based on mean flux values. See Sect. 3.3 for a detailed breakdown of aquatic fluxes. Large lakes are not shown. 23

Figure 2.5. Histograms of site-specific average CH_4 fluxes. a) Terrestrial fluxes. b) Aquatic diffusive fluxes. c) Aquatic ebullitive fluxes. Grey bars represent net zero or net uptake fluxes. 39

Figure 2.6. Histograms for the number of sampling days contributing to the average warm-season or ice-free season flux value. A) Terrestrial flux sampling days. B) Aquatic diffusion flux sampling days. C) Aquatic ebullition sampling days. The orange dotted lines in panels b and c represent the number of recommended sampling days needed to arrive at a flux estimate within 20% accuracy (11 days for diffusion and 39 days for ebullition; Wik et al. 2016b). 39

Figure 2.7. Relationships between site-averaged warm-season CH_4 flux and environmental variables. Environmental variables include water table, soil temperature at 5-25 cm depth, active layer depth, latitude, air temperature, organic layer thickness, ecosystem respiration (ER), gross primary productivity (GPP), and soil pH. Regression lines and R-square values are shown for significant relationships. Note the log scale. CH_4 flux was linearly related to water table and soil temperature and was logarithmically related to GPP (dotted line). Points below the red dotted line represent net uptake fluxes. * $P < 0.05$ ** $P < 0.01$ *** $P < 0.001$ 41

Figure 2.8. Warm-season CH_4 fluxes classfied by categorical variables. Orange circles represent mean flux values. The number of sites for each category is represented in the column to the right (n) and statistical differences among the categories are indicated by the letters (Sig). Permafrost zones are from Brown et al. 2002. Permafrost condition represents the presence of permafrost in the top 2 meters as reported by the authors. See text for definitions used to classify vegetation cover. Outlier fluxes greater than 380 are not shown. 42

Figure 2.9. Relationship between methane flux and BAWLD land cover classes. A) Terrestrial fluxes per each class. B) Aquatic fluxes including diffusion and ebullition per each class. Orange dots represent the arithmetic mean flux values and black lines represent median flux values. Boxes represent 25^{th} and 75^{th} percentiles. Outlier fluxes over 380 are not shown. The letters represent significant differences in fluxes among classes. Similar letters indicate no significant difference. 44

Figure 2.10. Relationships between site-averaged ice-free diffusive and ebullitive CH_4 fluxes (note the log scale) and environmental variables. Environmental variables include surface area, waterbody depth, latitude, dissolved organic carbon (DOC) concentration, water temperature, and pH. Regression lines and R-square values are shown for significant relationships. Log diffusive CH_4 flux was linearly related to surface area, depth, latitude, water temperature, and DOC. Log ebullitive fluxes were linearly related to surface area, latitude, DOC, and water temperature. * $P < 0.05$. ** $P < 0.01$. *** $P < 0.001$. 46

Figure 2.11. Ice-free season diffusion (left) and ebullitive (right) CH_4 fluxes as described by categorical variables. Orange circles represent mean flux values. The number of sites for each category is represented in the column to the right (n) in the representative colors for diffusion (light blue) and ebullition (dark blue). The letters (Sig) indicate statistical differences among the categories. Lake Size represents binned surface areas for < 0.1 km^2 (Small), 0.1 – 10 km^2 (Midsize), and > 10 km^2 (Large). Lake Type represents the BAWLD classification of waterbody types including Peatland, Yedoma, and Glacial lakes. Fluxes higher than 380 are not shown. ... 47

Figure 2.12. Average warm-season and ice-free CH_4 emissions across the Boreal-Arctic region. a) Warm-season wetland CH_4 fluxes. b) Ice-free aquatic CH_4 fluxes (includes both ebullition and diffusion). Note the different scales between panel a and panel b. The flux rates refer to the total unit area in a grid cell in grams of CH_4. 52

Figure 2.13. Geographical distribution and flux frequencies and for each terrestrial class. Relative land cover for each type is represented in green on the map. Site locations are represented by orange circles. Note the log scale for CH_4 flux. Land cover distributions from Olefeldt, Hovemyr, Kuhn et al. 2021. Histograms of non-transformed flux data can be found in Fig. A.2.8. 57

Figure 2.14. Relative total flux contribution (mean flux*total class area) for each land cover shown with the relative contribution of flux measurements for each class. A) Wetland classes. B) Aquatic classes. The bars represent the percent of total flux contribution and percent of reported flux sites for each class. Aquatic flux contributions represent average ebullition + average diffusion fluxes. 58

Figure 2.15. Flux frequencies and geographical distribution for each aquatic class. Relative land cover for each class type is represented in blue on the map. Site locations are represented by orange circles. Note the log scale for CH_4 flux. Land cover distributions from Olefeldt, Hovemyr, Kuhn et al. 2021. Histograms of non-transformed flux data are shown in Fig. A.2.9. 59

Figure 3.1. Locations of study lakes within the Interior Plains of western Canada. The Interior Plains study region is outlined with black line, and is comprised of the Taiga Plains (north) and Boreal Plains (south, largely permafrost free) ecozones. Permafrost zones are indicated by blue shadings (Brown et al. 2002). Five lakes were monitored for seasonal greenhouse gas emission at each study location, indicated by orange circles. The distribution of peatlands within both the study region and the broader circumpolar region is shown in the top right inset, showing that the study region is one of the major northern peatland regions (Olefeldt,

Hovemyr, Kuhn et al. 2021). Bottom right photos show one lake from each study location, with all lakes surrounded by treed peatlands. 66

Figure 3.2. Trends in magnitude and variability of lake greenhouse gas emissions across permafrost zones. Emissions of a) diffusive CO_2 and b) CH_4 were measured during the early, mid, and late open water season from five lakes each within the continuous (Cont.), discontinuous (Disc.), and sporadic (Spor.) permafrost zones, as well as south of the permafrost region (None). Boxplots indicate the 25th, median, and 75th percentiles of emissions, and the yellow diamonds indicate the average emissions. Different letters above the boxplots for CH_4 indicate statistically significant differences between permafrost zones, accounting for repeated measurements throughout the season (see Methods and Table A.3.2). Diffusive and ebullitive CH_4 flux significant differences are presented separately. Outlier CO_2 fluxes below -800 and about +1000 are not shown. Methane fluxes have not been corrected for diel variation in this figure. 67

Figure 3.3. Influence of lake water chemistry and lake characteristics on greenhouse gas emissions across permafrost zones. a) Redundancy analysis (RDA) ordination plot for CO_2 and CH_4 emissions, where explanatory variables include water chemistry variables along with maximum lake depth and mean annual air temperature (MAAT). The RDA shows that lake CO_2 and CH_4 fluxes were not correlated, with CH_4 emissions associated with lake depth, water temperature, and mean annual air temperature (circled in blue) while CO_2 emissions were more closely associated with higher concentrations of nutrients, DOC, and chlorophyll *a* (circled in green). Base_Cations represents summed Ca, Mg, and Na concentrations. Potassium (K) is shown on its own as it followed a dissimilar trend to the other cations. Circle symbols indicate individual lakes, colored by permafrost zonation. Structural equation models were constructed individually for b) CO_2 and c) CH_4. Arrows with solid lines and asterisks represent statistically significant pathways (*p* values = * <0.05, ** <0.01, *** <0.001), while dotted lines represent non-significant pathways. The values by each arrow represent standardized model coefficients, indicating post positive and negative relationships. Goodness of fit (Fisher's C values) were 12.90 and 4.85, respectively for the CO_2 and CH_4 models, while *P* values were 0.40 and 0.30. *P* values > 0.05 indicate that model structure does not differ from that expected by the data..... 69

Figure 3.4 Influence of climate and permafrost conditions on greenhouse gas emissions from peatland lakes. Lakes in the continuous permafrost zone were found to be net sources of CO_2 and had low CH_4 emissions, while lakes outside the permafrost region were CO_2 sinks and had high CH_4 emissions. Absence of permafrost allows for increased hydrological connectivity to the surrounding landscape, potentially both deeper flow-paths through mineral soils and near-surface flow-paths through the surrounding peatlands. In this study, we found that lakes outside the permafrost region had generally higher pH and higher concentrations of ions, nutrients, and

chlorophyll-a – suggesting that elevated primary productivity (PP) outweighs respiration (R) in lakes outside the permafrost region. Lake diffusive CH_4 emissions were primarily linked to lake water temperatures and were 8-times greater south of the permafrost boundary compared to within the continuous permafrost zone. 71

Figure 3.5. Trends in methane-related functional genes among permafrost zones. a) Relative abundance of the a) methanogenesis marker mcrA (methyl coenzyme A reductase) and methanotrophy markers b) mmoX (methane monooxygenase subunit-A) and c) pmoA (particulate methane monooxygenase) increased moving south along the transect. Boxplots represent median and quartile ranges for samples taken from each lake once mid-summer 2019 from the continuous (Cont.), discontinuous (Disc.), and sporadic (Spor.) permafrost zones, as well as south of the permafrost region (None). Note the different y-axis scales. Differences are not statistically significant, likely due to low sample sizes (n=5 for every zone except the discontinuous zone where n=4). 73

Figure 3.6. Net radiative forcing due to changing CO_2 and CH_4 emissions from Taiga Plains peatland lakes under RCP 2.6 and 4.5 scenarios. a) The global RCP 2.6 and 4.5 temperature scenario pathways for the 21st century have been multiplied by a factor of three to account for Arctic amplification in the Taiga Plains, western Canada (Government of the Northwest Territories, 2018). b) Modelled current and future CO_2 and CH_4 emissions and total emissions (CO_2 + CH_4) from peatland lakes on the Taiga Plains. Error bars represent 95% confidence intervals from the model output. c) The 21st century radiative forcing resulting from altered lake CO_2 and CH_4 fluxes under the RCP 2.6 and 4.5 scenarios. Radiative forcing is referenced to the year 2020. A scenario of no warming is included, under which the net radiative forcing is only influenced by lake CO_2 emissions while steady CH_4 emissions are in equilibrium with the atmosphere. Radiative forcing due to altered lake CO_2 and CH_4 emissions is expressed as 10^{-15} fW divided by the total lake area of the Taiga Plains. The shaded areas represent the standard deviations from the flux models. Under both the RCP 2.6 and 4.5, we find that the net radiative forcing is dominated by increasing CH_4 emissions and only partly offset by reduced CO_2 emissions. 75

Figure 4.1. Study location. a) Study location in the southern Taiga Plains ecozone. b) Aerial photo of Eli Lake. The lake sampling locations are indicated in white text with white arrows. Inter. = Intermediate location. The white arrow and N symbol represent the orientation of the photo. The surface area of the lake is 0.005 km^2. The small blue object near the southern edge of the lake is a kayak for scale. Permafrost extent from Brown et al. 2002. Continental borders base layer from Wessel et al. 1996 89

Figure 4.2. a) Conceptual diagram of Eli lake and b) water column and sediment profiles. 98

Figure 4.3. Methane fluxes across the lake locations. a) Ebullitive fluxes. b) Diffusive fluxes. Boxplots represent the median and quartile ranges. The black circles represent the average and the small grey circles represent individual measurements. Different letters above the boxplots indicate significant differences amont the lake locations. 101

Figure 4.4. Bubble concentrations of a) CH_4 and b) CO_2, and c) volumetric bubble fluxes for individual bubble traps. Boxplots represent the median and quartile ranges. The grey circles represent the average. Note the different scales for bubble CH_4 and CO_2 concentrations. 102

Figure 4.5. Methane fluxes from chamber measurements across the different lake locations (a) and over the sampling months (b). Boxplots represent the median and quartile ranges. The black circles represent the average and the small grey circles represent individual measurements. Different letters above the boxplots indicate significant differences among lake locations and months. 103

Figure 4.6. Ebullitive CO_2 fluxes across the lake locations (a) and over the sampling months (b). Boxplots represent the median and quartile ranges. The black circles represent the average and the small grey circles represent individual measurements. Different letters above the boxplots represent significant differences among lake locations or sampling months. 105

Figure 4.7. Diffusive CO_2 fluxes across lake locations (a) and over the sampling months (b). Negative values represent net uptake of CO_2 from the atmosphere**.** Boxplots represent the median and quartile ranges. The black circles represent the averages and the small grey circles represent individual measurements. The dashed line represents the source or sink cutoff. The flux units represent mg of carbon in CO_2 106

Figure 4.8. Sediment temperature vs a) CH_4 ebullition, b) CH_4 diffusion, and c) CH_4 chamber fluxes. Error bars represent one standard deviation. No standard deviations are presented for diffusive fluxes. Black text represents linear regression output for fluxes across both lake locations. 107

Figure 4.9. Dissolved concentrations of CH_4 in the sediment porewater. Plots represent measurements taken for CH_4 in 2017 (a, b) and 2018 (c,d). 109

Figure 4.10. Potential CH_4 production rates of in the sediments. a) Depth profile of productions rates. b) Production rates at 100 cm sediment depths. c) Production rates at 200 cm sediment depths. Error bars represent one standard deviation. Different letters indicate significant differences among lake locations. The absence of letters indicates no significant difference in production rates. Gdw = grams dry weight. 110

Figure 4.11. Fraction modern carbon for CH_4 and CO_2 bubbles, water column DIC, and water column DOC. Error bars represent the minimum and maximum fM values reported, including analytical uncertainty. Corresponding mean ^{14}C ages are shown next to samples with pre-modern fM values. Notice the y-axis break. The average estimated carbon ages are presented next to each point. Yrs BP = ^{14}C years before present (1950 AD). 111

Figure A.2. 1. Correlation between thaw depth and CH_4 uptake. Positive numbers represent net uptake from the atmosphere. Colors represented different ecosystem class. Neutral (i.e. zero) fluxes were not included in the regression analyses. 148

Figure A.2. 2. Boxplots of CH_4 uptake as a factor of shrub cover. Positive numbers represent net uptake from the atmosphere. Orange dots represent mean uptake within a given category. P = Present; D = Dominant; A = Absent. Neutral fluxes (i.e. zero) were not included the boxplots. 149

Figure A.2. 3. Model cross-validation output for a) soil temperature and b) wetland CH_4 fluxes. 149

Figure A.2. 4. Model cross-validation output for aquatic diffusive CH_4 fluxes. LAL = Large Lakes. MGL = Midsize Glacial Lakes. MPL = Midsize Peatland Lakes. MYL = Midsize Yedoma Lakes. SGL = Small Glacial Lakes. SPL = Small Peatland Lakes. SYL = Small Yedoma Lakes. 150

Figure A.2. 5. Warm-season emissions for each wetland class and their associated model uncertainty (does not include the uncertainty from individual class areas). 151

Figure A.2. 6. Ice-free season diffusive emissions for each aquatic class and their associated model uncertainty (does not include the uncertainty from class areas). LAL = Large Lakes. MGL = Midsize Glacial Lakes. MPL = Midsize Peatland Lakes. MYL = Midsize Yedoma Lakes. SGL = Small Glacial Lakes. SPL = Small Peatland Lakes. SYL = Small Yedoma Lakes. 152

Figure A.2. 7. Relationship between waterbody surface area and water column depth.... 153

Figure A.2. 8. Non-transformed flux frequencies across the terrestrial land cover classes. A constant of 10 was added to include CH_4 uptake..... 154

Figure A.2. 9. Non-transformed flux frequencies across the aquatic land cover classes. .. 155

Figure A.3. 1. Correlation matrices for lake variables overaged over the whole sampling period. Variables include average diffusive carbon dioxide flux (CO2_flux), average diffusive methane flux (CH4_flux), water temperature (H2O_Temp), absorbance at 254 nm (A254), chlorophyll a (CHL.A), percent dissolved oxygen (DO_Per), PH, total dissolved nitrogen (TDN), potassium (K), specific conductivity (Cond), base cations ($Na^+ + Ca^{2+} + Mg^{2+}$; Base_Cat), latitude (LAT), total dissolved iron (Fe), dissolved organic carbon (DOC), dissolved phosphate (PO4.P), max lake depth (Max_Depth), lake surface area (SA), mean annual air temperature (MAAT). 160

Figure A.3. 2. Average daytime log CO_2 emissions vs average daytime log diffusive CH_4 emissions (large circles). Small dots represent individual daytime measuremens. CO_2 points on the left of the red line represent net uptake from the atmosphere. Methane emissions have not been corrected for diel variation. 161

Figure A.3. 3. Seasonal emission patterns. a) Daytime CO_2 exchange. b) Daytime diffusive CH_4 emissions and c) daytime ebullitive CH_4 emissions. Measurements were performed during the daytime between 8:00 and 18:00. Methane emissions have not been corrected for diel variation. Note the different units for CH_4 and CO_2 fluxes and the different y axis scales. 162

Figure A.3. 4. Linear models used for scaling. (a) Average 24-hour CH_4 emissions (corrected for diel changes; Sieczko et al. 2020) for each permafrost zone verse mean annual air temperature (MAAT). (b) Average daytime CO_2 emissions and mean annual air temperature. (c) The relationship between the number of ice-free days and mean annual temperature in each region. The points represent the mean of the average flux for each of the five lakes over the study

period in each permafrost zone. Error bars in a and b represent standard deviation between the five lakes while the error bars in c represent the largest variation in ice-cover days overserved over the 3 year period (+/- 14 days). 163

Figure A.3. 5. Decaheme cytochrome abundances and methanogenesis enzymes. A) Normalised abundance of iron reduction markers MtrA and MtrD (decaheme cytochromes) and homologues within each permafrost zone. Cont. = Continuous. Disc. = Discontinuous. Spor. = Sporadic. B) Methanogenesis enzymes shift with both iron acquisition and metabolism genes and aquatic base cation concentrations. We visualized methanogenesis enzyme composition with a non-metric multidimensional scaling (NMDS) ordination fitted with 2 axes (stress = 0.04). Environmental variables were superimposed using the envfit() function in the vegan package (Oksanen et al, 2019). Points are individual enzymes classed under Subsystem 3 function: Methanogenesis in SEED, and have been coloured according to whether they were associated with methylotrophic or other forms of methanogenesis. The green methylotrophic enzyme points fall along the iron acquisition/metabolism and base cations vector (arrows). The blue acetoclastic/hydrogentrophic points cluster away from the vectors towards the 0.0 axes markers. This indicates that methylotrophic enzymes are correlated with iron acquisition and metabolism and base cations, suggesting that communities shift from acetoclastic/hydrogenotrophic methanogenesis to methylotophic methanogenesis in the presence of high iron concentrations. 164

Figure A.3. 6. Simple model spin up for the radiative forcing model. Emission rates were held constant between 1900 and 2020 to arrive at a relative baseline for 2020 and the changes in emissions thereafter. The figure in the main text was referenced to the year 2020 and reflects the relative changes in radiative forcing from the year 2020 on. Radiative forcing units are per m^{-2} lake area. fW = 10^{-15} Watts. 165

Figure A.3. 7. Outlier lakes. a) Log phosphate (PO_4^{3-}) vs log CO_2 emissions plus 200 (lake averages from the entire sampling period) which highlights L2 (sporadic zone) as an outlier with high phosphate concentrations. High nutrient concentrations in this lake may be linked to the presence of a beaver. b) Log base cations ($Na^+ + Ca^{2+} + Mg^{2+}$) vs log daytime CH_4 emissions (sampling period averages) which highlights L5 (sporadic zone) as an outlier with high base cation concentrations. High ion concentrations in this lake likely indicate this lake receives direct input from a groundwater spring. c) Log Chla vs log CO_2 emissions plus 650 (whole period averages) which highlights W4 (discontinuous zone) as an outlier with extreme CO_2 uptake unrelated to Chla concentration. Note that W4 is not shown in panel a because it is out of the range of the frame. 166

Figure A.4. 1. Stratigraphic diagram based on macrofossil analysis of core from center of Eli Lake. Sphagnum to LigRoot expressed as relative percentage; items expressed as number found per sample; bulk density expressed as gcm^{-3}. Transitions and zones determined by shifts in vegetation composition and density. Stages of development classified as shallow open water wetland (SOWW)/marsh, fen with internal shifts from rich to poor, and current aquatic (i.e. limnic). Int Fen = intermediate fen. Aer = above ground vegetation parts. Root = below ground vegetation parts. Sed = sedge spp. Eric = Ericaceous spp. Lig = Unidentified wood. Carex = carex spp. Larix = larix laricina. Chara = Chara spp. Picea = Picea mariana. Eleocharis = Eleocharis spp. Mtrifoliata = Meyanthus Trifoliata..... 170

Figure A.4. 2. Monthly patterns in a) ebullitive CH_4 fluxes and b) diffusive CH_4 fluxes. Sep = September. 171

Figure A.4. 3. Potential production rates of carbon dioxide in the sediments. a) Depth profile of production rates. b) Production rates at 100 cm sediment depths. c) Production rates at 200 cm sediment depths. Error bars represent one standard deviation. 172

Figure A.4. 4. Examples of the different lake sediment types. a) Compact and less humified peat sediment from deeper sediment depths and b) highly humified, loose limnic sediments from the surface. 172

Figure A.4. 5. Porewater CH_4 concentrations from the MLP samplers deployed in 2017. 173

1. General Introduction

1.1 Boreal-Arctic methane emissions

Methane (CH_4) is a potent, climate-forcing trace gas (i.e. greenhouse gas) that is naturally emitted from wetlands and lakes, which are abundant in northern Boreal and Arctic regions (Lehner and Dohl, 2004; Messager et al. 2016). Accurate estimates of CH_4 emissions from the north are acutely needed to assess the global impact of increasing emissions in response to warming and the thawing of perennially frozen ground (i.e. permafrost). Current estimates of CH_4 fluxes from the Boreal-Arctic region (~>50º N) range between 21-77 Tg CH_4 yr^{-1} (Bastviken et al. 2011; McGuire et al. 2012; Zhu et al. 2013; Watts et al. 2014; Wik et al. 2016a; Tan et al. 2016; Walter Anthony et al. 2016; Treat et al. 2018; Thompson et al. 2018; Peltola et al. 2019; Matthews et al. 2020; Saunois et al. 2020), and make up a significant but unconstrained portion of global wetland and freshwater fluxes (211-402 Tg CH_4 yr^{-1}; Saunois et al. 2020). A key disparity and source of uncertainty in emission estimates involves differences in estimates from bottom-up and top-down scaling approaches.

Bottom-up estimates use process-based models or empirical, field-based chamber or eddy covariance flux measurements to extrapolate over a larger area (e.g. Wik et al. 2016 and Peltola et al. 2019). Top-down approaches use measurements of the atmospheric concentration of CH_4 and models of atmospheric transport to work backward to estimate net emissions across a region (e.g. McGuire et al. 2012, Thompson et al. 2018). The two approaches should, in theory, provide similar emission estimates, yet rarely do. Bottom-up estimates of CH_4 emissions from the arctic and sub-arctic are 2-3 times higher than top-down inversion model estimates and include high uncertainties (Saunois et al. 2020). Uncertainties and the likely overestimate of bottom-up emissions may stem from 1) inadequate land cover classifications (i.e. wetland and lake types) and spatial distribution maps 2) largely unknown patterns in lake fluxes within similar regions with varying climates or 3) from poor representations of mean flux estimates from individual lakes due to few measurements.

The objective of this thesis is to examine current CH_4 emissions from wetlands and lakes and assess the potential of future emissions from lakes at northern circumpolar, regional, and local scales. I start at the northern circumpolar scale and arrive at a new estimate of annual CH_4

emissions for wetlands and lakes, while also exploring the major gaps in flux data and knowledge of CH_4 in northern systems. In the subsequent chapters, I narrow in on the spatial scale, focusing on lake greenhouse gas (GHG) exchange from a previously understudied extent of western Canada. With each successive chapter, the spatial scale changes but I explore related questions centering on an overarching question- **what is the current magnitude of CH_4 emissions from northern wetlands and lakes and how will emissions from lakes change with warming and permafrost thaw?**

1.2 Methane cycling in natural systems and dominant CH_4-emitting characteristics

A limitation of many currently available circumpolar-scale land cover databases and remote sensing products is a lack of differentiation among wetland and lake ecosystems that are known to have differing CH_4 emissions. For both lakes and wetlands, the coarse grouping of land covers is partially driven by limitations in remote sensing (Melton et al. 2013), but also a lack of a uniform classification system for organizing wetland and lake types based on their CH_4-emitting characteristics. A key step to improving bottom-up estimates of CH_4 emissions from the circumpolar north is to use a uniform framework for classifying distinct, CH_4 emitting land cover classes and their associated flux magnitudes.

Net CH_4 flux to the atmosphere depends on a suite of physical and biological controls linked to microbial production and aerobic and anaerobic oxidation and is further impacted by the mode of transport to the atmosphere (Bastviken et al. 2004; Whalen et al. 2005). Methane is transported to the atmosphere via plant-mediated transport through aerenchyma of certain vascular graminoids (i.e. *Cyperaceae*, including *Carex spp*. and *Eriophorum spp*.), via ebullition (CH_4 bubbles), or by mixing in the water column from the source region to the air-water interface followed by diffusive flux across the air-water interface (Le Mer et al. 2001; Bastviken et al. 2004). While these basic underlying CH_4 processes are the same across ecosystems, the dominance of different production, oxidation, and transport processes vary within and among wetlands and lakes, leading to a wide range of reported CH_4 fluxes, including net uptake by some ecosystems. However, through the work of large scale flux syntheses, key controls on emissions across ecosystems have been identified (Olefeldt et al. 2013; Wik et al. 2016a; Treat et al. 2018).

For wetlands and non-wetlands (i.e. dry tundra and boreal uplands), CH_4 fluxes are largely associated with permafrost conditions and hydrology (Olefeldt et al. 2013; Treat et al. 2018) which, in turn, are linked to various controls on CH_4 emission including soil temperature (Olefeldt et al. 2017), water table conditions (Moore et al. 1994; von Fischer et al. 2010), vegetation cover (Olefeldt et al. 2013, Treat et al. 2018), and organic matter availability (Wagner et al. 2003; Christensen et al. 2003). Lake CH_4 emissions are highly influenced by lake morphology (Rasilo et al. 2015; Holgerson and Rayond, 2016), lake genesis (Wik et al. 2016a), and the closely linked underlying permafrost conditions (Walter et al. 2006), which are all associated with other key controls including sediment temperature (Wik et al. 2013), organic matter availability (Bastviken et al. 2004; Wik et al. 2018), lake trophic status (Del Sontro et al. 2016), and the number of annual ice-free days (Wik et al. 2014). Thus, there are a handful of land cover characteristics for wetlands and lakes that can be used to partition the relative magnitude of CH_4 emissions from different ecosystems across the landscape. The development of land cover databases that split ecosystems by these CH_4-emitting characteristics and complimentary flux databases represents an important step towards constraining bottom-up estimates of Boreal-Arctic CH_4 emissions and also estimating future emissions. In Chapter 2 of this thesis, I use a novel land cover model and comprehensive flux dataset, built around key CH_4-emitting land cover characteristics, to arrive at a new bottom-up estimate of CH_4 emissions from the Boreal-Artic region.

1.3 The influence of climate warming and permafrost thaw on lake GHG emissions

Northern Boreal and Arctic regions have the potential for substantial positive feedbacks to climate warming due to polar amplification and large carbon stores. Northern soils store approximately one-third of the earth's below ground carbon, with large quantities of this C stored in permafrost peatlands (Hugelius et al. 2020), unavailable for microbial decomposition. Increasing ambient air temperatures have led to accelerated rates of permafrost thaw and the release of this previously unavailable soil carbon to the atmosphere in the form of CH_4 or carbon dioxide (CO_2) (Schuur et al. 2008, Abbot et al. 2016; Walter Anthony et al. 2016). The physical effects of permafrost thaw, including active layer deepening, slumping, and subsidence have both localized and regional effects on lake biogeochemistry. Regional, or landscape-level, effects

of permafrost thaw include shifts in hydrological flow and wetland cover, with predictions of higher groundwater water connectivity and more wetlands with more thaw (Frey et al. 2009; Turetsky et al. 2019). Such changes in regional hydrology and wetland cover may alter the biogeochemical inputs lakes receive- including potentially more dissolved organic carbon (DOC), nutrients, and dissolved GHG's- and thus may alter net GHG emissions from lakes. Localized effects of permafrost thaw on lakes include land slumping as ground ice melts creating inundated or highly saturated environments (i.e. thermokarst or "thaw" lakes) conducive to anaerobic decomposition and the release of CH_4 and CO_2 (Walter et al. 2006; Schuur et al. 2008). Furthermore, GHG emissions from thaw lakes may be further accelerated due to the direct effects of warming on microbial activity (Yvon-Durocher et al. 2014). Understanding both the regional and localized effects of permafrost thaw, and the direct effects of warming, on GHG emissions from northern lakes is a crucial component towards our ability to assess the influence of climate warming on the global carbon budget.

1.3.1 Permafrost thaw across the landscape

In landscapes with widespread permafrost cover, deeper groundwater flow is constrained by the impermeable permafrost layer, forcing the surface hydrology to be dominated by near-surface lateral flows (i.e. "supra-permafrost" flow; Walvoord and Kuryluk, 2016) and highly disconnected peatland patches that drain into isolated thaw depressions (Quinton et al. 2019). As permafrost thaws, the physical barriers to surface and groundwater flow dissolve, leading to a wetter and more hydrologically connected landscape, including the conversion of drier, elevated permafrost bogs to saturated, nutrient-rich, and higher CH_4 emitting wetlands (Olefeldt et al. 2013; Quinton et al. 2019). Hydrologically well-connected lakes often receive greater inputs of DOC, dissolved CH_4 and CO_2, nutrients from organic-rich peatlands (Laudon et al. 2011; Burd et al. 2018; Wauthy et al. 2017), and also higher inputs of terminal electron acceptors and base cations from mineral soils, potentially increasing pH levels (Frey et al. 2009, Walvoord et al. 2012, Toohey et al. 2016). Increases in organic matter and nutrient delivery and within-lake productivity positively affect net CH_4 emissions through enhanced substrate availability (Bastviken et al. 2004; Davidson et al. 2015; Del Sontro et al. 2016). Alternatively, excess terminal electron acceptors may inhibit CH_4 production via competition with more thermodynamically favorable processes (Yu et al. 2016) or consumption of CH_4 through

anaerobic CH_4 oxidation (van Grinsven et al. 2020). Thus far, the influence of increasing hydrological connectivity on CH_4 fluxes from northern lakes is not well constrained.

Lake CO_2 emissions are also influenced by hydrologic connectivity. Net CO_2 exchange from lakes is controlled by a balance of CO_2 uptake through within lake primary productivity and CO_2 losses due to terrestrial inputs of DOC and dissolved CO_2, internal heterotrophic respiration, and photodegradation (Karlsson et al. 2009; Weyhenmeyer et al. 2015; Bogard et al. 2016; Nydahl et al. 2020). A well-connected lake may receive larger inputs of dissolved CO_2 and DOC, thus increasing CO_2 emissions through photodegradation and CO_2 outgassing. However, higher connectivity may also lead to greater pH and nutrient input and therefore decrease CO_2 emissions through shifts in carbonate chemistry or increases in primary productivity, respectively (del Giorgio & Peters 1994; Lapierre & del Giorgio et al. 2012; Pacheco et al. 2014; Finlay et al. 2015).

Northern peatland lakes and boreal lakes are typically large net CO_2 and CH_4 sources, as they generally are small, have organic-rich sediments, are nutrient-poor, unproductive, and receive vast inputs of external, terrestrial dissolved organic carbon (DOC) and dissolved CO_2 (la Pierre et al. 2015; Weyhenmeyer et al. 2015; Wik et al. 2016; Hastie et al. 2018; Serikova et al. 2019). While both CO_2 and CH_4 emissions from lakes are predicted to increase with climate warming (Wik et al. 2016a; Hastie et al. 2018; Guo et al. 2020), the balance between internal warming (i.e. increased microbial activity and CH_4 production) and external, thaw-driven factors that influence northern peatland lake CO_2 and CH_4 emissions are not well constrained. This is particularly true for peatland lakes in the Mackenzie River basin of western Canada, an understudied (concerning lake GHG emissions), but globally significant peatland region. In Chapter 3, I examine the influence of landscape-level permafrost thaw and warming temperatures on GHG emission from peatland lakes across a permafrost gradient throughout western Canada.

1.3.2 Localized effects of permafrost thaw on lake GHG emissions

Thermokarst lakes are well-documented hotspots of CH_4 emission, particularly from actively thawing lake edges underlain by yedoma soils (i.e. Pleistocene aeolian soils with high content of poorly degraded organic matter; Walter et al. 2006; Walter Anthony et al. 2016; Dean et al. 2020; Walter Anthony et al. 2021). In yedoma systems, enhanced CH_4 emissions from thaw

edges have been linked to the high lability and quantity of OM released from yedoma permafrost soils (Heslop et al. 2016; Douglas et al. 2020). These previous findings indicate that the response of CH_4 emissions to permafrost thaw may be highly dependent on the history and quality of OM stored in the permafrost. However, yedoma soils are not widespread throughout the northern region (Strauss et al. 2017) and little is known about CH_4 emissions from peatland thermokarst lakes, despite the widespread presence of peatlands across the northern landscape (Hugelius et al. 2020; Olefeldt, Hovemyr, Kuhn, et al. 2021; Fig. 1.1).

The quality and quantity of carbon stored in peatland permafrost differ from the fine, organic-rich loess carbon in yedoma deposits, potentially leading to different responses of CH_4 emissions from lakes upon thaw. Many permafrost peatlands formed through epigenetic processes wherein permafrost is initially absent, but the development of thick, peat layers eventually facilitates downward freezing into soils (Zoltai et al. 1993). As a result, much of the peat is exposed to microbial decomposition before freezing, potentially leading to more recalcitrant carbon that is not as easily mineralized post-thaw (Treat et al. 2016). However, the carbon content of peat can be much higher than yedoma deposits (Krüger et al. 2014), potentially leading to more carbon mineralization. Thus the response of CH_4 emissions from peatland lakes to thaw is largely unknown. Given the widespread nature of permafrost peatlands throughout the north (Olefeldt, Hovemyr, Kuhn, et al. 2021), understanding the fate and magnitude of peatland permafrost carbon upon thaw is crucial to constraining the impact of climate warming on northern carbon emissions. Furthermore, many previous lake studies have been limited in spatial extent and temporal coverages, potentially leading to poor representation of mean emissions (Wik et al. 2016b; Jansen et al. 2020). In Chapter 4, I explore the influence of permafrost thaw on CH_4 emissions from a small peatland lake in northern Alberta using high frequency spatial and temporal measurements.

1.4 The Boreal and Taiga Plains of western Canada

The Mackenzie River basin is a previously glaciated northern landscape in western Canada with abundant lakes (Messager et al. 2016) and peatlands, representing the third-largest peatland area in the north, after the West Siberian Lowlands and the Hudson Bay Lowlands (Fig. 1.1; Hugelius et al. 2020; Olelfedt, Hovemyr, Kuhn, et al. 2021). The region includes the Taiga Plains and Boreal Plains ecozones (herein referred to as the Interior Plains), an area that extends

from 70º N to 56º N. The region is characterized by generally flat topography, sedimentary bedrock overlain by thick, heterogeneous surficial geology (Geological Survey of Canada, 2014). The region has a relatively dry climate throughout, with mean annual precipitation between 300 and 450 mm and mean annual runoff between 50 and 150 mm, but it has a large gradient in mean annual average temperatures (MAAT) between -8 and +2°C. Peatlands in the Interior Plains started developing shortly after deglaciation ~10,000 years ago, and today have 2-6 m deep peat deposits (Halsey, Vitt, and Bauer, 1998; Hugelius et al. 2020; Heffernan et al. 2020). Permafrost expanded southward after the Holocene thermal maximum and reached its maximum extent following the Little Ice Age, ~1,000 years ago (Pelletier et al., 2017). Outside of the continuous permafrost zone, permafrost is isolated to elevated peat plateaus (Zoltai et al. 1993). Permafrost conditions and heterogeneous glacial deposits strongly influence peatland hydrology and thus the hydrological connectivity of lakes to their surrounding landscape in this region (Quinton et al 2019; Hokansson et al. 2019). These characteristics set the Interior Plains apart from the adjacent Taiga Shield, eastern Canadian Shield, and most of Scandinavia- all of which have typically thin overburdens and generally steeper topography, thus fewer peatlands and peatland lakes.

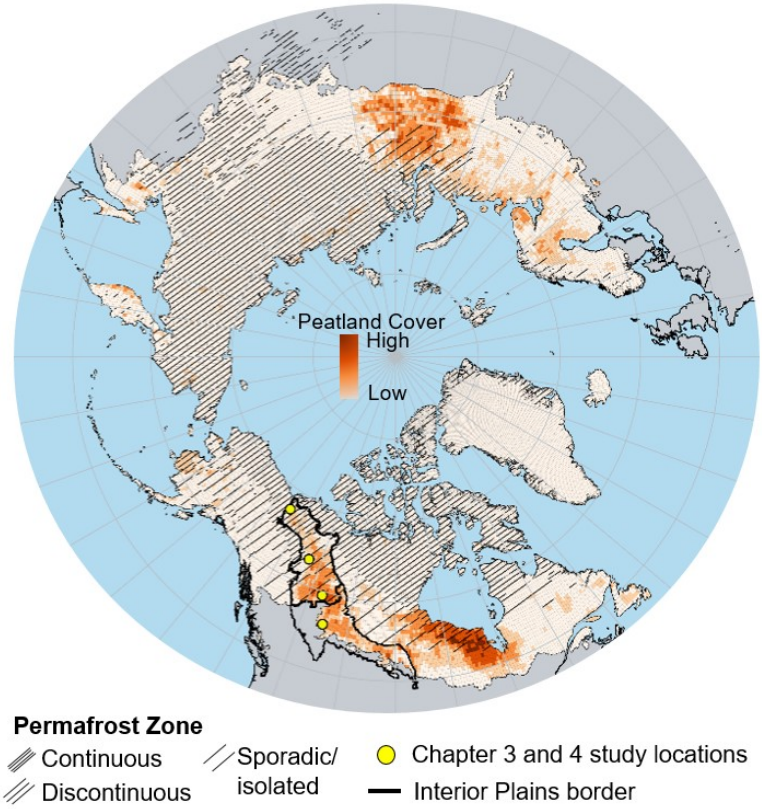

Figure 1.1. Northern circumpolar map including peatland and permafrost cover. The black outlines represent the Taiga (upper outline) and Boreal Plains ecozones. The yellow dots represent the study locations for Chapters 3 and 4. Peatlands include bogs, fens, and permafrost bogs extracted from Olefeldt, Hovemyr, Kuhn, et al. (2021). Permafrost distribution is from Brown et al. (2002).

1.5 Objectives

The main objective of this doctoral dissertation is to understand the current magnitude and potential sensitivity of CH_4 emissions from northern wetlands and lakes to climate warming across regional to local spatial scales. The dissertation is divided into five chapters, including an introduction, three data chapters, and a conclusion. In Chapter 2, I arrive at a new bottom-up estimate of CH_4 emissions for the northern Boreal and Arctic region using an extensive synthesis of all available flux data for the region, paired with a novel CH_4-centric land cover model. In this chapter, I also establish the crucial weaknesses and gaps in currently available CH_4 flux data and suggest avenues of future research that will help further constrain current emissions and also

better predict future changes in emissions. Chapter 2 sets the stage for Chapters 3 and 4 in which I explore, in detail, the potential effects of climate warming on CH_4 and CO_2 emissions from lakes across the Interior Plains. In Chapter 3, I assess the interactive effects of warming and landscape-level permafrost thaw and hydrological connectivity on CH_4 and CO_2 dynamics in lakes across a climate gradient throughout the Interior Plains. In Chapter 4, I zoom in further and explore the direct impacts of permafrost thaw on CH_4 emissions from one peatland lake using high frequency spatial and temporal measurements. In my fifth and final chapter, I provide concluding statements for each chapter and their linkages on the magnitude of CH_4 emissions from the Boreal-Arctic region and the potential impacts of climate warming and permafrost thaw on CH_4 emissions from northern lakes.

2. BAWLD-CH_4: A comprehensive dataset of methane fluxes from Boreal and Arctic ecosystems

Abstract

Methane (CH_4) emissions from the Boreal and Arctic region are globally significant and highly sensitive to climate change. There is currently a wide range in estimates of high-latitude annual CH_4 fluxes, where estimates based on land cover inventories and empirical CH_4 flux data or process models (bottom-up) generally are greater than atmospheric inversions (top-down). A limitation of bottom-up approaches has been the lack of harmonization between inventories of site-level CH_4 flux data and the land cover classes (i.e. ecosystem types) present in high-latitude spatial datasets. Here I present a comprehensive dataset of small-scale, surface CH_4 flux data from 540 terrestrial sites (wetland and non-wetland) and 1247 aquatic sites (lakes and ponds), compiled from 189 studies. The Boreal and Arctic Wetland and Lake Methane Flux Dataset (BAWLD-CH_4) was constructed in parallel with a compatible land cover dataset, sharing the same land cover classes to enable refined bottom-up assessments. BAWLD- CH_4 includes information on site-level CH_4 fluxes, but also on study design (measurement method, timing, and frequency) and site characteristics (vegetation, climate, hydrology, soil, and sediment types, permafrost conditions, lake area and depth, and our determination of land cover class). The different land cover classes had distinct CH_4 fluxes, resulting from definitions that were either based on or co-varied with key environmental controls. Fluxes of CH_4 from terrestrial ecosystems were primarily influenced by water table position, soil temperature, and vegetation composition, while CH_4 fluxes from aquatic ecosystems were primarily influenced by water temperature, lake size, and lake genesis. Models could explain more of the between-site variability in CH_4 fluxes for terrestrial than aquatic ecosystems, likely due to both less precise assessments of lake CH_4 fluxes and fewer consistently reported lake site characteristics. Finally, I incorporated land cover class and mean annual temperature as predictor variables in empirical models, alongside the newly developed land cover distribution areas, to arrive at new bottom-up annual CH_4 emission estimates of 30 (22.8-44) Tg CH_4 yr^{-1} and 6.6 (3.1-9.1) Tg CH_4 yr^{-1} for wetlands and lakes, respectively.

2.1 Introduction

Methane (CH_4) is a strong climate forcing trace gas that is naturally produced and emitted from wetlands and lakes, which are abundant in northern regions (Matthews and Fung 1987; Lehner and Doll et al. 2004; Messager et al. 2016). Current estimates of CH_4 fluxes from the northern Boreal and Arctic region (~>50º) range between 9 and 53 Tg CH_4 yr^{-1} from wetlands (McGuire et al. 2012; Zhu et al. 2013; Treat et al. 2018; Watts et al. 2014; Thompson et al. 2018; Peltola et al. 2019; Saunois et al. 2020) and between 12 and 24 Tg CH_4 y^{-1} from lakes (Bastviken et al. 2011; Wik et al. 2016a; Tan et al. 2016; Walter Anthony et al. 2016; Matthews et al. 2020; Saunois et al. 2020). Combined, CH_4 emissions from northern ecosystems make up a significant but uncertain portion of global wetland and freshwater fluxes (211-402 Tg CH_4 yr^{-1}) (Saunois et al. 2020). One reason for the wide range of high latitude CH_4 emissions estimates is the consistently lower estimates based on top-down approaches compared to bottom-up approaches. Top-down approaches use atmospheric observations of CH_4 concentrations with atmospheric-inverse modeling frameworks to estimate regional CH_4 budgets (e.g. , McGuire et al. 2012; Thompson et al. 2018) while bottom-up approaches merge land cover datasets and empirical CH_4 flux inventories or process-based models to scale emissions at regional levels (e.g. Wik et al. 2016a; Treat et al. 2018; Peltola et al. 2019). A key issue for bottom-up approaches is the lack of differentiation among different wetland and lake types despite clear evidence indicating differences in both the magnitude and drivers of CH_4 fluxes these classes (Olefeldt et al. 2013; Turetsky et al. 2014; Wik et al. 2016a).

Net CH_4 flux to the atmosphere depends on a suite of physical and biological controls linked to microbial production, oxidation, and transport via diffusion, ebullition, and plant-mediated processes (Bastviken et al. 2004; Whalen et al. 2005). While the basic underlying CH_4 processes are the same across all ecosystems, the dominance of different production, oxidation, and transport pathways varies within and among terrestrial (wetlands and non-wetlands) and lentic open water aquatic ecosystems (lakes and ponds), leading to a wide range of reported CH_4 fluxes at the site level with differences of up to four orders of magnitude (Olefeldt et al. 2013; Wik et al. 2016a; Treat et al. 2018). Despite the wide range in reported CH_4 fluxes, key over-arching controls on emissions from wetland and aquatic ecosystems have been identified through

the work of syntheses (Olefeldt et al. 2013; Wik et al. 2016a; Treat et al. 2018), suggesting that different ecosystems can be partitioned based on a handful of key CH_4-emitting characteristics.

For terrestrial ecosystems, CH_4 fluxes across the Boreal-Arctic region are primarily linked to permafrost conditions and hydrology (Olefeldt et al. 2013; Treat et al. 2018) which encompass other important controls on CH_4 emissions. For example, permafrost condition and hydrology can be directly linked to water table position and redox conditions (Moore et al. 1994; Fischer et al. 2010; Olefeldt et al. 2017), which in turn influence plant composition (i.e. plant function types including graminoids, *Sphagnum* mosses, shrubs, and trees; Olefeldt et al. 2013; Bridgham et al. 2013), microbial community composition (McCalley et al. 2014), productivity (Christensen et al. 2003), and organic matter availability (Wagner et al. 2003; Christensen et al. 2003). Both permafrost condition and hydrology can further be used as an indication of soil temperature with typically colder conditions in drier soils and permafrost-dominated landscapes (Olefeldt et al. 2017). Methane fluxes are typically highest from graminoid-dominant wetlands like marshes and fens which are frequently inundated, which in turn enhances primary productivity (Ström et al. 2012), creates a soil habitat conducive to CH_4-producing microbes (Woodcroft et al. 2018), and facilitates CH_4 transport through aerenchymatous roots and stems (Chanton et al. 1993; Ström and Christensen, 2007). Conversely, CH_4 fluxes are typically low from permafrost bogs and bogs which tend to have colder (in the case of permafrost bogs) and drier soil conditions (Beylea and Baird, 2006; Anderson et al. 2011), are less conducive to the presence of graminoid species and promote the consumption of CH_4 through oxidation (Bartlett et al. 1992; Moosavi and Crill, 1997).

Methane fluxes from aquatic ecosystems (lakes and ponds) are highly influenced by lake morphology (Rasilo et al. 2015; Holgerson and Raymond, 2016; Preskienis et al. 2021) and lake genesis (Wik et al. 2016a), including permafrost conditions (Walter et al. 2006), which are associated with other key controls and CH_4 fluxes. Lake morphology influences sediment temperature (Marinho et al. 2015), stratification and oxygen saturation (Riera et al. 1999), macrophyte presence (Wik et al. 2018), and turbulent transfer (MacIntyre et al. 2018). Lake morphology, permafrost condition, and lake genesis all determine organic substrate availability in sediments (Walter et al. 2006, Wik et al. 2016a) and trophic status (Bastviken et al. 2004; DelSontro et al. 2016). For example, peatland lakes and ponds, which form through degradation

and permafrost thaw processes in peatlands, are relatively high CH_4 emitters (Matveev et al. 2016; Kuhn et al. 2018; Burke et al., 2019). These waterbodies are underlain by organic-rich sediments and are typically small and shallow and less likely to be seasonally stratified, allowing for rapid sediment warming and carbon mineralization (Matveev et al. 2016). Glacial and post-glacial waterbodies, on the other hand, have relatively low CH_4 fluxes due to deeper water columns which limit ebullition, and also have mineral-rich sediments with typically less labile organic substrates (Schnurrenberger et al. 2003; DelSontro et al. 2016; Wik et al. 2016a). Therefore, while there are many physical and biogeochemical controls on aquatic CH_4 fluxes, size and lake genesis can be useful proxies for many of these underlying factors.

There are various methodologies used to measure surface CH_4 fluxes from terrestrial and aquatic ecosystems. Two approaches used in both terrestrial and aquatic ecosystems include micrometeorological eddy covariance (EC) techniques and chamber measurement techniques. Eddy covariance measurements are collected at high temporal frequencies from towers and typically cover a footprint of 100-10,000 m^2. The near-continuous nature of EC measurements provides valuable insight into the temporal patterns and drivers of CH_4 fluxes, however, towers are geographically limited across the Boreal-Arctic region and it can be difficult to attribute flux transport pathways and specific source areas at fine spatial scales (Knox et al. 2019: Delwiche et al. 2021). Conversely, static chamber measurements cover small spatial areas that allow for detailed assessments of environmental controls on fluxes (Bäckstrand et al. 2008; Olefeldt et al. 2013). Chamber-based methods quantify fluxes by calculating the change in chamber headspace concentration over a set time, which varies based on extraction methods (i.e. syringe, automated chamber, or portable gas analyzer). While chamber-based techniques have drawbacks, including surface disturbance, typically low sampling frequency, and high labor intensity, chambers are easily installed, can capture environmental controls of CH_4 fluxes at a sub-meter scale, and are cheaper options compared to installing and maintaining EC towers. Thus, I focus mostly on chamber-based flux measurements in this synthesis because they have been performed at a large number of sites across the Boreal and Arctic region and represent more of the geographic variation across the region.

In aquatic ecosystems, turbulence-driven modeling approaches, inverted funnels (i.e. bubbles traps), and ice bubble surveys (IBS) are additionally used to quantify CH_4 fluxes. Modeling approaches calculate net hydrodynamic flux (herein referred to as diffusion) to the

atmosphere by determining the concentration of dissolved CH_4 in the water column and an estimate of the gas transfer velocity *k* (see Sect. 2.2.4 for more information). Bubble traps capture the volume of bubble gas released from sediments; ebullitive flux can be estimated by using the concentration of CH_4 found in the bubble (Wik et al. 2013). Finally, IBS are used to quantify the spatial abundance and types of bubble formations trapped within lake ice over the winter (Walter et al. 2010). Importantly, these surface-based methods can be used to assess controls of CH_4 exchange at scales of individual ponds, lakes, and portions of open-water wetlands, providing key insights into the environmental processes controlling CH_4 flux to the atmosphere (Olefeldt et al. 2013; Wik et al. 2016a).

Here I expanded, updated, and merged previous CH_4 flux syntheses for northern wetlands (Olefeldt et al. 2013) and lakes (Wik et al. 2016a) to create a small-scale (sub-meter) surface-based dataset for CH_4 fluxes collected from 189 studies across the Boreal-Arctic region. The dataset was built in parallel with a novel, CH_4-specific land cover dataset for the circumpolar north- the Boreal-Arctic Wetland and Lake Dataset (BAWLD; Olefeldt, Hovemyr, Kuhn et, al. 2021), allowing for flux observations and spatial distribution of land cover features to be classified under the same criteria at a pan-Boreal-Arctic scale. This dataset provides an open platform for surface-based fluxes and associated environmental drivers from aquatic, wetland, and upland (i.e. non-wetland) ecosystems and can be utilized by both field researchers and the modeling community. Information in the dataset can be used to compare field results, identify new research opportunities, or build and test models. This dataset includes and uniformly classifies lake, wetland, and upland surface CH_4 flux data for the circumpolar north. In this study, I show CH_4 flux distributions and environmental drivers from various terrestrial (wetland and upland) and aquatic ecosystems, compare the results to previous CH_4 flux syntheses, highlight key gaps in the data, and suggest future research directions.

2.2 Dataset description and BAWLD land cover classification

The dataset is composed of two components including 1) terrestrial ecosystems (vegetated wetland and non-wetland ecosystems) and 2) lentic aquatic ecosystems (lakes, ponds, and open water pools; hereafter referred to as “aquatic ecosystems”). This synthesis does not include lotic systems (streams and rivers), which are already synthesized in Stanley et al. (2015). The datasets for terrestrial and aquatic ecosystems are reported as separate components due to

differences between both the drivers of CH_4 fluxes and data collection methods. The terrestrial dataset extends the work by Olefeldt et al. (2013), who compiled CH_4 flux estimates for wetlands in the permafrost zones designated by Brown et al. (2002). My dataset expands on this initial work to include flux data from non-permafrost and non-wetland sites throughout the Arctic and Boreal region (Olson et al. 2001) and flux data from studies between 2012 and February 2020. I updated the initial dataset to include separate entries for individual sites that reported flux and water table data for multiple years. I expanded the number of site-year flux estimates in the original terrestrial dataset by 83% and expanded the number of independent studies by 86%, leading to a total of 555 warm-season (~May through October depending on the location) flux estimates and 121 studies (Fig. 2.1a). The aquatic dataset extends the work by Wik et al. (2016a) which is a compilation of CH_4 flux data for lakes and ponds north of 50º N. I expand on this initial work to include studies between 2016 and February 2020. Additionally, I updated the original aquatic dataset to include the within-lake location for ebullition measurements and the equation used to model the gas velocity coefficient *k*. I expanded the number of lakes in the dataset by 71% and the number of studies by 66%, summing to a total of 1251 lakes and 68 independent studies (Fig. 2.1b). Finally, each terrestrial and aquatic site was reclassified into a new land cover classification, further explained below.

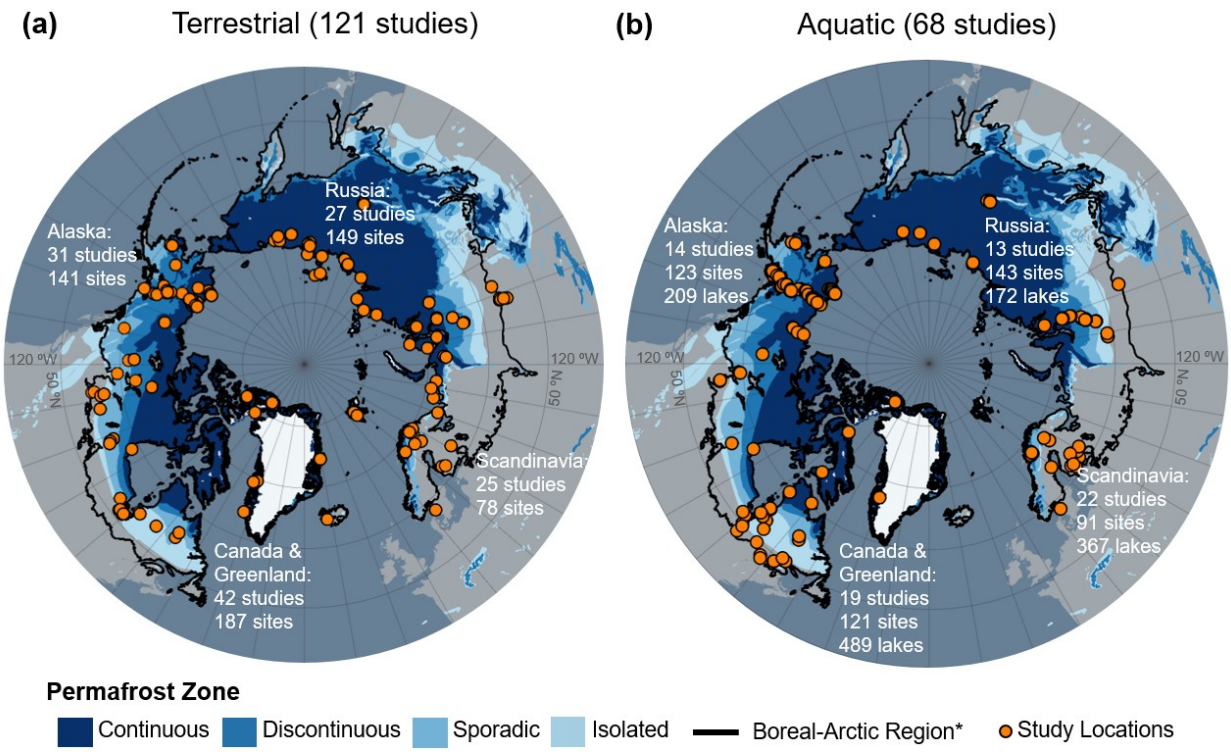

Figure 2.1. Maps of the individual sites (orange circles) incorporated in BAWLD-CH4. a) Sites included in the terrestrial flux dataset. b) Sites included in the aquatic flux dataset. The number of "sites" in the terrestrial data set represents site-years, which in some cases represent multiple years of data from one site or data from the same site reported by different studies. "Sites" in the aquatic dataset represent the reported average fluxes for one or multiple lakes. In some cases, studies reported one mean value for multiple lakes, therefore the number of lakes and the number of sites are not the same. *Boreal-Arctic Region boundary from Olson et al. 2001. Permafrost zones are from Brown et al. 2002. Continental shoreline base layers are from Wessel et al. 1996.

2.2.1.0 Land cover classes in the Boreal Arctic Wetland and Lake Dataset

Land cover classes in the Boreal and Arctic Wetland and Lake Dataset (BAWLD; Olefeldt, Hovemyr, Kuhn, et al. 2021) were chosen and defined to enable upscaling of CH_4 fluxes at large spatial scales. As such, we aimed to include as few classes as possible to facilitate large-scale mapping, while still having sufficient classes to allow separation among groups of ecosystems with similarities in hydrology, ecology, and biogeochemistry and therefore net CH_4

fluxes. The BAWLD land cover classification is hierarchical; with four upland classes, five wetland classes, seven lentic aquatic classes, and three lotic aquatic classes. As mentioned previously, fluxes from lotic ecosystems (streams and rivers) have not been included in this dataset but are covered by Stanley et al. (2015).

2.2.1.1 Wetland classes

Wetlands are defined by having a water table near or above the land surface for sufficient time to cause the development of wetland soils (either mineral soils with redoximorphic features, or organic soils with > 40 cm peat), and the presence of plant species with adaptations to wet environments (Hugelius et al., 2020; Canada Committee on Ecological (Biophysical) Land Classification et al., 1997; Jorgenson et al., 2001). Wetland classifications for boreal and arctic biomes can focus either on small-scale wetland classes that have distinct hydrological regimes, vegetation composition, and biogeochemistry or on larger-scale wetlands that are comprised of distinct patterns of smaller wetland and open-water classes (Gunnarsson et al., 2014; Terentieva et al., 2016; Masing et al., 2010; Glaser et al., 2004). While larger-scale wetlands are easier to identify through remote sensing techniques (e.g. patterned fens comprised of higher elevation ridges and inundated hollows), our classification focuses on wetland classes due to greater homogeneity of hydrological, ecological, and biogeochemical characteristics that regulate CH_4 fluxes (Heiskanen et al., 2021).

Several boreal countries identify four main wetland classes, differentiated primarily based on hydrodynamic characterization; bogs, fens, marshes, and swamps (Gunnarsson et al., 2014; Canada Committee on Ecological (Biophysical) Land Classification et al., 1997; Masing et al., 2010). The BAWLD classification follows this general framework, but further uses the presence or absence of permafrost as a primary characteristic for classification and excludes a distinct swamp class, yielding five classes; *Bogs*, *Fens*, *Marshes*, *Permafrost Bogs*, and *Tundra Wetlands* (see Fig. 2.2 and Fig. 2.3). The swamp class was omitted due to the wide range of moisture and nutrient conditions of swamps, as well as the limited number of studies of swamp CH_4 fluxes. We instead included swamp ecosystems in expanded descriptions of *Bogs*, *Fens*, and *Marshes*. The presence or absence of near-surface permafrost was used as a primary characteristic to distinguish between *Permafrost Bogs* and *Bogs* and to distinguish *Tundra*

Wetlands from *Marshes* and *Fens*. The presence or absence of near-surface permafrost is considered key for controlling CH_4 emissions given its influence on hydrology, and for the potential of permafrost thaw and thermokarst collapse to cause rapid non-linear shifts to CH_4 emissions (Bubier et al., 1995; Turetsky et al., 2002; Malhotra and Roulet, 2015; Fig, 2.2 and Fig. 2.3). Finally, while some classifications include shallow (e.g. 2 m depth), open-water ecosystems within the definition of wetlands (Gunnarsson et al., 2014; Canada Committee on Ecological (Biophysical) Land Classification et al., 1997), we have included all open-water ecosystems without emergent vegetation within the lake classes (see below) due to the strong influence of emergent vegetation in controlling CH_4 emissions (Juutinen et al., 2003).

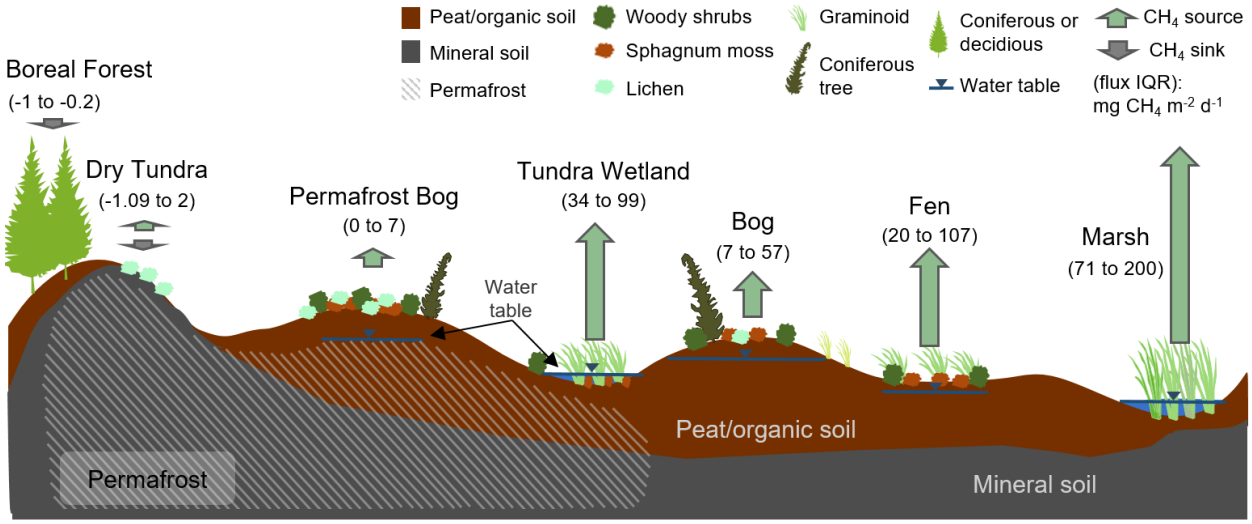

Figure 2.2. Conceptual diagram of the terrestrial land cover classes and their CH_4-emitting characteristics including permafrost conditions, hydrology, organic layer depth, and associated nutrient and vegetation characteristics. Numbers within the brackets represent the interquartile (IQR) flux ranges. Arrows are scaled based on mean flux values. See Sect. 2.3.2 for a detailed breakdown of terrestrial fluxes.

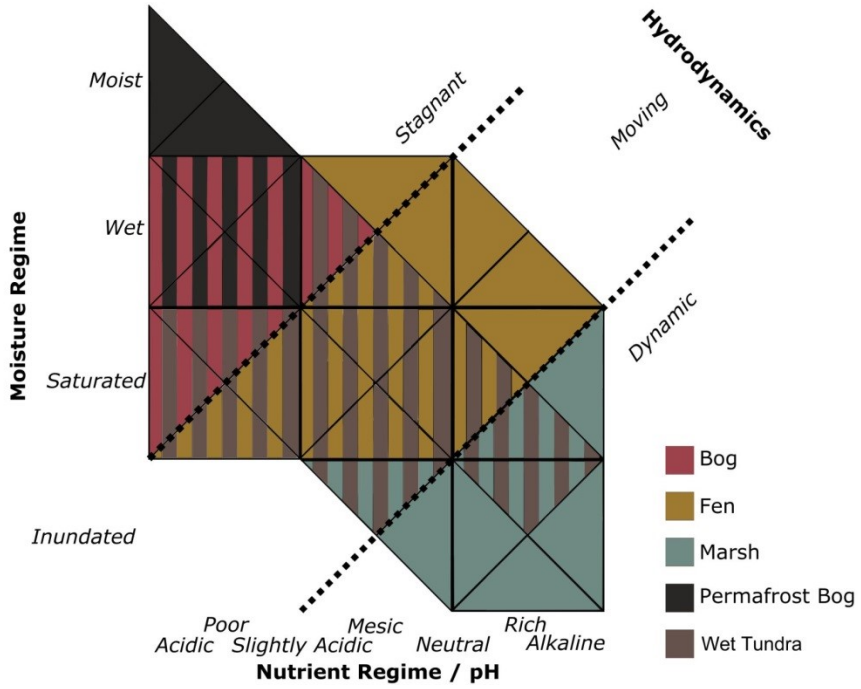

Figure 2.3. Definitions of the five wetland classes in BAWLD along axes of moisture regime and nutrient regime.

Bogs are described as ombrotrophic peatland ecosystems, i.e. only dependent on precipitation, and snowmelt for water inputs. Peat thickness is at least 40 cm, with maximum thickness > 10 m. The peat profile is not affected by permafrost, although in some climatically colder settings there may be permafrost below the peat profile. *Bogs* are wet to saturated ecosystems, often with small-scale (<10 m) microtopographic variability, with stagnant water and a water table that rarely is above the surface or more than 50 cm below the surface (Fig. 2.3). *Bogs* have low pH (<5), low concentrations of dissolved ions, and low nutrient availability resulting from a lack of hydrological connectivity to surrounding mineral soils. Vegetation is commonly dominated by *Sphagnum* mosses, lichens, and woody shrubs, and can be either treed or treeless (Beaulne et al., 2021). Our description of *Bogs* also includes what is commonly classified as treed swamps, which generally represent ecotonal transitions between peatlands and upland forests (Canada Committee on Ecological (Biophysical) Land Classification et al., 1997).

Fens are described as minerotrophic peatland ecosystems, i.e. hydrologically connected to surrounding mineral soils through surface water or groundwater inputs. A *Fen* peat profile is at least 40 cm thick (Gorham et al. 1991), although maximum peat thickness is generally less than for bogs. The peat profile is not affected by permafrost. *Fens* are wet to saturated

ecosystems, with generally slow-moving water (Fig. 2.3). *Fens* have widely ranging nutrient regimes and levels of dissolved ions depending on the degree and type of hydrological connectivity to their surroundings, ranging from poor fens to rich fens. Vegetation largely depends on wetness and nutrient availability, where more nutrient-poor fens can have *Sphagnum* mosses, shrubs, and trees, while rich fens are dominated by brown mosses, graminoids (sedges, rushes), herbaceous plants, and sometimes coniferous or deciduous trees (e.g. willows, birch, larch, black spruce). Our description of *Fens* also includes what is commonly classified as shrubby swamps, which often are associated with riparian ecotones and lake shorelines.

Marshes are minerotrophic wetlands with dynamic hydrology, and often high nutrient availability (Fig. 2.3). Vegetation is dominated by emergent macrophytes, including tall graminoids such as rushes, reeds, grasses, and sedges – some of which can persist in settings with >1.5 m of standing water. *Marshes* are saturated to inundated wetlands, often with highly fluctuating water levels as they generally are located along shorelines of lakes or coasts, along streams and rivers, or on floodplains and deltas. It is common for marshes to exhibit both flooded and dry periods. Dry periods facilitate the decomposition of organic matter and can prevent the build-up of peat. As such *Marshes* generally have mineral soils, although some settings allow for the accumulation of highly humified organic layers – sometimes indicating ongoing succession towards a peatland ecosystem. Salinity can vary depending on water sources, with brackish to saline conditions in some areas of groundwater discharge, or in coastal settings.

Permafrost Bogs are peatland ecosystems, although the peat thickness in cold climates is often relatively shallow. *Permafrost Bogs* have a seasonally thawed active layer that is 30 to 70 cm thick, with the remainder of the peat profile perennially frozen (i.e. permafrost). Excess ground-ice and ice expansion often elevate *Permafrost Bogs* up to a few meters above their surroundings, and as such, they are ombrotrophic and generally the wetland class with the driest soils (Fig. 2.3). *Permafrost Bogs* have moist to wet soil conditions, often with a water table that follows the base of the seasonally developing thawed soil layer. Ombrotrophic conditions cause nutrient-poor conditions, and the vegetation is dominated by lichens, *Sphagnum* mosses, woody shrubs, and sometimes stunted coniferous trees. *Permafrost Bogs* are often interspersed in a fine-scale mosaic (10 to 100 m) with other wetland classes, e.g. *Bogs* and *Fens*. Common *Permafrost*

Bog landforms include palsas, peat plateaus, and the elevated portions of high- and low-center polygonal peatlands.

Tundra Wetlands are treeless ecosystems with saturated to inundated conditions, most commonly with near-surface permafrost (Fig. 2.3). Tundra Wetlands can have either mineral soils or shallow organic soils, and generally receive surface or near-surface waters from their surroundings, as permafrost conditions preclude connectivity to deeper groundwater sources. Vegetation is dominated by short emergent vegetation, including sedges and grasses, with mosses and shrubs in slightly drier sites. *Tundra Wetlands* have a lower maximum depth of standing water than *Marshes,* due to the shorter vegetation. *Tundra Wetlands* can be found in basin depressions, in low-center polygonal wetlands, and along rivers, deltas, lake shorelines, and on floodplains in regions of continuous permafrost. Despite the name, limited wetlands with these characteristics (hydrology, permafrost conditions, and vegetation) can also be found within the continuous permafrost zone in boreal and sub-arctic regions (Virtanen et al., 2016).

2.2.1.2 Upland and other classes

Upland and other classes in BAWLD; *Glaciers, Rocklands, Dry Tundra,* and *Boreal Forests,* have in common that they are neither wetlands nor aquatic ecosystems. *Glaciers* are assumed to have neutral CH_4 fluxes, however, to our knowledge there are no published studies with field data. *Rocklands* are also expected to have very low CH_4 fluxes (Oh et al. 2020), potentially with more frequent CH_4 uptake than release – however, there were very few sites that fit within this class (n=5), therefore these flux estimates were combined with *Dry Tundra* sites.

The *Dry Tundra* class includes both lowland arctic tundra and alpine tundra; both treeless ecosystems dominated by graminoid or shrub vegetation. *Dry Tundra* ecosystems generally have near-surface permafrost, with seasonally thawed active layers between 20 and 150 cm depending on climate, soil texture, and landscape position (van der Molen et al., 2007; Heikkinen et al., 2004). Near-surface permafrost in *Dry Tundra* prevents vertical drainage, but lateral drainage ensures predominately oxic soil conditions. A water table is either absent or close to the base of the seasonally thawing active layer. *Dry Tundra* is differentiated from *Permafrost Bogs* by having thinner organic soil (<40 cm), and from *Tundra Wetlands* by their drained soils (average water table position >5 cm below soil surface).

Boreal Forests are treed ecosystems with non-wetland soils. Coniferous trees are dominant, but the class also includes deciduous trees in warmer climates and landscape positions. *Boreal Forests* may have permafrost or non-permafrost ground, where the absence of permafrost often allows for better drainage. Overall, it is rare for anoxic conditions to occur in *Boreal Forest* soils, and CH_4 uptake is prevalent, although low CH_4 emissions have been observed during brief periods during snowmelt or following summer storms (Matson et al., 2009), or conveyed through tree stems and shoots (Machacova et al., 2016). The *Boreal Forest* class also includes the few agricultural/pasture ecosystems within the boreal biome.

2.2.1.3 Aquatic classes

Lakes are in BAWLD considered to include all lentic open-water ecosystems (herein referred to as aquatic ecosystems), regardless of surface area and depth of standing water. It is common in ice-rich permafrost lowlands and peatlands for open-water bodies to have shallow depths, often less than two meters, even when surface areas are up to hundreds of km^2 in size (Grosse et al., 2013). While small, shallow open-water bodies often are included in definitions of wetlands (Canada Committee on Ecological (Biophysical) Land Classification et al., 1997; Gunnarsson et al., 2014; Treat et al., 2018), we include them here within the lake classes as controls on net CH_4 emissions depend strongly on the presence or absence of emergent macrophytes (Juutinen et al., 2003). Further classification of lakes in BAWLD is based on lake size and lake genesis, where lake genesis influences lake bathymetry and sediment characteristics (Fig. 2.4). Previous global spatial inventories of lakes include detailed information on size and location of individual larger lakes (Downing et al., 2012; Messager et al., 2016), but do not include open-water ecosystems <0.1 km^2 in size, and do not differentiate between lakes of different genesis (e.g. tectonic, glacial, organic, and yedoma lakes). Small water bodies are disproportionately abundant in some high latitude environments (Muster et al., 2019), have high emissions of CH_4 (Holgerson and Raymond, 2016), and therefore require explicit classification apart from larger water bodies. Furthermore, lake genesis and sediment type have been shown to influence net CH_4 flux from lakes (Wik et al., 2016). In BAWLD we thus differentiate between large (>10 km^2), midsize (0.1 to 10 km^2), and small (<0.1 km^2) lake classes, and further differentiate between three lake types for midsize and small lakes; peatland, yedoma, and glacial lakes (Fig. 2.4).

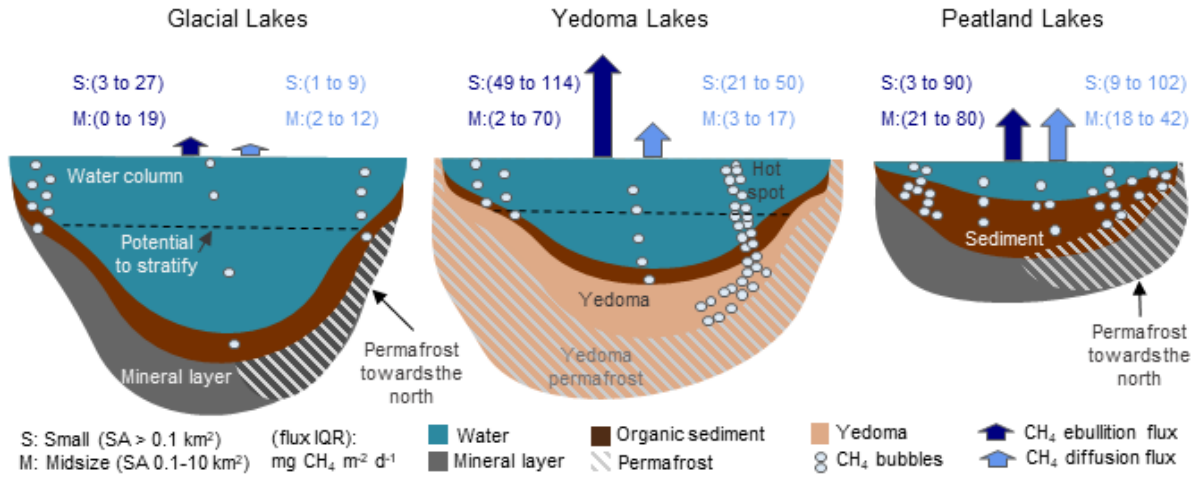

Figure 2.4. Conceptual diagram of the aquatic land cover classes. Key differences between the three overarching lake genesis "types" and their CH_4-emitting characteristics are shown, including sediment type, permafrost conditions, and water column depth. Fluxes (interquartile ranges-IQR) for each class size within the overarching types are shown above the lakes for both diffusive and ebullitive transport pathways. Arrows are scaled based on mean flux values. See Sect. 3.3 for a detailed breakdown of aquatic fluxes. Large lakes are not shown.

Small and *Midsize Peatland Lakes* are described as lakes with thick organic sediments that are mainly found adjacent to or surrounded by peatlands, or in lowland tundra regions with organic-rich soils. *Small Peatland Lakes* include the numerous small pools often found in extensive peatlands and lowland tundra regions, e.g. including the open-water parts of string fens and polygonal peatlands (Pelletier et al. 2014). *Peatland Lakes* generally form as a result of interactions between local hydrology and the accumulation of peat which can create open water pools and lakes (Garneau et al., 2018; Harris et al., 2020), but can also form in peatlands as a result of permafrost dynamics Sannel and Kuhry, 2011; Liljedahl et al., 2016). As such, these lakes with thick organic sediments are often shallow and have a relatively low shoreline development index. *Peatland lakes* typically have dark waters with high concentrations of dissolved organic carbon.

Small and *Midsize Yedoma Lake*s are exclusive to non-glaciated regions of eastern Siberia, Alaska, and the Yukon where yedoma deposits accumulated during the Pleistocene (Strauss et al., 2017). Yedoma permafrost soils are ice-rich and contain fine-grained, organic-rich

loess that was deposited by wind and accumulated upwards in parallel with permafrost aggradation, thus limiting decomposition and facilitating organic matter burial (Schirrmeister et al., 2013). Notable thermokarst features, including lakes, often develop when yedoma permafrost thaws, causing labile organic matter to become available for microbial mineralization (Walter Anthony et al., 2016). *Small Yedoma lakes* typically represent younger thermokarst features, whereas *Midsized Yedoma Lakes* represent later stages of thermokarst lake development. *Small Yedoma Lakes* are thus more likely to have actively thawing and expanding lake edges where CH_4 emissions can be extremely high, largely driven by hot spot ebullition emissions (Walter Anthony et al., 2016; Fig. 2.4). Century-scale development of yedoma lakes can shift the main source of CH_4 production from yedoma deposits to new organic-rich sediment that accumulated from allochtonous and autochthonous sources – resulting in such lakes here being considered as *Peatland Lakes*.

Small and *Midsize Glacial Lakes* include all lakes with organic-poor sediments – predominately those formed through glacial or post-glacial processes, e.g. kettle lakes and bedrock depressions. However, due to similarities in CH_4 emissions and controls thereof, we also include all other lakes with organic-poor sediments within these classes. *Glacial Lakes* typically have rocky bottoms or mineral sediments with limited organic content. Lakes in this class are abundant on the Canadian Shield and in Scandinavia but can be found throughout the boreal and tundra biomes. Many *Glacial Lakes* have a high shoreline development index, with irregular, elongated shapes. Generally, *Glacial Lakes* are deeper than lakes in the other classes, when comparing lakes with similar lake areas and are more likely to stratify seasonally than peatland lakes (Fig. 2.4).

Large Lakes are greater than 10 km^2 in surface area. Most *Large Lakes* are glacial or structural/tectonic in origin. Lake genesis is not considered for further differentiation within this land cover class.

2.2.2 Terrestrial methane flux dataset

The terrestrial CH_4 flux dataset includes warm-season (~May-October depending on the location) fluxes and was compiled using data from studies published before February 2020. I identified relevant studies using 1) JStor™, Google Scholar™ and Web of Science™ searches

with the terms (peatland OR wetland OR bog OR fen OR marsh OR upland) AND (north* OR boreal OR arctic OR sub-arctic) AND (methane OR CH_4 OR greenhouse gas*); 2) references from published studies; and 3) contributions of unpublished data (n=2). If multiple, yearly CH_4 flux and water table measurements were reported from one site or if multiple studies reported fluxes from the same site, the data were entered as separate individual lines and were considered each their own "site." Sites that underwent manipulations (soil temperature, water table, nutrients, etc.) were not included in the dataset, however, any control or undisturbed sites included within manipulation studies were included. Sites that had recently experienced disturbance from thermokarst processes were included. Winter flux measurements from terrestrial sites were excluded from this dataset (winter/ice-out emissions from aquatic ecosystems are included- see Sect. 2.2.3). I direct the reader to a comprehensive synthesis of seasonal winter estimates of CH_4 emissions from northern terrestrial ecosystems is presented in Treat et al. (2018).

The terrestrial dataset includes predominantly chamber measurements (n=519) at the sub-meter scale which allows for a detailed representation of specific land cover types (i.e. one land cover type per chamber measurement). However, a handful of eddy covariance measurements were included if the authors could clearly partition fluxes based on specific land cover classes (n=36). For more information on EC-based CH_4 synthesis, I direct the readers to the FLUXNET-CH_4 Community Product (Delwiche et al. 2021; Knox et al. 2019) and additional FluxNet resources (fluxnet.org). I grouped chamber measurements from specific studies by "Site", which I defined as surfaces with similar vegetation composition (dominant, present, absent) and physical characteristics (including water table position, permafrost conditions, organic layer depth, soil moisture, and pH) within proximity to each other (typically 1 – 100 m radius). In most cases, chambers and sites were already classified by these standards, however, sometimes it was necessary to combine or split chamber measurements presented by the authors into our site classifications. By combining and splitting sites this way, I were able to classify sites into BAWLD land cover classes. Average daily warm-season fluxes were then calculated from the average CH_4 flux from each site over the study's measurement period.

In addition to CH_4 flux data, I extracted various site descriptors and categorical and continuous environmental variables (see Table 2.1 for detailed metadata and additional variables

not discussed here). For all sites, I included information on the site name (Site), location (LatDec/LongDec, Country), the months measurements were taken (SampMonths), the flux measurement method (Meth), the author's description of the site (SiteDescrip), and vegetation composition. Most studies did not classify land cover types with similar BAWLD criteria, therefore I assigned BAWLD land cover classifications. Permafrost zone was assigned according to Brown et al. (2002). When reported by the authors, I also extracted continuous variables including Mean Annual Air Temperature (MAAT), Mean Annual Precipitation (MAP), growing season length, Net Ecosystem Productivity (NEP), Ecosystem Respiration (ER), Gross Ecosystem Photosynthesis (GPP_{Per}), air temperature (T_{Per}), soil temperature at 0-5 cm (TSoilA) and 5-25 cm (TSoilB), water table depth (WT_{Av}), organic layer depth (Org), active layer depth (AL), pH, and soil moisture (SoilMoist), all averaged over the same period as the flux measurements. The categorical variables collected include absence or presence of permafrost within the top two meters (PfConA), permafrost thaw (PfTh), and vegetation composition (absent, present, dominant) for graminoid (*Carex* spp. and *Eriophorum* spp; referred to as "Sedge" in the dataset), sphagnum moss (Sphag), non-sphagnum moss (Moss), tree, and shrub species. Vegetation composition of the functional plant type was considered dominant if that type made up greater than 50% of the reported biomass or areal coverage or was one of only two species present at the site. Trees were assigned as the dominant vegetation type if the canopy was described as closed. Gridded (0.5 by 0.5 degrees) climate variables including mean annual temperature (referred to as GRID_T) and mean annual precipitation (CD_Pcp_An) were extracted from WorldClim2 (http://www.worldclim.com/version2).

Table 2.1. Attribute information for the terrestrial flux dataset.

Column_Name	Variable_Name	Units_Info	Description	Controlled_Vocab
RefID	Reference ID	-	Number ID attached to independent publications	-
Dataset	Dataset Name	Olefeldt, Kuhn	Data entered originally included by Olefeldt et al or new data entered by Kuhn et al. All were updated to include additional information not include originally by Olefeldt et al.	Olefeldt, Kuhn
Reference	Reference	-	Author name and year published	-
LatDec	Latitude	Decimal Degrees	Coordinates given by the authors	-

LongDec	Longitude	Decimal Degrees	Coordinates given by the authors	-
Site	Site Name	-	Names of site provided by the authors	-
SiteID	Shortened SiteID	-	An abbreviated version of the site name	-
Country	Country	-	Country where the research took place	USA: United States, Canada, Russia, Sweden, Norway, Greenland, Finland
ID	Measurement location ID	-	Name of the individual plot	-
Ecosystem	Ecosystem Classification		Short name for the ecosystem type described by the authors	-
SiteDescrip	Site Description	-	A description of the site given by the authors	-
Class	Land cover Class	-	BAWLD land cover classification	Bog, Fen, Marsh, WetTundra (Tundra Wetlands), DryTundra, Boreal: Boreal Forest, PermBog = Permafrost bog
Seas	Season/s	T, S, F	Seasons the measurements took place in	T: Thaw/spring, S: Summer, F-fall
Year.P	Publication Year	Year	Year the study was published	-
Year.M	Measurement year/s	Year	Year/s the fieldwork took place	-
SampleDays	Sampling Days	Days	Number of measurement days	-
Month.Numbers	Number of sampling months	Months	The number of months in which sampling occurred	-
SampMonths	Sampling Months	-	The months that sampling took place in	Jn: June, J: July, A: August, S: September, O: October
Meth	Method	C, E, CE	Methane flux measurement method	C: Chamber, E: Eddy Covariance
Coll	Collars	Number of collars	Number of collars used to estimate the average methane flux at a site	-
Occ	Occasions	Flux measurements	Number of times a flux was measured at an individual collar	-
GrowSL	Growing Season Length	Days	Length of the growing season as reported by the authors	-
CH4An	Annual Fluxes	g m^{-2} yr^{-1}	Annual methane fluxes as reported by the authors	-

CH4Av	Average daily methane fluxes	mg CH_4 m^{-2} d^{-1}	Average growing season methane fluxes	-
CH4Md	Median daily methane flux	mg CH_4 m^{-2} d^{-1}	Median growing season flux, if reported by authors	-
CH4Mx	Max daily methane flux	mg CH_4 m^{-2} d^{-1}	Maximum methane flux over the growing season, if reported by authors	-
NEPPer	Net Ecosystem Primary Productivity	g C m^{-2} yr^{-1}	-	-
ERPer	Ecosystem Respiration	g C m^{-2} yr^{-1}	-	-
GPPPer	Gross Ecosystem Productivity	g C m^{-2} yr^{-1}	-	-
MAAT	Mean Annual Temperature	Celsius	Meant Annual Temperature reported by the authors	-
MAP	Mean Annual Precipitation	mm	Meant Annual Precipitation reported by the authors	-
TPer	Air Temperature	Celsius	Reported air temperature at the time of the methane measurement	-
TSoilA	Surface Soil Temperature	Celsius	Temperature of the soil from 5-25 cm depths	-
TsoilB	Deep Soil Temperature	Celsius	Temperature of the soil below 25 cm	-
TSoilDepth	Soil Temperature Depth	cm	Measurement Depth for TsoilB, if no deep temp reported, this depth represents TsoilB	-
WTAv	Water Table Average	cm	Average water table depth over the growing season, positive values represent water above the soil surface	-
WTMax	Water Table Max	cm	Max (highest) water table depth over the growing season, positive values represent water above the soil surface	-
WTMin	Water Table Min	cm	Minimum (lowest) water table depth over the growing season, positive values represent water above the soil surface	-
WTFluc	Water Table Fluctuation	cm	Fluctuation of the water table depth over the growing season (range between max and min)	-
SoilMoist	Soil Moisture	%	Soil Moisture percentage	-
SoilMostD	Soil Moisture Depth	cm	Depth the soil moisture was measured	-
Org	Organic Layer Depth	cm	Thickness of the organic layer	-

AL	Active Layer Depth	cm	Active layer depth at the time of measurement	-
Thaw	Thaw Depth	cm	Thaw depth	-
PfReg	Permafrost Region	C, D, S, N	Permafrost region where the study took place. Determined by mapping the coordinates over Brown et al. 1999 permafrost cover map	N: No permafrost, S: Sporadic/Isolated, D: Discontinuous, C: Continuous
PfConA	Permafrost Present	Y/N	Permafrost present in the top 2 meters, reported by the authors	Y: Yes, N: No
PfTh	Permafrost Thaw Present	Y/N	Permafrost thaw present, reported by the authors	Y: Yes, N: No
pH	pH	-	Soil pH	-
Sedge	Sedge	A, P, D	Sedge presence	A: Absent, P: Present, D: Dominant
Sphag	Sphagnum Cover	A, P, D	Sphagnum moss presence	A: Absent, P: Present, D: Dominant
Moss	Moss Cover	A, P, D	Non-sphagnum moss presence	A: Absent, P: Present, D: Dominant
Trees	Tree Cover	A, P, D	Tree presence	A: Absent, P: Present, D: Dominant
Shrubs	Shrub Cover	A, P, D	Shrub presence	A: Absent, P: Present, D: Dominant
Grid_T	Mean Annual Temperature (gridded)	Celcius	Gridded (0.5 by 0.5 degree) mean annual temperature from WorldClim2	-
TotalID	Unique site ID	-	Unique ID used as the random factor in mixed model analysis	-
CD_Pcp_An	Mean annual precipitation (gridded)	mm	Gridded (0.5 by 0.5 degree) mean annual precipitation from WorldClim2	
BIOME	Biome	11, 6	Biome as defined by Olson et al. 2001 and the World Wildlife Fund	11: Tundra, 6: Boreal

2.2.3 Aquatic methane flux dataset

The aquatic flux dataset includes ice-free season (~May-October depending on the location) and winter/ice-out fluxes and was compiled using data from studies published before February 2020. I identified new studies using 1) JStor™, Google Scholar™ and Web of Science™ searches with the terms (lake* OR pond*) AND (north* OR boreal OR arctic OR sub-arctic) AND (methane OR CH_4 OR greenhouse gas*); 2) references from published studies; and 3) contributions of unpublished data (n =1). If multiple, yearly measurements were given for one site by the same study, I averaged the flux values (following the initial protocol taken by Wik et al. 2016a). If different studies reported fluxes from the same lake then these data were reported as separate entries. In instances where ice-free fluxes and storage/ice-out fluxes were reported for the same lake, those data were entered on separate lines, but the number of lakes was designated as NA for the winter measurement as to not add to the total lake count. I defined sites based on reported average CH_4 fluxes. For example, some studies reported one average flux value for a group of lakes and this was considered one "site," however, the number of lakes was noted. Studies that only reported CH_4 concentrations and not a flux estimate were not included.

Similar to the terrestrial dataset, the aquatic dataset focuses on small-scale measurement techniques that allow for flux estimates to be attributed to one specific land cover class. Therefore ice-free season diffusive fluxes included in this dataset were measured using dissolved CH_4 concentrations and modeling approaches (n = 254) or floating chambers (n = 181), while ebullitive fluxes were measured by bubble trap (n = 187) or floating chamber (n = 34). Diffusive modeling approaches include an estimate of the gas transfer coefficient, *k*. Gas transfer velocity estimates are commonly calculated using equations established by Cole and Caraco (1998). However, more recent efforts with EC systems, chambers, and either calculation or measurement of the near-surface turbulence that enables flux across the air-water interface indicates that fluxes using Cole and Caraco's (1998) wind-based model of gas transfer velocities underestimate fluxes from non-sheltered and some sheltered waterbodies by a factor of two to four (Heiskanen et al. 2014; Mammarella et al. 2015; MacIntyre et al. 2020). Highly sheltered waterbodies, such as small lakes surrounded by trees, may be an exception and can have reduced mean lake *k* values (Markfort et al. 2010). While I do not recalculate fluxes in this synthesis, I indicate which *k* calculations were used so that future studies and can easily identify and recalculate fluxes when

required. Only a handful of eddy covariance (EC) measurements (n = 5) were included in the dataset. I included a limited number of EC measurements due to difficulties that most studies had in attributing the fluxes to lakes specifically. I classified all EC fluxes as diffusive fluxes as it is hard to separate between ebullition and diffusion within this measurement technique, however, for this reason, EC measurements were excluded from statistical analysis for ice-free season fluxes

I further delineated aquatic fluxes by transport pathway including ebullition (bubbles), diffusion (hydrodynamic flux), and winter storage/ice-out flux. Ebullition and diffusion measurements were averaged over the ice-free season to represent a mean daily flux estimate across a lake. In some cases, if measurements were only taken from one zone of the lake (i.e. just lake edge or just lake center) I averaged the fluxes and assumed whole-lake fluxes. Some studies only reported a seasonal ice-free flux estimate. If they also reported the number of days in the ice-free season, I then calculated the average daily flux rate. Storage flux includes the annual release of CH_4 that accumulates within and under the ice over the winter and includes estimates from ice bubble surveys (IBS). Our storage flux estimate does not include estimates of spring or fall circulation fluxes, wherein CH_4 that is stored in the deep portion of the water column is released upon season turnover of the water column (Karlsson et al. 2013; Sepulveda-Jauregui et al. 2015). I also include an estimate of the ice-free season ebullition and diffusive fluxes if provided by the authors or if the authors provided the number of ice-free days. Note that flux measurements that include the transport of CH_4 through littoral vascular plants were not included as aquatic fluxes, but as *Marsh* or *Tundra Wetland* fluxes within the terrestrial dataset.

In addition to aquatic CH_4 flux data, I also collected various site descriptors and categorical and continuous environmental variables (See Table 2.2 for detailed attribute information and additional variables not discussed here). For all sites I extracted information about the site name and location (latitude/longitude and country), the number of lakes for a reported flux estimate, sampling season (SEASON) and within lake sampling location (E.LOCATION), sampling pathway (PATHWAY), the general sampling dates (YEAR/MONTH) and the number of times sampled (D.DAYS/E.DAYS). When available, I added a column for the equation used to estimate the gas transfer velocity constant (k) using modeling approaches (K600_EQ). Categorical variables included lake sediment type

(BOTTOM), permafrost zone (PERMA.ZONE), presence of talik (TALIK), ecoregion (ECOREGION), and the original lake types outlined by Wik et al. (2016a) (LAKE.TYPE). BAWLD specific categorical variables include the overarching lake genesis type (TYPE), binned water body size (SIZE), and BAWLD land cover class (CLASS). When reported, I extracted the following continuous variables: surface area (SA), water body depth (DEPTH), water temperature (TEMP), dissolved organic carbon concentration (DOC), and pH. Gridded (0.5 by 0.5 degrees) climate variables including mean annual temperature (GRID_T) and mean annual precipitation (CD_Pcp_An) were extracted from WorldClim2 (http://www.worldclim.com/version2).

Table 2.2. Attribute details for the aquatic fluxes dataset.

Column_Name	Variable_Name	Units_Info	Description	Controlled_Vocab
ID	Row ID	Numbers	Unique identifier for individual rows	
NUM	Study number	-	Number ID for independent publications	-
STUDY	Reference	-	Author name and year published	-
DATASET	Dataset	WIK, KUHN	Data entered originally included by Wik et al or new data entered by Kuhn et al.	WIK, KUHN
YEAR	Publishing year	-	Year the study was published	-
COUNTRY	Country	-	Country where the research took place	USA: United States, Canada, Russia, Sweden, Norway, Greenland, Finland
SITE	Lake name	-	Names of the lakes provided by the authors	-
NUMBER.LAKES	Number of Lakes	-	Number of lakes represented by the flux value presented	-
LAT	Latitude	Decimal Degrees	Coordinates given by the authors	-
LONG	Longitude	Decimal Degrees	Coordinates given by the authors	-
ECOREGION	Ecoclimate Region	CB,SB,ST,AT	Ecoclimatic regions as define by Olson et al. 2001	CB: Continental Boreal, SB: Subarctic boreal, ST: Subarctic tundra, AT: Arctic tundra
PERMA.ZONE	Permafrost Zone	N,S,D,C	Permafrost region where the study took place. Determined by mapping the coordinates over Brown et al. 1998 permafrost cover map	N: No permafrost, S: Sporadic/Isolated, D: Discontinuous, C: Continuous
LAKE.TYPE	Lake Type	BP,PP,GP,T,U	Lake type originally outlined by Wik et al. 2016	BP: Beaver Pond, PP: Peatland Pond, GP: Glacial/post-glacial, T:

				Thermokarst, U: Unspecified
BOTTOM	Bottom Sediment Type	M,O,P,Y,U	Sediment type as described by the authors	M: Minerogenic, O: Organic, P:Peat, Y:Yedoma, U:Unspecified
TALIK	Talik Present	Y,N	Is a talik present under the lake	Y: Yes, N: No
SA	Water body surface area	km^2	Surface area reported by authors or determined by GIS if only the coordinates were given	-
DEPTH	Water body depth	meters	Mean lake depth reported by the authors; if mean was not reported, then the max was used	
SEASON	Sampling Days	Ice free, Winter	The time of the year the sampling took place. "Winter" includes winter ice surveys and ice-out measurements	Ice-free, Winter
YEAR.S	Sampling year(s)	year	The year or years the sampling took place	
MONTH	Sampling Months	Month names	The month or months the sampling took place	September, October, November, etc
PATHWAY	Method	D,E,S	The transport pathways measured	D:Diffusion, E: Ebullition, S:Storage, DE: Diffusion/Ebullition, DS: Diffusion/storage
D.METHOD	Diffusive measurement method	CH,WS,EC	The measurement method for diffusion	CH: Floating Chamber, WS: Water Sample, EC: Eddy Covariance
K600_EQ	K600 equation	-	Equation used to estimate the piston gas velocity coefficient (k) when calculating diffusive fluxes	-
K_REF	K600 reference		-	Citation for the k equation used
E.METHOD	Ebullition measurement method	BT, WS,IS	The measurement method for ebullition	BT: Bubble trap, CH: Chamber, IS: Ice survey
E.LOCATION	Ebullition measurement location	C,E,W	Location of the reported ebullition measurement	C: Center, E: Edge, W: Whole lake estimate
S.METHOD	Storage/ice out measurement method	BT,IS,WS	The measurement method for storage/Ice out	BT: Bubble trap, WS: Water sample, IS: Ice survey
D.DAYS	Diffusive measurement days	Days	Number of individual days diffusion was measured at the same lake	-

E.DAYS	Ebullition measurement days	Days	Total number of days a bubble trap was set to measure ebullition	-
LENGTH	Field sampling campaign length	Days	The duration of the field sampling campaign for each lake	-
CH4.D.FLUX	Diffusive fluxes	mg CH_4 m^{-2} d^{-1}	Mean daily diffusive fluxes	-
CH4.E.FLUX	Ebullitive fluxes	mg CH_4 m^{-2} d^{-1}	Mean daily ebullitive fluxes	-
SEASONAL.D	Seasonal Diffusive flux	grams m^{-2} yr^{-1}	Total diffusive fluxes over the season. Only included if the authors reported this value or the number of ice-free days	-
SEASONAL.E	Seasonal Ebullitive Fluxes	grams m^{-2} yr^{-1}	Total ebullitive fluxes over the season. Only included if the authors reported this value	-
SEASONAL.S	Seasonal Storage/ice-out	grams m^{-2} yr^{-1}	Below ice methane storage released upon ice-out in the spring	-
IBS	Ice Bubble Storage Fluxes	grams m^{-2} yr^{-1}	Ice-bubble methane storage released upon ice-out	-
TEMP	Water Temperature	Celsius	Water temperature as reported by the authors	-
DOC	Dissolved Organic Carbon	mg L^{-1}	DOC concentrations as reported by the authors	-
PH	PH	-	Water column pH as reported by the authors	-
ICEFREE.DAYS	Number of Ice free days	Days	Number of ice-free days as reported by the authors	-
CLASS	Lake landcover class	LL, MGL, MPL, MYL, SGL, SPL, SYL	BAWLD land cover class type (includes size and lake origin type)	LL: Large Lakes, MGP: Midsize glacial, MPL: Midsize Peatland, MYL: Midsize Yedoma, SGL: Small glacial, SPL: Small peatland, SYL: Small Yedoma
SIZE	Categorical waterbody size	S, M, L	BAWLD land cover size class only	S: Small (<0.1km^2), M: Midsize (0.1-10 km^2), L (>10 km^2)
TYPE	Land cover class type only	Y, P, G	BAWLD land cover lake origin type only	G- Glacial, P- Peatland, Y- Yedoma
CD_Pcp_An	Mean annual precipitation (gridded)	mm	Gridded (0.5 by 0.5 degrees) mean annual precipitation from WorldClim2	-
BIOME	Biome	11, 6	Biome as defined by Olson et al. 2001	11: Tundra, 6: Biome
GRID_T	Mean annual temperature (gridded)	Celcius	Gridded (0.5 by 0.5 degrees) mean annual temperature from WorldClim2	

NOTES	Notes on the data	-	Miscellaneous notes on the data

2.2.4 Statistics

All statistical analyses were performed in R statistical software (Version 1.1.383; www.r-project.org). I tested for significant relationships between log-transformed warm-season (terrestrial sites) or ice-free season (aquatic sites) average CH_4 fluxes and several covariates using a combination of linear regression and linear mixed-effects models when necessary (R Package 3.3.3; Lme4 Package; Bates et al. 2014). To include sites with CH_4 uptake or near zero fluxes I added a constant of 10 (terrestrial fluxes) or 1 (aquatic fluxes) before log transformation. Mixed-effects modeling was used when a given model included sites with multiple yearly measurements or if multiple studies reported fluxes from the same site (R "nmle" package; Pinheiro et al., 2017). In these cases, site ID was included as a random effect in the analysis to help account for lack of independence across repeated measurements and to weight potential biases (Treat et al. 2018). Almost no studies in the terrestrial or aquatic datasets provided information on all of the variables, therefore, individual statistical analyses have different sample sizes, however, the same subset of data was used to select the best performing mixed models (n = 206 and n = 149 for the terrestrial and diffusive aquatic mixed models, respectively). The significance of individual predictor variables in the mixed models was evaluated using forward model selection. Model performance was conducted using size-corrected Akaike information criterion (AICc; "AICcmodavg" package; Mazerolle & Mazerolle, 2017), wherein a decrease in AICc by 2 or more as an indication of a superior model (as in Olefeldt et al. 2013 and Dieleman et al. 2020). All models were tested against each other and the null model. The null model only included the random effects. Non-parametric Tukey's HSD post-hoc tests were performed to assess differences in median fluxes among sub-categories if the overall model was determined significant. All aquatic diffusive and ebullitive fluxes were analyzed separately. Eddy covariance flux estimates for aquatic ecosystems (n = 5) were not included in the statistical analysis since ebullitive and diffusive fluxes could not be partitioned. I modeled the temperature dependence (Q_{10}) of CH_4 following Rasilo et al. (2015).

2.2.5 Scaling

To spatially extrapolate CH_4 emissions across the Arctic-Boreal study domain, I used empirical models with gridded (0.5˚ by 0.5˚) climate variables and land cover classes (Olefeldt, Hovemyr, Kuhn, et al. 2021) as fixed variables and individual site as a random factor to account for repeated measures. I did not include CH_4 exchange from upland environments (*Dry Tundra* and *Boreal Forests*) due to low sample sizes from those classes. For wetlands, I used a two-step empirical modeling approach: first, I modeled soil temperature (TsoilB) using the interactive relationship between MAAT and average water table (WTAv) for each class (Eq. 2.1):

Equation 2.1: TSoilB = MAAT*WTAv

To model warm-season wetland CH_4 fluxes I then used the calculated soil temperature and land cover class as predictor variables (Eq. 2.2):

Equation 2.2: $\log CH_4$ = Class + TSoilB

For diffusive emissions from aquatic ecosystems over the ice-free season, I modeled fluxes based on the relationship between lake class and gridded MAAT (Eq. 2.3). Ebullitive emissions were not explicitly modeled using empirical relationships due to the low performance of those models, therefore, I used the relationship between diffusive and ebullitive emissions from lakes that reported both transport pathways (0.51 of total emissions are from ebullition; similar approach taken by Wik et al. 2016a and Matthews et al. 2020).

Equation 2.3: $\log CH_4$(diffusion) = Class + MAAT

Model performance was tested using a cross-validation approach by which I left out a subset of data, re-ran the model, and then compared the model output verse the withheld observed soil temperature (Fig. A.2.3a), wetland fluxes (Fig. A.2.3b), or aquatic diffusive fluxes (Fig. A.2.4). The wetland flux model performed better (R^2 = 0.77) than the aquatic model (R^2 = 0.39) during the validation tests. Model performance is explored in more detail in Sect. 2.4.1.

The empirical models were built to estimate daily flux values. To extrapolate over the warm-season or ice-free season I estimated the number of warm-season and ice-free days based

on gridded climate data. For the number of warm-season days, I used a simplified approach wherein I took the months with positive mean temperatures and multiplied them by 30. In some grid cells, there were no months with positive mean temperatures. In those cases, I assumed the minimum number of warm-season days was 30. To calculate the number of ice-free days, I used an equation provided by Weyhenmeyer et al. (2011) which uses an arc cosine relationship between MAAT and the yearly temperature range to estimate the number of ice-free days. The arc cosine relationship does not hold for regions where the daily temperatures are below zero for less than 55 days or longer than 310 days (Weyhenmeyer et al. 2011). In these cases, I used a simplified approach based on the number of months with mean temperatures above zero and set the minimum number of ice-free days to 30.

To quantify uncertainty for the warm-season or ice-free season estimates of CH_4 emissions I used a Monte Carlo approach (as in Dieleman et al. 2020). First, I established the 95% confidence intervals (CI) for coefficients within the empirical models using a bootstrap command ("bootMer", 1000 stimulations). I then generated a random number from a normal distribution within this CI range for each co-efficient in each grid cell. I then repeated this process 200 times leading to 200 matrices (23469 X 200 elements). For the wetland emissions, this was repeated for both soil temperature and flux, thus soil temperature also randomly varied within each cell as the flux model coefficients varied. I assumed additive uncertainty between the estimated flux and estimated area for each class as the two uncertainties are unrelated. Thus, the final output includes the average emission estimate over the 200 simulations and the lower and upper bounds represent the 95% CIs multiplied by the respective 95% CIs for the area. Because each class has a coefficient in the scaling model, individual class emissions and uncertainty were also calculated. I also compared the model uncertainty to the area uncertainty by multiplying the central model estimate times the low and high area uncertainty estimates and comparing that to the uncertainty associated with just the model output (i.e. area was held constant).

To estimate total annual emissions I estimated winter emissions from wetlands make up 20% of the total annual emissions (Treat et al. 2018) and winter/ice-out emissions from aquatic ecosystems make up 23% of annual emissions (Wik et al. 2016a). I assumed these calculations introduced the same percent of uncertainty and added it accordingly.

2.2.6 Limitations

Due to limitations of the studies where data were extracted from, some parts of the annual period are not considered in the dataset. Thus this dataset focuses on small-scale, surface-based spatial patterns in CH_4 fluxes associated with specific land cover classes and does not represent temporal patterns in fluxes. For both terrestrial and aquatic datasets, I extracted data on the average CH_4 fluxes over warm periods or ice-free periods. While I do include an estimate of winter/ice-out fluxes from aquatic ecosystems, the dataset does not include autumnal turnover fluxes from aquatic ecosystems, which may represent a substantial portion of annual emissions (Ferndandez et al. 2014; Klaus et al. 2018). Nor do I include shoulder season or winter fluxes from terrestrial ecosystems, which can represent substantial components of the annual flux (Treat et al. 2018; Zona et al. 2016). Furthermore, the data extraction methods were not designed to assess inter-annual changes in fluxes as this dataset compiles the data of multiple studies over a large range of years (1986-2020). Despite data limitations, the datasets represent an important step forward regarding the spatial variability in fluxes among different land cover types.

2.3.0 Results

2.3.1 Summary statistics

In total, I extracted 555 site-year CH_4 estimates from terrestrial (wetland and non-wetland) ecosystems. The majority of reported fluxes (site-years) were from Canada and Greenland (34%), followed by Russia (27%), Alaska (25%), and Scandinavia (14%) (Fig. 2.1a). Terrestrial fluxes followed a bimodal distribution, split by net positive fluxes (82% of all reported fluxes) and net uptake or zero-emission (18% of all reported fluxes; Fig. 2.5a). The median number of measurement days per site-year flux for chamber measurements was 10 and the median number of collars per site measurement was five (Fig. 2.6a). Of the site-year fluxes reported from aquatic ecosystems, there were 441 diffusive estimates and 175 ebullitive ice-free season estimates, and 125 estimates of winter/ice-out fluxes (including storage, winter ebullition, or ice bubble surveys). Aquatic sites were distributed throughout the Boreal-Arctic region (Fig. 2.1b). Diffusive fluxes showed a unimodal distribution, while ebullition showed bimodal peaks near 100 and 0 mg CH_4 m^{-2} d^{-1} (Fig. 2.5b, 2.5c). The median number of measurement days per site-year flux was three and 15 for diffusion and ebullition, respectively (Fig. 2.6b; 2.6c). Winter/ice-out fluxes were reported as annual estimates and are shown in Table 2.5.

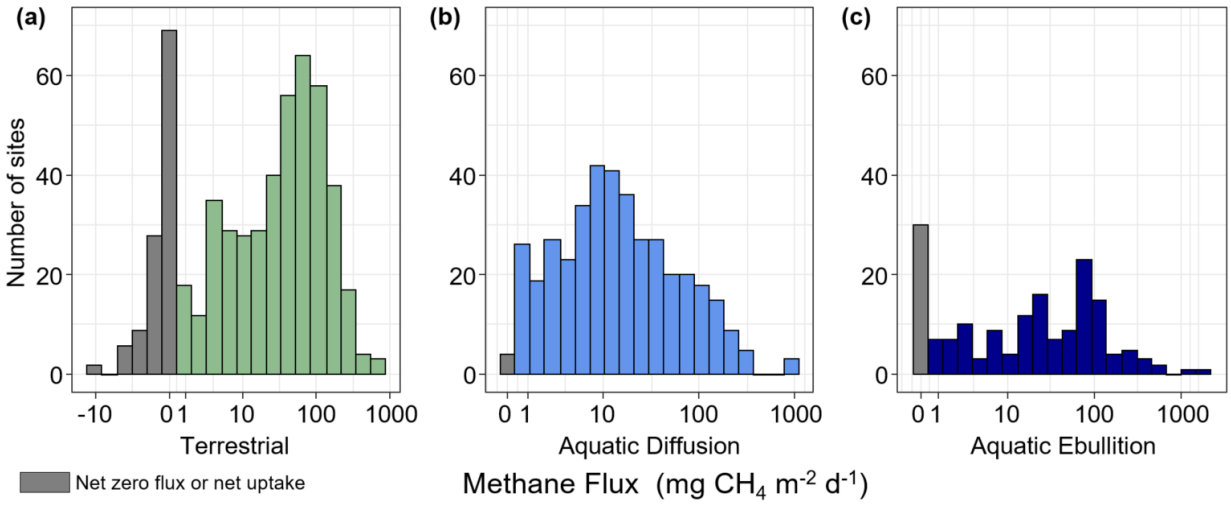

Figure 2.5. Histograms of site-specific average CH_4 fluxes. a) Terrestrial fluxes. b) Aquatic diffusive fluxes. c) Aquatic ebullitive fluxes. Grey bars represent net zero or net uptake fluxes.

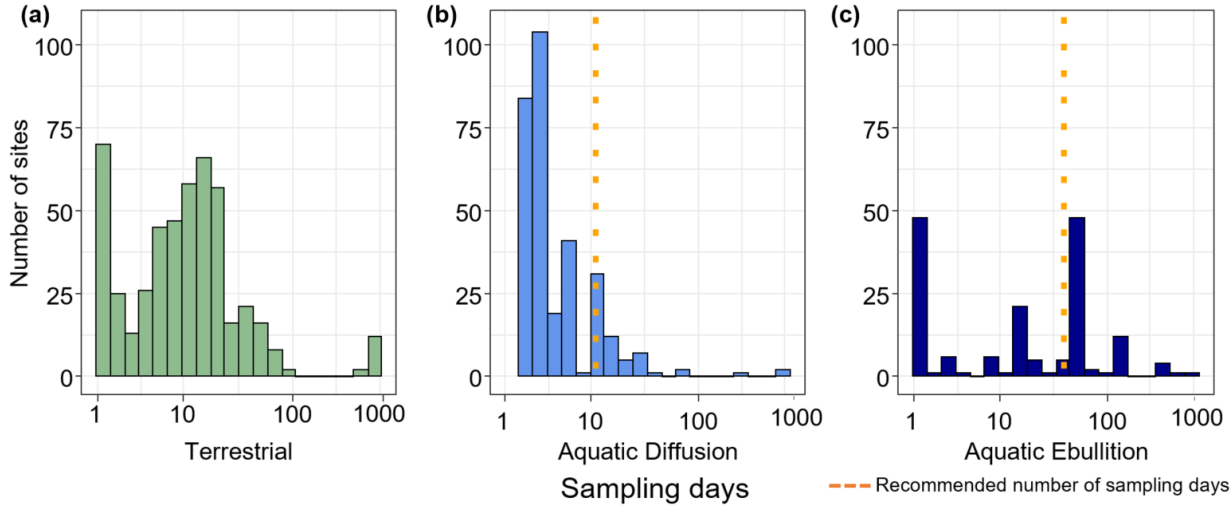

Figure 2.6. Histograms for the number of sampling days contributing to the average warm-season or ice-free season flux value. A) Terrestrial flux sampling days. B) Aquatic diffusion flux sampling days. C) Aquatic ebullition sampling days. The orange dotted lines in panels b and

c represent the number of recommended sampling days needed to arrive at a flux estimate within 20% accuracy (11 days for diffusion and 39 days for ebullition; Wik et al. 2016b).

2.3.2 Correlations with terrestrial methane fluxes

Of the continuous variables, water table (WT_{Av}) and soil temperature (TSoilA at 5-25 cm) were significantly and linearly correlated with log CH_4 (WT_{Av}: $\chi^2 = 121$, $P < 0.0001$, $R^2m = 0.28$, df = 380; TSoilA: $\chi^2 = 54.6$, $P < 0.0001$, $R^2 = 0.21$, df = 283; Fig. 2.7) and gross primary productivity (GPP) was logarithmically correlated with CH_4 ($\chi^2 = 5.8$, $P = 0.016$, $R^2m = 0.15$; df = 56; Fig. 2.7). However, given the relatively low sample size for GPP (n = 57), I do not include GPP in mixed model analyses. The temperature sensitivity (Q_{10}) for all terrestrial emissions was 2.8 (Table A.2.1). Of the categorical variables, there was no difference between the different permafrost zones ($\chi^2 = 0.88$, P = 0.83, df= 539), but CH_4 fluxes were higher from sites without permafrost present in the top two meters ($\chi^2 = 16.37$, P < 0.0001, df = 482; Fig. 2.8). For vegetation composition, sites dominated by shrubs had lower fluxes than those sites with shrubs present or absent ($\chi^2 = 34.66$, $P < 0.001$, df = 2; Fig. 2.8). The strongest relationship between vegetation composition and CH_4 flux was emergent graminoid cover. Sites with dominant graminoid composition had higher fluxes than sites where graminoids were present or absent ($\chi^2 = 148.95$, $P < 0.0001$, df = 2; Fig. 2.8). The best explanatory model for terrestrial CH_4 emissions was an additive model that included site-level predictors of water table, soil temperature, and graminoid cover alongside the broader classification of land cover class ($R^2m = 0.69$; $P < 0.0001$, df = 224; Table A.2.2). There was no effect on model performance using interactive effects (DeltaAICc = 0.84), however, the R^2m did increase to 0.73 (Table A.2.2). Notably, on their own, individual models with just the site-level predictors or with just land cover type explained close to the same amount of variation in CH_4 fluxes ($R^2m = 0.55$ and 0.54, respectively). Methane uptake fluxes, when analyzed separately, were positively correlated with thaw depth (i.e. more uptake with greater thaw depths; $R^2m = 0.55$, $\chi^2 = 19.61$, $P < 0.0001$, df = 22; Fig. A.2.1). No other continuous variables were correlated with CH_4 uptake, however, sites, where shrubs were present, had significantly higher uptake than sites where shrubs were absent or dominant (Tukey PostHoc, $P < 0.001$ for both, df = 2; Fig A.2.2).

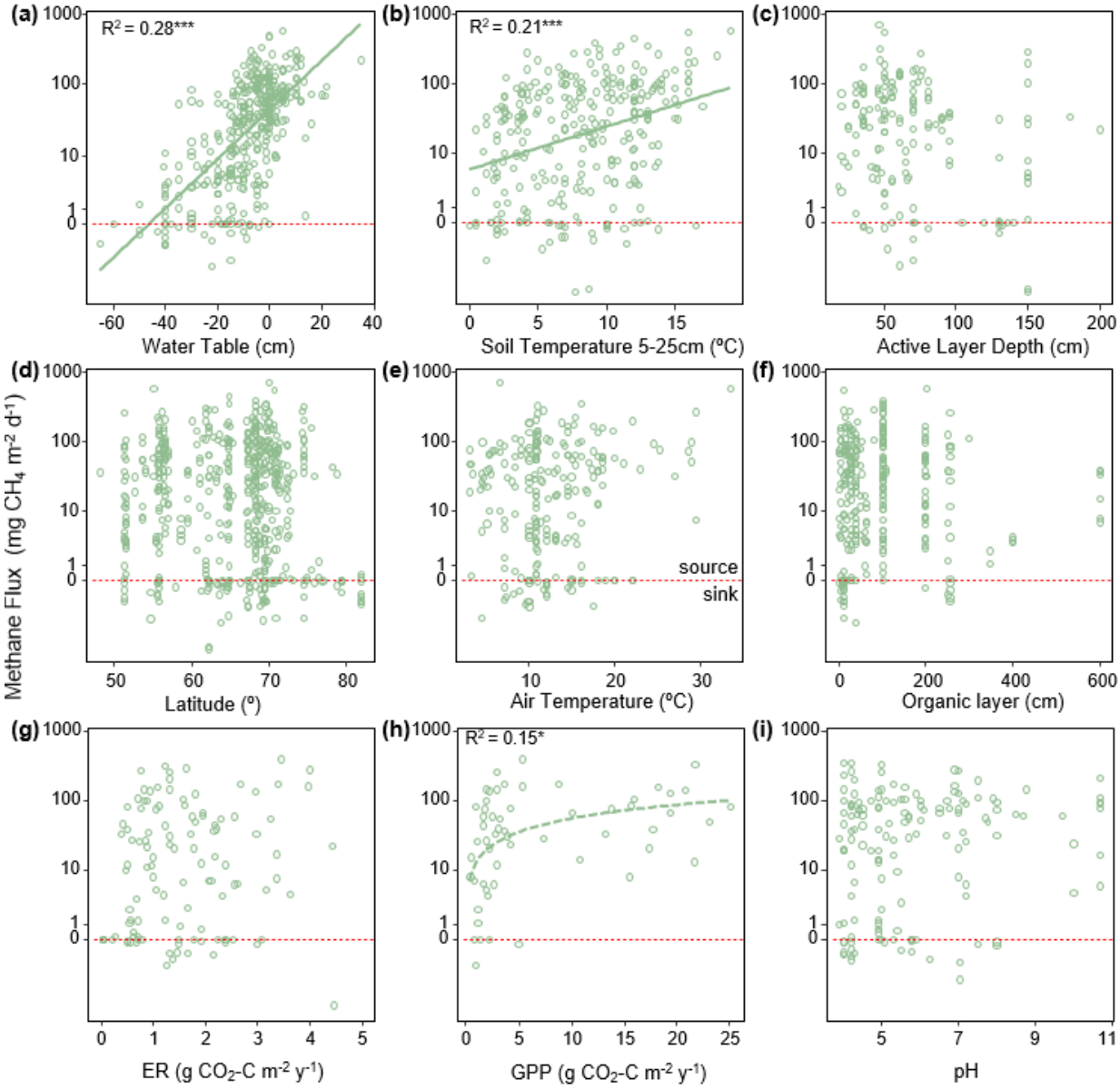

Figure 2.7. Relationships between site-averaged warm-season CH_4 flux and environmental variables. Environmental variables include water table, soil temperature at 5-25 cm depth, active layer depth, latitude, air temperature, organic layer thickness, ecosystem respiration (ER), gross primary productivity (GPP), and soil pH. Regression lines and R-square values are shown for significant relationships. Note the log scale. Log CH_4 flux was linearly related to water table and soil temperature and was logarithmically related to GPP (dotted line). Points below the red dotted line represent net uptake fluxes. * $P < 0.05$ ** $P < 0.01$ *** $P < 0.001$

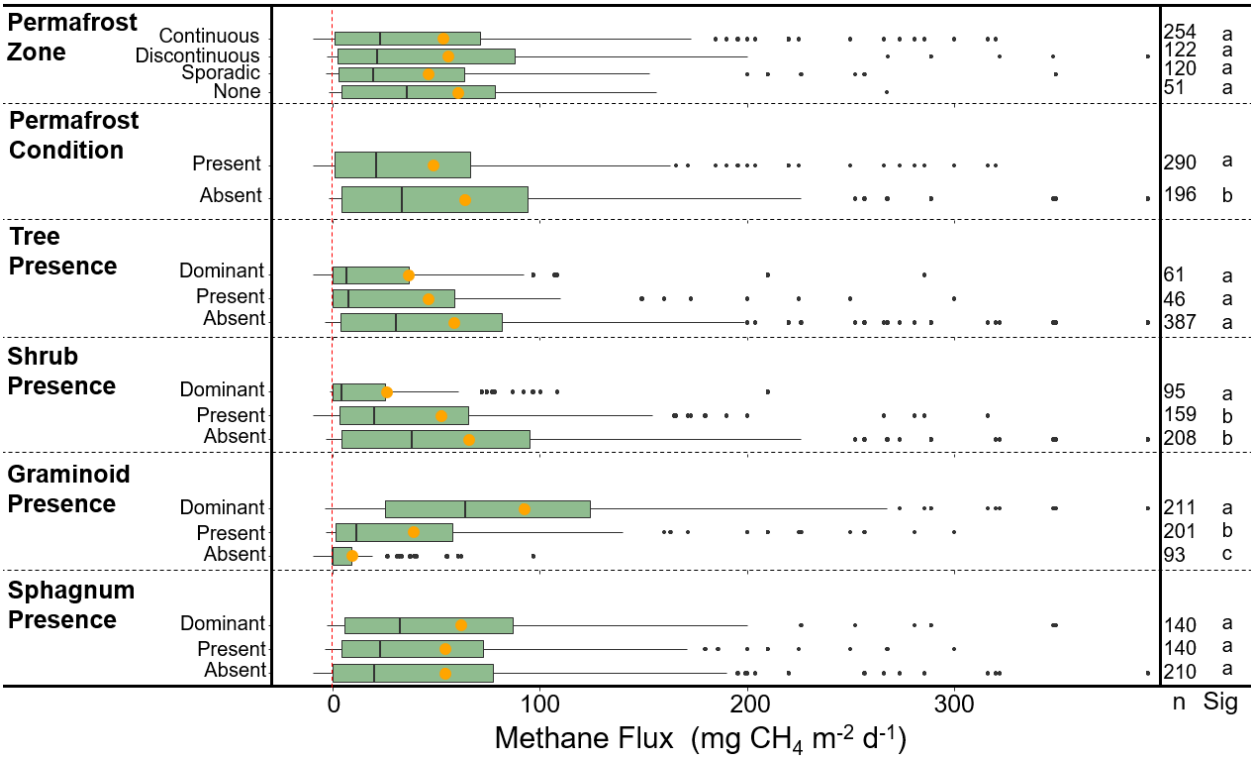

Figure 2.8. Warm-season terrestrial CH_4 fluxes classified by categorical variables. Orange dots represent the arithmetic mean flux values and black lines represent median flux values. Boxes represent 25th and 75th percentiles. The number of sites for each category is represented in the column to the right (n) and statistical differences among the categories are indicated by the letters (Sig), wherein subcategories with the same letters are not significantly different. Permafrost zones are from Brown et al. 2002. Permafrost condition represents the presence of permafrost in the top 2 meters as reported by the authors. See text for definitions used to classify vegetation cover. Outlier fluxes greater than 380 are not shown.

There were significant differences in fluxes among the BAWLD terrestrial land cover classes (χ^2 = 253. 69, $P < 0.001$, df = 6; Fig. 2.9a, Table 2.3). Median fluxes were highest from *Marshes, Tundra Wetlands, and Fens* (mean water table = +2, -0.4, and -6 cm, respectively). Median fluxes from *Bogs* were lower than the *Marshes, Tundra Wetlands, and Fens*, but higher than *Permafrost Bogs, Dry Tundra, and Boreal Forests*. *Permafrost Bogs* were the only wetland class that fell into the lowest emitting group of classes. However, the frozen and elevated nature of *Permafrost Bogs* typically leads to lower water table conditions more similar to *Dry Tundra* and *Boreal Forests* (mean water table = -22, -15, and -40 cm, respectively). However, it must be

noted that in most *Boreal Forest* sites the water table is not in the top two meters, therefore water table is not commonly measured or reported. The mean water table depth presented here is likely an over estimate that represents wetter *Boreal Forest* sites that had measurable water tables in the top two meters. *Boreal Forest* ecosystems were the only class to have negative median CH_4 flux for the entire class (net uptake). *Permafrost Bogs* and *Dry Tundra* classes also included net uptake site-year CH_4 estimates (n= 17 and 31, respectively). One *Wetland Tundra* site in the Canadian High Arctic showed net CH_4 uptake for one of the three years it was measured (Emmerton et al. 2014). Notably, the apparent temperature sensitivity of CH_4 flux from the drier terrestrial sites (*Boreal Forest, Dry Tundra,* and *Permafrost Bogs:* $Q_{10} = 3.7$*)* was higher than from the wet terrestrial sites (*Marshes, Tundra Wetlands, Bogs, and Fens;* $Q_{10} = 2.8$).

Table 2.3. Characteristics of BAWLD terrestrial classes based on environmental variables. The number of sites (site years) and contributing studies are shown for each class. Also shown are the mean, median, and quartiles for site average CH_4 flux, water table, soil temperature between 5 and 25 cm (TSoilB), sedge cover, pH, ecosystem respiration (ER), and gross primary productivity (GPP). *In some cases one study contributed flux data for multiple classes.

		Boreal Forest	**Dry Tundra**	**Permafrost Bog**	**Bog**	**Fen**	**Tundra Wetlands**	**Marsh**
Sites		30	63	81	87	109	109	33
Studies*		15	30	34	36	33	47	20
CH_4	Mean	-1.1	3.83	7.79	43.45	79.61	81.54	171.61
Flux	Median	-0.4	-0.01	2.32	24.55	54	65	106.00
(mg CH_4 m^{-2} d^{-1})	25th	-0.87	-1.09	0	6.92	20	34	70.50
	75th	-0.17	2.4	6.9	57.35	107.20	99.30	200
Water	Mean	-38.37	-14.67	-22.16	-12.65	-5.98	-0.40	2
Table	Median	-42.50	-14.50	-20	-11	-5	0	0
(cm)	25th	-50	-19.50	-37.25	-20	-10	-5	-3.5
	75th	-25.3	-8.3	-10.3	-5	-1	4	5
	n	6	30	62	67	91	91	23
TSoilB	Mean	9.4	4.7	5	10.7	11.6	5.6	11.6
(ºC)	Median	10	3.85	4.2	11.24	12	5	11

	25th	8.8	2	2.5	9.2	9.5	3.6	8.8
	75th	11	6.7	6.9	12.20	13.4	7.4	15
	n	14	20	53	51	60	59	17
Average	Dom	0%	17%	14%	23%	61%	61%	91%)
Sedge Cover	Pres	27%	59%	53%	49%	34%	38%	9%
	Absent	73%	28%	21%	28%	5%	1%	0%
	n	26	54	78	82	107	105	32
pH	Median	4.2	5.8	4.9	4.9	6.7	6.1	5.8
	n	9	12	11	29	42	25	10
ER	Median	2.3	1.5	1	1.6	1.93	1.4	3.25
(g C m^{-2} yr^{-1})	n	6	18	55	20	14	27	5
GPP	Median	-	2.2	1.6	7.4	15.5	2.4	3.4
(g C m^{-2} yr^{-1})	n	-	3	9	13	17	11	2

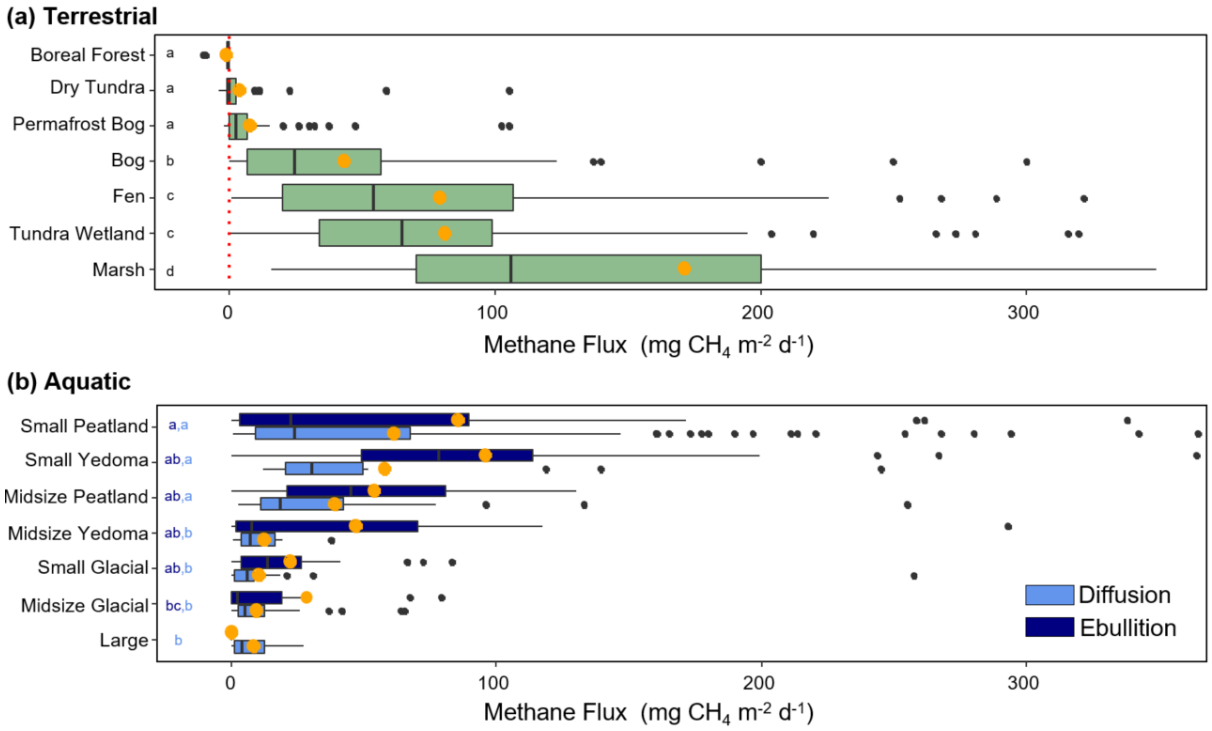

Figure 2.9. Relationship between CH_4 flux and BAWLD land cover classes. A) Terrestrial fluxes per each class. B) Aquatic fluxes including diffusion and ebullition per each class. Orange dots represent the arithmetic mean flux values and black lines represent median flux values.

Boxes represent 25th and 75th percentiles. Outlier fluxes over 380 are not shown. The letters represent significant differences in fluxes among classes. Similar letters indicate no significant difference.

2.3.3 Correlations with aquatic methane fluxes

Diffusive CH_4 fluxes from aquatic ecosystems were negatively correlated with the continuous variables logged surface area (χ^2 =73.0, $P < 0.0001$, $R^2m = 0.20$, df = 235; Fig. 2.10a), logged waterbody depth (χ^2 =23.5, $P < 0.0001$, $R^2m = 0.09$, df= 275; Fig. 2.10b), latitude ($F = 54.6$, $P < 0.0001$, $R^2 = 0.13$, df = 361; Fig. 2.10c), and positively correlated with DOC ($F = 71.7$, $P < 0.0001$, $R^2 = 0.21$, df = 261; Fig. 2.10d) and water temperature ($F = 57.2$, $P < 0.001$, $R^2 = 0.19$, df = 236; Fig. 2.10e). The apparent Q_{10} for diffusive emissions was 4.3 (Table A.2.1). Diffusive CH_4 fluxes were highest from the sporadic permafrost zone ($\chi^2 = 17.2$, $P = 0.002$, df = 3; Fig. 2.11). Furthermore, diffusive fluxes were significantly higher from small lakes compared to midsize and large lakes ($\chi^2 = 30.5$, $P < 0.0001$, df = 2; Fig. 2.11) and from lakes with peaty/organic-rich sediments compared to lakes with *Yedoma* and *Glacial* sediment types (χ^2 =103.9, $P < 0.0001$, df = 2; Fig. 2.11). The best explanatory model for diffusive CH_4 fluxes was an additive model including an interaction between lake surface area (continuous) and type (i.e. overarching lake genesis) alongside water temperature as predictor variables ($F = 14.9$, $P < 0.0001$, adj.$R^2 = 0.41$, $df = 149$; Table A.2.3). Land cover class on its own explained 25% of the flux variation ($F = 22.8$, $P < 0.0001$, $df = 149$).

Ebullitive CH_4 fluxes from aquatic ecosystems were positively correlated with logged DOC ($F = 12.25$, $P = 0.0008$, adj.$R^2 = 0.14$, df = 71; Fig. 2.10d) negatively correlated with surface area ($F = 13.88$, $P = 0.0003$, adj.$R^2 = 0.08$, df = 164; Fig. 2.10a) and latitude ($F = 5.38$, $P = 0.02$, adj.$R^2 = 0.03$, df = 160; Fig. 2.10c) and were weakly correlated with water temperature ($F = 5.55$, $P = 0.02$, adj.$R^2 = 0.06$, df = 67; Fig. 2.10e). The apparent Q_{10} for ebullitive emissions was 2.4 (Table A.2.1). There was no apparent relationship with lake depth and ebullitive fluxes ($F = 0.02$, $P = 0.91$, df = 151; Fig. 2.10b). There were no differences in ebullitive emissions between the permafrost zones with the exception of lower ebullitive emissions from the continuous zone compared to the sporadic zone (Tukey' HSD, $P < 0.001$; Fig. 2.11). Similar to diffusive fluxes, ebullitive fluxes were higher from the small lake classes compared to midsize

lakes (Wilcoxon Rank Sum, $P = 0.0006$, note that *Large lakes* did not have a large enough sample size (n=1) to be included in the post-hoc analysis). Finally, ebullitive fluxes were similarly higher from *Peatland* and *Yedoma lakes* compared to *Glacial lakes* (Tukey' HSD, $P = 0.006$ and 0.001, respectively). The best explanatory model for ebullitive fluxes using a subset of the data with complete information for predictor variables of interest (i.e. SA, SITE, CLASS, SIZE, DOC, TYPE, LAT, GRID_T) included just water body surface area (continuous) as a predictor variable ($F = 19.85$, $P = 0.0001$, adj.$R^2 = 0.21$, df = 68).

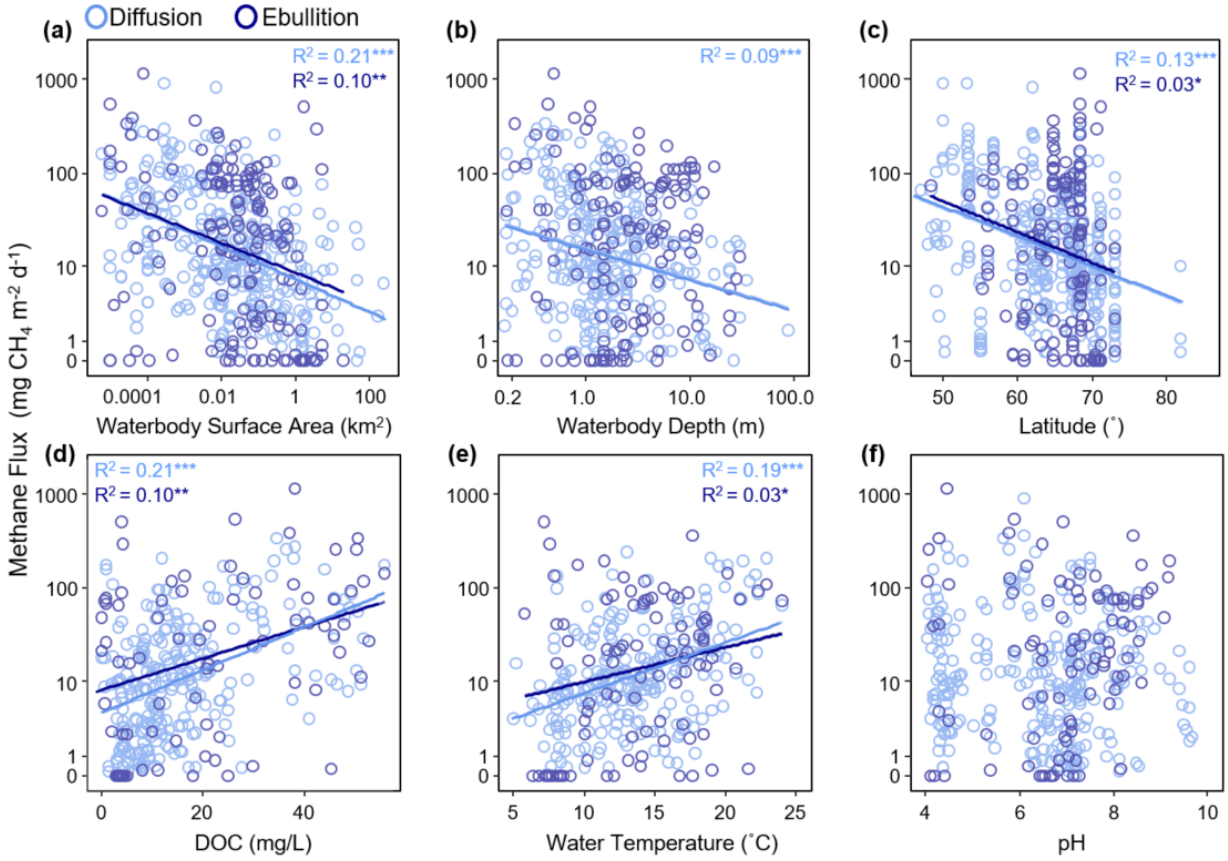

Figure 2.10. Relationships between site-averaged ice-free diffusive and ebullitive CH_4 fluxes (note the log scale) and environmental variables. Environmental variables include surface area, waterbody depth, latitude, dissolved organic carbon (DOC) concentration, water temperature, and pH. Regression lines and R-square values are shown for significant relationships. Log diffusive CH_4 flux was linearly related to surface area, depth, latitude, water temperature, and DOC. Log ebullitive fluxes were linearly related to surface area, latitude, DOC, and water temperature. * P <0.05. ** P < 0.01. *** P < 0.001.

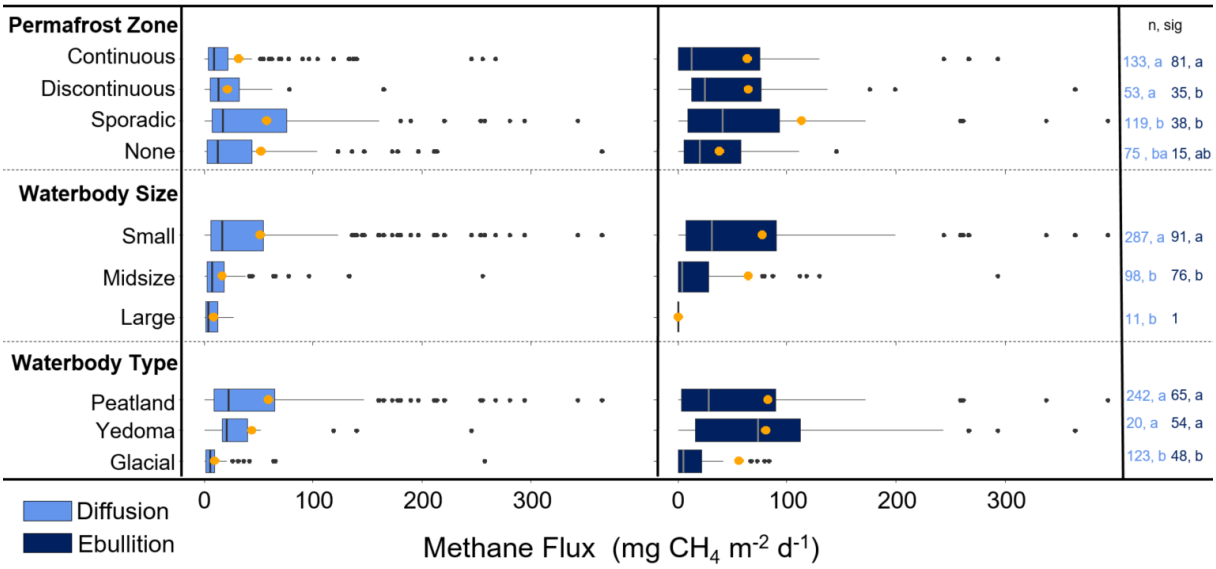

Figure 2.11. Ice-free season diffusion (left) and ebullitive (right) aquatic CH_4 fluxes as described by categorical variables. Orange circles represent mean flux values. The number of sites for each category is represented in the column to the right (n) in the representative colors for diffusion (light blue) and ebullition (dark blue). The letters (Sig) indicate statistical differences among the categories. Lake Size represents binned surface areas for < 0.1 km^2 (Small), 0.1 – 10 km^2 (Midsize), and > 10 km^2 (Large). Lake Type represents the BAWLD classification of waterbody types including Peatland, Yedoma, and Glacial lakes. Fluxes higher than 380 are not shown.

There were clear differences in diffusive CH_4 fluxes among the aquatic class types, but few differences were observed for ebullitive fluxes. Diffusive fluxes were higher from the *Peatland* and *Yedoma lake* classes (both small and midsize), associated with organic-rich sediments, compared to mineral-rich glacial and large lakes ($\chi^2 = 119.8$, $P < 0.001$, df = 6; Fig. 2.9b; Table 2.4). While ebullition fluxes appear to follow a similar trend to diffusive fluxes, the only significant difference was between *Small Yedoma lakes* and *Midsize Glacial lakes* (Tukey' HSD, $P < 0.001$; Fig. 2.9b). However, the lack of statistical differences found for ebullition between lake classes may in part be due to fewer and more variable ebullition measurements compared to diffusion (Table 2.4). Reported winter/ice-out emission estimates (including storage flux and Ice Bubble Survey (IBS) flux) were scarce in comparison to reported ice-free season emissions. *Small Glacial Lakes* and *Midsize Glacial Lakes* had the most reported winter ice-out

emission estimates (n= 20 and 31, respectively). Average winter emissions (storage flux + IBS) generally were lower than annual estimates of ice-free diffusive and ebullitive emissions (Table 2.5); however, statistical tests were not performed across all of the classes due to low sample sizes from some of the classes. Winter ebullition estimates (i.e. direct ebullition emission to the atmosphere from seeps during the ice-cover winter season) were not included in winter emission sums because of the non-uniform spatial nature of these emission types (Sepulveda-Jauregui et al. 2015; Wik et al. 2016a), but are shown in Table 2.5. In the future, more estimates of winter emissions from aquatic systems are needed to more accurately estimate total annual emissions.

Table 2.4. Characteristics of the BAWLD aquatic classes based on CH_4 and environmental variables. The number of sites and contributing studies are shown for each class and flux pathway. Also shown are the mean, median, and quartiles for site average diffusive and ebullitive CH_4 flux, waterbody surface area, water body depth, and dissolved organic carbon concentrations (DOC). *In some cases one study contributed flux data for multiple classes and pathway types. One ebullition outlier point (flux = 1815 mg CH_4 m^2 d^{-1}) was excluded from the Midsize Glacial class as it was influenced by beaver activity (Sepulveda-Jauregui et al. 2015).

		Large Lakes	**Midsize Glacial**	**Small Glacial**	**Midsize Yedoma**	**Midsize Peatland**	**Small Peatland**	**Small Yedoma**
Studies*		7	23	15	18	13	39	6
Lakes* D		168	447	52	7	43	400	17
Lakes* E		1	34	19	38	26	50	34
Diffusive	Mean	8.6	9.5	10.5	12.3	39.1	61.2	57.8
CH_4 Flux (mg CH_4 m^{-2} d^{-1})	Med	3.8	5.1	5.8	6.8	18.4	16.4	30.5
	25th	1.1	2.4	1.1	3.4	11.0	9.1	20.5
	75th	12.2	12.3	8.6	16.5	42	101.6	49.7
	n	11	68	55	6	24	218	14
Ebullitive	Mean	0	24.12	22.1	46.8	54.0	85.6	95.9
CH_4 Flux (mg CH_4 m^{-2} d^{-1})	Med	0	1.65	13.3	7.5	45.1	22.5	78.3
	25th	0	0	3.4	1.8	20.8	3.2	49.1
	75th	0	15.4	26.5	70.1	80.5	89.4	113.8
	n	1	35	19	15	7	57	33
Surface	Mean	52.9	1.2	0.03	1.2	1.03	0.0123	0.03

Area (km^2)	Med	42.6	0.5	0.02	0.56	0.25	0.002	0.02
	25th	17	0.2	0.01	0.32	0.13	0.0001	0.008
	75th	48.4	1.4	0.05	1.2	0.48	0.01	0.04
	n	16	106	61	16	24	201	48
Depth (m)	Mean	21.4	7.7	4.6	4.7	2.0	1.2	4.9
	Med	15.6	4.6	3.15	2.8	1.4	1	4.3
	25th	9	1.8	2.5	2.1	1	0.5	2.6
	75th	26.5	11.4	6.7	4.8	1.6	1.7	6
	n	13	90	46	16	17	178	49
DOC	Mean	7.7	7.3	13.4	7.8	12.0	20.3	23.2
($mg\ L^{-1}$)	Med	8	4.6	7.6	4.7	10.6	16.6	16.3
	25th	5.9	3.2	4.2	4.0	8.4	11.0	14.9
	75th	8.1	8.1	11.3	4.8	11.3	25.8	35.3
	n	11	62	33	8	17	162	11

Table 2.5. Winter fluxes, including storage, ice bubble storage (IBS), and winter ebullition for each class type. Annual estimates of ice-free diffusion and ebullition are included for comparison. ** Winter ebullition from constant seeps not included in sum winter/ice-out emissions.

Class	Annual Flux (g CH_4 m^{-2} yr^{-1})	Storage	Ice Bubble Storage	Winter Ebullition (Seeps)**	Ice-free Diffusion	Ice-free Ebullition
Small Peatland Lakes	Mean (n)	1.3 (4)	1.3 (4)	9.5 (4)	10.50 (97)	12.61 (38)
	Median	1.5	1.5	2.3	4.50	5.50
	25th	0.8	0.8	1.7	1.62	1.26
	75th	1.9	1.9	10.1	12.10	14.33
Small Glacial Lakes	Mean (n)	1.3 (14)	1.3 (14)	1.1 (6)	0.78 (46)	4.72 (8)
	Median	0.5	0.5	1.2	0.70	4.95
	25th	0.1	0.1	0.7	0.13	3.98
	75th	2.6	2.6	0.6	1.14	7.52
Small Yedoma Lakes	Mean (n)	0.4 (6)	0.4 (6)	2.3 (10)	6.18 (11)	11.14 (16)
	Median	0	0	1.1	3.20	3.70
	25th	0	0	0.4	2.70	1.50
	75th	0.5	0.5	3.8	5.70	14.55
Midsize Peatland Lakes	Mean (n)	0.9 (1)	0.9 (1)	1 (1)	4.02(6)	6.47 (4)
	Median	-	-	-	2.85	6.04
	25th	-	-	-	1.65	3.85
	75th	-	-	-	5.63	8.66
Midsize Glacial Lakes	Mean (n)	0.3 (19)	0.3 (19)	0.4 (12)	1.59 (54)	3.37(21)
	Median	0	0	0.3	0.6	0.92
	25th	0	0	0.1	0.26	0.35
	75th	1.7	1.7	0.5	1.41	1.7

Midsize Yedoma Lakes	Mean (n)	1.2 (3)	1.2 (3)	0.2 (3)	1.71 (5)	6.12 (5)
	Median	0.6	0.6	0.2	1.10	2.10
	25th	0.5	0.5	0.15	0.50	0.70
	75th	1.7	1.7	0.25	2.00	11.80
Large Lakes	Mean (n)	0 (4)	0 (4)	-	1.38 (9)	-
	Median	0	0	-	0.8	-
	25th	0	0	-	0.25	-
	75th	0	0	-	1.3	-

2.3.4 Joint analysis of terrestrial and aquatic fluxes

I performed a joint analysis of fluxes from both the aquatic and terrestrial datasets with regional predictor variables (Class, MAAT, MAP, Permafrost Zone, and Biome) using mixed models to assess the potential for universal drivers across all Boreal-Arctic ecosystems. The best model included Class and MAAT ($\chi^2 = 345.6$, $P < 0.0001$, $R^2m = 0.47$, df = 18: Table A.2.4). However, Class alone explained 44% of the variation in fluxes (compared to 47% in the best model; Table A.2.4), suggesting that ecosystem classification based on CH_4 emitting characteristics, alongside corresponding spatial extent, is one of the most important variables to consider when scaling CH_4 fluxes across the Boreal-Arctic region.

2.3.5 Upscaled methane fluxes

I used empirical models together with gridded climate variables and land cover distributions (Olefeldt, Hovemyr, Kuhn, et al. 2021) to estimated warm-season and ice-free season CH_4 emissions across the Boreal-Arctic region. Average CH_4 emissions from wetlands were 24.7 (18.5-35.7) Tg CH_4 yr^{-1} (Table 2.6) and average CH_4 emissions from aquatic ecosystems were 5.1 (3.7-7.7) Tg CH_4 yr^{-1} (Table 2.6). Total annual emissions (including winter and ice-out emission estimates) were 30 (22.8-44) Tg CH_4 yr^{-1} for wetland and 6.6 (3.1-9.1) Tg CH_4 yr^{-1} for aquatic ecosystems. The largest source of CH_4 for wetlands over the warm-season was from *Fens* (9.9 Tg CH_4 yr^{-1}) and the lowest source was *Permafrost Bogs* (1.1 Tg CH_4 yr^{-1}; Fig. A.2.5). Geographically, emissions were highest from West Siberian Lowlands, Hudson Bay Lowlands, and the southern Taiga Plains of western Canada where wetlands are most prominent (Fig. 2.12a; Hugelius et al. 2020). Aquatic diffusive emissions were highest from *Small Peatland Lakes* (1.14 Tg CH_4 yr^{-1}) and *Large/Midsize Glacial Lakes* (together = 1.03 Tg; Fig. A.2.6). Ebullitive emissions (paint by numbers) were highest from *Small* and *Midsize Peatland Lakes* (~1.7 and ~1.3 Tg CH_4 yr^{-1} each). Geographically, emissions were highest from the West

Siberian Lowlands, where *Small Peatland Lakes* are abundant, and the Canadian Shield where glacial lakes are present at a high density (Fig. 2.12b; Messager et al. 2016).

Uncertainty from the wetland empirical models (~4 Tg CH_4 yr^{-1}) was less than the associated uncertainty from the land cover area (~13 Tg CH_4 yr^{-1}), suggesting the land cover area is less constrained than flux estimates. Within the wetland classes, the highest model uncertainty (i.e. flux uncertainty) was from *Fens* (~ 2 Tg CH_4 yr^{-1}; Fig. A.2.5). For aquatic ecosystems the highest model uncertainty was from *Small Peatland Lakes* (~ 0.3 Tg CH_4 yr^{-1}) and *Midsize Glacial Lakes* (~0.14 Tg CH_4 yr^{-1}; Fig. A.2.6).

Table 2.6. Annual CH_4 emission estimates from Boreal-Arctic wetland and aquatic ecosystems.

Study	Domain (latitude)	Tg CH_4 $year^{-1}$	Notes
Aquatic (bottom-up)			
Walter et al. 2007	>45	25.3 (15-36)	Only 1.1 Tg from diffusion
Bastviken et al. 2011	>50	13.4	
Wik et al. 2016	>50	16.5 (7.5-25.5)	
Tan et al. 2015	>60	11.86	
Matthews et al. 2020	>50	15.8 (13.8-17.7)	
This study (ratio)	~>50-55	6.6 (3.1-9.1)	Moving southern boundary
This study (PBN ebullition)	~>50-55	10.1 (5.7-14.5)	Moving southern boundary
Wetlands (bottom-up)			
Treat et al. 2018	>40	37 (30-43)	
Peltola et al. 2019	>45	38, 31, 32	3 outputs from 3 different wetland cover maps
Zhu et al. 2016	>45	44-54.7	
Watts et al. 2015	>45	53	
This study	~>50-55	30 (22.8-44)	Moving southern boundary
Inverse model (top-down)			
Thompson et al. 2018	>45	33.6	Doesn't explicitly include lakes
Bruhwiler et al. 2014	>47	23	Doesn't explicitly include lakes
Spahni et al. 2011	>45	28.2 (26-30.4)	Doesn't explicitly include lakes

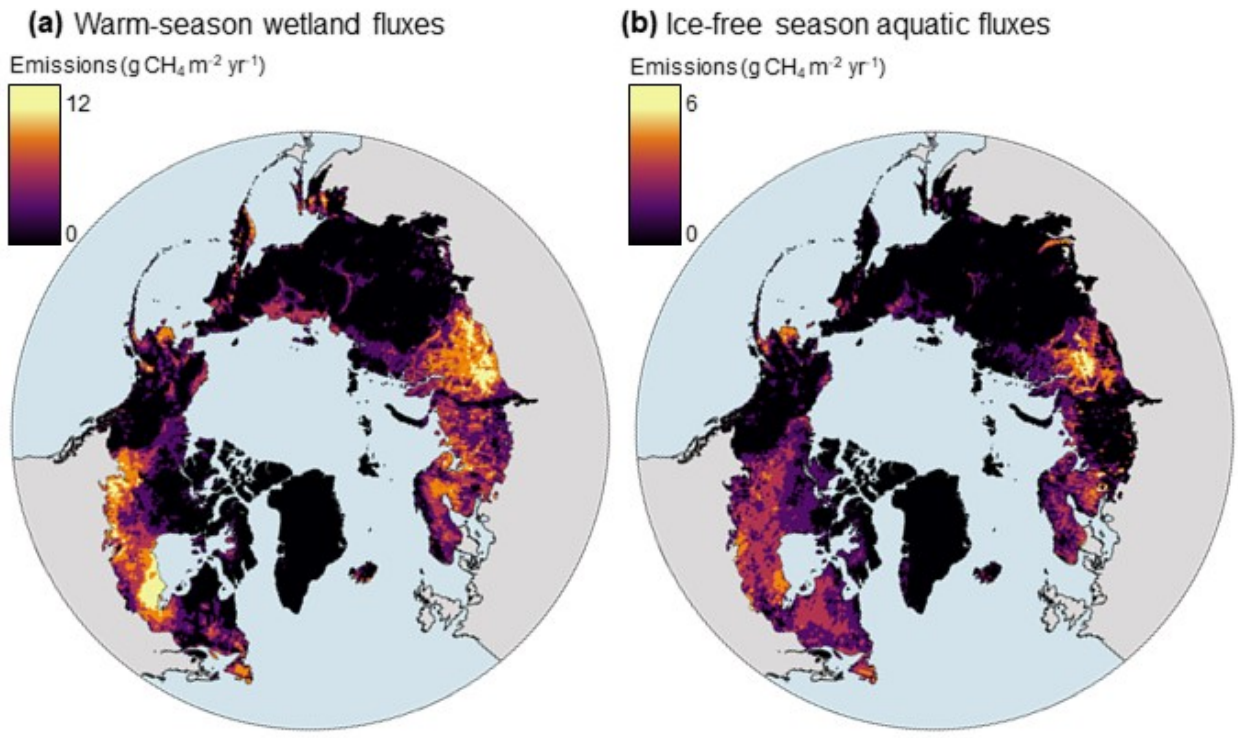

Figure 2.12. Average warm-season and ice-free CH_4 emissions across the Boreal-Arctic region. a) Warm-season wetland CH_4 fluxes. b) Ice-free aquatic CH_4 fluxes (includes both ebullition and diffusion). Note the different scales between panel a and panel b. The flux rates refer to the total unit area in a grid cell in grams of CH_4.

2.4.0 Discussion

2.4.1 Flux variation largely explained by land cover classes

In this review, I assessed the controls on CH_4 emissions from 189 studies across terrestrial and aquatic ecosystems in the Boreal-Arctic region. A central component to this study was the inclusion of new land cover classes split by CH_4-emitting characteristics common across terrestrial and aquatic ecosystems, respectively. Terrestrial classes were split by permafrost conditions and hydrology (and vegetation and nutrient conditions therein) whereas aquatic classes were split by size and lake genesis (i.e. type). I found that much of the observed CH_4 flux variability from terrestrial and aquatic ecosystems could be explained by this land cover classification system (Fig. 2.9). When modeling fluxes for both aquatic and terrestrial

ecosystems together with regional-level predictors (variables assigned to sites based on the gridded product including Biome, Permafrost Zone, MAAT, and MAP) land cover class explained most of the variation (44%) with statistically significant, but small contributions in explained variation from gridded MAAT (3% of 47% total variation explained; Table A.2.2). This suggests that differences in land cover classes are the most important consideration for estimating CH_4 flux at this scale, with some influence of MAAT.

For terrestrial fluxes alone, land cover class as a predictor variable explained 55% of the flux variation. Site-level predictors, including water table, temperature, and vegetation conditions explained 54% of the variation in the fluxes when analyzed separately. The best model for terrestrial fluxes included these site-level variables and land cover class and explained 69-73% of the variation (depending on additive or interactive effects; Table A.2.2). This model likely performed better than land cover class on its own because the extra information added from the continuous soil temperature and water table variables captured the variation in these conditions within each class. While permafrost presence came out as a non-significant term in the best model (Table A.2.2), the effects of permafrost presence and absence, including confounding temperature effects, were already intertwined into the land cover classes.

For aquatic ecosystems, the best models for diffusive and ebullitive fluxes contained different predictor variables. The best model for diffusive fluxes explained 41% of CH_4 flux variability and included an interactive effect between surface area and lake type (*Peatland, Yedoma*, and *Glacia*l) and water temperature. Land cover classes (i.e. lake types split by small and medium categorical sizes) did not come out as significant in this model because the continuous variable of surface area captures the size variation within each lake type. However, land cover class modeled on its own explained 25% of the flux variation. The significant effect of surface area is consistent with previous global synthesis efforts that found small water bodies tend to have higher CH_4 fluxes likely due to the compounding effects of higher substrate availability and warmer temperatures compared to larger water bodies (Holgerson and Raymond, 2016; DelSontro et al. 2018). Notably, previous synthesis efforts also found that water body depth was a significant predictor variable of diffusive fluxes (Wik et al. 2016a, Li et al. 2020). While depth did not come out as significant in my model, the effect of waterbody depth is taken into account with the lake types and areas embedded within. For example, I found diffusive

fluxes are typically higher from *Peatland lake* types compared to *Glacial lakes*, which have average depths of 1.6 meters and 6.7 meters, respectively. Waterbody depth is also an important factor contributing to water body temperature (i.e. warmer waters in shallower waterbodies), thus the effect of waterbody depth may also be confounded with that of the temperature variable.

The best model for ebullition contained waterbody surface area as a predictor and explained 21% of the variation in the fluxes. Previous synthesis efforts have linked ebullition fluxes to both temperature (Aben et al. 2017) and waterbody depth (Wik et al. 2016a). The weak or absent relation with temperature and depth here is not surprising especially given the broad depth range of the lakes evaluated, nor contradicts the previously observed relationships, because it is likely that the temperature and depth influence is clearer over time and space, respectively, in each specific system. In this dataset, such patterns may be masked by differences in measurement strategies (i.e. number of measurements per season or measurement distributions over the lake) or among overall system characteristics. It is also possible the effects of depth are confounded with surface area as the two metrics are highly correlated (Fig. A.2.7). While this dataset represents one of the largest collections of ebullitive emissions from northern lakes so far, this emission pathway is still largely underrepresented and waterbody depth and temperature are not always reported with the flux estimates. Furthermore, I collected information on surface water temperature for this dataset because it was the most widely available temperature metric. Sediment temperature is a better metric to collect in hand with ebullition due to production and transport directly from the sediments (Aben et al. 2017; Wik et al. 2013). Future studies should work to report sediment temperature and water column temperature alongside their flux measurements.

2.4.2 Annual estimates of methane from northern wetland and aquatic ecosystems

The annual estimates (warm-season + winter) of wetland CH_4 emissions (~30 Tg CH_4 yr^{-1}) and lake CH_4 emissions (~6.6 Tg CH_4 yr^{-1}) are on the low end but within similar ranges of annual emissions reported from other bottom-up studies (average = ~40 and ~17 Tg CH_4 yr^{-1} for wetlands and aquatic ecosystems, respectively; Table 2.6). The total annual estimate of CH_4 emissions (~36.6 Tg CH_4 yr^{-1}; wetland + aquatic) is closer to the total emission estimated by top-

down models (23-33.6 Tg CH_4 yr^{-1}; Table 2.6) compared to the average of previous bottom-up estimates (~57 Tg CH_4 yr^{-1}). While the domain sizes for each literature estimate differ slightly, I suggest my lower annual estimates are associated with distinguishing between wetland and aquatic land cover classes. Previous scaling estimates included fewer wetland or lake classes (for example Watts et al. 2016 and Wik et al. 2016a), potentially leading to higher average emissions. For the few studies that do incorporate distinct wetland and lake types (Treat et al. 2018, Matthews et al. 2020), wetlands and aquatic ecosystems are not explicitly included in the same land cover maps. Lower annual emissions found in my study may be linked to the incorporation of wetland and aquatic land covers within the same model, thus reducing the change of "double-counting" or over counting emissions through confounding wetland or aquatic areas (Thornton et al. 2015). Lower emissions from aquatic ecosystems may also be linked to the empirical modeling approach. My model may not be able to capture higher emissions from aquatic ecosystems and does not explicitly model ebullitive emissions, which can make up to 77% of total CH_4 emissions from yedoma lakes (Walter et al. 2008). However, my approach of using a ratio of diffusion to ebullition is similar to the most recent approaches (Wik et al. 2016a; Matthews et al. 2020).

Despite generally lower annual estimates using this new bottom-up approach, my estimate is still higher than top-down model estimates, suggesting there are more sources of uncertainty not accounted for in my approach and/or in the top-down modeling approaches. Additional sources of uncertainty from the bottom-up perspective may include the accuracy of measured field fluxes and the land cover area. The accuracy of field measurements is discussed in more detail in Sect 2.4.3. While BAWLD is the best available wetland and aquatic ecosystem area database product currently available at this scale, it consists of relatively low spatial resolution (0.5 by 0.5 degree grid cells) and the percent land cover area was determined by expert assessment. Emission uncertainty may be more constrained as remote sensing products and the ability to identify distinct wetland and aquatic land cover areas improve. Furthermore, top-down models rely on a priori information provided by bottom-up estimates and the same land cover models (Saunois et al. 2020). Inverse model emission estimates may more closely resemble ours if the same land cover maps and a priori information are used. Additional uncertainties from top-down modeling approaches include stable isotope signature sources, tower locations, or estimates of CH_4 oxidation rates in the atmosphere (Saunois et al. 2020).

Finally, I did not include CH_4 uptake from upland environments (i.e. *Boreal Forests, Dry Tundra*, and some *Rocklands*) in my annual estimate due to low sample sizes from those ecosystems. Recent work suggests uplands in the Boreal-Arctic region could uptake ~9 Tg CH_4 yr^{-1} (Oh et al. 2020). If I assume the sink capacity is 9 Tg CH_4 yr^{-1}, my annual estimate is ~27.6 Tg CH_4 yr^{-1} which is much closer to inverse model estimates. However, CH_4 uptake across the Boreal Arctic region is still highly uncertain and more field measurements from *Boreal Uplands*, *Dry Tundra*, and *Rocklands* are needed.

2.4.3 Directions for future research

While my small-scale, surface CH_4 flux datasets for northern ecosystems are the most extensive datasets compiled to date for the Boreal-Arctic region, I identified key gaps in the data and areas of improvement that future studies should focus on. While the geographical gaps represented in Figure 2.1a suggest widespread geographic under-representation of terrestrial ecosystems, especially across central Russia and the Canadian Territories of Nunavut and Northwest Territories, these regions are comprised primarily of *Boreal Forest* and *Dry Tundra* ecosystems, respectively (Fig. 2.13e, 2.13g). Study sites for many of the other land cover types, for example, *Bogs* and *Fens*, were relatively well distributed across the Boreal and Arctic region (Fig. 2.13a, 2.13b). However, to assess how well or poorly represented a land cover class is, class area and flux magnitude must also be considered (Fig. 2.14a). For example, *Fens* are a high-emitting land cover class and are spatially abundant, leading to a high total flux contribution across the study region (~41%, Fig. 2.14a), however, the relative number of *Fen* sites represented in the available literature is not proportional to the total flux contribution (~26%). This, alongside the large spread of reported flux magnitudes (Fig. 2.9a) and the calculated uncertainty from the scaling exercise, suggests future studies should focus on *Fens* to better constrain the flux magnitude. Conversely, *Permafrost Bogs* are low contributors to the total wetland flux (~4%) and are well represented throughout the literature (~19%), suggesting fewer direct flux measurements are needed from these ecosystems.

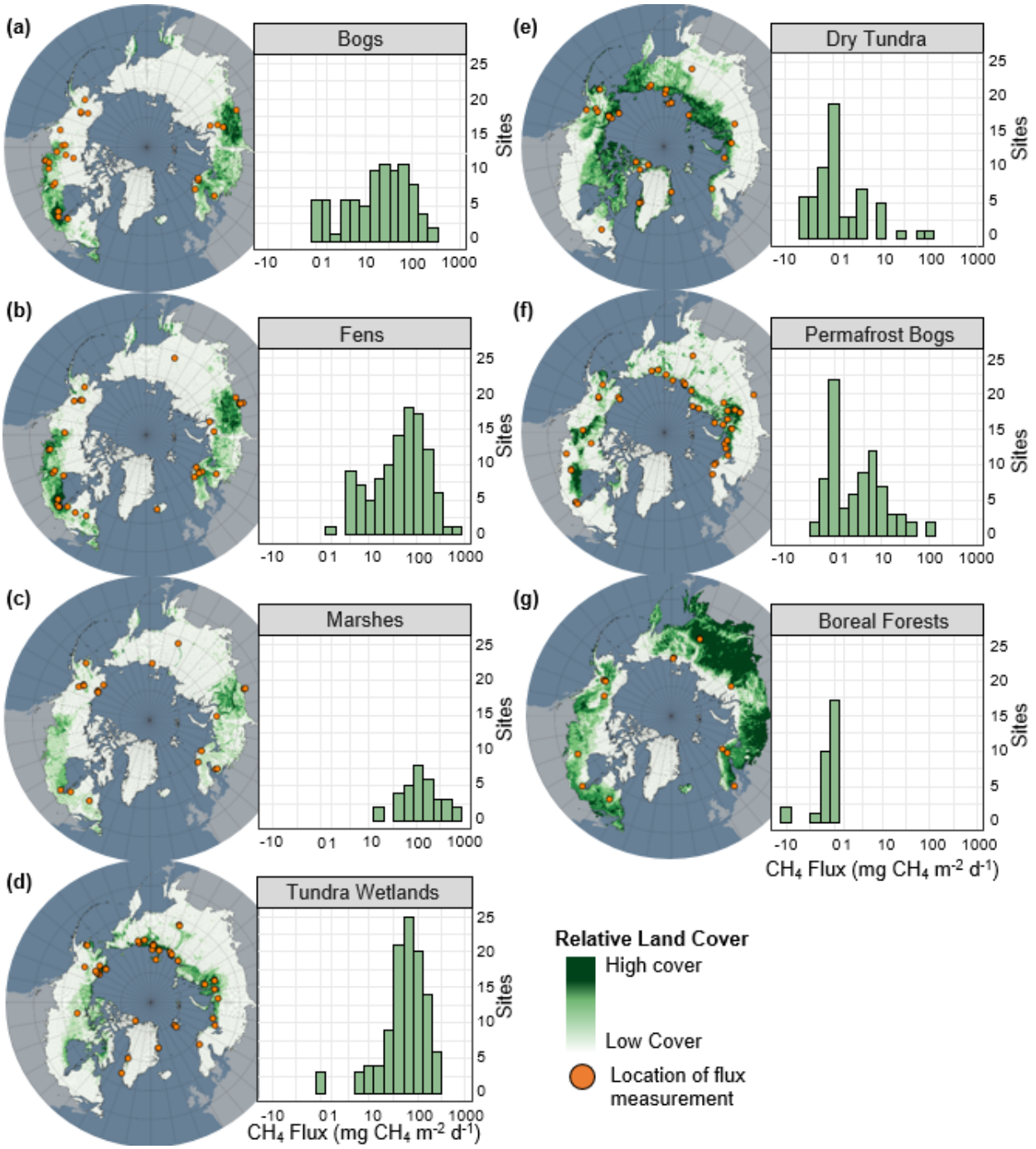

Figure 2.13. Geographical distribution and flux frequencies and for each terrestrial class. Relative land cover for each type is represented in green on the map. Site locations are represented by orange circles. Some circles represent more than one land cover site. Note the log

scale for CH_4 flux. Land cover distributions from Olefeldt, Hovemyr, Kuhn et al. 2021. Histograms of non-transformed flux data can be found in Fig. A.2.8.

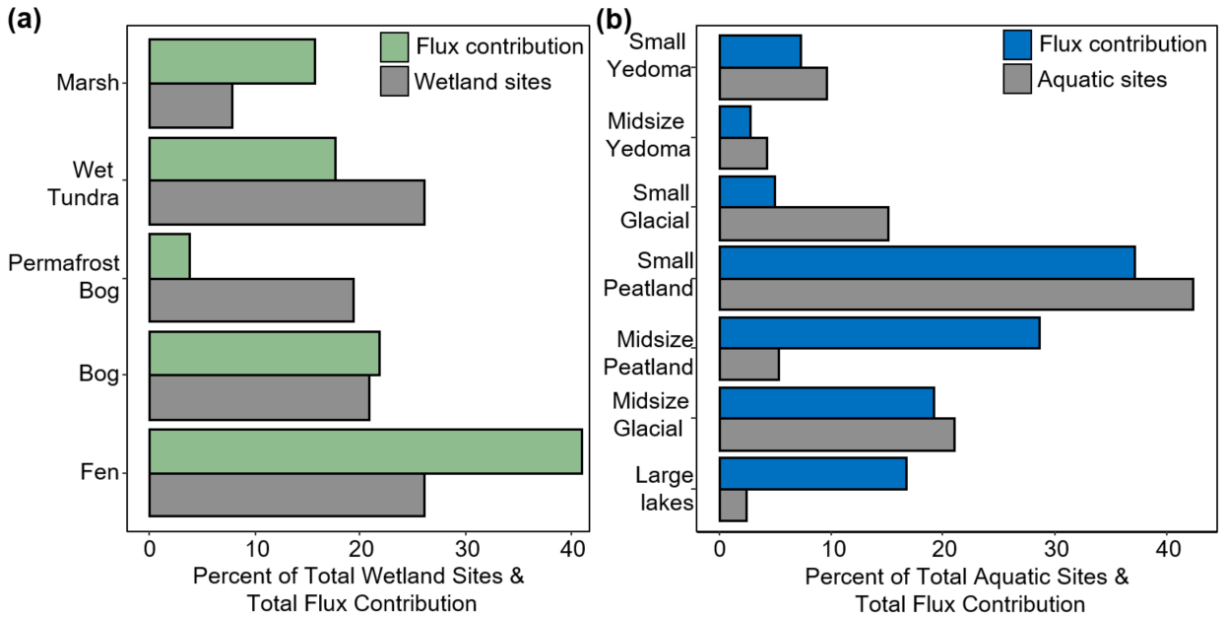

Figure 2.14. Relative total flux contribution (mean flux*total class area) for each land cover shown with the relative contribution of flux measurements for each class. A) Wetland classes. B) Aquatic classes. The bars represent the percent of total flux contribution and percent of reported flux sites for each class. Aquatic flux contributions represent average ebullition + average diffusion fluxes.

For aquatic ecosystems, there are key data gaps in geography and flux pathway representation with relatively few measurements of ebullition and ice-out fluxes compared to diffusive fluxes. Geographically there are very few flux measurements from lakes in the western Canadian Shield (Fig. 2.1b), despite this region containing the most lakes per unit area throughout the north (Messager et al. 2016). This data gap is further highlighted by very few flux estimates from *Large lakes* and *Midsize-Glacial lakes*, which are numerous throughout the western Canadian Shield (Fig. 2.15a, 2.15d). Notably, *Large lakes* are the least represented of all of the aquatic classes (~2.4% of measurements), but could potentially contribute ~17% of the total flux, mostly from diffusive emissions. Interestingly, uncertainty calculations from the scaling model suggest *Small Peatland Lakes* have the highest flux uncertainty, despite being well represented (~42% of measurements and 37% of potential total flux contribution). Conversely,

Midsize Peatland lakes had the second-highest model uncertainty and are under-represented (~5% of measurements) compared to their estimated flux contribution (~28%).

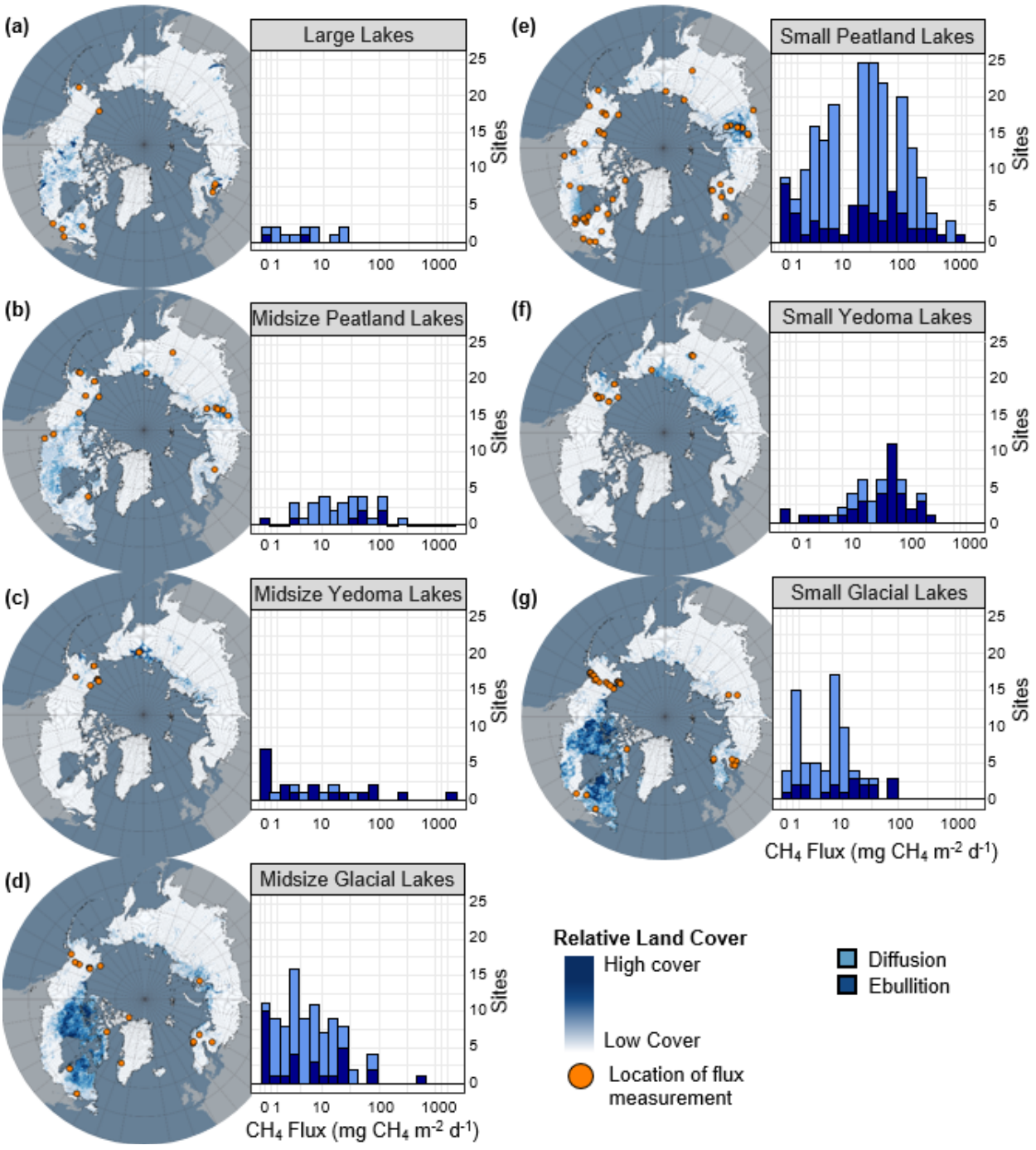

Figure 2.15. Flux frequencies and geographical distribution for each aquatic class. Relative land cover for each class type is represented in blue on the map. Site locations are represented by

orange circles. Note the log scale for CH_4 flux. Land cover distributions from Olefeldt, Hovemyr, Kuhn et al. 2021. Histograms of non-transformed flux data are shown in Fig. A.2.9.

There are fewer ebullition measurements compared to diffusive flux measurements from aquatic ecosystems (21% and 79% of ice-free fluxes, respectively). Average ebullitive fluxes were greater than diffusive estimates for all of the land cover classes except *Large Lakes* (Fig. 2.7b), and thus represent an important component of total CH_4 fluxes from these systems, however, none of the models performed in this study could explain a large amount of the variation in ebullitive fluxes. More ebullition measurements, across all the land cover classes, will help to constrain our understanding of CH_4 transport mechanisms and drivers. However, it is important to note that more representative ice-free season flux estimates are needed for both ebullition and diffusion. Wik et al (2016b) suggest that ~11 diffusive day flux measurements and ~39 ebullition day flux measurements are required to calculate a mean ice-free flux estimate within 20% of the true value. 86% of diffusive estimates were under the recommended 11-day mark and 58% of ebullition estimates were below the recommended 39-day mark (Fig. 2.5b, 2.5c). Jansen et al. (2020) posit that an even higher frequency of sampling is required (14-22 days and 135 days for diffusion and ebullition, respectively). Under-sampling potentially reduces the accuracy of mean CH_4 flux estimates leading to the relatively poor fitness and explanatory power of the aquatic regression analysis in this study compared to the terrestrial models' performances. This is especially true for ebullitive emissions, which were poorly explained by the reported predictor variables available for this dataset. Calculation of mean ice-free fluxes from a greater number of flux measurements is an important step forward towards better constraining CH_4 fluxes from aquatic ecosystems. Finally, there are very few flux estimates for lakes over the shoulder seasons and winter/ice-out compared to the ice-free season (Table 2.5). While shoulder season flux estimates, including autumnal turnover, were not included in this dataset, winter/ice-out measurements make up only 7% of all aquatic flux measurements collected. Winter/ice-out emissions could potentially contribute a significant portion of annual fluxes from aquatic ecosystems (Karlsson et al. 2013; Sepulveda-Jauregui et al. 2015) and therefore represent an important gap in CH_4 flux data.

2.5.0 Conclusions

Methane fluxes from northern ecosystems represent an important component of the global CH_4 cycle (Saunois et al. 2020). BAWLD-CH_4 is a comprehensive flux dataset that uniquely represents flux data from both terrestrial and aquatic ecosystems across the Boreal-Arctic region. BAWLD-CH_4 has many potential applications including benchmarking for process-based models, empirical scaling models and informing future research directions. Importantly, I show that land cover class, split by CH_4-emitting ecosystem characteristics, is a significant flux predictor variable across terrestrial and aquatic ecosystems and I suggest that future studies should scale CH_4 emissions based on CH_4-emitting land cover characteristics. I show that while land cover class explains most of the flux variation for wetland and aquatic ecosystems when analyzed jointly, both types of classes are sensitive to MAAT. My annual estimates of wetland CH_4 emissions (~30 Tg CH_4 yr^{-1}) and lake CH_4 emissions (~6.6 Tg CH_4 yr^{-1}) are on the low end, but within the range, of annual emissions reported from other bottom-up studies (averages = ~40 and ~17 Tg CH_4 yr^{-1} for wetlands and aquatic ecosystems, respectively), but are still higher than averaged top-down estimates (~28 Tg CH_4 yr^{-1}). Finally, I found that a higher percentage of terrestrial CH_4 fluxes could be explained by land cover class and site-level variables than for diffusive and ebullitive fluxes from aquatic ecosystems (73% vs 41% and 21%, respectively). Under-sampling of aquatic ecosystems is likely responsible for the lower explained variation observed in my models compared to terrestrial ecosystems. Future studies should increase the number of sampling days for both diffusive and ebullitive fluxes as well as capture the potential for season turnover and CH_4 release from aquatic ecosystems to arrive at more representative ice-free CH_4 flux estimates from the Boreal-Arctic region.

3. Permafrost and climate strongly influence CH_4 and CO_2 emissions from peatland lakes

Abstract

Changing greenhouse gas (GHG) emissions from northern lakes due to warming and permafrost thaw may become a globally significant climate feedback. Here, I monitored seasonal GHG emissions from 20 peatland lakes across a 1,600 km transect in western Canada. From continuous permafrost to warmer non-permafrost regions, I observed a shift from source to sink for carbon dioxide (CO_2) emissions and an 8-fold increase of methane (CH_4) emissions. Trends in CO_2 and CH_4 emissions were driven by different processes. Less permafrost was associated with greater hydrological connectivity, nutrient availability, and thus increased primary productivity and uptake of CO_2. Conversely, trends in CH_4 emissions were driven by temperatures but augmented by shifts in microbial communities and dominant anaerobic processes. The results suggest that the net radiative forcing from altered GHG emissions of boreal peatland lakes this century will be dominated by increasing CH_4 emissions and only partially offset by reduced CO_2 emissions.

3.1 Introduction

Small lakes emit globally significant amounts of carbon dioxide (CO_2) and methane (CH_4) to the atmosphere (Holgerson and Raymond, 2016; Wik et al. 2016a; Hastie et al. 2018), yet the sensitivity of emissions to climate change is poorly constrained. Fueling the biogeochemistry of small lakes are the relatively warm and organic-rich sediments in shallow waters, and the inflow of nutrients, dissolved gases, terminal electron acceptors, and organic matter from the surrounding landscape (Lapierre and del Giorgio et al. 2012; Wik et al. 2016a; DelSontro et al. 2016; Waulthy et al. 2018). Small, shallow lakes with organic-rich sediments are abundant across northern peatlands, which cover ~3% of the global land surface (Hugelius et al. 2020; Olefeldt, Hovemyr, Kuhn, et al. 2021). Arctic amplification has caused temperatures in northern peatland regions to increase much faster than the global average, and these regions are furthermore experiencing rapid permafrost thaw (Olefeldt et al. 2016; Treat and Jones, 2018). To understand the climate sensitivity of peatland lake CO_2 and CH_4 emissions it is thus necessary to account for both the direct effects of warming and the indirect effects arising from increased hydrological connectivity following permafrost thaw (McKenzie et al. 2021).

Lake CH_4 and CO_2 emissions are both influenced by the direct effects of climate warming on microbial activity. For CH_4, increasing temperatures influence both CH_4 production (methanogenesis) and oxidation (methanotrophy), but effects on methanogenesis generally dominate and result in high sensitivity of the net CH_4 emissions (Yvon-Durocher et al. 2011; Yvon-Durocher et al. 2014). Temperature sensitivity of net CH_4 emissions is however often assessed within individual ecosystems, e.g. seasonally, and it is uncertain whether this sensitivity reflects spatial differences among lakes at broad geographical scales. Heterotrophic respiration and net emission of CO_2 are also temperature-dependent (Gudasz et al. 2010; Kosten et al. 2010), but relationships between lake net CO_2 emissions and temperatures are often less clear than for CH_4 (Sobek et al. 2005; Lapierre et al. 2015). While most boreal peatland lakes are net sources of CO_2 (Lapierre et al. 2015; Weyhenmeyer et al. 2015, Hastie et al. 2018), net CO_2 emissions are influenced not only by respiration but also by CO_2 uptake through primary productivity, which in turn is influenced by nutrient availability and water column light conditions (Lapierre & del Giorgio et al. 2012; Pacheco et al. 2014).

Permafrost thaw in peatland regions may have additional indirect effects on lake CO_2 and CH_4 emissions through several processes. Thaw opens both shallow and deep groundwater connections, bringing water to lakes with high concentrations of dissolved organic matter (DOM), nutrients, and weathering products, respectively (Frey et al. 2009; Laudon et al. 2011). Within-lake primary productivity increases with greater nutrient availability, often associated with groundwater inputs but can be inhibited if concentrations of dissolved organic carbon (DOC) causes substantial light attenuation (Ask et al. 2009; Bogard et al. 2020). Delivery of dissolved CO_2 and CH_4 produced in surrounding organic soils can also cause high lake emissions (Weyhenmeyer et al., 2015; Payton et al. 2015), while connectivity to deeper groundwater may increase pH and reduce lake CO_2 emissions through pH-driven changes in carbonate equilibrium (Finlay et al. 2015). Higher CH_4 emissions may also be driven by the availability of labile organic matter, supplied from the surrounding landscape, littoral emergent vegetation, or from within-lake primary productivity (Bastviken et al. 2004; Davidson et al. 2015; Del Sontro et al. 2016; Emilson et al. 2018). Further, shorter ice-free days may increase annual CH4 emissions (Guo et al. 2020). Conversely, increased delivery of terminal electron acceptors, e.g. sulfate and iron, may inhibit methanogenesis (Sivan et al. 2011: Yu et al. 2016). Indirect effects of climate warming through permafrost thaw may thus either enhance or dampen the direct effects of climate warming leading to hitherto unclear climate feedbacks from a broader scope than just temperature effects.

3.2 Lake greenhouse gas emissions across a permafrost transect

I monitored CO_2 and CH_4 emissions during two ice-free seasons from 20 shallow lakes across a 1,600 km permafrost transect within the Interior Plains of western Canada (Fig. 3.1). Lakes were clustered at four sites, with five lakes per site. All lakes were surrounded by peatlands, had thick organic sediments, and ranged in size between 0.4 and 10 ha. Diffusive gas emissions were sampled using floating chambers between 7 and 12 times over two ice-free seasons, with two or three individual flux measurements at each lake visit. Sampling started shortly after ice-off (~May/June) and ended just before ice-on (~September/October). Ebullition of CH_4 was measured at a subset of twelve lakes, three per site, using inverted funnel bubble traps. Ebullition was measured three to five times at each lake and included three traps set near the lake edge and three in the lake center. Water chemistry was assessed during each lake visit,

and included measurements of pH, water temperature, specific conductivity, and dissolved oxygen, along with sampling and subsequent analysis of dissolved organic carbon (DOC), light absorbance at 254 nm (A_{254}), nutrients, major ions, and Chlorophyll-*a* (Chl*a*) all taken from the surface of the water column. Shotgun metagenomic sequencing was used to examine microbial community functions in the top 15 cm of near-shore sediments in all lakes, focusing on genes involved in methanogenesis and methanotrophy.

The Interior Plains of western Canada represents a unique opportunity to use a space-for-time approach to assess climate sensitivity of lake CO_2 and CH_4 emissions, as the region has broadly similar surficial geologies throughout the whole transect. The region is characterized by generally flat topography, sedimentary bedrock overlain by thick, heterogeneous surficial geology (Geological Survey of Canada 2014), and widespread peatlands with abundant lakes (Fig. 3.1 inset). The region has a relatively dry climate throughout, with mean annual precipitation between 300 and 450 mm and mean annual runoff between 50 and 150 mm, but it has a large gradient in mean annual average temperatures (MAAT) between -8 and +2°C (Table A.3.1). Peatlands in the Interior Plains started developing shortly after deglaciation ~10,000 years ago, and today have 2-5 m deep peat deposits (Halsey, Vitt, and Bauer, 1998; Hugelius et al. 2020). Permafrost expanded southward after the Holocene thermal maximum and reached its maximum extent following the Little Ice Age, ~1,000 years ago (Pelletier et al., 2017). Permafrost conditions strongly influence peatland hydrology and thus the hydrological connectivity of lakes to their surrounding landscape in this region (Quinton et al 2019). Widespread permafrost precludes deeper groundwater flow but also blocks shallow flow paths and much peatland runoff enters hydrologically isolated depressions rather than connecting with lakes (Vitt et al. 2000; Quinton et al 2019). Consequently, with less permafrost in warmer climates, there is increased connectivity of lakes with the surrounding peatlands, while lake position in the landscape determines the potential for regional groundwater recharge or discharge (Hokansson et al. 2019).

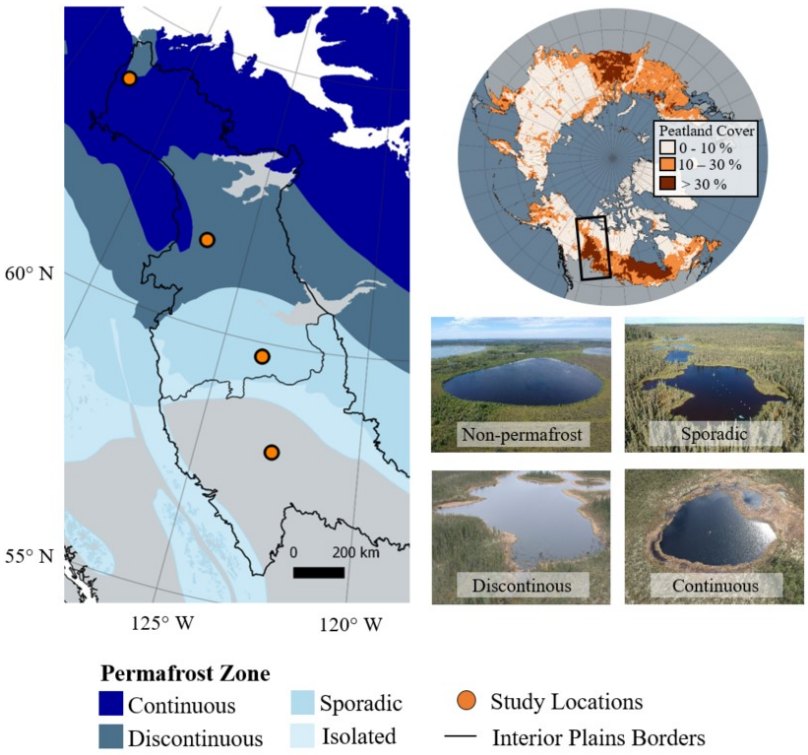

Figure 3.1. Locations of study lakes within the Interior Plains of western Canada. The Interior Plains study region is outlined with a black line and is comprised of the Taiga Plains (north) and Boreal Plains (south, largely permafrost free) ecozones. Permafrost zones are indicated by blue shadings (Brown et al. 2002). Five lakes were monitored for seasonal greenhouse gas emission at each study location, indicated by orange circles. The distribution of peatlands within both the study region and the broader circumpolar region is shown in the top right inset, showing that the study region is one of the major northern peatland regions (Olefeldt, Hovemyr, Kuhn, et al. 2021). The bottom right photos show one lake from each study location, with all lakes surrounded by treed peatlands.

I found that lakes in regions with less permafrost and warmer climates had lower CO_2 emissions, or even CO_2 uptake, and much higher CH_4 emissions, than lakes further north (Fig. 3.2a, Fig. 3.2b). Lakes in warmer climates also had higher pH, concentrations of base cations, DOC, phosphate (PO_4^{3-}), and Chl*a*. Between-lake variability also increased from colder to warmer climates for both CO_2 and CH_4 emissions, and water chemistry (Fig. A.3.1). While CO_2 and CH_4 emissions both varied with latitude, they were only weakly related to each other (Fig. A.3.2). Below I explore the distinct drivers of CO_2 and CH_4 emissions, and use the information

to project future emissions and the net radiative forcing resulting as a feedback to climate warming under different RCP scenarios.

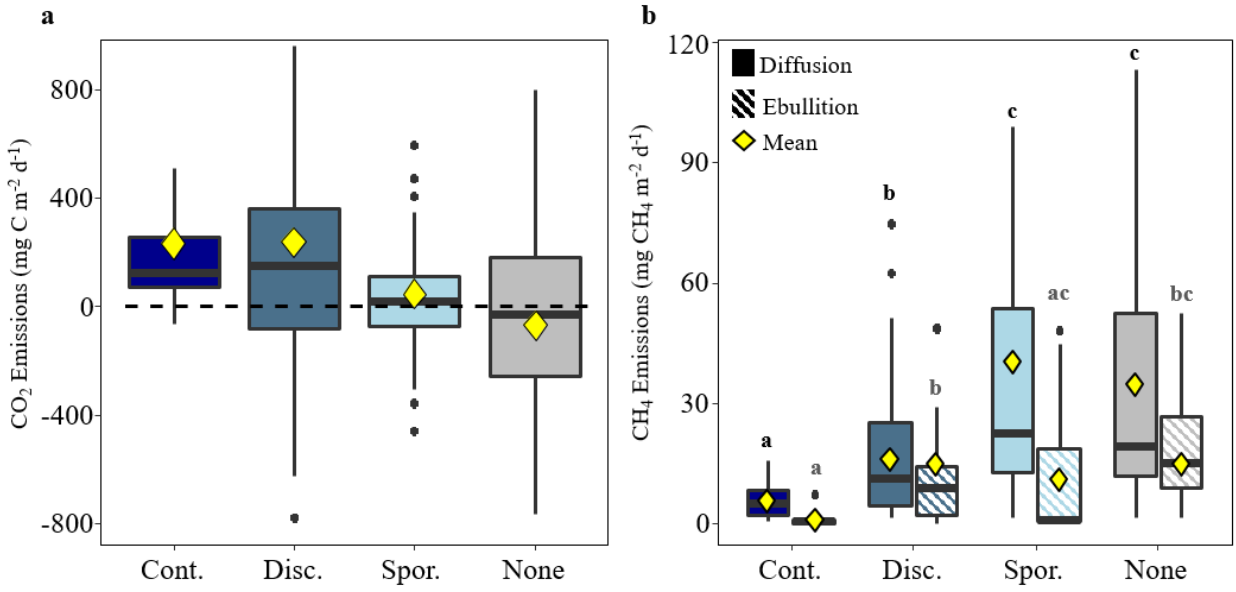

Figure 3.2. Trends in magnitude and variability of lake greenhouse gas emissions across permafrost zones. Emissions of a) diffusive CO_2 and b) CH_4 were measured during the early, mid, and late open water season from five lakes each within the continuous (Cont.), discontinuous (Disc.), and sporadic (Spor.) permafrost zones, as well as south of the permafrost region (None). Boxplots indicate the 25th, median, and 75th percentiles of emissions, and the yellow diamonds indicate the average emissions. Different letters above the boxplots for CH_4 indicate statistically significant differences between permafrost zones, accounting for repeated measurements throughout the season (see Methods and Table A.3.2). Diffusive and ebullitive CH_4 flux significant differences are presented separately. Positive CO_2 fluxes represent a net sources while negative fluxes represent a net sink of CO_2 from the atmosphere. Outlier CO_2 fluxes below -800 and about +1000 mg C m^{-2} d^{-1} are not shown. Methane fluxes have not been corrected for diel variation in this figure (See Methods).

3.3 Connectivity, primary productivity, and CO_2 emissions

My study shows that climate change is likely to reduce peatland lake CO_2 emissions, as its positive effects on primary productivity appeared greater than effects on respiration across the

transect. I attribute this result primarily to indirect effects of climate through increased hydrological connectivity of lakes to the surrounding landscape. Across the transect, diffusive CO_2 emissions were lower for lakes with higher concentrations of Chl*a*, which also were lakes with higher DOC, light absorbance, PO_4^{3-}, and pH (Fig. 3.3a). These water chemistry attributes are characteristic of near-surface water in nutrient-rich groundwater-connected peatlands (i.e. fens) that are relatively more widespread in discontinuous and non-permafrost zones (Vitt et al. 2000; Wood et al. 2015; Fig. 3.4). While there was a trend of decreasing CO_2 emissions in warmer climates, a structural equation model (SEM) highlighted that this link was mediated through effects on lake water chemistry ($R_2 = 0.78$, Fisher's C = 12.9, $P = 0.40$; $P > 0.05$ = good fit; Fig. 3.3b). In the SEM, I hypothesized that higher MAAT allows for less permafrost and increased lake connectivity with groundwater-fed peatlands, raising lake DOC, phosphate, and pH, which in turn increases primary productivity, indicated by higher Chl*a* (Engel et al. 2020), and shifts the carbonate equilibrium from CO_2 to bicarbonate, both causing reduced CO_2 emissions. Notably, CO_2 emission from ebullitive fluxes did not follow a strong north to south trend but emissions were generally higher from the non-permafrost zone than the continuous zone (Fig. A.3.3b), suggesting a potential link between temperature and sediment respiration. However the magnitude of ebullitive CO_2 fluxes was minor compared to diffusive emissions (~7% of the total flux for lakes where both pathways were measured), likely due to the high solubility of CO_2 in water, and did not change the latitudinal trends or net sink/source capacity of individual lakes.

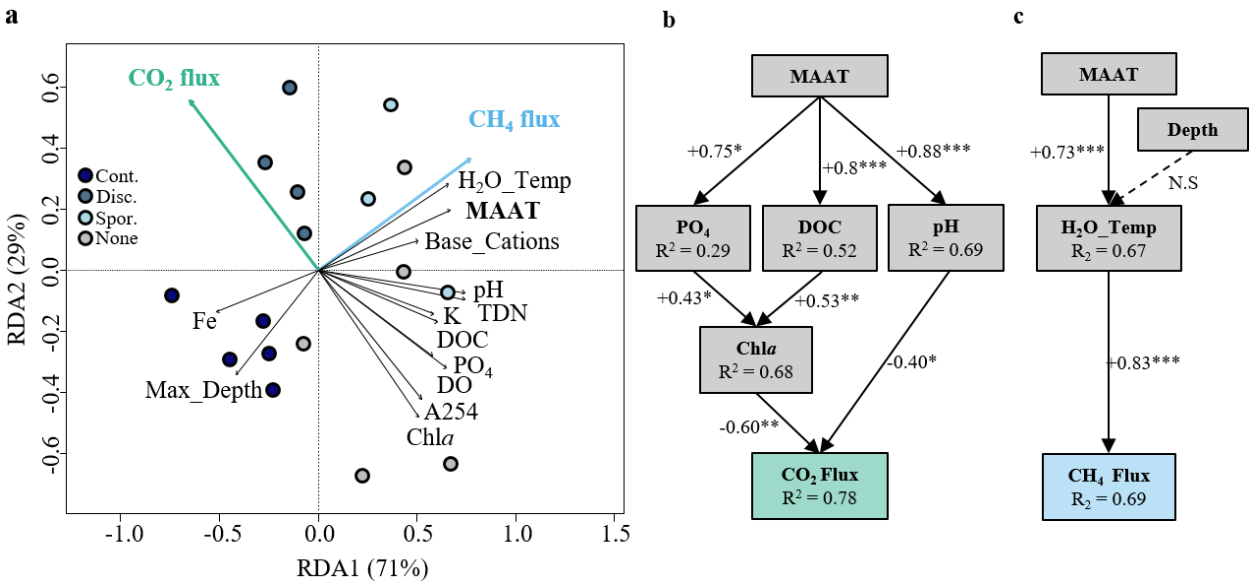

Figure 3.3. Influence of lake water chemistry and lake characteristics on greenhouse gas emissions across permafrost zones. a) Redundancy analysis (RDA) ordination plot for CO_2 and CH_4 emissions, where explanatory variables include water chemistry variables along with maximum lake depth and mean annual air temperature (MAAT). The RDA shows that lake CO_2 and CH_4 fluxes were not correlated, with CH_4 emissions associated with lake depth, water temperature, and mean annual air temperature, while CO_2 emissions were more closely associated with higher concentrations of nutrients, DOC, and chlorophyll *a*. Base_Cations represents the molar sum of Ca, Mg, and Na. Potassium (K) is shown on its own as it followed a dissimilar trend to the other cations. Circle symbols indicate individual lakes, colored by permafrost zonation. Structural equation models were constructed individually for b) CO_2 and c) CH_4. Arrows with solid lines and asterisks represent statistically significant pathways (*p* values = * <0.05, ** <0.01, *** <0.001), while dotted lines represent non-significant pathways. The values by each arrow represent standardized model coefficients, indicating post positive and negative relationships. Goodness of fit (Fisher's C values) were 12.90 and 4.85, respectively for the CO_2 and CH_4 models, while *P* values were 0.40 and 0.30. *P* values > 0.05 indicate that model structure does not differ from that expected by the data.

My findings of decreasing diffusive CO_2 emissions from lakes with higher DOC concentrations contrast most other boreal lake surveys (LaPierre et al. 2015; Weyhenmeyer et al. 2015). Previous studies have shown strong positive relationships between lake DOC

concentrations and CO_2 emissions, suggesting that greater connectivity to terrestrial sources of DOC either enhances lake respiration and/or suppresses primary productivity through light attenuation, resulting in higher net CO_2 emissions (Ask et al. 2012; LaPierre et al. 2015). I speculate that the difference between my results and previous studies stems from the inclusion solely of small peatland lakes with relatively high DOC concentrations (range 17-50 mg L^{-1}). Other surveys include lakes of various origin and size, and thus lakes with much lower DOC concentrations (e.g. Ask et al. 2012; LaPierre et al. 2015). For the peatland lakes in this study, it is possible that further elevated DOC concentrations in warmer climates have limited additional influence on respiration or primary productivity – while co-varying increases in nutrient availability drive greater primary productivity. This study thus suggests that peatland lake CO_2 emissions are likely to respond to climate change in a different way than other lake types, such as deeper lakes in Shield regions of Canada and Scandinavia.

3.4 Temperature sensitivity, microbial ecology, and CH_4 emissions

Both ebullitive and diffusive CH_4 emissions were greater in warmer climates, with emissions from lakes in the non-permafrost zone being ~8 times greater than emissions from lakes in the continuous permafrost zone throughout the ice-free season. Between-lake variability in CH_4 emissions was also greatest in the sporadic and non-permafrost zones (Fig 3.2b). Ebullitive emissions represented ~28% of the total C emissions from lakes where it was measured; a fraction that did not vary systematically across the transect. Ebullitive CH_4 emissions were generally highest in spring, while diffusive emissions were highest during summer or fall (Fig. A.3.3d and A.3.3c; Table A.3.3). Higher MAAT and water temperature were strongly related to higher diffusive CH_4 emissions, while higher base cation concentrations, decreasing lake depth, and lower concentrations of iron were weakly associated with higher emissions (Fig. 3.3a). The lack of a strong relationship between diffusive CH_4 emissions and lake size and depth, as is often found (Holgerson and Raymon, 2016), was not surprising as all studied lakes were relatively small, shallow (Table A.3.4), and likely non-stratified seasonally. The SEM analysis showed a significant relationship of MAAT with water temperature, which in turn influenced diffusive CH_4 emissions ($R^2 = 0.67$, Fischer C = 4.3, $P = 0.3$; Fig. 3.3c; see Methods). The apparent temperature sensitivity (Q_{10}) of diffusive CH_4 emissions across the transect to changes in water temperature was 16, substantially higher than the Q_{10} of ~4 that is

commonly found for the direct temperature response of CH_4 emissions within individual ecosystems (Yvon-Durocher et al. 2014).

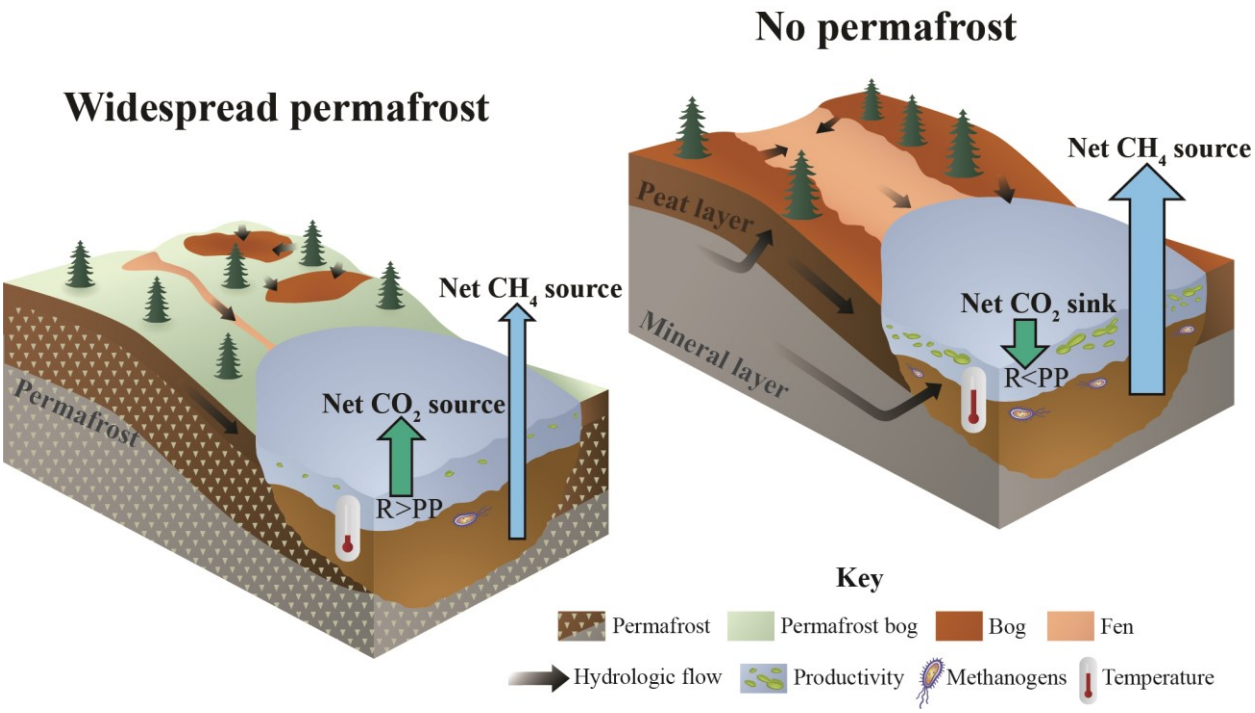

Figure 3.4 Influence of climate and permafrost conditions on greenhouse gas emissions from peatland lakes. Lakes in the continuous permafrost zone were found to be net sources of CO_2 and had low CH_4 emissions, while lakes outside the permafrost region were CO_2 sinks and had high CH_4 emissions. The absence of permafrost allows for increased hydrological connectivity to the surrounding landscape, potentially both deeper flow-paths through mineral soils and near-surface flow-paths through the surrounding peatlands. In this study, I found that lakes outside the permafrost region had generally higher pH and higher concentrations of ions, nutrients, and chlorophyll-a – suggesting that elevated primary productivity (PP) outweighs respiration (R) in lakes outside the permafrost region. Lake diffusive CH_4 emissions were primarily linked to lake water temperatures and were 8-times greater south of the permafrost boundary compared to within the continuous permafrost zone.

The high apparent temperature sensitivity of CH_4 emissions across the transect suggests the observed direct response to water temperature was amplified by additional factors, possibly shifts in microbial communities, redox conditions, or substrate quality (Rasilo et al. 2015). Of these, I found the least support for increasing CH_4 emissions being driven by shifts in substrate quality. Greater lake primary productivity in warmer climates was hypothesized to increase the availability of labile substrate for methanogenesis (Sepulveda-Jauregui et al. 2018), but I found only a weak relationship between CH_4 emissions and Chl*a* (Fig. 3.3a). Permafrost thaw was also hypothesized to increase the availability of labile substrates through thermokarst lake expansion. However, visual evidence of ongoing thermokarst lake expansion was found in all permafrost zones, and the highest CH_4 emissions were found in the non-permafrost zone. Lastly, it is possible that shifts in surrounding wetland and littoral vegetation towards denser, taller emergent macrophyte species in warmer climates could provide external sources of labile organic substrates and dissolved CH_4 to the lake (Emilson et al. 2018), although I did not observe any apparent links between shoreline vegetation and CH_4 emissions.

Several lines of evidence instead suggested that shifts in redox conditions and microbial communities contributed to the high climate sensitivity of CH_4 emissions. My assessment of microbial functional gene abundances showed that warmer climates were associated with a preferential increase of the methanogenesis marker methyl coenzyme A reductase (mcrA) over the methanotrophy markers, methane monooxygenase subunit A (mmoX), and particulate methane monooxygenase (pmoA) (Fig. 3.5). While gene abundances do not necessarily correlate with microbial activity (Freitag and Prosser, 2009), this trend was similar to that of observed CH_4 emissions (Fig. 3.2b). A lower abundance of mcrA in the northern lakes may be reflective of a temperature effect, wherein methanogenesis is suppressed under colder conditions. However, I also found evidence suggesting suppression of methanogenesis in the continuous permafrost zone through greater dominance of more thermodynamically favourable iron reduction. Lakes in the continuous permafrost zone trended towards higher concentrations of iron (Fe) in the water (Table A.3.4), and higher abundances of Fe(III) reduction marker genes (decaheme cytochromes) in sediments (Fig. A.3.4a). These conditions could also promote anaerobic CH_4 oxidation (Ettwig et al, 2016). Higher normalized counts of genes involved in iron acquisition and metabolism in colder climates were furthermore associated with a shift in enzymatic composition from hydrogenotrophic and acetoclastic methanogenesis towards the

stoichiometrically less productive methylotrophic form (Teh et al, 2007; Fig. A.3.4b). The mechanisms driving higher dissolved iron and abundances of decaheme cytochromes within the continuous permafrost zone is unclear, but the negative relationship between lake iron, pH, and base cation concentrations suggests that hydrological connectivity to deeper groundwater sources is important (Fig. 3.3a).

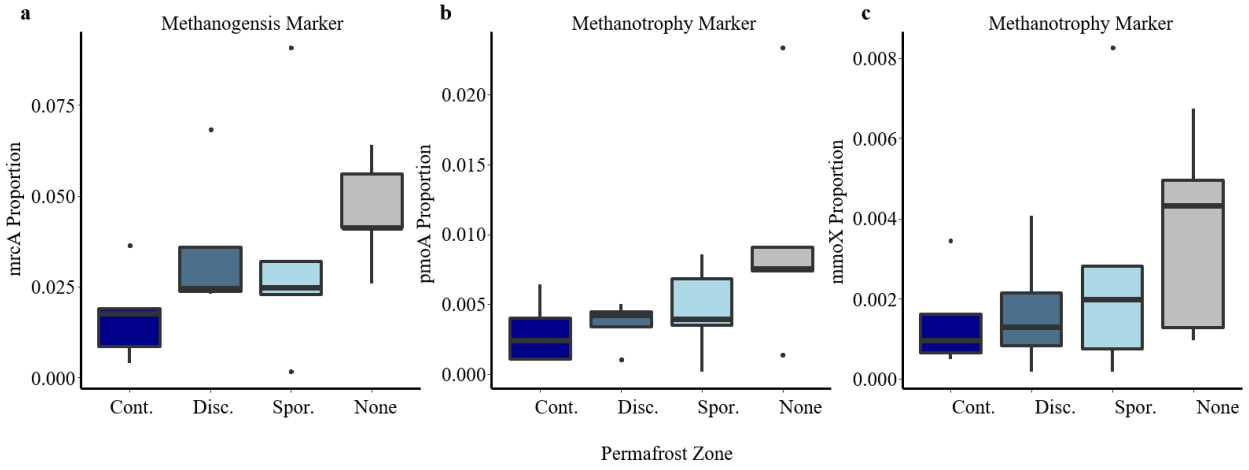

Figure 3.5. Trends in methane-related functional genes among permafrost zones. a) Relative abundance of the a) methanogenesis marker mcrA (methyl coenzyme A reductase) and methanotrophy markers b) mmoX (methane monooxygenase subunit-A) and c) pmoA (particulate methane monooxygenase) increased moving south along the transect. Boxplots represent median and quartile ranges for samples taken from each lake once mid-summer 2019 from the continuous (Cont.), discontinuous (Disc.), and sporadic (Spor.) permafrost zones, as well as south of the permafrost region (None). Note the different y-axis scales. Differences are not statistically significant, likely due to low sample sizes (n=5 for every zone except the discontinuous zone where n=4).

Similar to lake CO_2 emissions, this study suggests that peatland lake CH_4 emissions are likely to respond to climate change differently from other lake types; likely with a higher climate sensitivity driven by increasing CH_4 production in organic-rich sediments. Greater climate sensitivity of peatland lakes is noteworthy as their current CH_4 emissions currently are higher than emissions from most other boreal lake types (Kuhn et al. 2021). I note however that the observed CH_4 emissions in this study (average diffusion = 27 mg CH_4 m^{-2} d^{-1} and ebullition = 11 mg CH_4 m^{-2} d^{-1}) were in the low range of what has been reported previously for boreal peatland

lakes (diffusive interquartile range [IQR] = 9-101 mg CH_4 m^{-2} d^{-1}, ebullitive IQR = 3-89 mg CH_4 m^{-2} d^{-1}; Kuhn et al. 2021). Furthermore, the latitudinal trends in GHG emissions were more pronounced than found from lakes in other northern regions (Sepulveda-Jauregui et al. 2016; Serikova et al. 2019) Differences in lake CH_4 emissions between major peatland regions may be due to landscape characteristics and Holocene history which influence water chemistry and organic matter quality, but differences can also be due to climate and measurement methods (including timing, placement, and number of measurements). My study implements a methodology that constrains seasonal diffusive and ebullitive CH_4 fluxes from a large number of lakes across a permafrost transect – yielding robust findings.

3.5 Future peatland lake GHG emissions and net radiative forcing

I used an atmospheric perturbation radiative forcing model to assess the relative importance of projected shifts in peatland lake CO_2 and CH_4 emissions within the Taiga Plains region until 2100 (Frolking et al. 2006). This model considers the larger radiative forcing efficiency of CH_4 compared to CO_2 (Myhre et al. 2013), and the shorter atmospheric lifetime of CH_4 (Allen et al. 2018), however it does not account for current and future changes in carbon sedimentation rates (e.g Lundin et al. 2015). I assumed that emissions and the number of ice-free days will change linearly with increasing temperatures, based on the trends observed across the transect (Fig. A.3.4), and assessed changes in emissions based on the RCP Scenarios 2.6 and 4.5, adjusted for temperature amplification in the Taiga Plains (Fig 3.6a; IPCC, 2013; Government of the Northwest Territories, 2018). Peatland lakes <10 km^2 in size cover ~260,000 km^2 within the Taiga Plains (Olefeldt, Hovemyr, Kuhn, et al. 2021) and were estimated to emit 0.20 ± 0.08 Tg CO_2-C y^{-1} and 0.048 ± 0.01 Tg CH_4-C y^{-1} under the current climate. Emissions of CO_2 were estimated to decrease, on average, by 16.5% and 68% under the RCP 2.6 and 4.5 scenarios, respectively (Fig. 3.6b), while CH_4 emissions increased by 31% and 121%, respectively (Fig. 3.6b). Overall, increasing CH_4 emissions dominated the net radiative forcing under both RCP scenarios. Increasing CH_4 emissions added, on average, 5 and 15 fW m^{-2} by 2100 under RCP 2.6 and 4.5, respectively, which was only partially offset by reduced CO_2 emissions equivalent to -1 and -2 fW m^{-2}, respectively, when compared to the no-warming scenario (Fig. 3.6c).

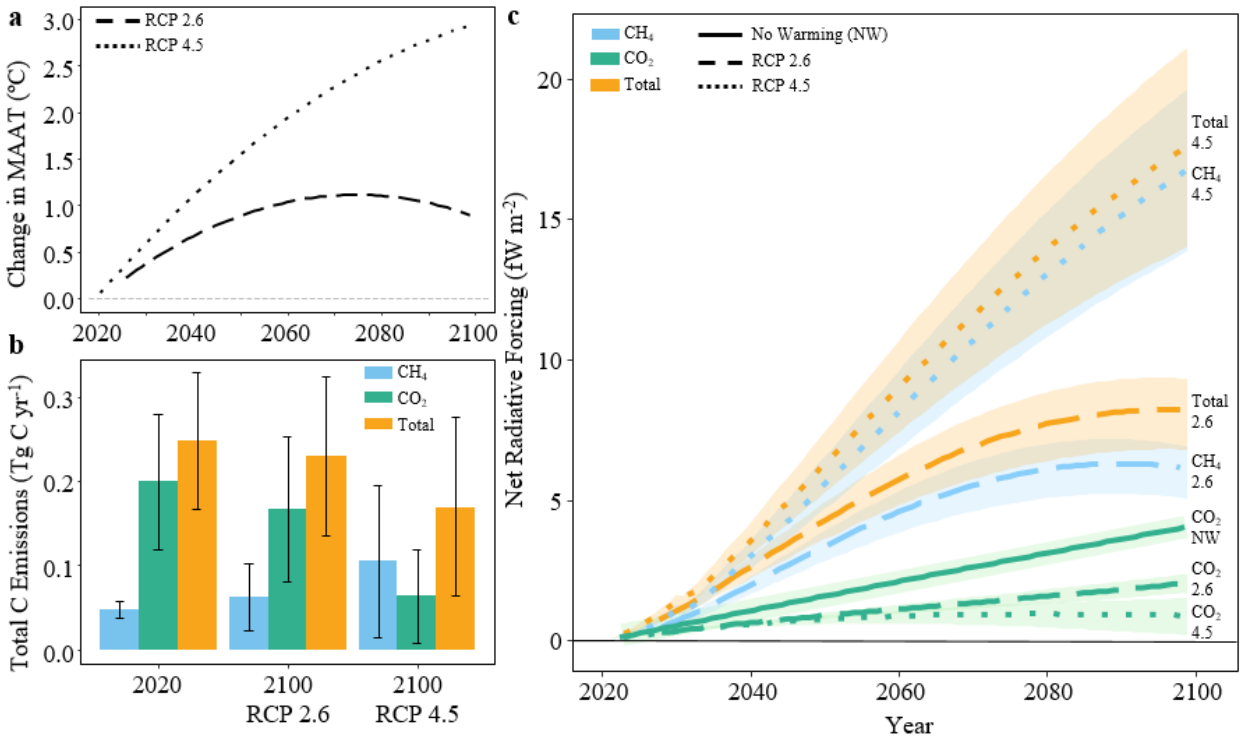

Figure 3.6. Net radiative forcing due to changing CO_2 and CH_4 emissions from Taiga Plains peatland lakes under RCP 2.6 and 4.5 scenarios. a) The global RCP 2.6 and 4.5 temperature scenario pathways for the 21st century have been multiplied by a factor of three to account for Arctic amplification in the Taiga Plains, western Canada (Government of the Northwest Territories, 2018). b) Modelled current and future CO_2 and CH_4 emissions and total emissions (CO_2 + CH_4) from peatland lakes on the Taiga Plains. Error bars represent 95% confidence intervals from the model output. c) The 21st-century radiative forcing resulting from altered lake CO_2 and CH_4 fluxes under the RCP 2.6 and 4.5 scenarios. Radiative forcing is referenced to the year 2020. A scenario of no warming is included, under which the net radiative forcing is only influenced by lake CO_2 emissions while steady CH_4 emissions are in equilibrium with the atmosphere. Radiative forcing due to altered lake CO_2 and CH_4 emissions is expressed as 10^{-15} fW divided by the total lake area of the Taiga Plains. The shaded areas represent the standard deviations from the flux models. Under both the RCP 2.6 and 4.5, I find that the net radiative forcing is dominated by increasing CH_4 emissions and only partly offset by reduced CO_2 emissions.

This study shows that climate change is likely to cause reduced CO_2 emissions but greatly increased CH_4 emissions from boreal peatland lakes over ice-free periods. My projections of future peatland lake CO_2 and CH_4 emissions are limited to the ice-free season, and rely on a space-for-time approach with inherent assumptions, but are likely to be robust. Further data are required for an assessment of ice-out emissions in the region; several studies have shown that ice-out emissions generally scale with emissions from the ice-free season (Wik et al. 2016a). Furthermore, I acknowledge that my measurements represent day-time conditions and that night-time conditions may lead to higher respiration in some lakes and may alter the net ice-free estimates of CO_2 exchange (Gómez-Gener et al. 2021). However, the results still highlight key mechanistic differences between CO_2 and CH_4 dynamics in lakes across the study region. Water chemistry and microbial community data allowed for the identification of processes likely responsible for the observed, and opposing CH_4 and CO_2 emissions trends along the transect. I showed that peatland lake CO_2 and CH_4 emissions were driven by different processes and thus not strongly inter-correlated. Both the direct effect of warming and the indirect effect of permafrost thaw was important, where the absence of permafrost in warmer regions allowed for greater variability in lake hydrological connectivity and thus also greater variability in CO_2 and CH_4 emissions. The influence of permafrost thaw on lake productivity and reduced CO_2 emissions, and the extremely high-temperature sensitivity of CH_4 emissions, are likely associated with characteristics of peatland lakes and the hydrology of their surrounding landscape. While further data from other major peatland regions are needed to support my findings, my study strongly suggests that peatland lakes, which make up 18% of all northern lake area (Olefeldt, Hovemyr, Kuhn,s et al. 2021), need to be considered separately from other lake types when assessing the impact of climate change on future greenhouse gas emissions.

3.6 Methods

3.6.1 Sampling sites

The studied region includes Taiga Plains and Boreal Plains ecozones of the Interior Plains in boreal western Canada, an area that extends from 70º N to 56º N. This region encompasses the lands of the Metis, Dene Tha', Woodland Cree, Big Stone Cree in Alberta and the lands of the Inuvialuit Settlement Region, Gwich'in Settlement Area, and the Dehcho of the Northwest Territories. The region is characterized by thick peat deposits and generally flat

topography (Zoltai et al. 1993; Hugelius et al. 2020) and has a subhumid to dry and cool climate. The region was previously glaciated and is dominated by glacial and glaciolacustrine surficial geologies (Government of Canada 2014). Across the latitudinal transect, the ecosystems include similar tree species including aspen (*Populus tremuloides*), balsam poplar (*Populus balsamifera*), white spruce (*Picea glauca*), jack pine (*Pinus banksiana*), larch (*Larix laricina*), and black spruce (*Picea mariana*).

I sampled 20 lakes located in four sites within the study region (Fig. 3.1), spanning across different climatic and permafrost zones (Table A.3.4). At each site, I chose five study lakes that had surface areas between 0.3 to 10.1 hectares (ha). Physical characteristics for each lake can be found in Supplementary Table 3. Sampling took place at all sites during the ice-free seasons in 2018 and 2019. I designed the sampling campaigns to capture seasonal patterns at each site from just after ice-out to just before ice on. Each lake was sampled a minimum of 7-12 times to get a statistically accurate representation of annual diffusive greenhouse gas emissions (Wik et al. 2016b). At the northernmost site of Fort McPherson, each lake was sampled 7-9 times due to logistical limitations of getting to the sites. Exact sampling dates can be found in the metadata (https://doi.org/10.7939/DVN/LF4WDG).

3.6.2 Water sampling

Surface water chemistry was measured from a boat at the location of flux measurements and the center of the lakes. At each lake, I sampled dissolved CH_4 concentrations using a headspace method (Karlsson et al. 2013) and measured dissolved oxygen, specific conductivity, pH, and temperature in the top 10 cm using a handheld water monitor (Yellow Springs Instrument ProDO). Water samples for dissolved organic carbon (DOC), total dissolved nitrogen (TN), and specific ultraviolet absorbance ($SUVA_{254}$) were sampled from the center of the lake following protocols outlined in Burd et al. 2018. Concentrations of DOC and TN were measured by a TOC-L combustion analyzer with a TNM-L module (Shimadzu, Kyoto, Japan). SUVA absorbance at 254 nm was measured from 200 to 700 nm (UV-1280, UV-VIS Spectrophotometer, Shimadzu Corporation, Japan) and was corrected by Milli-Q water blanks. I calculated SUVA by first correcting decadal absorbance at 254 nm (cm^{-1}) for interference by Fe as outlined by Weishaar et al., (2003).

Water samples for ion concentrations were filtered and frozen on the day of sampling and kept frozen until analysis. Anions were measured using Ion chromatography (Dionex Ion chromatography DX 600, Thermo Fisher Scientific, US). Cations were measured by ICP-OES (iCAP6300 Duo, Thermo Fisher Scientific, US). Samples for Chlorophyll-*a* analysis were collected using opaque Nalgene bottles. Duplicate samples for each lake were refrigerated and vacuum filtered on the day of collection using 47-mm diameter, ethanol-rinsed GF/F filters Grade GF/F, Whatman). The filters were then placed in petri dishes, wrapped in aluminum foil, and were frozen immediately until analyses at the University of Alberta Biogeochemical Analytical Service Laboratory using a Shimadzu RF-1501 spectrofluorophotometer.

3.6.3 Microbial sampling

Between 28 July and 31 August 2019, I collected three top layer (~15 cm) sediment samples from the edge of each lake where flux measurements were taken. Samples were pooled per lake and DNA was extracted in duplicate from 0.65 g dry sediment per sample using the DNeasy PowerSoil kit (QIAGEN N.V., Hilden, Germany). Sequencing libraries were prepared from 250 ng DNA per sample with the NEBNext Ultra II FS DNA Library Prep kit according to the manufacturer's instructions (New England Biolabs, Ipswich, MA, USA). Samples were sequenced paired-end (300 cycles) using a NextSeq 500/550 High Output Kit v2,5 (Illumina, Inc, San Diego, CA, USA). Contamination was negligible, as assessed with both negative (nuclease-free water) and positive (ZymoBIOMICS Microbial Community Standard, Zymo Research Corporation, Irvine, CA, USA) controls. I estimated the abundance of functional marker genes involved in methanogenesis: methyl coenzyme A reductase (mcrA) and methanotrophy: methane monooxygenase subunit A (mmoX) and particulate methane monooxygenase (pmoA), expressed relative to the total number of SILVA 16S hits for each sample with GraftM (Boyd et al, 2018). Whole-metagenome functional profiling relative to the SEED database (used to identify decaheme cytochrome genes and methanagenesis enzyme composition data) was performed with SUPER-FOCUS (Silva et al, 2015), and reads were normalised using the geometric mean of pairwise ratios (Chen et al, 2018). I were unable to extract enough DNA sample from one lake in the discontinuous zone (W1) to perform analysis.

3.6.4 Greenhouse gas fluxes

Methane and CO_2 fluxes were measured with small, lightweight chambers (volume = 13.55 L, area = 0.062 m^2), covered in reflective tape to keep the inside of chambers from warming. All chamber measurements were taken on the edge of the lakes 1-2 meters from the shore to avoid littoral vegetation. While there is evidence for both under- and over-estimating lake fluxes based on near shore measurements (Shilder et al. 2013; Matveev et al. 2016), all of the study lakes were surrounded by black spruce trees near the lake edge, providing similarly sheltered wind conditions and comparable environments for comparison across the transect. The chambers were connected to a portable greenhouse gas analyzer (Los Gatos Research, California) in a closed path that recorded the linear change in GHG concentrations within the chamber over time. On each sampling occasion, 3-4 chamber flux measurements of 2-5 minute durations were taken and then averaged to estimate daytime flux estimate. Typically, each lake was measured on 1 to 3 days per trip and 7-12 days total. Fluxes were calculated using linear regression (slope) of the change in GHG gas concentration (ppm) inside the chamber over time and the ideal gas law, air temperature, and atmospheric pressure at the time of sampling (Equation 1). Negative slopes for CO_2 measurements were interpreted as CO_2 uptake. CH_4 slopes with R^2 less than 0.90 were excluded in the daytime average slope calculations.

Equation 1: $Flux = S * (\frac{P*V}{R*T*A}) * M * C$

where S is the slope from the linear change in gas concentrations within the chamber over time (atm $minute^{-1}$), P is barometric pressure (atm), R is the universal gas constant (L atm K^{-1} mol^{-1}), V is the volume of the chamber (L), T is the average air temperature inside the chamber (K), A is the area of the chamber (m^{-2}), M is the molar mass of the CH_4 or C-CO_2 (mol mg^{-1}) and C is a conversion factor to convert from per minute to per day.

I measured ebullitive CH_4 and CO_2 fluxes using bubble traps. The traps were built using inverted funnels (area = 0.073 m^2) equipped with a syringe and stopcock. Due to the intense and time-consuming nature of installing and sampling bubble traps in remote locations, three out of five lakes at each site were equipped with bubble traps, including three traps along the lake edge and three traps in the lake center. Water column depths below the traps ranged from 0.5 meters (L5/L1 edges) to 2.5 meters (W1/F2 centers; Table A.3.4). Traps were set at the beginning of each trip and were sampled 2-4 days later. Accumulated gas bubbles were collected manually

using syringes, and the gas volume was recorded. To obtain the concentrations of the bubbles I reset the traps and disturbed the sediments, immediately collecting 30 ml of sample volume, stored in 20 ml glass vials sealed with rubber septa. This was done to avoid any potential errors associated with oxidation effects on gases that sit in the traps over the 2-4 day period. Samples were analyzed within one to two weeks after collection at the University of Alberta using a SRI-8610C gas chromatograph equipped with an FID detector. I calculated the ebullitive flux as outlined by Wik et al. (2013).

3.6.5 Upscaling

I estimated current lake CH_4 and CO_2 emissions from the Taiga Plains by multiplying the area of small and midsized peatland lakes from the Boreal Arctic Wetland and Lake Database (BAWLD; Olefeldt, Hovemyr, Kuhn, et al. 2021) by the mean CH_4 and CO_2 flux specific to the MAAT reported for each 0.5 x 0.5 degree grid cell of the database and the number of ice-free days. Daytime diffusive CH_4 emissions were multiplied by a diel correction factor (0.70) to account for diel patterns in CH_4 emissions between day and night (i.e. "24-hour fluxes"; Sieczko et al. 2020). Mean CH_4 and CO_2 emissions and the number of ice-free days were calculated based on linear relationships between mean annual temperature, CH_4 or CO_2 flux, and ice-free days observed across the latitudinal transect (Fig. A.3.5). Total mean CH_4 emission (diel corrected diffusion+ ebullition) was used in upscaling. Carbon dioxide emissions were not corrected for nighttime-factor, but evidence suggests diel patterns in CO_2 respiration are less, bordering negligible for darker, DOC-rich waters (Gómez-Gener et al. 2021) so diel patterns are likely minimal for the lakes that are positive CO_2 emitters. Furthermore, daylight hours across the transect are long, with closer to full days of sunlight throughout most of the summer period in the northern sites. Thus, applying the diel factor for daily CH_4 emissions is likely a conservative estimate. Though I do acknowledge that the lakes that experience net uptake of CO_2 during the daytime may be small sinks at nighttime- especially for periods closer to fall and spring. I only scaled across grid cells within the Taiga Plains that were within the temperature MAAT range of the study and not the entire extent of the Interior Plains. See Data Availability for information on the land cover database.

3.6.6 Radiative forcing

I used a radiative forcing model that applies simple impulse-response functions and assumed the same warming potential timeframes for CH_4 and CO_2 as outlined in Joos et al. (2013). I modeled the carbon pools for CH_4 and CO_2 and mixed atmosphere assumptions following the methods and code by Gunther et al. (2020). While CH_4 was modeled as one pool with a simple exponential decay rate, CO_2 was split into five pools with varying decay rates (Frolking et al. 2006). I did not consider climatic effects of CO_2 from CH_4 oxidation per Myhre et al. 2013. I compared the radiative forcing trajectories under two global temperature change scenarios (RCP 2.6 and RCP 4.5; IPCC's AR5). To account for the effects of Arctic temperature amplification observed across the Northwest Territories, I multiplied the projected changes in average global temperatures for each RCP by three, which is more conservative than the most recent analysis by the Government of the Northwest Territories which suggest that the region could be warming four times faster (NWT Government, 2018). I did not include RCP scenario 8.5 because the projected temperature increases are greater than the range of temperatures experienced across the study transect (range = 9 ˚C; Table A.3.1). Prior to 2020, I performed a simplified model spin-up, starting in 1900 (as in Turetsky et al. 2020). In the spin, we applied current CO_2 and CH_4 fluxes at a constant rate over a 120 year period (Fig. A.3.6). The purpose of the simplified model spin-up is to bring the model close to an equilibrium point (Turetsky et al. 2019). I then used the year 2020 as a reference point for changes in instantaneous net radiative forcing (Helbig et al. 2017). The model accounts for future changes in CO_2 and CH_4 emissions and the number of ice-free days associated with warming (Fig. A.3.5). Uncertainty for the radiative forcing model was calculated based on one standard deviation of the scaling model coefficients.

3.6.7 Statistical analysis

All statistical analyses were performed in R statistical software (Version 3.8, RStudio Inc, www.r-project.org). Predictor variables for all models were log-transformed for statistical analyses except water temperature, DOC, and pH. Daytime GHG emission comparisons between zones were performed using mixed effects models (R Package 3.3.3; Lme4 Package Bates et al. 2019) with the fixed effect of Permafrost Zone and random effects of individual lake to account

for repeated measures, and season to account for variation in emissions between early, mid, and late-season emissions (Fig. A.3.3; Table A.3.3). Each mixed model for CO_2, diffusive CH_4, and ebullitive CH_4 was compared to the respective null model, which only included the random effects, using ANOVA. Individual pairs were then compared using a post-hoc, non-parametric t-test (Barroti adjustment). For simple linear regression, structural equation modeling (SEM), and redundancy (RDA) analysis, we used mean values over the entire sampling period and excluded three outlier lakes from analysis in the SEM. The outlier points include lakes L2, L5, and W4 (See Table A.3.4 for more information on lake IDs). The lakes were designated as outliers due to extreme differences in nutrient concentrations, solute chemistry, and CO_2 emissions, respectively (Fig. A.3.7). The RDA was performed using the vegan package's *rda()* function with CO_2 and diffusive CH_4 emission set as the response variables. Methane and CO_2 fluxes were log-transformed to normalize the data. Finally, changes to the functional composition of microbial communities were tested using permutational multivariate analysis of variance with vegan's *adonis2* function based on a Euclidean distance matrix.

I used structural equation models (SEMs) to quantify the direct and indirect effects of MAAT on environmental variables and average daytime CO_2 and CH_4 emissions (R Package, piecewiseSEM; code adapted from St. Pierre et al. 2019). The SEM defines causal links between variables of interest through a system of predefined interconnected linear equations (Shipley et al. 2009). It then tests the significance of individual paths and the entire model as a whole. The significance of individual paths is determined by a P-value < 0.05. However, the model as a whole is defined as a good fit if $P > 0.05$ from a Fisher's test of directed separation, as this means that the proposed model structure adequately captures the variability in the model variables and the designated paths (Shipley et al. 2009). Designated model paths must be supported by known links between variables based on prior work. For CO_2, the links and associated references are 1) Chl*a* (as a proxy for productivity) and CO_2 (Engel et al. 2020), 2) phosphate and lake productivity (Carpenter et al. 2001; Schindler et al. 2009), 3) DOC and productivity (Kissman et al. 2013; Klug et al. 2002), and 4) MAAT and phosphate and DOC (Laudon et al. 2012; Weyhenmeyer and Karlsson, 2009). For CH_4, the links and prior work included 1) water temperature and CH_4 flux (Zeikus et al. 1976; Yvon-Durocher et al. 2014; Del Sontro et al. 2016), 2) water temperature and lake depth (Fang and Stefan, 1999), and c) MAAT

and water temperature (Schneider et al. 2010). Iron was not included in the CH_4 SEM because clear links between permafrost zone and higher dissolved iron could not be established.

4. Extreme methane emissions from a peatland thermokarst lake edge driven by millennial-aged peat and released through ebullition

Abstract

Peatland lakes are abundant across the northern boreal region and are sources of methane (CH_4) and carbon dioxide (CO_2) fluxes. Warming at high latitudes has led to accelerated rates of permafrost thaw and subsequent carbon fluxes from thaw impacted lakes. I examined the effects of permafrost thaw on CH_4 and CO_2 fluxes from one peatland lake in the discontinuous permafrost location of western Canada. Average CH_4 fluxes were 41 ± 14 mg CH_4 m^{-2} d^{-1} and 114 ± 77 mg CH_4 m^{-2} d^{-1} for diffusion and ebullition, respectively. The highest ebullitive fluxes were from the thaw edge (236 ± 61 mg CH_4 m^{-2} d^{-1}) and the highest diffusive fluxes were from the thaw edge and stable edge (~57 and 46 mg CH_4 m^{-2} d^{-1}, respectively). CO_2 was a minor component of total ebullitive fluxes (~7%) and diffusive measurements suggest the lake is a net sink of CO_2. Radiocarbon (^{14}C) analysis of the sediment bubbles showed that ^{14}C-CH_4 from the thaw edge is older (~1211 ^{14}C years BP) than the stable edge and center (modern and 102 ^{14}C years BP, respectively), suggesting the CH_4 from the thaw edge is largely sourced from old permafrost carbon. Radiocarbon ages for CO_2 were similar to ^{14}C-CH_4 ages across the lake locations. My results suggest small peatland lakes throughout western Canada may be hotspots for CH_4 fluxes, particularly ebullitive fluxes, and that permafrost thaw may further enhance ebullitive fluxes and the release of old carbon from thaw edges.

4.1 Introduction

Small peatland lakes are globally important sources of greenhouse gases (GHG), methane (CH_4), and carbon dioxide (CO_2) (Holgerson et al. 2016; Wik et al. 2016a; Serikova et al. 2018). Peatland lakes are particularly abundant throughout the circumpolar north where organic-rich northern boreal peatlands are abundant (Messager et al. 2016; Hugelius et al. 2020; Olefeldt, Hovemyr, Kuhn, et al. 2021; Muster et al. 2019). Greenhouse gas fluxes from northern peatland lakes are expected to increase as temperatures warm, leading to higher microbial activity and the thawing of perennially frozen ground (i.e. permafrost), which makes previously stored organic matter (OM) available for decomposition (Walter Anthony et al. 2018). However, there are still large uncertainties related to the magnitude of annual CH_4 fluxes from northern lakes (Wik et al. 2016a; Saunois et al. 2020; Kuhn et al. 2021); especially in regard to the magnitude of CH_4 emissions from thermokarst peatland lakes. Some of the uncertainty can also be attributed to poor representation of flux estimates through limited sampling frequencies and spatial representation across lakes (Wik et al. 2016b; Jansen et al. 2020; Kuhn et al. 2021). Few studies provide both temporally and spatially high-resolution flux data for small, organic-rich peatland lakes (Kuhn et al. 2021).

Methane is predominantly produced in the sediments of lakes through the microbial breakdown of OM and is transported from lake sediments to the atmosphere through plant-mediated diffusion, ebullition (CH_4 bubbles), or diffusion from the water column to the atmosphere (Bastviken et al. 2004). In lakes without emergent vegetation, ebullition often accounts for the majority of CH_4 fluxes (Walter Anthony et al. 2016; Wik et al. 2016a) and is predominately controlled by OM availability, water depth, sediment temperature, solar radiation, and changes in pressure (Wik et al. 2013; Del Sontro et al. 2016; Aben et al. 2017). However, estimates of ebullitive fluxes are poorly represented for most lakes, particularly peatland lakes (Kuhn et al. 2021), due to the time-consuming and labor-intensive ebullition measurements (see Wik et al. 2013 and Wik et al 2016b). While diffusive CH_4 fluxes are generally easier to measure in the field and are therefore more commonly measured (Kuhn et al. 2021), diffusion alone is likely under-represents net CH_4 fluxes because most CH_4 diffusing through the sediment and water column does not make it to the atmosphere, and is instead consumed through CH_4 oxidation and converted to CO_2 (Bastviken et al. 2002). Further, diffusive fluxes are often

sourced from different parts of the sediment compared to ebullitive fluxes (Gonzales Moguel et al. 2021). Diffusive CH_4 fluxes reaching the atmosphere are largely controlled by water column depth and turbulence across the water-atmosphere interface (MacIntyre et al. 2020). To accurately represent the magnitude of CH_4 fluxes from lakes, both ebullition and diffusion should be considered.

Carbon dioxide is also emitted to the atmosphere from northern lakes and is predominantly sourced from the breakdown of terrestrial OM and inputs of inorganic carbon (i.e. dissolved CO_2) from surrounding terrestrial ecosystems (Prairie and Cole 2009; Weyhenmeyer et al. 2015). However, internal lake production of CO_2 through anaerobic respiration, autotrophic respiration, or the oxidation of CH_4 can dominate CO_2 evasion in some northern lakes (Bogard et al. 2019). Lakes with higher nutrient statuses can also sequester CO_2 from the atmosphere through primary productivity facilitated by pelagic algae or benthic macrophytes (Del Georgio and Peters, 1994; Pachecho et al. 2014). Net evasion of CO_2 from lakes thus depends on the balance of external inputs of inorganic carbon, within-lake respiration, and primary productivity. Most boreal peatland lakes are oligotrophic and receive large inputs of terrestrially derived pCO_2 and thus are considered to be net sources of CO_2 (Weyhenmyer et al. 2015; Hastie et al. 2018).

Rapid warming in northern ecosystems is causing accelerated rates of permafrost thaw, leading to the development of thermokarst lakes and the expansion of lakes already present across the landscape (Olefeldt et al. 2016; Turetsky et al. 2019; Walter Anthony et al. 2021). Permafrost thaw along lake edges mobilizes previously frozen soil OM into lakes, where it is subsequently inundated and then potentially mineralized and released to the atmosphere as CH_4 or CO_2 (Walter et al. 2006; Schuur et al. 2008). Thermokarst lakes have been well documented as hot spots of CH_4 and CO_2 flux derived from old permafrost carbon, particularly from actively thawing lake edges with yedoma sediments (i.e. Pleistocene Aeolian soils with high content of poorly degraded organic matter; Walter et al. 2006; Tank et al. 2009; Walter Anthony et al. 2016; Dean et al. 2020; Walter Anthony et al. 2021). High CH_4 fluxes from yedoma thaw lakes have been linked to the high bioavailability of OM in the sediments and the underlying, carbon-rich loess permafrost soils (Heslop et al. 2015), resulting in millennial old CH_4 release, as determined through from radiocarbon dating techniques (Schuur et al. 2016). Studies in non-yedoma permafrost soils also indicate that the response of CH_4 and CO_2 fluxes and age of carbon emitted to permafrost thaw is highly dependent on the history and quality of OM stored in

permafrost (Treat et al. 2016; Elder et al. 2018; Estop-Aragonés et al. 2020). The distribution of yedoma and non-yedoma soils in the landscape may be thus important to accurately represent lake GHG fluxes following thaw. Yedoma lakes are not widespread throughout the northern region (~3.5 % of all northern lake area; Olefeldt, Hovemyr, Kuhn et, al. 2021), but account for most studies on thaw effects on lake GHG fluxes (e.g. Walter et al. 2006; Walter et al. 2010; Walter Anthony et al. 2018; Heslop et al. 2020; Dean et al. 2020, etc.). In contrast, little is known about GHG fluxes and ^{14}C ages from peatland thermokarst lakes despite peatland lakes covering ~18% of the northern aquatic landscape (Olefeldt, Hovemyr, Kuhn et, al. 2021). Of the handful of studies that have looked at ^{14}C ages of GHGs and carbon in peatland thaw lakes and ponds, ebullitive CH_4 tends to be older than ebullitive CO_2 and diffusive CH_4 and CO_2, but younger than lake dissolved and particulate organic carbon (Bouchard et al. 2015; Matveev et al. 2016; Gonzalez Moguel et al. 2021; Prėskienis et al. 2021). However, given the heterogeneity of peatland formation and composition across the north (Hugelieus et al. 2020), there is a need for more studies from peatland lakes and ponds to better constrain the magnitude of CH_4 emissions and the potential effect of permafrost thaw on the release of old carbon.

This study focuses on a small peatland lake in the southern Taiga Plains region of western Canada wherein a large portion of the permafrost has developed epigenetically and has a cyclical lifetime of aggradation and degradation (Zoltai et al. 1993; Pelletier et al. 2017; Heffernan et al. 2020). During epigenetic aggradation, permafrost is initially absent, but shifts in the climate towards cooler conditions and the development of thick peat layers eventually facilitate downward freezing into the soil (Zoltai et al. 1993). As a result, deeper, older peat is present long before permafrost develops and peat is thus exposed to microbial mineralization for hundreds to thousands of years before freezing. Therefore, epigenetic processes may lead to more recalcitrant, less labile (i.e. a lower "quality" of carbon) OM, mainly in the form of sphagnum mosses, that is not as easily mineralized post-thaw (Treat et al., 2014; Heffernan et al. 2020), potentially leading to lower CH_4 fluxes from peatland thaw lakes compared to yedoma lakes. Alternatively, despite a potentially lower OM quality in permafrost peatlands, the large quantity of OM made available for mineralization in peatlands may favor high CH_4 fluxes post-thaw (Krüger et al. 2014). In summary, our understanding of the consequences of permafrost thaw on the magnitude of CH_4 fluxes from peatland lakes remains highly unconstrained.

Here I assessed the spatial and temporal patterns of CH_4 and CO_2 fluxes from a small peatland lake in the discontinuous permafrost location of the Taiga Plains. I focus on the comparison of fluxes from the center of the lake with two edge locations, including a lake edge with active thermokarst and one which showed no signs of recent thermokarst. I hypothesized that CH_4 and CO_2 fluxes across the entire lake would be relatively high compared to other northern lakes due to the lake's relatively small size, shallow water column, and thick, organic-rich peat sediments. I further hypothesized that net fluxes of CH_4 and CO_2 would be higher and sourced from older carbon at the lake's thaw edge due to the mobilization of "old" (i.e. centennial- to millennial-aged carbon), previously frozen OM made recently available for microbial processing through permafrost thaw. To address my hypotheses, I combined measurements of CH_4 and CO_2 ebullition and diffusion across the entire lake extent over three ice-free seasons with sediment concentration profiles, sediment macrofossil analysis, ex-situ potential CH_4 and CO_2 production incubations and, ^{14}C dating to estimate the age of CH_4 and CO_2 released through ebullition across the lake.

4.2 Methods

4.2.1 Site Description

The study lake ("Eli") is located near Lutose, Alberta, Canada (59.5°N, 117.2°W; Fig. 4.1.a) in the discontinuous permafrost zone of the Mackenzie River Basin in the Taiga Plains ecozone (Brown et al., 2002; Heginbottom, Dubreuil, and Harker, 1995). The general study region encompasses the lands of the Metis and Dene Tha'. The mean annual temperature of the region is -1.8 C and the mean annual precipitation is ~391 mm (Climate-Data.org, 2021), comprising a sub-humid and cool climate. The study region is characteristic of the broader Taiga Plains Ecoregion (Government of the Northwest Territories, 2007), wherein peatland complexes are comprised of a mosaic of elevated permafrost peat plateaus dominated by black spruce (*Picae mariana*), Labrador tea shrubs (*Rhododendron groenlandicum*), and lichens (*Cladonia spp*.) which are adjacent to saturated, permafrost free wetlands and lakes. Peat initiation occurred ~10,000 years ago (Pelletier et al. 2017). Permafrost in the local area is isolated to peat plateaus and developed between 1000 and 2000 years ago (Loisel et al., 2014; Pelletier et al., 2017; Heffernan et al. 2020). The average peat depths in the region vary from 2-6 m (Vitt, Halsey, and Zoltai, 2000). Furthermore, peatland lakes are abundant throughout the Taiga Plains landscape

(Olefeldt, Hovemyr, Kuhn, et al. 2021) and there is evidence that many of these lakes are expanding due to thermokarst activity (Coleman et al. 2015).

Eli Lake is a small (surface area = 0.005 km^2; Fig. 4.1b) and shallow (water depth = 1 m) lake underlain by limnic (i.e. sediment composed of OM from terrestrial inputs and autochthonous production) and peat sediments (i.e. peat that formed before the development of the lake). The lake is bordered by elevated peat plateaus underlain by permafrost and also by wetland vegetation (i.e. *carex* and *eriophorum spp*.) in some locations. Where the lake is bordered directly by elevated peat plateaus, physical slumping of the shoreline is observed. Benthic, non-emergent, macrophytes are present sporadically throughout the lake.

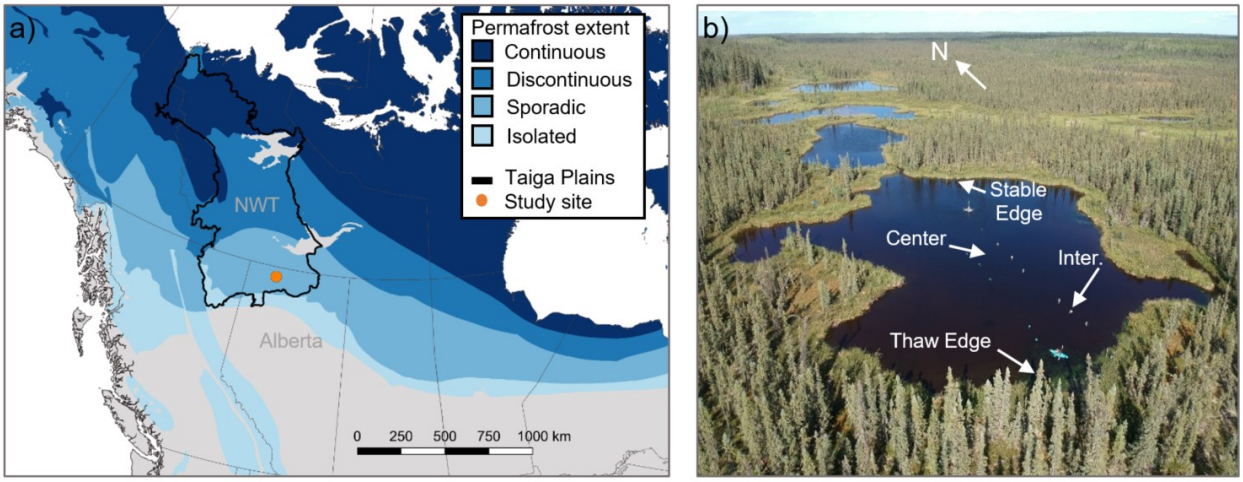

Figure 4.1. Study location. a) Study location in the southern Taiga Plains ecozone. b) Aerial photo of Eli Lake. The lake sampling locations are indicated in white text with white arrows. Inter. = Intermediate location. The white arrow and N symbol represent the orientation of the photo. The surface area of the lake is 0.005 km^2. The small blue object near the southern edge of the lake is a kayak for scale. Permafrost extent from Brown et al. 2002. Continental borders base layer from Wessel et al. 1996

4.2.2 Flux measurement timeframe

Sampling took place over the ice-free periods in 2017, 2018, and 2019. In 2017, sampling started in May and ended in early September for a total of 10 diffusive CH_4 sampling days and seven ebullitive sampling times (24 days of bubble trap deployment in total). In 2018 there were

three sampling campaigns (May, July, August) for six diffusive CH_4 and CO_2 sampling days and three ebullitive sampling points (10 days of bubble trap deployment in total). In 2018, diffusive CH_4 fluxes were not measured from the intermediate lake location (between the thaw edge and center location, see Sect. 4.2.3). In 2019 there were three additional sampling campaigns in May, June, and September in which only diffusive CO_2 and surface water chemistry were measured (six diffusive CO_2 sampling days). For statistical analysis, the September sampling trip in 2017 and the one day of September samples from 2019 were included with the August trips. In August 2017, the thaw edge was sampled less frequently than the other lake locations due to shallow water depths limiting access to the bubble traps from the kayak or shoreline without disturbing the sediments. A detailed sampling schedule can be found in the appendix (Table A.4.1).

4.2.3 Ebullitive fluxes

A sampling transect was established across the lake in 2017. The transect included four locations: a thaw-impacted thermokarst edge ("thaw edge"), an intermediate location between the thaw edge and center, the lake center, and a stable edge where the lake is bordered by wetland vegetation (predominantly sedges) instead of permafrost peat plateau and associated vegetation (predominantly shrubs and black spruce trees). The thaw edge was identified by signs of permafrost thaw including slumping and tilted trees next to the adjacent permafrost plateau. Three inverted funnels ("bubble traps"; polyethylene, area = 0.073 m^2) and three floating chambers (volume = 13.55 L, area = 0.062 m^2) were deployed in each of the four lake locations to measure ebullitive and diffusive fluxes, respectively. The bubble traps and floating chambers were accessed via kayak or shoreline. Ebullitive fluxes (bubble fluxes) were measured following Wik et al. (2013). Traps were set at the beginning of each trip and were sampled 2 to 4 days later. Accumulated gas from bubbles was collected manually using syringes, and the gas volume was recorded. To measure the CH_4 and CO_2 concentrations of the bubbles I reset the traps and disturbed the sediments, immediately collecting 30 mL of gas sampled, stored in 20 mL glass vials sealed with rubber septa. This procedure aimed to avoid any potential errors associated with oxidation effects on gas samples that remain in the traps over the 2-4 day collection period. Concentrations of CH_4 and CO_2 in the bubble samples were collected once a month, therefore in some instances, bubble gas concentrations were not measured on every sampling occasion (Table A.4.1). Gas samples were analyzed within seven days after collection at the University of

Alberta using a SRI-8610C gas chromatograph equipped with an FID detector. To obtain CH_4 and CO_2 ebullition rates, the bubble gas concentrations were applied to the volume of bubbles collected over the sampling period (Wik et al. 2013).

4.2.4 Net CH_4 fluxes and diffusive fluxes

I measured diffusive fluxes from the lake using two approaches- floating chambers and dissolved CH_4 concentration-based estimates. Floating chambers were used to measure diffusive and net CH_4 fluxes (Bastviken et al. 2004). The chambers were deployed and sampled after 20-28 hours. This was done once or twice per sampling trip. The floating chambers were not equipped with bubble shields (Jansen et al. 2019) and thus collected CH_4 from both diffusion and ebullition (i.e. "net" emissions). To separate the contributions of ebullitive and diffusive flux in the chambers, I calculated the experimentally derived piston gas exchange velocities (k_{600} values; Jahne et al. 1987). k_{600} values that were two times higher than the minimum calculated k_{600} value were considered to be impacted by ebullition (Bastviken et al. 2004; see below for more information on k_{600} calculations).

I modeled diffusive CH_4 flux using dissolved CH_4 concentrations at the surface of the water column, the dissolved gas concentration at equilibrium with atmospheric CH_4, and an estimate of the k_{600} value This method avoids the contribution of ebullition and estimates k_{600} values based on wind speed following Cole and Caraco (1998; eq. 4.1).

Equation 4.1: $k_{600} = 2.07 + 0.215 \times U_{10}^{1.7}$

Where k_{600} is the gas exchange coefficient (cm hr^{-1}) and U_{10} is the wind speed (m s^{-1}) at a 10 m height. Notably, the meteorological station wind meter on the study lake is positioned at two meters, therefore a conversion factor was used to scale wind speed from two to 10 meters (Smith et al. 1985). Wind speeds were averaged over three-hour and then over 24-hour periods. A detailed description of the wind-based modeling approach used, including converting between k_{600} and specific k_{CH4} values can be found in Laurion et al. (2011).

Diffusive CO_2 fluxes were directly measured in 2018 and 2019 with a small, lightweight chamber (volume = 13.55 L, area = 0.062 m^2), connected to a portable greenhouse gas analyzer (Los Gatos Research, California) in a closed path that recorded the linear change in CO_2

concentrations within the chamber over time. The chambers were covered in reflective tape to prevent warming in the chambers. Due to the limitations of deploying the instrument at the center of the lake diffusive CO_2 fluxes were only measured at the thaw edge and stable edge, approximately 0.5 to 1 meters from the shore to avoid littoral vegetation. On each sampling occasion, I took 3-4 individual chamber flux measurements of 2-4 minute duration and then averaged them to estimate daily flux. Typically, the first 30 seconds and last 30 of the fluxing period were discarded due to the disturbance to the surface water when placing and picking up the chamber. Fluxes were calculated using linear regression (slope) of the change in headspace CO_2 gas concentration (atm) inside the chamber over time and the ideal gas law, air temperature, and atmospheric pressure at the time of sampling (Equation 2). Negative slopes and fluxes for CO_2 measurements are reported as CO_2 uptake by the lake while positive slopes and fluxes indicate CO_2 flux to the atmosphere.

Equation 2: $Flux = S * (\frac{P*V}{R*T*A}) * M * C$

Where S is the slope from the linear change in gas concentrations within the chamber over time (atm minute^{-1}), P is barometric pressure (atm), R is the universal gas constant (L atm K^{-1} mol^{-1}), V is the volume of the chamber (L), T is the average air temperature inside the chamber (K), A is the area of the chamber (m^{-2}), M is the molar mass of C-CO_2 (mol mg^{-1}) and C is a conversion factor to convert from minutes to days (i.e. 1/1440). All CH_4 fluxes are presented in mg CH_4 (molecular weight = 16.04 mg mmol^{-1}) and all CO_2 fluxes are presented in mg carbon (molecular weight = 12.01 mg mmol^{-1})

4.2.5 Water chemistry and meteorological measurements

Surface water chemistry was measured from a kayak at each location within the lake. At each location, I measured dissolved oxygen, specific conductivity, pH, and temperature in the top 10 cm of the water column using a handheld water monitor (Yellow Springs Instrument ProDO). Water samples for dissolved organic carbon (DOC) and total dissolved nitrogen (TN) were sampled from the center of the lake and filtered in the field (0.7 µm; Grade GF/F, Whatman) and acidified with 20% HCl to reduce the pH below two and prevent further microbial activity (Burd et al. 2018). The samples were stored in amber bottles to prevent photodegradation and were kept at 4 ºC until analysis. Concentrations of DOC and TN were

measured by a TOC-L combustion analyzer with a TNM-L module (Shimadzu, Kyoto, Japan. Water samples for ion concentrations were filtered and frozen on the day of sampling and kept frozen until analysis. Anions (Cl^-, PO_4^{3-}, SO_4^{2-}, NO_3^-) were measured using Ion chromatography (Dionex Ion chromatography DX 600, Thermo Fisher Scientific, US). Cations (Na^+, Mn^{2+}, K^+, Ca^{2+}, Fe^{3+}, NH_4^+) were measured by ICP-OES (iCAP6300 Duo, Thermo Fisher Scientific, US). All ions were measured in 2018 and 2019 and only Cl^- and SO_4^{2-} were measured in 2017. Water samples for chlorophyll-a (Chl*a*) analysis were collected from the center of the lake in 2018 and 2019 using opaque Nalgene bottles. Duplicate samples for each lake were refrigerated and vacuum filtered on the day of collection using 47-mm diameter, ethanol-rinsed GF/F filters (Whatman). The filters were then placed in Petri dishes, wrapped in aluminum foil, and were frozen immediately until analyses at the University of Alberta Biogeochemical Analytical Service Laboratory using a Spectrofluorophotometer (Shimadzu RF-1501).

Samples for dissolved CH_4 and dissolved inorganic carbon (DIC: sum of CO_3^{2-}, HCO_3^-, H_2CO_3; i.e. DIC) concentrations were collected from the surface of the water from each lake location one to two times per sampling trip. I collected five mL of water using a six mL plastic syringe and was injected into a pre-prepared 10 mL vial (Wheaton) with 20 uL of 20% HCl (Karlsson et al. 2010). The vials were stored upside down at room temperature until analysis of the headspace gas concentrations which occurred no later than seven days after sampling. Dissolved gas concentrations were then calculated following Henry's Law (Sander et al. 2015).

Continuous bi-hourly measurements of sediment temperatures (°C) were recorded using loggers (Hobo 8k Pendant Onset Computer, Bourne, MA, USA) installed at five and 50 cm sediment depths in the thaw edge, stable edge, and center in 2017. Loggers from the stable edge malfunctioned in June 2017 and are therefore not included in any analysis. Meteorological variables were recorded onsite from a floating weather station (Hobo RX3000 Remote Monitoring weather station) over both the 2017 and 2018 open-water seasons. The weather station was equipped with Hobo Smart Sensors (Onset Computer, Bourne, MA, USA). Air temperature and air pressure were recorded every five minutes using a Hobo 12-bit Temperature Smart Sensor (S-TMB-M002) and Hobo Pressure Sensor (S-BPB-M002). Photosynthetically active radiation (PAR) was measured every five minutes using a Hobo Photosynthetic Light Smart Sensor (S-LIA-M003). Finally, the wind speed was measured every five minutes using a

Hobo Wind Smart Sensor (S-WSB-M003). Both wind speed and PAR sensors were placed two meters above the water-air interface. All measurements were aggregated to daily averages in post-processing.

Relative lake depths were measured in March 2017 by drilling into the ice along a transect from the thaw edge to the center lake location and then at the stable edge and measuring the length of the ice and water column.

4.2.6 Sediment porewater CH_4 concentrations

Porewater samplers were used to measure dissolved concentrations of CH_4 in the lake sediments and were installed in the thaw edge, center, and stable edge. The samplers are 60 cm long and consist of 60 chambers of five mL each at one cm resolution. The chambers were filled with deionized water and covered with a permeable membrane before installation. A full description of the samplers can be found in Hesslein (1976). Upon installation, ~10 cm of the sampler was kept above the sediment-water interface and reached a depth of ~50 cm below the sediment-water interface. The samplers were installed in June and August of 2017 and 2018 and were left to equilibrate for 3-4 weeks. In 2017 the samplers were installed on June 20th and sampled on July 14th and then were reset and sampled again on August 9th. In 2018 the samplers were installed on June 14th, 2018, and were sampled on July 5th, 2018. The samplers were installed a second time from July 5th to August 12th, 2018. Dissolved porewater CH_4 concentrations were sampled by extracting two mL of porewater from a single porewater chamber using a needle and syringe. Sample extraction was repeated at two cm depth intervals. Water samples were injected into six mL glass vials, pre-flushed with nitrogen, and acidified with 20 μL of 20% HCl. To measure porewater CH_4 concentrations at deeper sediment depths, multilevel piezometers (MLPs; Beer and Blodau, 2007) were installed at the thaw edge, center, and stable edge in May of 2017 and then were sampled seven weeks later in July 2017. The MLPs consisted of eight to 15 segments, each containing a 12 ml crimped vial with deionized water and permeable membrane (0.2 μm) to allow for diffusion of solutes in the vial. Dissolved CH_4 samples were extracted directly from the vials by extracting two mL of porewater and injecting it into pre-acidified vials, similar to the porewater sampling technique. The MLPs were installed at depths between 70 and 170 cm. Sample analysis and determination of CH_4 concentrations were performed as described above for the surface water samples.

4.2.7 Radiocarbon analysis

Bubble samples were collected in July and August of 2018 for ^{14}C-CH_4 analysis. Samples were collected directly from the bubble traps and were injected into pre-prepared glass vials equipped with rubber septa following the same protocol described above. Three samples were collected from the thaw edge, center, and stable edge for a total of nine samples. Methane and CO_2 concentrations in each vial were measured at the University of Alberta and then the vials were shipped to the National Environmental Isotope Facility (NEIF) in the United Kingdom. Samples were prepared to graphite at the NEIF Radiocarbon laboratory and sent to the Scottish Universities Environmental Research Centre (SUERC) AMS laboratory for ^{14}C analysis (Allocation No. 2128.1018) following protocols described by Garnett et al. (2016). Unique lab codes for each sample can be found in Table A.4.2. Due to low concentrations of CO_2 in many of the bubble samples, radiocarbon data were only reported for three samples from the thaw edge and one sample from the stable edge. Water samples for ^{14}C and stable carbon isotope ($\delta^{13}C$) analysis of DOC and DIC were collected from the center of the lake with a hand pump at a water depth of 0.5 to 1 meters. Water samples were filtered on-site with a 0.7 μm pre-baked glass fiber filter and storing the filtered water in pre-baked and acid-washed 1L vials. Samples were analyzed at the A. E. Lalonde AMS Laboratory in Ottawa, Canada following protocols established by Crann et al. (2017) and St-Jean et al. (2017). Radiocarbon data are expressed in fraction modern (fM) which is the ^{14}C to ^{12}C ratio in the sample relative to that of the oxalic acid-1 standards (Stuiver and Polach, 1977 and as in Elder et al. 2018) and as conventional radiocarbon ages (years BP, where 0 BP = AD 1950) at the ±1σ level (as in Gonzalez Moguel et al. 2021).

4.2.8 Lake peat sediment cores and macrofossil analysis

Lake peat sediment cores were taken from the center of the study lake during ice-cover in March 2017 and from the stable and thaw edges of the lake in March 2018 to determine organic layer depth and to investigate the site history through macrofossil analysis. A manual ice auger was used to drill through the ice, and a Russian peat corer (4.5 cm inner-diameter, Eijkelkamp, Giesbeek, Netherlands) was used to take sediment cores in 50 cm increments. To account for disturbance of the upper few centimeters of each core, an 10 cm overlap was achieved by coring

alternately between two holes, ~20 cm apart, to a depth of 380 cm at the lake center and ~200 cm at the edges. Cores were frozen upon extraction and were kept frozen until analysis. Each 50 cm core section from the center core was further segmented at 2 cm intervals, and macrofossils were analyzed every 10 cm. The samples were prepared by thawing and diluting with deionized water and filtered through a 150 μm sieve to remove any particles too small to identify. Macrofossil analysis was carried out following the protocols described by Mauquoy et al. (2010) as in Heffernan et al. (2020). Data analysis was performed in the C2 program for ecological and paleo-ecological data analysis and visualization (Juggins, 2003) to create a stratigraphic diagram. The transition from limnic sediment to peat sediment in the cores at the thaw edge, lake center, and stable edge were visually assessed in the field immediately upon extraction based on changes in color and humification (Fig. A.4.4). The transitions in the center core were additionally determined by shifts in vegetation composition and bulk density of the samples.

4.2.9 Surface sediment cores and incubations

Surface sediment cores (i.e. limnic sediments) were taken from the edges and center of each lake in July 2017 using a gravity corer (UWETEC). Depths of the surface cores ranged from 20-45 cm depending on water depth and success of corer deployment. Cores were sectioned in the field at two cm increments and immediately placed in bags (WhirlPack), closed with no air bubbles, and placed in a cooler until they could be frozen at -18 C approximately 1 to 2 hours post coring. In the lab, sectioned cores were thawed and then homogenized at depths 0-4 cm and 10-14 cm. Peat sediments from the deep cores were homogenized at depths of 20-30 for the thaw edge, 60-70 cm for the stable edge, and 70-80 cm for the lake center to capture the peat sediment just below the limnic sediment transition. Additional peat sediments were homogenized from 100-110 cm and 190-200 cm depths at all locations. After sediments were homogenized, three subsets of 20-30 grams of wet sediments from each depth were added to 37.5 mL glass jars (Wheaton). Nitrogen-degassed Millipore water was then added to each jar until half of the total volume of the jar was filled. Jars were covered in tinfoil, capped with rubber septa (Wheaton), and crimped close. Two needles attached with two-way stopcocks were inserted into the rubber septa for headspace gas sample extraction.

Prior to the start of the incubation measurements, each jar was shaken and then flushed with nitrogen for one minute repeating this procedure three times to degas as much oxygen as

possible and arrive at an anoxic state. The time was recorded after the first headspace gas sample was taken. The jars were sampled at 0 (start of the experiment), 1, 2, 3, 7, 10, and 14 days. At each sampling occasion, the jars were shaken for 30 seconds and left to sit for another 30 seconds to allow porewater gas to fully equilibrate with the headspace. One mL of nitrogen was injected and mixed into the headspace using a syringe attached to one of the stopcocks and then 1 mL of headspace sample was extracted using a syringe attached to the other stopcock and the sample was directly injected into the gas chromatogram. Methane production rates were calculated using the nitrogen dilution-corrected slope of headspace concentrations over the sampling period and are expressed in micrograms of CH_4-C or CO_2-C per gram of dry weight (gdw) sediment sample. In between sampling occasions, the jars were kept in dark conditions at a controlled temperature of 14˚C.

4.2.10 Statistical analysis

All statistical analyses were performed using R software (Version 1.1.383, RStudio Inc, www.r-project.org). Differences in daily CH_4 fluxes among the lake locations and months were performed using mixed effects models (R Package 3.3.3; Lme4 Package; Bates et al. 2015). Methane fluxes were log-transformed before analysis to fit assumptions of normality. Lake location and sampling month were set as fixed effects in their respective models. Individual bubble traps and chambers were set as random effects to account for repeated measures. Each mixed model was compared against the respective null model, which only included the random effects, using analysis of variance (ANOVA; “anova” command). Individual pair relationships were then determined using a post-hoc, non-parametric t-test (Barroti adjustment). I used Kruskal-Wallis rank-sum tests to examine the temporal variation of fluxes within each lake location among months and to test for differences between modeled CH_4 diffusive fluxes and chamber fluxes and differences in diffusive CO_2 exchange between the stable and thaw edge. Follow-up pairwise relationships were examined using post hoc Dunn’s test with Bonferri method (dunn.test package; Dinno, 2017). To examine the relationship between environmental variables and CO_2 and CH_4 flux, fluxes within each location were averaged daily as water chemistry was only measured at one spot within each location on the sampling day. Correlations between CH_4 and CO_2 fluxes and environmental variables (air temperature, water temperature, conductivity, pH, air pressure, dissolved oxygen, PAR) were performed across the entire lake

extent using nonparametric Kendall correlation tests. Based on the Kendall's Tau (Ƭ) value, correlations were classified as weak (± 0.1-0.30), moderate (± 0.3-0.5), or strong (± > 0.5) (Cohen et al. 2013 as in Burke et al. 2019). Positive (+) Ƭ values represent a positive relationship with flux and negative (-) Ƭ values represent a negative relationship with flux. Relationships between CH_4 flux and sediment temperature were assessed using linear models (R Package 3.3.3; Lme4 Package; Bates et al. 2015). Unless otherwise noted, results are presented as the average ± one standard deviation. Output from statistical tests are presented in Tables A.4.3 through A.4.7.

4.3 Results

4.3.1 Sediment and water chemistry characteristics

Both organic-rich limnic and peat sediments were found throughout the three meters deep core at the lake center (Fig. 4.2a,b; Fig. A.4.1). Below three meters, the sediments transitioned to a mineral deposit of clay and silt composition. Macrofossil analysis suggests the center of the lake was initiated as an open-water wetland before transitioning to various fen stages and then into its current limnic state (limnic sediment thickness ~70 cm; Fig. 4.2a,b). At the stable edge, limnic sediments were ~60 cm thick. The thaw edge has the thinnest limnic sediment layer (~20 cm), indicating ongoing lake expansion (Fig. 4.2a,b).

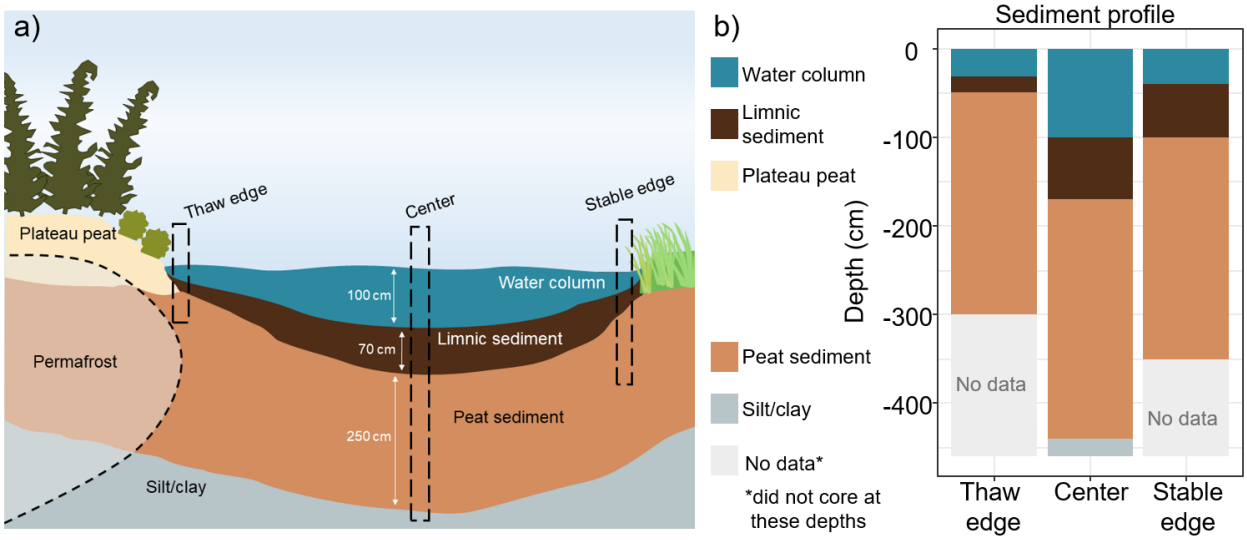

Figure 4.2. a) Conceptual diagram of Eli lake and b) water column and sediment profiles.

Water chemistry metrics show Eli is a mesotrophic lake with relatively high concentrations of DOC (44.3 mg L^{-1}) and ammonium (NH_4^+; 36.4 µg L^{-1}) and moderate levels of phosphate (PO_4^{3-}) and chlorophyll-*a* (Chl*a*; Table 4.1). The average surface water pH over the study period was 7.5 but reached as high as 8.7. Average conductivity and dissolved sulfate (SO_4^{2-}) concentrations were 358.9 µS cm^{-1} and 29.9 mg L^{-1}, respectively (Table 4.1). The average water column DIC concentration was 8.9 mg L^{-1}.

Table 4.1. Average (± one standard deviation) surface water characteristics (2017-2019) from the center of the lake.

DOC (mg L^{-1})	TN (mg L^{-1})	DIC (mg L^{-1})	pH	Cond (µS cm^{-1})	PO_4^{3-}-P (µg L^{-1})	SO_4^{2-}-S (mg L^{-1})	NH_4^+-N (µg L^{-1})	Chl*a* (µg L^{-1})
44.3	1.7	8.9	7.5	358.9	7.5	29.9	36.4	7.9
(10.0)	(0.4)	(3.7)	(0.5)	(65.6)	(2.5)	(14.5)	(8.2)	(5.2)

4.3.2 Methane fluxes

The average ebullitive CH_4 flux for Eli Lake was 124 ± 77 mg CH_4 m^{-2} d^{-1} (average and one standard deviation among the four locations). Ebullitive fluxes varied across lake locations and were highest at the thaw edge with 236 ± 61 mg CH_4 m^{-2} d^{-1} ($\chi^2 = 25.78$, $P < 0.001$, df = 3; Fig. 4.3a; Table A.4.3). There was a trend of decreasing ebullitive fluxes from the edges to the center of the lake where the water column is deepest (depth = 1 m) and the average flux was 62 ± 34 mg CH_4 m^{-2} d^{-1} (Fig. 4.3a, Table 4.2). This pattern is consistent with the volume of bubbles collected at each lake location (Fig. 4.4c). The average CH_4 concentration from the bubble samples across all lake locations was 42 ± 13% (n=121). Bubble CH_4 concentrations were not statistically different among the four lake locations ($\chi^2 = 3.93$, $P = 0.27$, df =3) but the highest concentration was measured at the thaw edge (62% CH_4) and the lowest at the lake center (11% CH_4; Fig. 4.4a). When combining all lake locations over the study period, there was no effect of month on ebullitive CH_4 flux ($\chi^2 = 2.56$, P =0.046, df =3). I also found no significant effects of month when analyzing each lake location individually (Table A.4.4). However, ebullitive fluxes clustered around high values when sediments were warmest in July at the thaw edge and had an increasing trend during the ice-free season at the stable edge (Fig. A.4.2).

Table 4.2. **Summary results (± one standard deviation) for GHG fluxes at each lake location.** E_flux = ebullitive flux. D_flux = diffusive flux. [CH_4] = dissolved CH_4 concentration.

Location	Water depth (m)	D_flux (mg CH_4 m^{-2} d^{-1})	E_flux (mg CH_4 m^{-2} d^{-1})	Chamber flux (mg CH_4 m^{-2} d^{-1})	[CH_4] (uM)	E_flux (mg C-CO_2 m^{-2} d^{-1})	D_flux (mg C-CO_2 m^{-2} d^{-1})
Thaw Edge	0.3	57.4 (22.8)	236.4 (60.6)	199.5 (115.4)	7.1 (3.1)	9.9 (60)	-79 (191)
Intermediate	0.7	36.6 (21.3)	107.4 (56.1)	158.3 (72.2)	5.2 (3.0)	5.3 (56)	-
Center	1	24.2 (13.2)	61.9 (33.87)	130.17 (87.1)	3.5 (1.7)	2.3 (34)	-
Stable Edge	0.4	46.1 (28.2)	92.67 (95.68)	157.7 (62.4)	5.0 (3.7)	8.5 (96)	-126 (211)

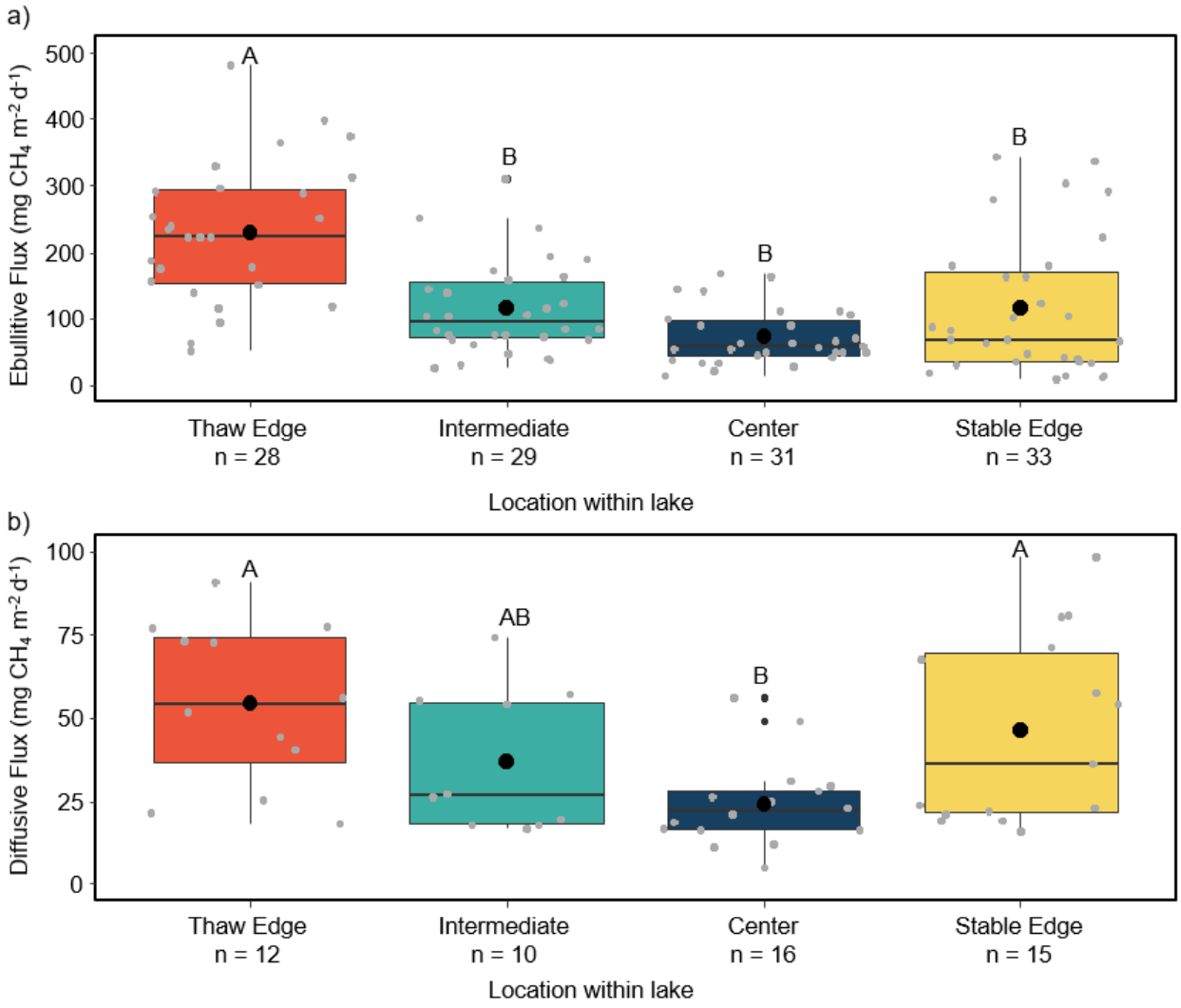

Figure 4.3. Methane fluxes across the lake locations. a) Ebullitive fluxes. b) Diffusive fluxes. Boxplots represent the median and quartile ranges. The black circles represent the average and the small grey circles represent individual measurements. Different letters above the boxplots indicate significant differences among the lake locations.

The average diffusive CH_4 flux from the lake was 41 ± 14 mg CH_4 m^{-2} d^{-1} and ranged between 5 and 81 mg CH_4 m^{-2} d^{-1}. Diffusive fluxes were significantly higher at the thaw edge and stable edge compared to the intermediate and center locations ($\chi^2 = 27.68$, $P < 0.001$, df =3; Fig. 4.3b; Table A.4.3). I found no effect of month on diffusive fluxes when combining all lake locations ($\chi^2 = 4.81$, $P = 0.19$, df =3). Temporal patterns were variable for each location but diffusive fluxes were usually higher in July at the edges (Fig A.4.2).

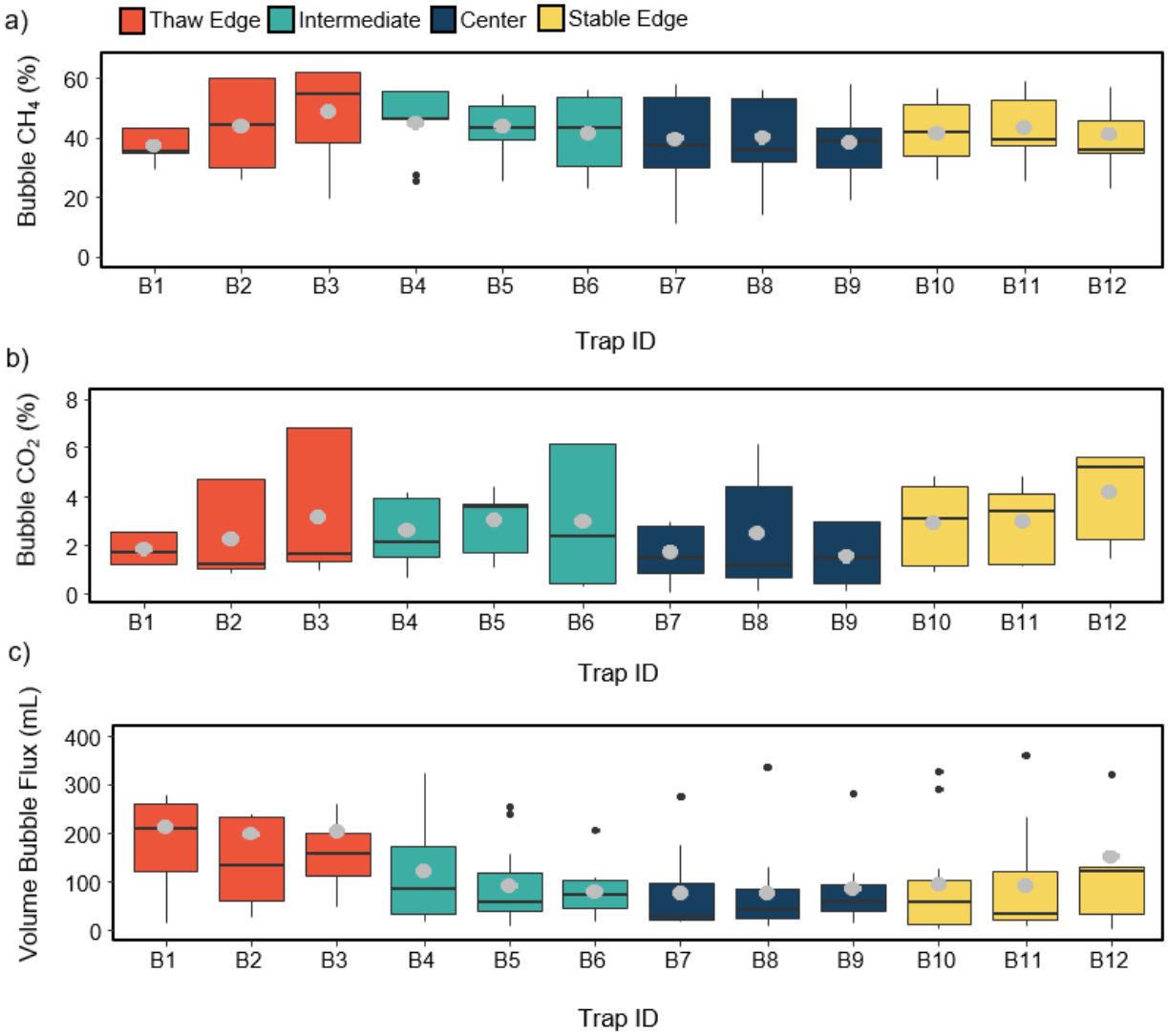

Figure 4.4. Bubble concentrations of a) CH_4 and b) CO_2, and c) volumetric bubble fluxes for individual bubble traps. Boxplots represent the median and quartile ranges. The grey circles represent the average. Note the different scales for bubble CH_4 and CO_2 concentrations.

The average chamber flux across the lake locations was 161 ± 29 mg CH_4 m^{-2} d^{-1}. Chamber measurements were significantly higher than diffusive fluxes when compared across the whole lake and within each lake location ($\chi^2 = 76.86$, $P < 0.001$, df =1). This difference indicates that chamber measurements are more representative of net CH_4 fluxes than what would be accounted for only by diffusive as shown by the large influence of ebullition in the measurements. Approximately 30% of estimated K_{600} values from the chamber measurements

were twice as high as the minimum calculated K_{600} value, indicative of ebullition. I found a minimal influence of lake location on chamber fluxes ($\chi^2 = 8.65$, $P = 0.03$, df =3), with the only significant difference found between the intermediate and center locations (293 and 152 mg CH_4 m^{-2} d^{-1}, respectively; Fig. 4.5a). Chamber fluxes varied temporally ($\chi^2 = 28.11$, $P < 0.001$, df =3) and were highest in June and July (Fig. 4.5b; Table A.4.4).

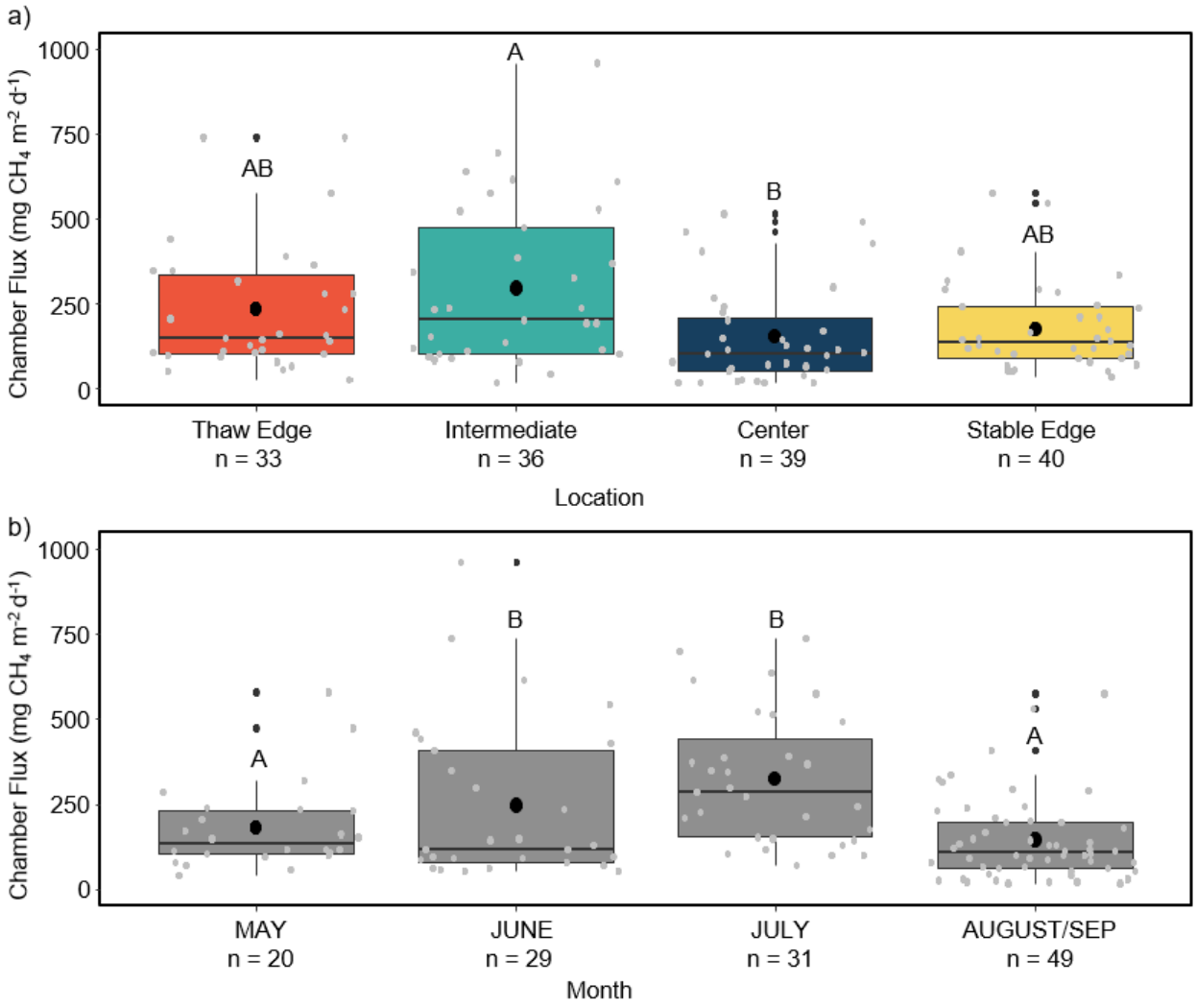

Figure 4.5. Methane fluxes from chamber measurements across the different lake locations (a) and over the sampling months (b). Boxplots represent the median and quartile ranges. The black circles represent the average and the small grey circles represent individual measurements. Different letters above the boxplots indicate significant differences among lake locations and months.

4.3.3 Carbon dioxide fluxes

The average ebullitive CO_2 flux was 6.4 ± 7.3 mg CO_2-C m^{-2} d^{-1}, which represents a minor fraction of the total carbon (mg C m^{-2} d^{-1}) flux from bubbles (~7%). Average bubble CO_2 concentrations were 2.64% ± 1.84% (n = 121; Fig. 4.4b). Bubble CO_2 concentrations were weakly related to lake location ($\chi^2 = 8.97$, $P = 0.03$, df =3) with the only significant differences between the center and stable edge (Z-value = 3.04, $P = 0.013$; Table A.4.5). However, lake location was a significant factor influencing ebullitive CO_2 fluxes ($\chi^2 = 21.3$, $P < 0.001$, df =3) with the lowest fluxes at the center and without statistical differences between the edges and the intermediate location (Fig. 4.6a; Table A.4.6). Ebullitive CO_2 fluxes had an increasing trend over the open water season with the highest average fluxes in July and August/September that statistically differed from May (Fig. 4.6b; Table A.4.6).

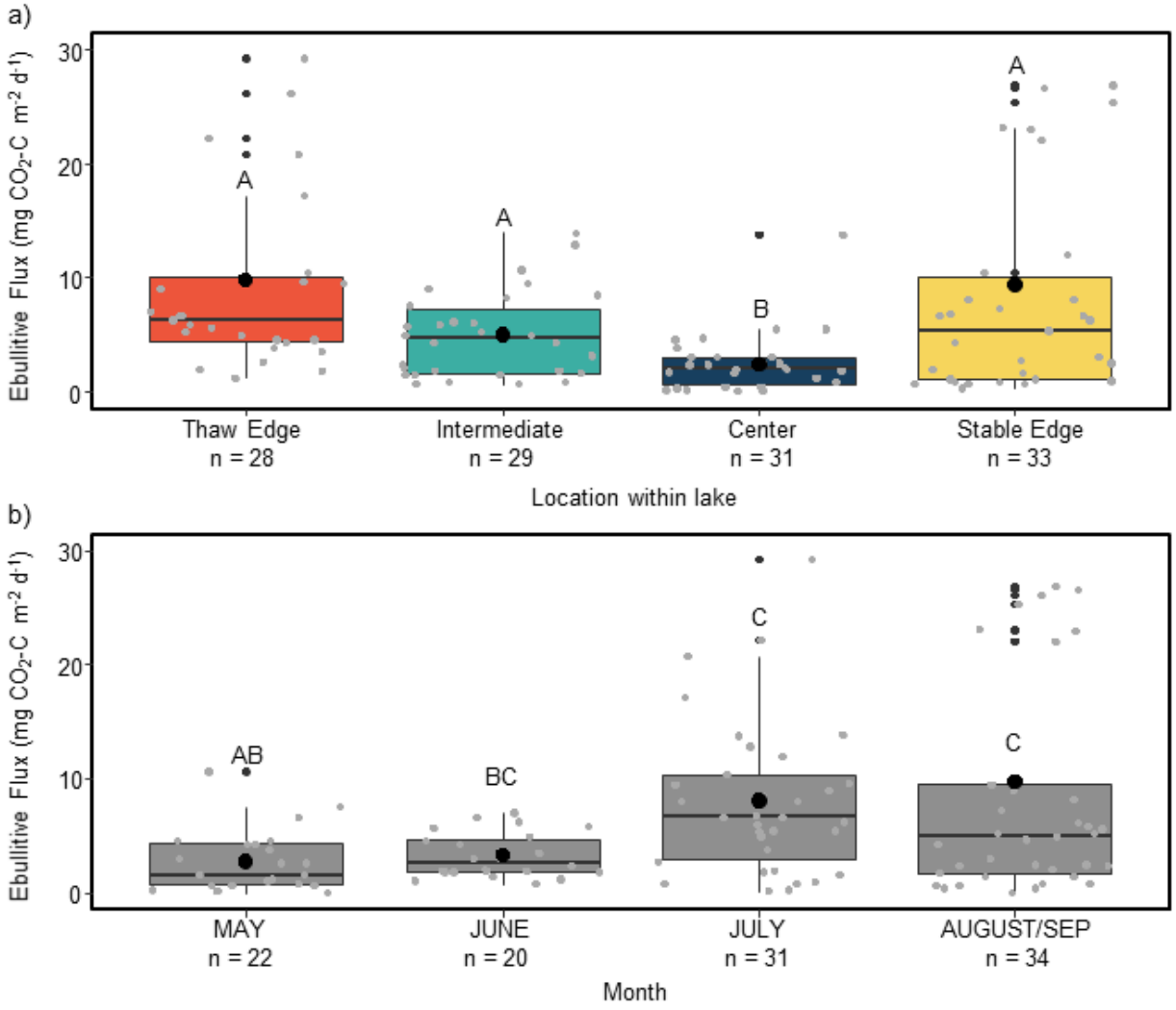

Figure 4.6. Ebullitive CO_2 fluxes across the lake locations (a) and over the sampling months (b). Boxplots represent the median and quartile ranges. The black circles represent the average and the small grey circles represent individual measurements. Different letters above the boxplots represent significant differences among lake locations or sampling months.

The stable edge and thaw edge were usually net sinks in terms of diffusive CO_2 exchange (-126 ± 211 and –79 ± 191 mg CO_2-C m^{-2} d^{-1}, respectively) and were not statistically different from each other ($\chi^2 = 0.45$, $P = 0.50$, df =1; Fig. 4.7a). Average CO_2 exchange was negative (net uptake) for all months but, the median flux was positive in August (i.e. net source) when most diffusive CO_2 measurements took place (Fig. 4.7b). Statistical differences between months were not performed due to low sample sizes in June (n =1 for stable and thaw edge).

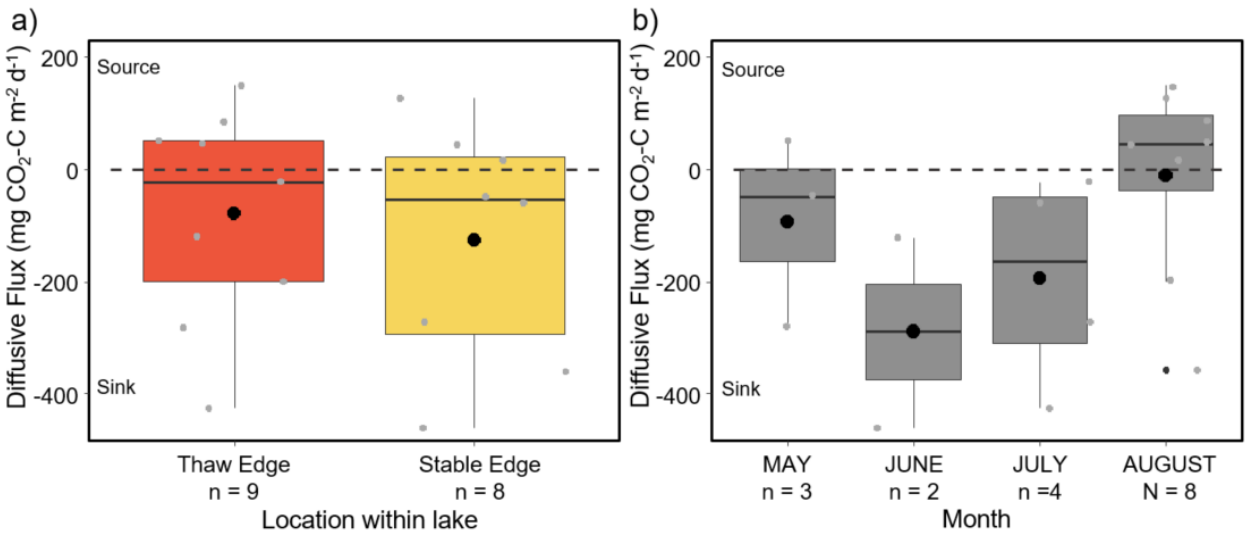

Figure 4.7. Diffusive CO_2 fluxes across lake locations (a) and over the sampling months (b). Negative values represent the net uptake of CO_2 from the atmosphere**.** Boxplots represent the median and quartile ranges. The black circles represent the averages and the small grey circles represent individual measurements. The dashed line represents the source or sink cutoff. The flux units represent mg of carbon in CO_2.

4.3.4 Flux correlations with environmental variables

Diffusive and ebullition CH_4 fluxes weakly correlated with the daily average environmental and meteorological parameters. Diffusive CH_4 flux was moderately correlated with water temperature (τ = 0.30, P = 0.002) and weakly correlated with air pressure (τ = -0.28, p = 0.003; Table A.4.7). The strongest correlation was between chamber fluxes and PAR (τ = 0.46, P = 0.0001), suggesting high incoming solar radiation could increase net CH_4 fluxes but this correlation was not observed with ebullitive and diffusive fluxes. Sediment temperatures were generally 5°C colder at the center of the lake compared to the thaw edge (May-August average; Fig. 4.8), however, sediment temperature did not significantly correlate with any of the measured fluxes when tested across both lake locations (Fig. 4.8). Ebullitive CO_2 fluxes did not correlate with any of the environmental variables measured in this study (Table A.4.7). Diffusive CO_2 fluxes were moderately but not significantly correlated with conductivity (τ = 0.35, P = 0.08).

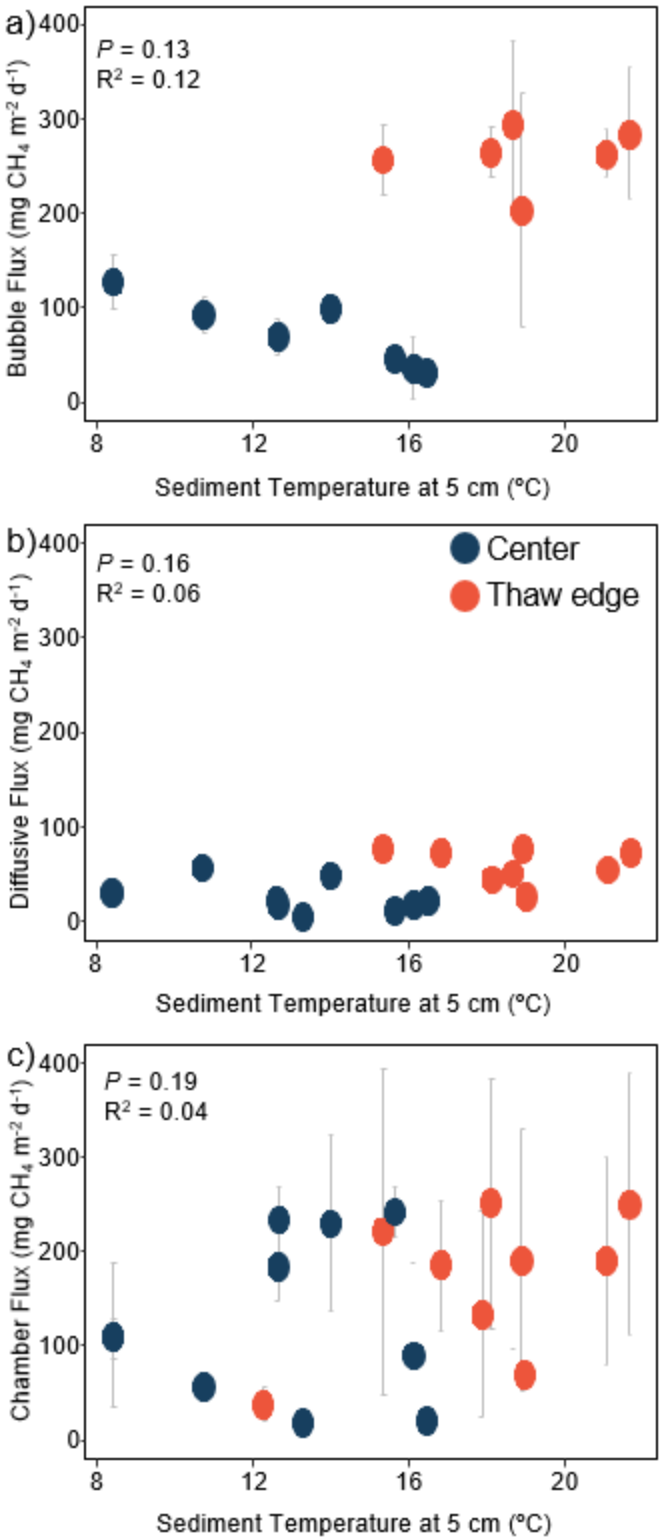

Figure 4.8. Sediment temperature vs a) CH_4 ebullition, b) CH_4 diffusion, and c) CH_4 chamber fluxes. Error bars represent one standard deviation. No standard deviations are

presented for diffusive fluxes. Black text represents linear regression output for fluxes across both lake locations.

4.3.5 Porewater concentrations

Dissolved sediment porewater CH_4 concentrations showed a relatively consistent profile among sampling times (i.e. months) and lake locations, sharply increasing within a few cm below the sediment and showing a much weaker gradient between depths ~10 to 50 cm (Fig. 4.9). Further down concentrations generally increased slightly as observed from profiles using the MLPs down to ~150 cm (Fig. A.4.5). A potentially faulty deployment of the sampler in the center may have lead to reduced concentrations between 0 and 20 cm in August 2018. The profiles showed lower concentrations and little variation among lake locations in 2017, especially in July and except for higher values with depth at the center in August. Concentrations were generally higher and there were greater differences among lake locations in the 2017 MLP profile (Fig. A.4.5) and in the 2018 surface sediments with higher values in the thaw edge (640 to 800 µM; 5-50 cm depths) compared to the other locations during July 2018 (480 to 650 µM for the same depth range).

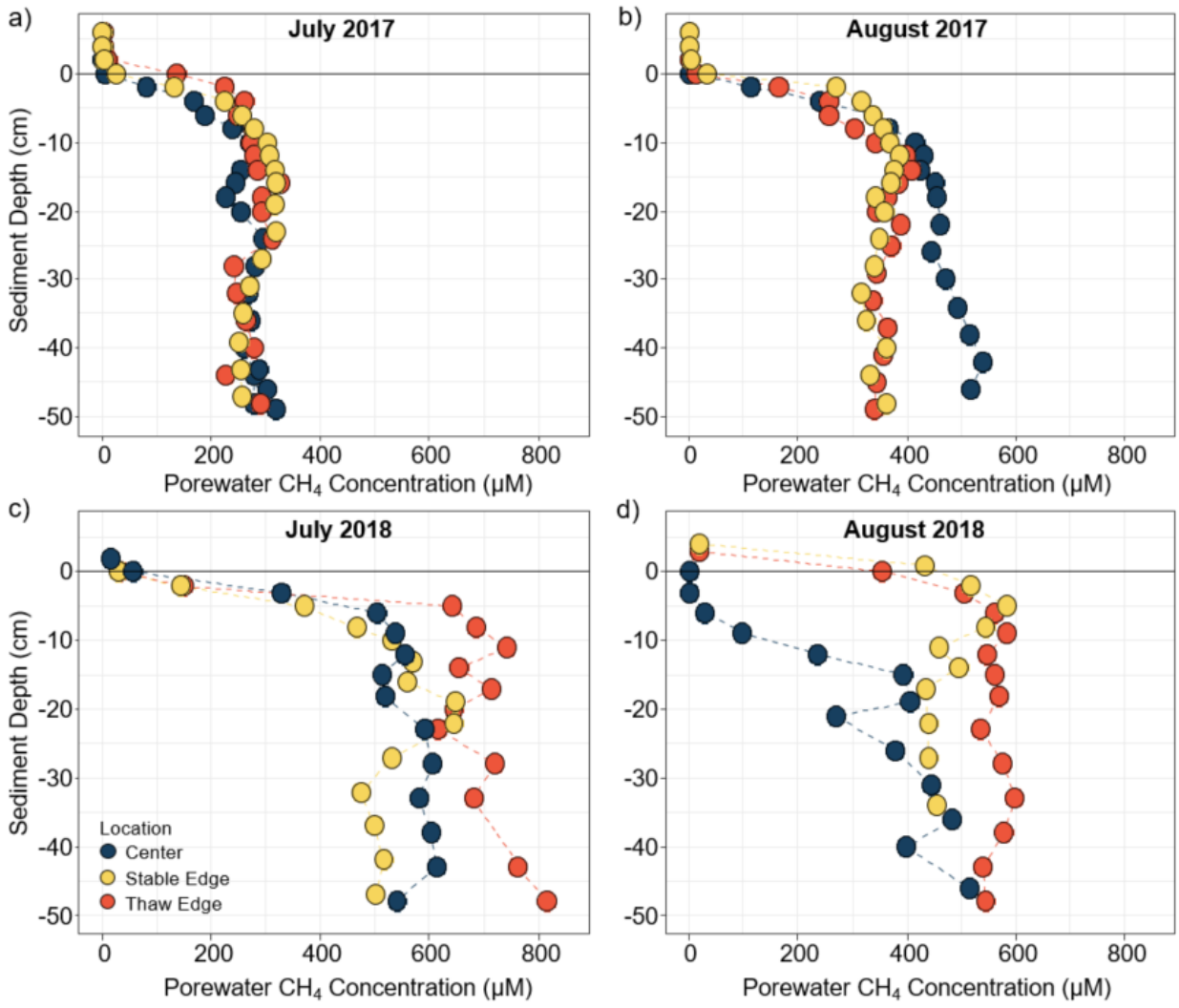

Figure 4.9. Dissolved concentrations of CH_4 in the sediment porewater. Plots represent measurements taken for CH_4 in 2017 (a, b) and 2018 (c,d).

4.3.6 Potential production rates from incubations

I found a consistent pattern across all lake locations of declining CH_4 production rates with sediment depth and highest rates at 0-4 cm followed by 10-14 cm depths (Fig. 4.10a). Production rates at 0-4 cm depths were generally higher in the stable edge sediments (6.1 ± 0.7 μg CH_4-C $gdw^{-1}d^{-1}$) compared to the center (4.2 ± 1.4 μg CH_4-C $gdw^{-1}d^{-1}$) and thaw edge (4.1 ± 1.2 μg CH_4-C $gdw^{-1}d^{-1}$) but these differences were not statistically significant ($P = 0.15$, F = 2.7, df = 2). Production rates at 10-14 cm were significantly higher at the stable edge (ANOVA; $P = 0.003$, F = 18.5, df = 2). At nearest depths below the transition from limnic to terrestrial

sediment, production rates were highest at the thaw edge (0.06 µg CH_4-C $gdw^{-1}d^{-1}$) compared to the stable edge and the center (0.0009 and 0.0006 µg CH_4-C $gdw^{-1}d^{-1}$, respectively; $P = 0.005$, F = 14.9, df = 2). However, the transition from limnic to peat sediments at the thaw edge was considerably more shallow (~20 cm) compared to the stable edge (~60 cm) and center (~70 cm). While all lake locations showed similar patterns of declining production rates with depth, the deepest samples (190-200 cm) showed rates an order of magnitude higher at the thaw edge (5e-4 ± 1e-4 µg CH_4-C $gdw^{-1}d^{-1}$) compared to the center and stable edge ($P = 0.002$, F = 23.2, df = 2; ; Fig. 4.10c). Potential CO_2 production rates followed the same trend with depth as for CH_4 and were of a similar magnitude at the 0-4 cm (1.6 to 5.3 µg CO_2-C $gdw^{-1}d^{-1}$; Fig. A.4.3) leading to CO_2:CH_4 production ratios between 0.4 and 1.3.

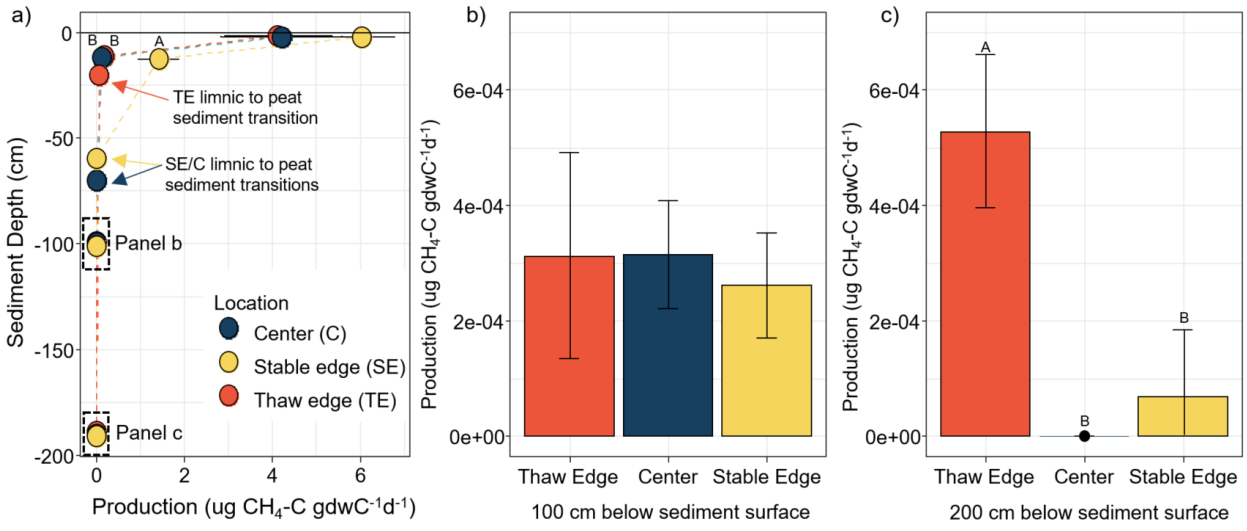

Figure 4.10. Potential CH_4 production rates in the sediments. a) Depth profile of productions rates. b) Production rates at 100 cm sediment depths. c) Production rates at 200 cm sediment depths. Error bars represent one standard deviation. Different letters indicate significant differences among lake locations. The absence of letters indicates no significant difference in production rates. Gdw = grams dry weight.

4.3.7 Radiocarbon

Analysis of CH_4 released as bubbles showed a lower ^{14}C content at the thaw edge (0.86 ± 0.004 fM) compared to the stable edge (>1.00 fM) and lake center (0.99 ± 0.005 fM; Fig 4.11). Radiocarbon ages of CH_4 bubbles were modern in the stable edge, 1211 ^{14}C years before present

(BP) in the thaw edge on average, and ranged from modern to 102 ^{14}C years BP at the center (Fig. 4.11, Table A.4.2). Radiocarbon ages and fM values of CO_2 from bubbles at the thaw edge (0.84 fM, 1420 years BP) and stable edge (0.996 fM, 50 ^{14}C years BP) were similar those of CH_4 (Table A.4.3; Fig. 4.11). Water column DIC was modern (1.00 fM) while DOC had the lowest fM (0.62 fM) and the older ^{14}C age (3804 ^{14}C yrs BP) of all measured samples (Table A.4.2; Fig. 4.11). Stable carbon isotope values (δ^{13}C) were approximately -4‰, for DIC and -26.9‰ for DOC.

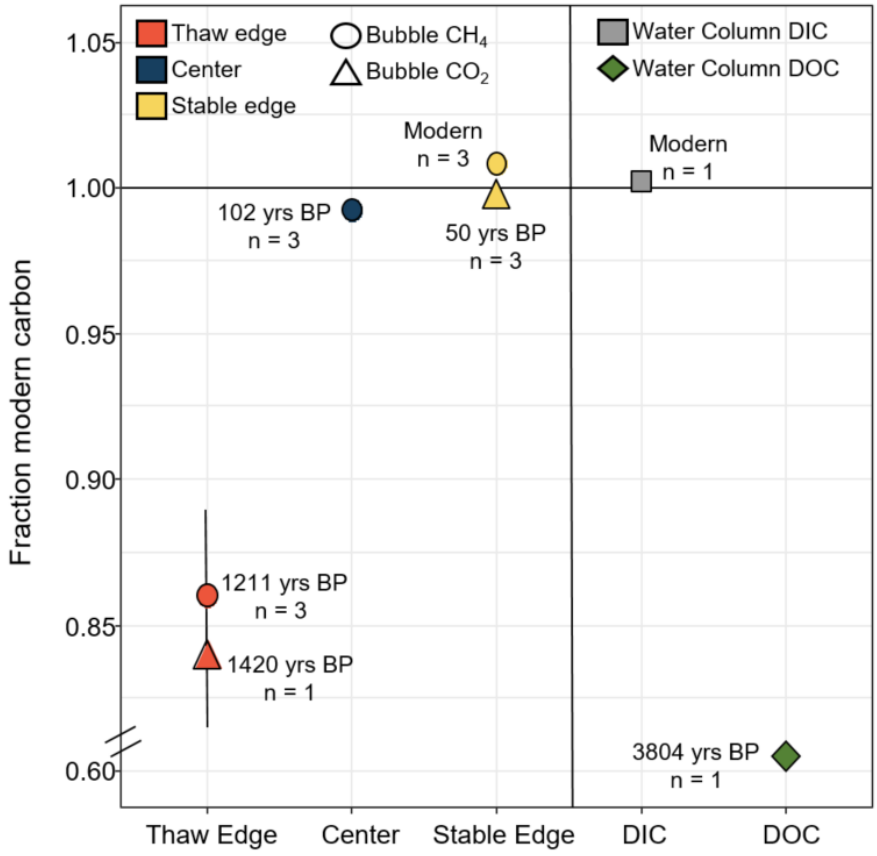

Figure 4.11. Fraction modern carbon for CH_4 and CO_2 bubbles, water column DIC, and water column DOC. Error bars represent the minimum and maximum fM values reported, including analytical uncertainty. Corresponding mean ^{14}C ages are shown next to samples with pre-modern fM values. Notice the y-axis break. The average estimated carbon ages are presented next to each point. Yrs BP = ^{14}C years before present (1950 AD).

Table 4.3. Summary results for ^{14}C ages and fM carbon at each lake location. fM = fraction Modern (1.00 = 1950 AD). Mod = modern ^{14}C age. Parenthesis correspond to the ± uncertainty ranges also shown in Fig. 4.11.

Location	^{14}C-CH_4 (year BP)	CH_4 fM	^{14}C-CO_2 (year BP)	CO_2 fM
Thaw Edge	1211 (180)	0.86 (0.02)	1420	0.84
Intermediate	-	-	-	-
Center	102 (87)	0.99 (0.01)	-	-
Stable Edge	mod	1.01 (0.01)	50 (65)	0.996 (0.008)

4.4 Discussion

In this study, I monitored CH_4 and CO_2 fluxes from a small, thaw-impacted peatland lake (Eli Lake) for three ice-free seasons. Spatial variation within the lake was the primary control on CH_4 flux variability, rather than temporal variation and associated environmental variables. Ebullitive CH_4 fluxes were highest from the thaw edge while diffusive CH_4 fluxes were highest from the thaw edge and stable edge. Ebullitive CO_2 fluxes were a minor component of the total bubble carbon release while negative diffusive CO_2 measurements suggest the lake is a net sink of CO_2 during the ice-free period. Radiocarbon analysis of the bubbles showed that CH_4 and CO_2 at the thaw edge had lower fM values than the stable edge and center, implying the gases include a substantial contribution from old permafrost carbon. Below I expand on my findings of the magnitude and controls on CH_4 and CO_2 fluxes from the study lake and explore the potential connections between permafrost thaw, old carbon, and GHG fluxes.

4.4.1 Spatial variability of methane fluxes

Location within the lake was a stronger indicator of the magnitude of CH_4 fluxes than any of the environmental variables measured over time (i.e. water chemistry and meteorological variables). Ebullitive CH_4 fluxes were highest from the thaw edge while diffusive fluxes were

highest from the two edge locations where the water depths were also the shallowest. Higher diffusive fluxes from the edges may be due to limited oxidation occurring in shallower water columns or due to differences in OM availability with higher terrestrial inputs near the lake shore (Del Sontro et al. 2016). Warmer temperatures at the lake edges, as I found for the thaw edge, may also drive higher CH_4 production rates in the surface sediments. Net CH_4 fluxes (chamber measurements), were positively correlated with PAR across all locations, suggesting some effect on net fluxes could arise from incoming solar radiation with sunny days potentially causing higher temperature. Similar observations have been reported in lakes in northern Sweden (Wik et al. 2014). While I collected limited data, sediment temperature was not a strong predictor of CH_4 release even though fluxes were generally higher where sediment temperatures were warmer (Fig. 4.8). The lack of a strong relationship between sediment temperature and flux within each lake location suggests that CH_4 release is more strongly controlled by differences in temperature or OM availability occurring between lake locations than by temporal variation in temperature within each lake location (Praetzel et al. 2020).

4.4.2 Sources of methane production

Potential CH_4 production rates derived from incubations of the surface sediments (0-4 cm and 10-14 cm) did not correlate with observed spatial patterns in ebullitive fluxes. Production rates were generally higher at the stable edge than at the thaw edge at the surface (Fig. 4.10). Higher production rates in the stable edge surface sediments may be related to the presence of sedge species along the shoreline, which release highly labile organic acids in the form of root exudates (Ström et al. 2012). The addition of labile, and contemporary OM from sedges into the adjacent sediments could explain both higher production rates and the strong modern signature of the carbon age in ebullitive samples at the stable edge (See Sect. 4.4.3; Table 4.2). Together, the lower surface sediment production rates (incubations) and higher ebullitive fluxes at the thaw edge compared to the stable edge suggest CH_4 emissions from the thaw edge must be produced by additional sources beyond the surface sediments.

Concentrations of dissolved CH_4 in thaw edge sediments were generally higher than the other lake locations (Fig. 4.9a), despite lower potential CH_4 production rates in the surface sediments. This suggests CH_4 production occurs deeper in the thaw edge sediment column or that dissolved CH_4 enters the lake from outside sources. While recently thawed deep peat at the

thaw edge may be more recalcitrant than surface OM inputs at the stable edge (Treat et al. 2016), it may be comparatively more labile than similarly deep sediment (peat) at the other lake locations. For example, sediment OM at 200 cm depths had more time to decompose at the other lake locations compared to the thaw edge given the more recent frozen conditions (Heslop et al. 2015), thus potentially leading to lower production rates. Incubation results support this reasoning about OM lability as I found greater potential CH_4 production rates from the thaw edge at 200 cm depths (Fig. 4.10c) compared to the center and stable edges. While these rates at depth are much lower compared to rates at the surface, there is also much more OM available at depth (1-2.5 meters) than at the surface sediments (i.e. high production likely limited to top 5-20 cm; Pratetzel et al. 2020). However, incubations were performed at 14ºC which is likely a higher temperature than that experienced in situ in deep sediments, and the influence of this relatively high temperature on CH_4 production must also be considered (Hopple et al. 2020). Alternatively, dissolved CH_4 might enter the lake from the adjacent plateau active layer (Olid et al. 2021; Pacheco et al. 2014) or be produced at and transported from the permafrost-active layer interface (Douglas et al. 2020) to the lake sediments. Under both deeper sediment production and external active layer/permafrost transport scenarios, CH_4 produced and emitted from the thaw edge may be sourced from older, recently thawed permafrost carbon. Evidence of old carbon emissions from the thaw edge is supported by radiocarbon dating discussed in the following section.

4.4.3 Old carbon from lake thaw edge

I found that the CH_4 bubbles emitted from the thaw edge had a lower fraction modern (fM) than bubble samples from the rest of the lake locations (Fig. 4.11). The presence of old ^{14}C-CH_4 (~0.86 fM and ~1211 ^{14}C years BP) in the thaw edge bubbles suggests some CH_4 is partially sourced from older, recently thawed permafrost carbon. Notably, there are no sedges at the thaw edge, thus it is also possible that the lower fM carbon at that location is due to less modern carbon inputs. However, the center of the lake also lacks sedges and aquatic plants and had higher fM carbon and more modern ^{14}C age in the bubbles compared to the thaw edge, suggesting the old signal I observed at the thaw edge is not solely driven by lack of modern sources. The fM and age of ^{14}C-CH_4 ebullitive samples from the thaw edge are within the range of ^{14}C-CH_4 ages reported from thermokarst peatlands and non-yedoma thermokarst lakes in eastern Canada and the north slope of Alaska (modern-5000 ^{14}C years BP), but older than CH_4

emitted from thermokarst bogs (Estop-Aragonés et al. 2020). For further context, peat initiation in the study region occurred ~9,000 years (Heffernan et al. 2020). ^{14}C-CO_2 ages closely mirrored the ages of ^{14}C-CH_4 (~0.84 fM and ~1400 ^{14}C years BP), signifying CO_2 in the bubbles may be derived from either oxidation of CH_4 (Elder et al. 2018) or that CH_4 and CO_2 are sourced from similarly aged substrate and anaerobic production pathways. Modern ages of CH_4 and CO_2 bubbles from the stable edge are likely due to the latter as opposed to oxidation, as the ratios of CO_2:CH_4 potential production rates are close to 1 (Fig. A.4.3), indicating methanogenesis is the dominant anaerobic pathway (Corbett et al. 2015).

Radiocarbon ages of DIC in the water column were modern while ^{14}C-DOC ages were old (~3800 ^{14}C years BP), suggesting that much of the DOC is derived from carbon fixed before permafrost aggradation in the local area (Heffernan et al. 2020). Modern-aged ^{14}C-DIC in the water column suggests DIC is sourced from the dissolution of atmospheric CO_2, respiration of modern carbon fixed within the water column, or from terrestrial inputs of modern pCO_2 (Del Georgio and Peters, 1994; Ask et al. 2009). Fixation of modern atmospheric CO_2 is supported by the net uptake of diffusive CO_2 fluxes measured by floating chambers (Fig. 4.7). Furthermore, the $\delta^{13}C$ value for DIC was -4‰, which is relatively enriched and is consistent with the dissolution of atmospheric CO_2 being the primary source (Bade et al. 2004), but it could also point to fractionation as a result of either autotrophic or heterotrophic respiration (Bade et al. 2004). Interestingly, the oldest observed radiocarbon ages were from water column DOC (Fig. 4.11). The ^{14}C-DOC age observed in this study closely resembles reported ages of DOC in the porewaters of peat plateau active layers (Tanentzap et al. *in review*), as the water table often follows the active layer and is exposes older peat (up to ~4000 years old) to oxic conditions (Quinton et al. 2019). This suggests the DOC in the lake is primarily derived from terrestrial sources. The ^{14}C-DOC sample also had a $\delta^{13}C$ value of -26.9‰, which indicates terrigenous origin (Karlsson et al. 2003). The observations of older DOC compared to CH_4 and CO_2 are also in line with previous peatland thaw lake studies (Gonzales Moguel et al. 2021).

While age mixing models are required to fully partition C age sources, the much older DOC ages relative to the rest of the carbon species measured in this study suggests that CH_4 and CO_2 produced within the lake sediment bubbles are not derived from the old fraction of DOC, although I cannot rule this out. Old DOC may flocculate and become part of the lake sediment

and then subsequently be mineralized (Downing et al. 2008; Tranvik et al. 2009), however, under this scenario I would expect older ages of CH_4 and CO_2 across the entire lake extent, not just the thaw edge. Methane and CO_2 could be derived from a slightly younger and more labile fraction of the DOC. While this study is limited by a small sample size of radiocarbon measurements it is also enhanced by the variety of forms of carbon represented through ebullitive CH_4 and CO_2, and water column DIC and DOC, which are rarely measured simultaneously (Estop-Aragonés et al. 2020; Gonzales Moguel et al. 2021). To draw more definitive conclusions about the contribution of old permafrost carbon to net CH_4 fluxes from lakes, additional radiocarbon samples should be taken from potential source materials (i.e. permafrost, active layer peat, limnic sediments), particulate organic carbon, and dissolved CH_4 samples.

4.4.4 Influence of local and regional characteristics on lake CH_4 fluxes

The average CH_4 flux over the sampling period was 41 ± 14 mg CH_4 m^{-2} d^{-1} and 124 ± 77 mg CH_4 m^{-2} d^{-1} for diffusion and ebullition, respectively. The average ebullition fluxes are on the higher end of reported estimates for small peatland lakes (< 0.01 km^2) across the north (ebullition IQR = 23-89; Kuhn et al. 2021) while diffusive fluxes are on the low end of reported fluxes (diffusion IQR = 38-94 mg CH_4 m^{-2} d^{-1}; Kuhn et al. 2021). Ebullitive to diffusive flux ratios from the stable edge are similar to the ratios observed across peatland lakes (~50% ebullition; Kuhn et al. 2021). Interestingly, the thaw edge was dominated by ebullitive fluxes (76% of net fluxes) which is similar to observations from actively thawing yedoma lake edges (79%; Walter et al. 2016), suggesting there is a common link between permafrost thaw and CH_4 transport pathway. Conversely, thermokarst peatland lakes in eastern Canada and northern Sweden reported a much lower ebullitive to diffusive ratios (~15% for northern Sweden; Burke et al. 2019; Kuhn et al. 2018 and 14% for eastern Canada; Matveev et al. 2016). Differences in lake morphology, local peat development, and regional landscape characteristics could lead to observed differences in flux magnitude and dominant transport pathway between my study lake and other peatland thaw lakes (Kuhn et al. *In Review*). The relationship between CH_4 fluxes and these characteristics is explored in detail below in the context of the available literature.

Differences in lake morphology may lead to differences in CH_4 production and flux among peatland lakes. Eli Lake is shallow with a maximum depth of one meter at the center and a relatively flat bathymetry (Fig. 4.2a) while, for example, the peatland lakes studied in eastern

Canada have generally greater depths (~2 m), stratified conditions, and steeply sloping sides (Matveev et al. 2016). Shallower water column depths in Eli Lake could results in generally warmer sediments both at the surface and deeper, thus increasing CH_4 production (Yvon-Durocher et al. 2014), while also creating non-stratified water-column conditions more conducive to ebullition (Bastviken et al. 2004). Sediments beneath shallow waters also experience less hydrostatic pressure and a higher sensitivity to changes in air pressure, compared to deeper waters, which may lead to a higher volume of bubbles released (Wik et al. 2013; Langenegger et al. 2019). Differences in bathymetry and surface area could also influence terrestrial carbon sediment loading, with higher loading rates in steeper lakes and smaller thaw ponds leading to potentially more labile carbon at the center of the lake and higher diffusive fluxes (Matveev et al. 2016; Holgerson and Raymond, 2016).

Furthermore, differences in landscape characteristics between the Taiga Plains and shield-dominated regions (i.e. landscapes underlain by Precambrian rock) could drive differences in lake water biogeochemistry and carbon cycling. The Taiga Plains is characterized by thick peat deposits, heterogeneous glacial deposits, and generally flat topography, which is associated with complex groundwater hydrology which can lead to higher nutrient concentrations in lakes connected to groundwater sources (Hokansson et al. 2019). For example, Eli is a mesotrophic to eutrophic lake with groundwater influence as indicated by high specific conductivity (Table 4.1). The shield regions of eastern Canada and Scandinavia have thin soils, undulating topography and thus abundant lakes with more mineral-rich sediments and generally less groundwater and peatland interactions (see Couture et al. 2012 and Houle et al. 2014) and lower concentrations of solutes and nutrients (Matveev et al. 2016; Kuhn et al. 2018; Table A.4.8). Lakes throughout the Taiga Plains thus receive higher relative concentrations of solutes, OM, and nutrients from surrounding terrestrial ecosystems, compared to lakes in shield regions, potentially leading to higher trophic status, sedimentation rates, and associated CH_4 production and flux across the entire lake extent. The higher trophic status of Taiga Plains lakes may also lead to more CO_2 uptake, as observed in the CO_2 fluxes from the edges of Eli Lake (Fig. 4.7). However, notably, the high DOC concentrations and generally darker waters of the lake suggest within-lake primary productivity (CO_2 uptake) is occurring in the top few cm of the water column.

Finally, assuming the study lake and the peatland lakes reported in other northern peatland studies are representative of lakes in their respective regions, I can speculate that local peat history and OM depth may lead to differences in CH_4 emissions between peatland lakes. Eli Lake is underlain by over three meters of organic-rich limnic and peat sediments (Fig. 4.2b) and there are up to 6 meters of peat in the surrounding permafrost peatlands (Heffernan et al. 2020). Despite the importance of sediment OM quality and depth for CH_4 emissions (Wik et al. 2018), few studies report organic sediment depths for northern peatland lakes to compare with. Measurements of the surrounding peat depths in peatland complexes in eastern Canada and Scandinavia, where similar peatland lakes have been studied (e.g. Matveev et al. 2016, Rasilo et al. 2016, Burke et al. 2019; Kuhn et al. 2018), are only 1-3 meters deep (Fillion et al. 2014; Pellitier et al. 2007; Malmer & Wallen, 1996). Assuming sediment OM depths in peatland lakes are related to surrounding terrestrial peat depth, differences in local peat depths may be the reason why I observed differences greater ebullitive emissions than in other studies. Thicker limnic sediments and peat sediments in the study lake could provide more substrate for CH_4 production and ebullition. Furthermore, many of the peatland lakes in eastern Canada and Scandinavia are surrounded by small permafrost peatland mounds that formed 200-400 years ago (Matveev et al. 2016; Malmer & Wallen, 1996), compared to more spatially extensive permafrost plateaus in the Taiga Plains that formed ~1500 years ago (Heffernan et al. 2020; Loisel et al., 2014; Pelletier et al., 2017). Differences in permafrost history may lead to differences in OM lability due to decomposition of peat during non-frozen periods i.e. peatlands that developed permafrost more recently may have more recalcitrant OM (Treat et al. 2016) and thus lakes with such OM may have lower CH_4 production and emissions (Douglas et al. 2020). Future research should work towards assessing the links between permafrost history, peat/limnic sediment quality and quantity, and CH_4 emissions from peatland thaw lakes.

4.5 Conclusion

In this study, I measured spatial and temporal CH_4 and CO_2 emissions from a small peatland thaw lake. I paired GHG emission data with physiochemical variables, sediment profiles, ex situ incubations, and radiocarbon dating to investigate key controls on GHG emissions. Strong and differing spatial correlations of ebullitive and diffusive CH_4 fluxes across the lake highlight the need for high spatial resolution of flux measurements and further suggests that whole lake estimates extrapolated from flux measurements taken at the edge may lead to

overestimates of net emissions. Ebullitive CH_4 emissions from the study lake accounted for most carbon gas released from the lake, similar to yedoma thaw lakes, and were much higher than ebullitive emissions from peatland thaw lakes in eastern Canada and Scandinavia. This suggests not all peatland lakes are similar in regard to CH_4 emissions characteristics and that other factors including local peat history, morphology, regional land cover characteristics, and trophic status must also be considered. Finally, I found the oldest CH_4 and CO_2 emitted via ebullition at the thaw edge suggesting old carbon may be sourced from recently thawed permafrost. My results suggest small peatland lakes throughout western Canada and similar landscapes may be hotspots for CH_4 emissions, particularly through ebullitive emissions, and that permafrost thaw may further enhance ebullitive emissions and the release of old carbon from thaw edges.

5. Summary, conclusions, and directions for future research

5.1 Summary of findings

Northern wetlands and lakes represent an important but unconstrained globally significant source of CH_4 emissions, and emissions are projected to increase with climate warming. Through the first component of this research, I used a novel land cover model and parallel flux database to arrive at a new bottom-up estimate of CH_4 emissions from wetlands and lakes in the Arctic-Boreal region. In the second component of this research, I show that climate warming and permafrost thaw will influence both CH_4 and CO_2 emissions from northern peatland lakes. More broadly, the results show that land cover, including different wetland and lake types and regional landscape features, have unique CH_4-emitting characteristics and potentially divergent responses in emissions to climate warming.

The results in Chapter 2 indicate that CH_4 emissions are closely tied to land cover. Using distinct wetland and aquatic land cover classes may reduce bottom-up estimates of annual CH_4 emissions. Fluxes of CH_4 from terrestrial ecosystems were primarily influenced by water table position, soil temperature, and vegetation composition- thus, wetlands with high water tables and dense sedge cover, including *Marshes, Fens, and Permafrost Wetlands*, had the highest CH_4 fluxes. Methane fluxes from aquatic ecosystems (lakes) were primarily influenced by water temperature, lake size, and lake genesis (i.e., type). Therefore, CH_4 fluxes were generally highest from small, organic-rich peatland and yedoma lakes. The best explanatory model for terrestrial CH_4 emissions was an interactive model that included site-level predictors of water table, soil temperature, and graminoid cover alongside land cover class ($R^2m = 0.73$). The best model for diffusive aquatic emissions explained 41% of the variation and included an interaction between surface area and lake type alongside water temperature. The best model for ebullitive aquatic emissions explained considerably less flux variation at 25%, with surface area as the only significant predictor variable. When including terrestrial and aquatic ecosystem fluxes alongside regional-scale predictor variables (i.e., land cover class, MAAT, MAP, Permafrost Zone, and Biome), land cover class was suggested to be the most important predictor variable (explaining 44% out of the total 47% variability).

My annual estimates of wetland CH_4 emissions (~30 Tg CH_4 yr^{-1}) and lake CH_4 emissions (~6.6 Tg CH_4 yr^{-1}) are on the low end, but within the range, of annual emissions reported from other bottom-up studies (averages = ~40 and ~17 Tg CH_4 yr^{-1} for wetlands and aquatic ecosystems, respectively), but are still higher than averaged top-down estimates (~28 Tg CH_4 yr^{-1}). Discrepancies in annual emissions may be linked to the accuracy of field fluxes, land cover area uncertainty, CH_4 uptake, or top-down model uncertainties such as prior estimates, tower locations, isotope tracers, or estimates of CH_4 oxidation rates in the atmosphere (Saunois et al. 2020). However, more direct comparisons with similarly masked areas are needed to compare across studies properly. Future research directions are explored in more detail in Sect. 5.2.

Chapter 3 builds on the need for a more accurate representation of current CH_4 fluxes from northern lakes and investigates the potential response of both CH_4 and CO_2 emissions to climate warming using a space-for-time approach. The results show that CH_4 and CO_2 varied along a climate/permafrost gradient across western Canada but had opposing trends and associated drivers. Methane emissions increased moving south along the gradient and were driven primarily by temperature and augmented by shifts in microbial communities. Conversely, CO_2 emissions decreased moving south, with net uptake of CO_2 in the southern-most lakes, associated with less permafrost cover and greater hydrological connectivity, nutrient availability, and within-lake primary productivity. Using radiative forcing models projected to 2100, I examined the effect of opposing responses of CH_4 and CO_2 to climate warming. I found that increasing CH_4 emissions added, on average, 5 and 15 fW m^{-2} by 2100 under RCP 2.6 and 4.5, respectively, which was only partially offset by reduced CO_2 emissions equivalent to -1 and -2 fW m^{-2}, respectively, when compared to the no-warming scenario. The influence of permafrost thaw on lake productivity and reduced CO_2 emissions, and the high-temperature sensitivity of CH_4 emissions, are likely associated with characteristics of peatland lakes and the hydrology/landscape history of their surrounding landscape. While further data from other major peatland regions are needed to support my findings, my study strongly suggests that peatland lakes need to be considered separately from other lake types when assessing the impact of climate change on future GHG emissions.

While the landscape-level effects of permafrost thaw on GHG emissions are explored in Chapter 3, in Chapter 4, I assess the direct effects of permafrost thaw on emissions due associated with thermokarst processes and also explore the spatial variability of CH_4 emissions across one lake. While the release of old permafrost carbon has been well-documented from yedoma lakes (for example, Walter et al. 2006; Dean et al. 2020; Walter Anthony et al. 2021), little is known about the magnitude and age of carbon released as a consequence of permafrost that in peatland lakes. Spatial variation in fluxes across the lake was the primary control on CH_4 emissions compared to temporal and environmental controls. The highest ebullitive emissions were from the thaw edge (236 ± 61 mg CH_4 m^{-2} d^{-1}) and the highest diffusive emissions were from the thaw edge and stable edge (~57 and 46 mg CH_4 m^{-2} d^{-1}, respectively) with lower emissions from the center for both transport pathways. I show that ebullitive CH_4 and CO_2 emissions from the thaw edge are sourced from older carbon (~1211 ^{14}C years BP) compared to elsewhere in the lake (~modern ^{14}C ages), potentially indicating the release of previously stored permafrost carbon. Notably, CO_2 was only a minor component of total ebullitive fluxes (~7%) but was as old or older than bubble CH_4 ages, which differs from other peatland thaw lake studies which found modern CO_2 ages in the bubbles (Gonzales-Moguel et al. 2021). Furthermore, diffusive CO_2 measurements show the lake is a net sink of CO_2, suggesting modern CO_2 is not emitted from the lake during the ice-free period. My results suggest small peatland lakes throughout western Canada may be hotspots for CH_4 emissions, particularly through ebullition, and that permafrost thaw may further enhance ebullitive emissions and the release of old carbon from thaw edges.

5.2 Future research directions

The results presented in this thesis help towards constraining bottom-up emissions estimates of CH_4 and CO_2 from wetlands and lakes across the Boreal-Arctic region and towards assessing the impact of climate warming on lake GHG emissions. My findings suggest CH_4 emissions are strongly associated with land cover classes and that CH_4 emissions from peatland lakes are likely to increase with warmer temperatures and accelerated permafrost thaw, while CO_2 emissions from peatland lakes might decrease. Given anthropogenic CH_4 emissions are projected to correspond to temperature increases above 3˚C, there is an urgent need for large reductions in global CH_4 emissions to meet the temperature targets set by the Paris agreement

(Collins et al., 2013; Nisbet et al., 2019). Therefore, it is also a research priority to constrain the magnitude of natural CH_4 emissions, including from northern latitudes, and assess how natural emissions might change with climate warming to constrain the total annual CH_4 budget and set realistic reduction goals. Below I suggest potential directions for future research to constrain current GHG emissions estimates from the Boreal-Arctic region and to better assess how emissions may change with warming.

In Chapter 2, through empirical model exploration of the controls on CH_4 fluxes, including a scaling exercise across the entire study domain, I highlighted key gaps in the current CH_4 flux data. First, I show that empirical models performed better for terrestrial fluxes than aquatic diffusive and ebullitive fluxes. I suggest poor model performance for fluxes from aquatic ecosystems is, in part, linked to under-sampling, which potentially reduces the accuracy of mean CH_4 flux estimates leading to the relatively poor fitness and explanatory power of the aquatic regression analysis. Future studies should aim to measure diffusive and ebullitive emissions more times over the ice-free season as outlined in Wik et al. 2016b and Jansen et al. 2020. Furthermore, my synthesis focused on ice-free and warm-season emissions only with rough estimates of ratios between winter/ice-out emissions and warm-season emissions. Winter/ice-out and shoulder season emissions represent a potentially significant portion of the annual aquatic and terrestrial CH_4 budget (Karlsson et al. 2013; Sepulveda-Jauregui et al. 2015; Zona et al. 2016; Treat et al. 2018); thus, future research should focus on these less commonly studied seasonal periods. Finally, to compare my results directly against other bottom-up and top-down model estimates, the domains should be masked to similar areas, and the inverse models should use my estimate as a priori information and BAWLD as the land cover map.

While I show that scaling emissions by CH_4-specific land cover classes reduces estimates of annual CH_4 emissions compared to previous bottom-up estimates, I highlight specific ecosystems that are less constrained through uncertainty analysis of individual classes. The least constrained classes include *Fens, Small Peatland Lakes*, and *Large/Midsize Glacial Lakes*, which had the highest variability in their model coefficients. The classes were also under-represented when comparing their potential flux contributions and the number of associated measurements (except *Small Peatland Lakes*, which were well represented by the number of measurements). I suggest future flux-based studies focus on these land cover classes to constrain uncertainty of annual emission estimates.

Lastly, while I do not scale CH_4 exchange from upland environments (i.e., *Dry Tundra, Boreal Forests*, and *Rocklands*) due to low sample sizes, the range of fluxes reported suggest upland environments could be sinks or small sources of CH_4 throughout the year. Given the vast area covered by upland ecosystems, minor differences in estimated fluxes from these areas could make a big difference in the annual CH_4 budget across the Boreal-Arctic region and potentially lead to similar bottom-up and top-down estimates if incorporated into bottom-up models. Recent process-based modeling efforts suggest Boreal-Arctic uplands are a large net sink of CH_4 (~ -9 Tg yr^{-1}; Oh et al. 2019). However, ground-based studies in these ecosystems are limited. I suggest the best path towards constraining CH_4 emission from upland environments is to install more eddy covariance towers in these areas instead of using chambers. Eddy covariance towers may better capture the potential variability in the sink or source capacity from uplands while capturing better representations of the entire ecosystem output (i.e., potential uptake or release of CH_4 from large trees are not included in chamber measurements; Pangala et al. 2015).

In Chapter 3, I show that CH_4 and CO_2 emissions from peatland lakes may have opposing responses to climate warming and permafrost thaw, with higher CH_4 emissions and potentially more uptake of CO_2. The strong association between warmer temperatures and increasing CH_4 emissions from peatland lakes agrees with previous findings based on laboratory studies and field studies across different regions (e.g. Yvon-Durocher et al. 2014; Aben et al. 2017). My results further affirm that future studies can rely on this temperature relationship to project emissions with climate warming. Interestingly, my findings of decreasing CO_2 emissions from peatland lakes with warming do not match findings from lakes in different northern regions (e.g. Bogard et al. 2016; Hastie et al. 2018). The results of these other studies suggest all northern boreal lakes are and will continue to be net sources of CO_2 (see Hastie et al. 2018). Here I show that some boreal peatland lakes are sinks of CO_2 during the ice-free seasons, and more lakes may become sinks as permafrost thaws and hydrologic connectivity shifts. I suggest the differences in CO_2 exchange observed in my study lakes compared to other northern lakes are associated with landscape history, groundwater connectivity, and nutrient delivery. Future research should examine the role of geological substrate and potential shifts from surface water to groundwater on lake nutrient status and CO_2 exchange.

In Chapter 4, I show that CH_4 emissions from a small peatland lake are relatively high and vary over space with the highest emissions from the permafrost thaw edge. Radiocarbon dating suggests that ebullitive emissions from the thaw edge are sourced from older, potentially recently thawed permafrost OM. I found the ages of CH_4 found in the bubbles is similar to other peatland thermokarst lakes (Estop-Aragonés et al. 2020), but the magnitude of ebullitive emissions is much greater (Burke et al. 2019; Matveev et al. 2016) and more similar to yedoma thermokarst lakes (Walter et al. 2008). While in Chapter 2 I show that CH_4 emissions from most peatland lakes act more similarly to one another than they do to yedoma or glacial lakes, I do not explicitly compare thermokarst lakes. The results from Chapter 4 suggest differences in the magnitude of ebullitive emissions observed between the peatland thaw lake in my study and other peatland thaw lakes may be linked to lake morphology, sediment OM quality/quality, and landscape history. Thus, I suggest moving forward that researchers incorporate landscape history, sediment OM quality and depth, and lake morphology when measuring CH_4 emissions.

To summarize, in Chapter 2, I demonstrate that Boreal-Arctic ecosystems can be split by overarching CH_4-emitting landscape characteristics, leading to a bottom-up estimate of annual CH_4 emissions closer to estimates provided by inverse models (i.e., top-down approaches). In Chapters 3 and 4, I show that climate warming and permafrost thaw will lead to more CH_4 emissions from peatland lakes but potentially less CO_2 emissions. In these chapters, I also demonstrate that the magnitude and climate response of CH_4 emissions from peatland thaw lakes may differ across regions depending on lake morphology, organic matter quality/quantity, and landscape history/composition. Together, these findings suggest that future research, including GHG emission models, should consider wetland and lake types and regional variability when estimating current emissions and projecting future emissions with warming. A state-factor approach outlined by Tank et al. (2020), which considers regional topography, permafrost extent/content, and parent material substance and history, is one example of a framework that could be used towards more unified approaches to assessing the role of regional and local variability in determining GHG emissions from peatland lakes. More generally, collaborative and coordinated field campaigns should utilize similar methodologies and ideological frameworks across diverse geographical locations and ecosystem types, with a particular focus on the under-represented and less constrained ecosystems outlined above.

Bibliography

Abbott, B.W., Jones, J.B., Schuur, E.A., Chapin III, F.S., Bowden, W.B., Bret-Harte, M.S., Epstein, H.E., Flannigan, M.D., Harms, T.K., Hollingsworth, T.N. and Mack, M.C., 2016. Biomass offsets little or none of permafrost carbon release from soils, streams, and wildfire: an expert assessment. *Environmental Research Letters*, *11*(3), p.034014.

Aben, R.C., Barros, N., Van Donk, E., Frenken, T., Hilt, S., Kazanjian, G., Lamers, L.P., Peeters, E.T., Roelofs, J.G., de Senerpont Domis, L.N. and Stephan, S., 2017. Cross continental increase in methane ebullition under climate change. *Nature communications*, *8*(1), pp.1-8.

Allen, M.R., Shine, K.P., Fuglestvedt, J.S., Millar, R.J., Cain, M., Frame, D.J. and Macey, A.H., 2018. A solution to the misrepresentations of CO 2-equivalent emissions of short-lived climate pollutants under ambitious mitigation. *Npj Climate and Atmospheric Science*, *1*(1), pp.1-8.

Andersen, R., Poulin, M., Borcard, D., Laiho, R., Laine, J., Vasander, H. and Tuittila, E.T., 2011. Environmental control and spatial structures in peatland vegetation. *Journal of Vegetation Science*, *22*(5), pp.878-890.

Ask, J., Karlsson, J. and Jansson, M., 2012. Net ecosystem production in clear-water and brown-water lakes. *Global Biogeochemical Cycles*, *26*(1).

Ask, J., Karlsson, J., Persson, L., Ask, P., Byström, P. and Jansson, M., 2009. Terrestrial organic matter and light penetration: Effects on bacterial and primary production in lakes. *Limnology and Oceanography*, *54*(6), pp.2034-2040.

Bade, D.L., Carpenter, S.R., Cole, J.J., Hanson, P.C. and Hesslein, R.H., 2004. Controls of δ13C-DIC in lakes: Geochemistry, lake metabolism, and morphometry. *Limnology and Oceanography*, 49(4), pp.1160-1172.

Bartlett, K.B., Crill, P.M., Sass, R.L., Harriss, R.C. and Dise, N.B., 1992. Methane emissions from tundra environments in the Yukon-Kuskokwim Delta, Alaska. *Journal of Geophysical Research: Atmospheres*, *97*(D15), pp.16645-16660.

Basiliko, N., Knowles, R. and Moore, T.R., 2004. Roles of moss species and habitat in methane consumption potential in a northern peatland. *Wetlands*, *24*(1), pp.178-185.

Bastviken, D., Cole, J., Pace, M. and Tranvik, L., 2004. Methane emissions from lakes: Dependence of lake characteristics, two regional assessments, and a global estimate. *Global biogeochemical cycles*, *18*(4).

Bastviken, D., Ejlertsson, J. and Tranvik, L., 2002. Measurement of methane oxidation in lakes: a comparison of methods. *Environmental science & technology*, *36*(15), pp.3354-3361.

Bastviken, D., Tranvik, L.J., Downing, J.A., Crill, P.M. and Enrich-Prast, A., 2011. Freshwater methane emissions offset the continental carbon sink. *Science*, *331*(6013), pp.50-50.

Bates, D., M€achler, M., Bolker, B., & Walker, S. 2015. Fitting linear mixed-effects models using lme4, vol. 67, p. 48.

Beaulne, J., Garneau, M., Magnan, G. and Boucher, É., 2021. Peat deposits store more carbon than trees in forested peatlands of the boreal biome. *Scientific reports*, *11*(1), pp.1-11

Beer, J. and Blodau, C., 2007. Transport and thermodynamics constrain belowground carbon turnover in a northern peatland. *Geochimica et Cosmochimica Acta*, 71(12), pp.2989-3002.

Bellisario, L.M., Bubier, J.L., Moore, T.R. and Chanton, J.P., 1999. Controls on CH4 emissions from a northern peatland. *Global Biogeochemical Cycles*, *13*(1), pp.81-91.

Belyea, L.R. and Baird, A.J., 2006. Beyond "the limits to peat bog growth": Cross-scale feedback in peatland development. *Ecological Monographs*, *76*(3), pp.299-322.

Bogard, M.J., St-Gelais, N.F., Vachon, D. and del Giorgio, P.A., 2020. Patterns of spring/summer open-water metabolism across boreal lakes. *Ecosystems*, pp.1-17.

Bogard, M.J. and del Giorgio, P.A., 2016. The role of metabolism in modulating CO2 fluxes in boreal lakes. *Global Biogeochemical Cycles*, *30*(10), pp.1509-1525.

Bogard, M.J., Kuhn, C.D., Johnston, S.E., Striegl, R.G., Holtgrieve, G.W., Dornblaser, M.M., Spencer, R.G., Wickland, K.P. and Butman, D.E., 2019. Negligible cycling of terrestrial carbon in many lakes of the arid circumpolar landscape. *Nature Geoscience*, *12*(3), pp.180-185.

Bouchard, F., Laurion, I., Prėskienis, V., Fortier, D., Xu, X. and Whiticar, M.J., 2015. Modern to millennium-old greenhouse gases emitted from ponds and lakes of the Eastern Canadian Arctic (Bylot Island, Nunavut). *Biogeosciences*, *12*(23), pp.7279-7298.

Boyd, J.A., Woodcroft, B.J. and Tyson, G.W., 2018. GraftM: a tool for scalable, phylogenetically informed classification of genes within metagenomes. *Nucleic Acids Research*, *46*(10), pp.e59-e59.

Bridgham, S.D., Cadillo-Quiroz, H., Keller, J.K. and Zhuang, Q., 2013. Methane emissions from wetlands: biogeochemical, microbial, and modeling perspectives from local to global scales. *Global change biology*, *19*(5), pp.1325-1346.

Brown, J., O. Ferrians, J. A. Heginbottom, and E. Melnikov. 2002. *Circum-Arctic Map of Permafrost and Ground-Ice Conditions, Version 2*. Boulder, Colorado USA. NSIDC: National Snow and Ice Data Center. doi: https://doi.org/10.7265/skbg-kf16. [11/20/2020]

Bruhwiler, L., Dlugokencky, E., Masarie, K., Ishizawa, M., Andrews, A., Miller, J., Sweeney, C., Tans, P. and Worthy, D., 2014. CarbonTracker-CH 4: an assimilation system for estimating emissions of atmospheric methane. *Atmospheric Chemistry and Physics*, 14(16), pp.8269-8293.

Bubier, J.L., Moore, T.R., Bellisario, L., Comer, N.T. and Crill, P.M., 1995. Ecological controls on methane emissions from a northern peatland complex in the zone of discontinuous permafrost, Manitoba, Canada. *Global Biogeochemical Cycles*, *9*(4), pp.455-470.

Burke, S.A., Wik, M., Lang, A., Contosta, A.R., Palace, M., Crill, P.M. and Varner, R.K., 2019. Long-term measurements of methane ebullition from thaw ponds. *Journal of Geophysical Research: Biogeosciences*, *124*(7), pp.2208-2221.

Burd, K., Tank, S.E., Dion, N., Quinton, W.L., Spence, C., Tanentzap, A.J. and Olefeldt, D., 2018. Seasonal shifts in export of DOC and nutrients from burned and unburned peatland-rich catchments, Northwest Territories, Canada. *Hydrology and Earth System Sciences*, *22*(8), pp.4455-4472.

Canada Committee on Ecological (Biophysical) Land Classification, National Wetlands Working Group, Warner, B. G., and Rubec, C. D. A., 1997. The Canadian wetland classification system, Wetlands Research Branch, University of Waterloo, Waterloo, Ont.

Canada, G. S. of. Canadian Geoscience Map. 2014. doi:https://doi.org/10.4095/295462.

Carpenter, S.R., Cole, J.J., Hodgson, J.R., Kitchell, J.F., Pace, M.L., Bade, D., Cottingham, K.L., Essington, T.E., Houser, J.N. and Schindler, D.E., 2001. Trophic cascades, nutrients, and lake productivity: whole-lake experiments. *Ecological monographs*, *71*(2), pp.163-186.

Chanton, J.P., Whiting, G.J., Happell, J.D. and Gerard, G., 1993. Contrasting rates and diurnal patterns of methane emission from emergent aquatic macrophytes. *Aquatic botany*, *46*(2), pp.111-128

Chen, L., Reeve, J., Zhang, L., Huang, S., Wang, X. and Chen, J., 2018. GMPR: A robust normalization method for zero-inflated count data with application to microbiome sequencing data. *PeerJ*, *6*, p.e4600.

Christensen, T.R., Jonasson, S., Callaghan, T.V. and Havström, M., 1995. Spatial variation in high-latitude methane flux along a transect across Siberian and European tundra environments. *Journal of Geophysical Research: Atmospheres*, *100*(D10), pp.21035-21045.

Christensen, T.R., Ekberg, A., Ström, L., Mastepanov, M., Panikov, N., Öquist, M., Svensson, B.H., Nykänen, H., Martikainen, P.J. and Oskarsson, H., 2003. Factors controlling large scale variations in methane emissions from wetlands. *Geophysical Research Letters*, *30*(7).

Cole, J.J., Prairie, Y.T., Caraco, N.F., McDowell, W.H., Tranvik, L.J., Striegl, R.G., Duarte, C.M., Kortelainen, P., Downing, J.A., Middelburg, J.J. and Melack, J., 2007. Plumbing the global carbon cycle: integrating inland waters into the terrestrial carbon budget. *Ecosystems*, *10*(1), pp.172-185.

Coleman, K.A., Palmer, M.J., Korosi, J.B., Kokelj, S.V., Jackson, K., Hargan, K.E., Mustaphi, C.J.C., Thienpont, J.R., Kimpe, L.E., Blais, J.M. and Pisaric, M.F., 2015. Tracking the impacts of recent warming and thaw of permafrost peatlands on aquatic ecosystems: a multi-proxy approach using remote sensing and lake sediments.

Collins, M., Knutti, R., Arblaster, J., Dufresne, J. L., Fichefet, T., Friedlingstein, P., ... & Booth, B. B. 2013. Long-term climate change: projections, commitments and irreversibility. In Climate Change 2013-The Physical Science Basis: Contribution of Working Group I to the Fifth

Assessment Report of the Intergovernmental Panel on Climate Change (pp. 1029-1136). Cambridge University Press.

Conrad, R., Claus, P. and Casper, P., 2009. Characterization of stable isotope fractionation during methane production in the sediment of a eutrophic lake, Lake Dagow, Germany. *Limnology and Oceanography*, *54*(2), pp.457-471.

Corbett, J.E., Tfaily, M.M., Burdige, D.J., Glaser, P.H. and Chanton, J.P., 2015. The relative importance of methanogenesis in the decomposition of organic matter in northern peatlands. *Journal of Geophysical Research: Biogeosciences*, *120*(2), pp.280-293.

Couture, S., Houle, D. and Gagnon, C., 2012. Increases of dissolved organic carbon in temperate and boreal lakes in Quebec, Canada. *Environmental Science and Pollution Research*, *19*(2), pp.361-371.

Crann CA, Murseli S, St-Jean G, Zhao X, Clark ID, Kieser WE. 2017. First status report on radiocarbon sample preparation at the A.E. Lalonde AMS Laboratory(Ottawa, Canada). Radiocarbon 59(3): 695–704.

Quinton, W., Berg, A., Braverman, M., Carpino, O., Chasmer, L., Connon, R., Craig, J., Devoie, É., Hayashi, M., Haynes, K. and Olefeldt, D., 2019. A synthesis of three decades of hydrological research at Scotty Creek, NWT, Canada. *Hydrology and Earth System Sciences*, *23*(4), pp.2015-2039.

Czikowsky, M.J., MacIntyre, S., Tedford, E.W., Vidal, J. and Miller, S.D., 2018. Effects of wind and buoyancy on carbon dioxide distribution and air-water flux of a stratified temperate lake. *Journal of Geophysical Research: Biogeosciences*, *123*(8), pp.2305-2322.

Dean, J.F., Meisel, O.H., Rosco, M.M., Marchesini, L.B., Garnett, M.H., Lenderink, H., van Logtestijn, R., Borges, A.V., Bouillon, S., Lambert, T. and Röckmann, T., 2020. East Siberian Arctic inland waters emit mostly contemporary carbon. *Nature Communications*, *11*(1), pp.1-10.

del Giorgio, P.A. and Peters, R.H., 1994. Patterns in planktonic P: R ratios in lakes: influence of lake trophy and dissolved organic carbon. *Limnology and Oceanography*, *39*(4), pp.772-787.

DelSontro, T., Beaulieu, J.J. and Downing, J.A., 2018. Greenhouse gas emissions from lakes and impoundments: Upscaling in the face of global change. *Limnology and Oceanography Letters*, *3*(3), pp.64-75

DelSontro, T., Boutet, L., St-Pierre, A., del Giorgio, P.A. and Prairie, Y.T., 2016. Methane ebullition and diffusion from northern ponds and lakes regulated by the interaction between temperature and system productivity. *Limnology and Oceanography*, *61*(S1), pp.S62-S77.

Delwiche, K.B., Knox, S.H., Malhotra, A., Fluet-Chouinard, E., McNicol, G., Feron, S., Ouyang, Z., Papale, D., Trotta, C., Canfora, E. and Cheah, Y.W., 2021. FLUXNET-CH4: A global, multi-ecosystem dataset and analysis of methane seasonality from freshwater wetlands. *Earth System Science Data Discussions*, pp.1-111.

Dieleman, C.M., Rogers, B.M., Potter, S., Veraverbeke, S., Johnstone, J.F., Laflamme, J., Solvik, K., Walker, X.J., Mack, M.C. and Turetsky, M.R., 2020. Wildfire combustion and carbon stocks

in the southern Canadian boreal forest: Implications for a warming world. *Global Change Biology*, *26*(11), pp.6062-6079.

Dinno, A. 2017. dunn.test: Dunn's test of multiple comparisons using rank sums

Douglas, P.M., Gonzalez Moguel, R., Walter Anthony, K.M., Wik, M., Crill, P.M., Dawson, K.S., Smith, D.A., Yanay, E., Lloyd, M.K., Stolper, D.A. and Eiler, J.M., 2020. Clumped isotopes link older carbon substrates with slower rates of methanogenesis in northern lakes. *Geophysical Research Letters*, *47*(6), p.e2019GL086756.

Downing, J.A., Cole, J.J., Duarte, C.M., Middelburg, J.J., Melack, J.M., Prairie, Y.T., Kortelainen, P., Striegl, R.G., McDowell, W.H. and Tranvik, L.J., 2012. Global abundance and size distribution of streams and rivers. *Inland Waters*, *2*(4), pp.229-236.

Downing, J.A., Cole, J.J., Middelburg, J.J., Striegl, R.G., Duarte, C.M., Kortelainen, P., Prairie, Y.T. and Laube, K.A., 2008. Sediment organic carbon burial in agriculturally eutrophic impoundments over the last century. *Global Biogeochemical Cycles*, *22*(1).

Elder, C.D., Xu, X., Walker, J., Schnell, J.L., Hinkel, K.M., Townsend-Small, A., Arp, C.D., Pohlman, J.W., Gaglioti, B.V. and Czimczik, C.I., 2018. Greenhouse gas emissions from diverse Arctic Alaskan lakes are dominated by young carbon. *Nature Climate Change*, *8*(2), pp.166-171

Emilson, E.J., Carson, M.A., Yakimovich, K.M., Osterholz, H., Dittmar, T., Gunn, J.M., Mykytczuk, N.C.S., Basiliko, N. and Tanentzap, A.J., 2018. Climate-driven shifts in sediment chemistry enhance methane production in northern lakes. *Nature Communications*, *9*(1), pp.1-6.

Emmerton, C.A., St Louis, V.L., Lehnherr, I., Humphreys, E.R., Rydz, E. and Kosolofski, H.R., 2014. The net exchange of methane with high Arctic landscapes during the summer growing season. *Biogeosciences*, *11*(12), pp.3095-3106.

Engel, F., Attermeyer, K. and Weyhenmeyer, G.A., 2020. A simplified approach to detect a significant carbon dioxide reduction by phytoplankton in lakes and rivers on a regional and global scale. *The Science of Nature*, *107*(4), pp.1-10.

Estop-Aragonés, C., Olefeldt, D., Abbott, B.W., Chanton, J.P., Czimczik, C.I., Dean, J.F., Egan, J.E., Gandois, L., Garnett, M.H., Hartley, I.P. and Hoyt, A., 2020. Assessing the potential for mobilization of old soil carbon after permafrost thaw: A synthesis of 14C measurements from the northern permafrost region. *Global Biogeochemical Cycles*, *34*(9), p.e2020GB006672.

Ettwig, K.F., Zhu, B., Speth, D., Keltjens, J.T., Jetten, M.S. and Kartal, B., 2016. Archaea catalyze iron-dependent anaerobic oxidation of methane. *Proceedings of the National Academy of Sciences*, *113*(45), pp.12792-12796.

Fang, X. and Stefan, H.G., 1999. Projections of climate change effects on water temperature characteristics of small lakes in the contiguous US. *Climatic Change*, *42*(2), pp.377-412.

Frenzel, P. and Karofeld, E., 2000. CH4 emission from a hollow-ridge complex in a raised bog: The role of CH4 production and oxidation. *Biogeochemistry*, *51*(1), pp.91-112.

Frey, K.E. and McClelland, J.W., 2009. Impacts of permafrost degradation on arctic river biogeochemistry. *Hydrological Processes: An International Journal*, *23*(1), pp.169-182.

Frolking, S., Roulet, N. and Fuglestvedt, J., 2006. How northern peatlands influence the Earth's radiative budget: Sustained methane emission versus sustained carbon sequestration. *Journal of Geophysical Research: Biogeosciences*, *111*(G1).

Gardner, R.C. and Davidson, N.C., 2011. The ramsar convention. In *Wetlands* (pp. 189-203). Springer, Dordrecht.

Garneau, M., Tremblay, L. and Magnan, G., 2018. Holocene pool formation in oligotrophic fens from boreal Québec in northeastern Canada. *The Holocene*, *28*(3), pp.396-407.

Garnett, M.H., Gulliver, P. and Billett, M.F., 2016. A rapid method to collect methane from peatland streams for radiocarbon analysis. *Ecohydrology*, *9*(1), pp.113-121.

Gibson, C., Cottenie, K., Gingras-Hill, T., Kokelj, S.V., Baltzer, J., Chasmer, L. and Turetsky, M., 2021. Mapping and understanding the vulnerability of northern peatlands to permafrost thaw at scales relevant to community adaptation planning. *Environmental Research Letters*.

Glaser, P.H., Siegel, D.I., Reeve, A.S., Janssens, J.A. and Janecky, D.R., 2004. Tectonic drivers for vegetation patterning and landscape evolution in the Albany River region of the Hudson Bay Lowlands. *Journal of Ecology*, *92*(6), pp.1054-1070.

Gómez-Gener, L., Rocher-Ros, G., Battin, T., Cohen, M.J., Dalmagro, H.J., Dinsmore, K.J., Drake, T.W., Duvert, C., Enrich-Prast, A., Horgby, Å. and Johnson, M.S., 2021. Global carbon dioxide efflux from rivers enhanced by high nocturnal emissions. *Nature Geoscience*, pp.1-6.

Gorham, E., 1991. Northern peatlands: role in the carbon cycle and probable responses to climatic warming. *Ecological Applications*, 1(2), pp.182-195.

Government of the Norwest Territories, Environment, D. O., & Resources, N. (2007). Ecosystem Classification Group, 1–184.

Government of the Northwest Territories. 2030 Nwt Climate Change Strategic Framework. 2018.https://www.enr.gov.nt.ca/sites/enr/files/resources/128climate_change_strategic_framework_web.pdf.

Grossart, H.P., Frindte, K., Dziallas, C., Eckert, W. and Tang, K.W., 2011. Microbial methane production in oxygenated water column of an oligotrophic lake. *Proceedings of the National Academy of Sciences*, *108*(49), pp.19657-19661.

Gudasz, C., Bastviken, D., Steger, K., Premke, K., Sobek, S. and Tranvik, L.J., 2010. Temperature-controlled organic carbon mineralization in lake sediments. *Nature*, *466*(7305), pp.478-481.

Gunnarsson, U. and Löfroth, M. 2013. The Swedish wetland survey: compiled excerpts from the national final report. Swedish Environmental Protection Agency.

Günther, A., Barthelmes, A., Huth, V., Joosten, H., Jurasinski, G., Koebsch, F. and Couwenberg, J., 2020. Prompt rewetting of drained peatlands reduces climate warming despite methane emissions. *Nature Communications*, *11*(1), pp.1-5.

Guo, M., Zhuang, Q., Tan, Z., Shurpali, N., Juutinen, S., Kortelainen, P. and Martikainen, P.J., 2020. Rising methane emissions from boreal lakes due to increasing ice-free days. *Environmental Research Letters*, *15*(6), p.064008.

Halsey, L.A., Vitt, D.H. and Bauer, I.E., 1998. Peatland initiation during the Holocene in continental western Canada. *Climatic Change*, *40*(2), pp.315-342.

Harris, L.I., Roulet, N.T. and Moore, T.R., 2020. Mechanisms for the development of microform patterns in peatlands of the Hudson Bay lowland. *Ecosystems*, 23(4), pp.741-767.

Hastie, A., Lauerwald, R., Weyhenmeyer, G., Sobek, S., Verpoorter, C. and Regnier, P., 2018. CO 2 evasion from boreal lakes: revised estimate, drivers of spatial variability, and future projections. *Global Change Biology*, *24*(2), pp.711-728.

Heffernan, L., Estop-Aragonés, C., Knorr, K.H., Talbot, J. and Olefeldt, D., 2020. Long-term impacts of permafrost thaw on carbon storage in peatlands: Deep losses offset by surficial accumulation. *Journal of Geophysical Research: Biogeosciences*, *125*(3), p.e2019JG005501.

Heginbottom, J.A., Dubreuil, M.A. and Harker, P.A., 1995. Canada, Permafrost. National Atlas of Canada. Natural Resources Canada, 5th Edition, MCR, 4177.

Heikkinen, J.E., Virtanen, T., Huttunen, J.T., Elsakov, V. and Martikainen, P.J., 2004. Carbon balance in East European tundra. *Global Biogeochemical Cycles*, *18*(1).

Heiskanen, J.J., Mammarella, I., Haapanala, S., Pumpanen, J., Vesala, T., MacIntyre, S. and Ojala, A., 2014. Effects of cooling and internal wave motions on gas transfer coefficients in a boreal lake. *Tellus B: Chemical and Physical Meteorology*, *66*(1), p.22827.

Heiskanen, L., Tuovinen, J.P., Räsänen, A., Virtanen, T., Juutinen, S., Lohila, A., Penttilä, T., Linkosalmi, M., Mikola, J., Laurila, T. and Aurela, M., 2021. Carbon dioxide and methane exchange of a patterned subarctic fen during two contrasting growing seasons. *Biogeosciences*, *18*(3), pp.873-896.

Helbig, M., Chasmer, L.E., Kljun, N., Quinton, W.L., Treat, C.C. and Sonnentag, O., 2017. The positive net radiative greenhouse gas forcing of increasing methane emissions from a thawing boreal forest-wetland landscape. *Global Change Biology*, *23*(6), pp.2413-2427.

Heslop, J.K., Walter Anthony, K.M., Sepulveda-Jauregui, A., Martinez-Cruz, K., Bondurant, A., Grosse, G. and Jones, M.C., 2015. Thermokarst lake methanogenesis along a complete talik profile. *Biogeosciences*, *12*(14), pp.4317-4331.

Heslop, J.K., Anthony, K.W., Winkel, M., Sepulveda-Jauregui, A., Martinez-Cruz, K., Bondurant, A., Grosse, G. and Liebner, S., 2020. A synthesis of methane dynamics in thermokarst lake environments. *Earth-Science Reviews*, p.103365.

Hesslein, R.H., 1976. An in situ sampler for close interval pore water studies 1. *Limnology and Oceanography*, *21*(6), pp.912-914.

Hokanson, K.J., Mendoza, C.A. and Devito, K.J., 2019. Interactions between regional climate, surficial geology, and topography: characterizing shallow groundwater systems in subhumid, low-relief landscapes. *Water Resources Research*, *55*(1), pp.284-297.

Holgerson, M.A. and Raymond, P.A., 2016. Large contribution to inland water CO 2 and CH 4 emissions from very small ponds. *Nature Geoscience*, *9*(3), pp.222-226.

Hopple, A.M., Wilson, R.M., Kolton, M., Zalman, C.A., Chanton, J.P., Kostka, J., Hanson, P.J., Keller, J.K. and Bridgham, S.D., 2020. Massive peatland carbon banks vulnerable to rising temperatures. *Nature Communications*, *11*(1), pp.1-7.

Houle, D., Khadra, M., Marty, C. and Couture, S., 2020. Influence of hydro-morphologic variables of forested catchments on the increase in DOC concentration in 36 temperate lakes of eastern Canada. *Science of The Total Environment*, *747*, p.141539.

Hugelius, G., Loisel, J., Chadburn, S., Jackson, R.B., Jones, M., MacDonald, G., Marushchak, M., Olefeldt, D., Packalen, M., Siewert, M.B. and Treat, C., 2020. Large stocks of peatland carbon and nitrogen are vulnerable to permafrost thaw. *Proceedings of the National Academy of Sciences*, *117*(34), pp.20438-20446.

Jahne, B., Heinz, G. & Dietrich, W. 1987. Measurement of the diffusion coefficients of sparingly soluble gases in water. *Journal of Geophysical Research*, 92, 10767–10776.

Jansen, J., Thornton, B.F., Cortés, A., Snöälv, J., Wik, M., MacIntyre, S. and Crill, P.M., 2020. Drivers of diffusive CH 4 emissions from shallow subarctic lakes on daily to multi-year timescales. *Biogeosciences*, *17*(7), pp.1911-1932.

Jansen, J., Thornton, B.F., Jammet, M.M., Wik, M., Cortés, A., Friborg, T., MacIntyre, S. and Crill, P.M., 2019. Climate-sensitive controls on large spring emissions of CH4 and CO2 from northern lakes. *Journal of Geophysical Research: Biogeosciences*, 124(7), pp.2379-2399.

Joos, F., Roth, R., Fuglestvedt, J.S., Peters, G.P., Enting, I.G., Bloh, W.V., Brovkin, V., Burke, E.J., Eby, M., Edwards, N.R. and Friedrich, T., 2013. Carbon dioxide and climate impulse response functions for the computation of greenhouse gas metrics: a multi-model analysis. *Atmospheric Chemistry and Physics*, *13*(5), pp.2793-2825.

Jorgenson, M.T., Racine, C.H., Walters, J.C. and Osterkamp, T.E., 2001. Permafrost degradation and ecological changes associated with a warmin gclimate in central Alaska. *Climatic Change*, *48*(4), pp.551-579.

Juggins, S. 2003. “C2 User Guide: Software for Ecological and Palaeoecological Data Analysis and Visualization.” User Guide. Newcastle upon Tyne, UK: Newcastle University. http://scholar.google.com/scholar?hl=en&btnG=Search&q=intitle:C2+Software+for+ecological+and+palaeoecological+data+analysis+and+visualisation#0.

Juutinen, S., Alm, J., Larmola, T., Huttunen, J.T., Morero, M., Martikainen, P.J. and Silvola, J., 2003. Major implication of the littoral zone for methane release from boreal lakes. *Global Biogeochemical Cycles*, *17*(4).

Karlsson, J., Christensen, T.R., Crill, P., Förster, J., Hammarlund, D., Jackowicz-Korczynski, M., Kokfelt, U., Roehm, C. and Rosén, P., 2010. Quantifying the relative importance of lake emissions in the carbon budget of a subarctic catchment. *Journal of Geophysical Research: Biogeosciences*, *115*(G3).

Karlsson, J., Giesler, R., Persson, J. and Lundin, E., 2013. High emission of carbon dioxide and methane during ice thaw in high latitude lakes. *Geophysical research letters*, *40*(6), pp.1123-1127.

Kelly, C.A. and Chynoweth, D.P., 1981. The contributions of temperature and of the input of organic matter in controlling rates of sediment methanogenesis 1. *Limnology and Oceanography*, *26*(5), pp.891-897.

Kip, N., Van Winden, J.F., Pan, Y., Bodrossy, L., Reichart, G.J., Smolders, A.J., Jetten, M.S., Damsté, J.S.S. and Den Camp, H.J.O., 2010. Global prevalence of methane oxidation by symbiotic bacteria in peat-moss ecosystems. *Nature Geoscience*, *3*(9), pp.617-621.

Kissman, C.E., Williamson, C.E., Rose, K.C. and Saros, J.E., 2013. Response of phytoplankton in an alpine lake to inputs of dissolved organic matter through nutrient enrichment and trophic forcing. *Limnology and Oceanography*, *58*(3), pp.867-880.

Klaus, M., Bergström, A.K., Jonsson, A., Deininger, A., Geibrink, E. and Karlsson, J., 2018. Weak response of greenhouse gas emissions to whole lake N enrichment. *Limnology and Oceanography*, *63*(S1), pp.S340-S353.

Klug, J.L., 2002. Positive and negative effects of allochthonous dissolved organic matter and inorganic nutrients on phytoplankton growth. *Canadian Journal of Fisheries and Aquatic Sciences*, *59*(1), pp.85-95.

Knox, S.H., Jackson, R.B., Poulter, B., McNicol, G., Fluet-Chouinard, E., Zhang, Z., Hugelius, G., Bousquet, P., Canadell, J.G., Saunois, M. and Papale, D., 2019. FLUXNET-CH4 synthesis activity: Objectives, observations, and future directions. *Bulletin of the American Meteorological Society*, *100*(12), pp.2607-2632.

Kosten, S., Roland, F., Marques, D.D.M., Van Nes, E.H. and Mazzeo, N., L. d. S. Sternberg, M. Scheffer, and JJ Cole (2010), Climate-dependent CO2 emissions from lakes. *Global Biogeochem. Cycles*, *24*.

Krüger, J.P., Leifeld, J. and Alewell, C., 2014. Degradation changes stable carbon isotope depth profiles in palsa peatlands. *Biogeosciences*, *11*(12), pp.3369-3380.

Kuhn, M., Lundin, E.J., Giesler, R., Johansson, M. and Karlsson, J., 2018. Emissions from thaw ponds largely offset the carbon sink of northern permafrost wetlands. *Scientific Reports*, *8*(1), pp.1-7.

Kuhn, M.A., Thompson, L.M., Tanentzap, A., Winder, J., Braga, L., Bastviken, D., Olefeldt, D., *In Review*. Permafrost and climate strongly influence CH_4 and CO_2 emissions from peatland lakes.

Kuhn, M.A., Varner, R.K., Bastivken, D., Crill, P., MacIntrye, S., Turetsky, M., Anthony, K.W., McGuire, A.D. and Olefeldt, D., 2021. BAWLD-CH_4: A Comprehensive Dataset of Methane Fluxes from Boreal and Arctic Ecosystems. Arctic Data Center [data set], https://doi.org/10.18739/A27H1DN5S

Langenegger, T., Vachon, D., Donis, D. and McGinnis, D.F., 2019. What the bubble knows: Lake methane dynamics revealed by sediment gas bubble composition. *Limnology and Oceanography*, *64*(4), pp.1526-1544.

Lapierre, J.F. and del Giorgio, P.A., 2012. Geographical and environmental drivers of regional differences in the lake pCO2 versus DOC relationship across northern landscapes. *Journal of Geophysical Research: Biogeosciences*, *117*(G3).

Lapierre, J.F., Seekell, D.A. and Del Giorgio, P.A., 2015. Climate and landscape influence on indicators of lake carbon cycling through spatial patterns in dissolved organic carbon. *Global Change Biology*, *21*(12), pp.4425-4435.

Larmola, T., Tuittila, E.S., Tiirola, M., Nykänen, H., Martikainen, P.J., Yrjälä, K., Tuomivirta, T. and Fritze, H., 2010. The role of Sphagnum mosses in the methane cycling of a boreal mire. *Ecology*, *91*(8), pp.2356-2365.

Laudon, H., Buttle, J., Carey, S.K., McDonnell, J., McGuire, K., Seibert, J., Shanley, J., Soulsby, C. and Tetzlaff, D., 2012. Cross-regional prediction of long-term trajectory of stream water DOC response to climate change. *Geophysical Research Letters*, *39*(18).

Laurion, I., Vincent, W.F., MacIntyre, S., Retamal, L., Dupont, C., Francus, P. and Pienitz, R., 2010. Variability in greenhouse gas emissions from permafrost thaw ponds. *Limnology and Oceanography*, *55*(1), pp.115-133.

Le Mer, J. and Roger, P., 2001. Production, oxidation, emission and consumption of methane by soils: a review. *European Journal of Soil Biology*, *37*(1), pp.25-50.

Lehner, B. and Döll, P., 2004. Development and validation of a global database of lakes, reservoirs and wetlands. *Journal of Hydrology*, *296*(1-4), pp.1-22.

Li, M., Peng, C., Zhu, Q., Zhou, X., Yang, G., Song, X. and Zhang, K., 2020. The significant contribution of lake depth in regulating global lake diffusive methane emissions. *Water Research*, *172*, p.115465.

Liljedahl, A.K., Boike, J., Daanen, R.P., Fedorov, A.N., Frost, G.V., Grosse, G., Hinzman, L.D., Iijma, Y., Jorgenson, J.C., Matveyeva, N. and Necsoiu, M., 2016. Pan-Arctic ice-wedge degradation in warming permafrost and its influence on tundra hydrology. *Nature Geoscience*, *9*(4), pp.312-318.

Loisel, J., Yu, Z., Beilman, D.W., Camill, P., Alm, J., Amesbury, M.J., Anderson, D., Andersson, S., Bochicchio, C., Barber, K. and Belyea, L.R., 2014. A database and synthesis of

northern peatland soil properties and Holocene carbon and nitrogen accumulation. *the Holocene*, *24*(9), pp.1028-1042.

Lundin, E.J., Klaminder, J., Bastviken, D., Olid, C., Hansson, S.V. and Karlsson, J., 2015. Large difference in carbon emission–burial balances between boreal and arctic lakes. *Scientific Reports*, *5*(1), pp.1-7.

Machacova, K., Bäck, J., Vanhatalo, A., Halmeenmäki, E., Kolari, P., Mammarella, I., Pumpanen, J., Acosta, M., Urban, O. and Pihlatie, M., 2016. Pinus sylvestris as a missing source of nitrous oxide and methane in boreal forest. *Scientific Reports*, *6*(1), pp.1-8.

MacIntyre, S., Bastviken, D., Arneborg, L., Crowe, A.T., Karlsson, J., Andersson, A., Gålfalk, M., Rutgersson, A., Podgrajsek, E. and Melack, J.M., 2021. Turbulence in a small boreal lake: Consequences for air–water gas exchange. *Limnology and Oceanography*, *66*(3), pp.827-854.

MacIntyre, S., Crowe, A.T., Cortés, A. and Arneborg, L., 2018. Turbulence in a small arctic pond. *Limnology and Oceanography*, *63*(6), pp.2337-2358.

Malhotra, A. and Roulet, N.T., 2015. Environmental correlates of peatland carbon fluxes in a thawing landscape: do transitional thaw stages matter?. *Biogeosciences*, *12*(10), pp.3119-3130.

Malmer, N. and Wallén, B., 1996. Peat formation and mass balance in subarctic ombrotrophic peatland around Abisko, northern Scandinavia. *Ecological Bulletins*, pp.79-92.

Mammarella, I., Nordbo, A., Rannik, Ü., Haapanala, S., Levula, J., Laakso, H., Ojala, A., Peltola, O., Heiskanen, J., Pumpanen, J. and Vesala, T., 2015. Carbon dioxide and energy fluxes over a small boreal lake in Southern Finland. *Journal of Geophysical Research: Biogeosciences*, *120*(7), pp.1296-1314.

Marinho, C.C., Palma-Silva, C., Albertoni, E.F., Giacomini, I.B., Barros, M.P.F., Furlanetto, L.M. and de Assis Esteves, F., 2015. Emergent macrophytes alter the sediment composition in a small, shallow subtropical lake: Implications for methane emission. *American Journal of Plant Sciences*, *6*(02), p.315.

Markfort, C.D., Perez, A.L., Thill, J.W., Jaster, D.A., Porté-Agel, F. and Stefan, H.G., 2010. Wind sheltering of a lake by a tree canopy or bluff topography. *Water Resources Research*, *46*(3).

Masing, V., Botch, M. and Lääne laid, A., 2010. Mires of the former Soviet Union. *Wetlands Ecology and Management*, *18*(4), pp.397-433.

Matson, A., Pennock, D. and Bedard-Haughn, A., 2009. Methane and nitrous oxide emissions from mature forest stands in the boreal forest, Saskatchewan, Canada. *Forest Ecology and Management*, *258*(7), pp.1073-1083.

Matthews, E. and Fung, I., 1987. Methane emission from natural wetlands: Global distribution, area, and environmental characteristics of sources. *Global Biogeochemical Cycles*, *1*(1), pp.61-86.

Matveev, A., Laurion, I., Deshpande, B.N., Bhiry, N. and Vincent, W.F., 2016. High methane emissions from thermokarst lakes in subarctic peatlands. *Limnology and Oceanography*, *61*(S1), pp.S150-S164.

Mauquoy, D., Hughes, P.D.M. and Van Geel, B., 2010. A protocol for plant macrofossil analysis of peat deposits. *Mires and Peat*, *7*(6), pp.1-5.

Mazerolle, M. J., & Mazerolle, M. M. J. 2015. Package "AICcmodavg" AICcmodavg; model selecion and multimodel inference based on(Q) AIC ©. CRAN R Project.

McCalley, C.K., Woodcroft, B.J., Hodgkins, S.B., Wehr, R.A., Kim, E.H., Mondav, R., Crill, P.M., Chanton, J.P., Rich, V.I., Tyson, G.W. and Saleska, S.R., 2014. Methane dynamics regulated by microbial community response to permafrost thaw. *Nature*, *514*(7523), pp.478-481.

McGuire, A.D., Christensen, T.R., Hayes, D., Heroult, A., Euskirchen, E., Kimball, J.S., Koven, C., Lafleur, P., Miller, P.A., Oechel, W. and Peylin, P., 2012. An assessment of the carbon balance of Arctic tundra: comparisons among observations, process models, and atmospheric inversions. *Biogeosciences*, *9*(8), pp.3185-3204.

McKenzie, J.M., Kurylyk, B.L., Walvoord, M.A., Bense, V.F., Fortier, D., Spence, C. and Grenier, C., 2021. Invited perspective: What lies beneath a changing Arctic?. *The Cryosphere*, *15*(1), pp.479-484.

Melton, J., Wania, R., Hodson, E.L., Poulter, B., Ringeval, B., Spahni, R., Bohn, T., Avis, C., Beerling, D., Chen, G. and Eliseev, A. 2013. Present state of global wetland extent and wetland methane modeling : conclusions from a model inter-comparison project (WETCHIMP), *Biogeosciences*, 10, pp. 753–788.

Messager, M.L., Lehner, B., Grill, G., Nedeva, I. and Schmitt, O., 2016. Estimating the volume and age of water stored in global lakes using a geo-statistical approach. *Nature Communications*, *7*(1), pp.1-11.

Moore, T.R., Heyes, A. and Roulet, N.T., 1994. Methane emissions from wetlands, southern Hudson Bay lowland. *Journal of Geophysical Research: Atmospheres*, *99*(D1), pp.1455-1467.

Moosavi, S.C. and Crill, P.M., 1997. Controls on CH4 and CO2 emissions along two moisture gradients in the Canadian boreal zone. *Journal of Geophysical Research: Atmospheres*, *102*(D24), pp.29261-29277.

Muster, S., Riley, W.J., Roth, K., Langer, M., Cresto Aleina, F., Koven, C.D., Lange, S., Bartsch, A., Grosse, G., Wilson, C.J. and Jones, B.M., 2019. Size distributions of Arctic waterbodies reveal consistent relations in their statistical moments in space and time. *Frontiers in Earth Science*, *7*, p.5.

Myhre, G., Shindell, D. and Pongratz, J., 2014. Anthropogenic and natural radiative forcing. Clim. Chang. 2013 Phys. Sci. Basis. Contrib. Work. Gr. I to Fifth Assess. Rep. Intergov. Panel Clim. Chang. Phys. Sci. Basis. Contrib. Work. Gr. I to Fifth Assess. Rep. pp. 1–44.

National Wetlands Working Group (NWWG): The Canadian Wetland Classification System, 2nd Edition. Warner, B.G. and C.D.A. Rubec (eds.), Wetlands Research Centre, University of Waterloo, Waterloo, ON, Canada. 68 p., 1997.

Nielsen, C.S., Hasselquist, N.J., Nilsson, M.B., Öquist, M., Järveoja, J. and Peichl, M., 2019. A novel approach for high-frequency in-situ quantification of methane oxidation in Peatlands. *Soil Systems*, *3*(1), p.4.

Nisbet, E.G., Manning, M.R., Dlugokencky, E.J., Fisher, R.E., Lowry, D., Michel, S.E., Myhre, C.L., Platt, S.M., Allen, G., Bousquet, P. and Brownlow, R., 2019. Very strong atmospheric methane growth in the 4 years 2014–2017: Implications for the Paris Agreement. *Global Biogeochemical Cycles*, *33*(3), pp.318-342.

Nydahl, A.C., Wallin, M.B. and Weyhenmeyer, G.A., 2020. Diverse drivers of long-term p CO2 increases across thirteen boreal lakes and streams. *Inland Waters*, *10*(3), pp.360-372.

Nykänen, H., Heikkinen, J.E., Pirinen, L., Tiilikainen, K. and Martikainen, P.J., 2003. Annual CO2 exchange and CH4 fluxes on a subarctic palsa mire during climatically different years. *Global Biogeochemical Cycles*, *17*(1).

Oh, Y., Zhuang, Q., Liu, L., Welp, L.R., Lau, M.C., Onstott, T.C., Medvigy, D., Bruhwiler, L., Dlugokencky, E.J., Hugelius, G. and D'Imperio, L., 2020. Reduced net methane emissions due to microbial methane oxidation in a warmer Arctic. *Nature Climate Change*, *10*(4), pp.317-321.

Oksanen, J., Blanchet, F.G., Friendly, M., Kindt, R., Legendre, P., McGlinn, D., Minchin, P.R., O'Hara, R.B., Simpson, G.L., Solymos, P. and Stevens, H.H., 2019. vegan: Community Ecology Package. R package version 2.5–6. 2019.

Olefeldt, D., Turetsky, M.R., Crill, P.M. and McGuire, A.D., 2013. Environmental and physical controls on northern terrestrial methane emissions across permafrost zones. *Global Change Biology*, *19*(2), pp.589-603.

Olefeldt, D., Goswami, S., Grosse, G., Hayes, D., Hugelius, G., Kuhry, P., McGuire, A.D., Romanovsky, V.E., Sannel, A.B.K., Schuur, E.A.G. and Turetsky, M.R., 2016. Circumpolar distribution and carbon storage of thermokarst landscapes. *Nature Communications*, *7*(1), pp.1-11.

Olefeldt, D., Euskirchen, E.S., Harden, J., Kane, E., McGuire, A.D., Waldrop, M.P. and Turetsky, M.R., 2017. A decade of boreal rich fen greenhouse gas fluxes in response to natural and experimental water table variability. *Global Change biology*, *23*(6), pp.2428-2440.

Olefeldt, D., Hovemyr, M., Kuhn, M.A., Bastviken, D., Bohn, T., Connolly, J., Crill, P., Euskirchen, E., Finklestein, S., Genet, H., Grosse, G., Harris, L., Heffernan, L., Helbig, M., Hugelius, G., Hutchins, R., Juutinen, S., Lara, M., Malhotra, A., Manies, K., McGuire, A.D., Natali, S., O'Donnell, S., Parmentier, F.J., Räsänen, A., Schaedel, C., Sonnentag, O., Strack, M., Tank, S., Treat, C., Varner, R.K, Virtanen, T., Warren, R., Watts, J.D., 2021. The fractional land cover estimates from the Boreal-Arctic Wetland and Lake Dataset (BAWLD), 2021. Arctic Data Center [data set], https://doi.org/10.18739/A2C824F9X

Olid, C., Zannella, A. and Lau, D.C., 2021. The role of methane transport from the active layer in sustaining methane emissions and food chains in subarctic ponds. *Journal of Geophysical Research: Biogeosciences*, *126*(3), p.e2020JG005810.

Olson, D.M., Dinerstein, E., Wikramanayake, E.D., Burgess, N.D., Powell, G.V., Underwood, E.C., D'amico, J.A., Itoua, I., Strand, H.E., Morrison, J.C. and Loucks, C.J., 2001. Terrestrial Ecoregions of the World: A New Map of Life on EarthA new global map of terrestrial ecoregions provides an innovative tool for conserving biodiversity. *BioScience*, *51*(11), pp.933-938.

Öquist, M.G. and Svensson, B.H., 2002. Vascular plants as regulators of methane emissions from a subarctic mire ecosystem. *Journal of Geophysical Research: Atmospheres*, *107*(D21), pp.ACL-10.

Pacheco, F.S., Roland, F. and Downing, J.A., 2014. Eutrophication reverses whole-lake carbon budgets. *Inland Waters*, *4*(1), pp.41-48.

Paytan, A., Lecher, A.L., Dimova, N., Sparrow, K.J., Kodovska, F.G.T., Murray, J., Tulaczyk, S. and Kessler, J.D., 2015. Methane transport from the active layer to lakes in the Arctic using Toolik Lake, Alaska, as a case study. *Proceedings of the National Academy of Sciences*, *112*(12), pp.3636-3640.

Peeters, F., Fernandez, J.E. and Hofmann, H., 2019. Sediment fluxes rather than oxic methanogenesis explain diffusive CH 4 emissions from lakes and reservoirs. *Scientific Reports*, *9*(1), pp.1-10.

Pelletier, L., Moore, T.R., Roulet, N.T., Garneau, M. and Beaulieu-Audy, V., 2007. Methane fluxes from three peatlands in the La Grande Riviere watershed, James Bay lowland, Canada. *Journal of Geophysical Research: Biogeosciences*, *112*(G1).

Pelletier, L., Strachan, I.B., Garneau, M. and Roulet, N.T., 2014. Carbon release from boreal peatland open water pools: Implication for the contemporary C exchange. *Journal of Geophysical Research: Biogeosciences*, *119*(3), pp.207-222.

Pelletier, N., Talbot, J., Olefeldt, D., Turetsky, M., Blodau, C., Sonnentag, O. and Quinton, W.L., 2017. Influence of Holocene permafrost aggradation and thaw on the paleoecology and carbon storage of a peatland complex in northwestern Canada. *The Holocene*, *27*(9), pp.1391-1405.

Peltola, O., Vesala, T., Gao, Y., Räty, O., Alekseychik, P., Aurela, M., Chojnicki, B., Desai, A.R., Dolman, A.J., Euskirchen, E.S. and Friborg, T., 2019. Monthly gridded data product of northern wetland methane emissions based on upscaling eddy covariance observations. *Earth System Science Data*, *11*(3), pp.1263-1289.

Perryman, C.R., McCalley, C.K., Malhotra, A., Fahnestock, M.F., Kashi, N.N., Bryce, J.G., Giesler, R. and Varner, R.K., 2020. Thaw transitions and redox conditions drive methane oxidation in a permafrost peatland. *Journal of Geophysical Research: Biogeosciences*, *125*(3), p.e2019JG005526.

Pinheiro, J., Bates, D., DebRoy, S., Sarkar, D., Heisterkamp, S., Van., Willigen, B., & Maintainer, 2017. R: Package "nlme". Linear and Nonlinear Mixed Effects Models, version 3-1. CRAN R Project.

Popp, T.J., Chanton, J.P., Whiting, G.J. and Grant, N., 2000. Evaluation of methane oxidation in therhizosphere of a Carex dominated fen in northcentral Alberta, Canada. *Biogeochemistry*, *51*(3), pp.259-281.

Praetzel, L.S.E., Plenter, N., Schilling, S., Schmiedeskamp, M., Broll, G. and Knorr, K.H., 2020. Organic matter and sediment properties determine in-lake variability of sediment CO 2 and CH 4 production and emissions of a small and shallow lake. *Biogeosciences*, *17*(20), pp.5057-5078.

Prėskienis, V., Laurion, I., Bouchard, F., Douglas, P.M., Billett, M.F., Fortier, D. and Xu, X., 2021. Seasonal patterns in greenhouse gas emissions from lakes and ponds in a High Arctic polygonal landscape. *Limnology and Oceanography*, *66*, pp.S117-S141.

Rasilo, T., Prairie, Y.T. and Del Giorgio, P.A., 2015. Large-scale patterns in summer diffusive CH 4 fluxes across boreal lakes, and contribution to diffusive C emissions. *Global Change Biology*, *21*(3), pp.1124-1139.

Riera, J.L., Schindler, J.E. and Kratz, T.K., 1999. Seasonal dynamics of carbon dioxide and methane in two clear-water lakes and two bog lakes in northern Wisconsin, USA. *Canadian Journal of Fisheries and Aquatic Sciences*, *56*(2), pp.265-274.

Rhew, R.C., Teh, Y.A. and Abel, T., 2007. Methyl halide and methane fluxes in the northern Alaskan coastal tundra. *Journal of Geophysical Research: Biogeosciences*, *112*(G2).

Roehm, C.L., Giesler, R. and Karlsson, J., 2009. Bioavailability of terrestrial organic carbon to lake bacteria: The case of a degrading subarctic permafrost mire complex. *Journal of Geophysical Research: Biogeosciences*, *114*(G3).

Sannel, A.B.K. and Kuhry, P., 2011. Warming-induced destabilization of peat plateau/thermokarst lake complexes. *Journal of Geophysical Research: Biogeosciences*, *116*(G3).

Saunois, M., Stavert, A.R., Poulter, B., Bousquet, P., Canadell, J.G., Jackson, R.B., Raymond, P.A., Dlugokencky, E.J., Houweling, S., Patra, P.K. and Ciais, P., 2020. The global methane budget 2000–2017. *Earth System Science Data*, *12*(3), pp.1561-1623.

Schilder, J., Bastviken, D., Van Hardenbroek, M. and Heiri, O., 2016. Spatiotemporal patterns in methane flux and gas transfer velocity at low wind speeds: Implications for upscaling studies on small lakes. *Journal of Geophysical Research: Biogeosciences*, *121*(6), pp.1456-1467.

Schirrmeister, L., Froese, D., Tumskoy, V., Grosse, G. and Wetterich, S., 2013. Yedoma: Late Pleistocene ice-rich syngenetic permafrost of Beringia. In *Encyclopedia of Quaternary Science. 2nd edition* (pp. 542-552). Elsevier.

Schneider, P. and Hook, S.J., 2010. Space observations of inland water bodies show rapid surface warming since 1985. *Geophysical Research Letters*, *37*(22).

Schnurrenberger, D., Russell, J. and Kelts, K., 2003. Classification of lacustrine sediments based on sedimentary components. *Journal of Paleolimnology*, *29*(2), pp.141-154.

Schuur, E.A., Bockheim, J., Canadell, J.G., Euskirchen, E., Field, C.B., Goryachkin, S.V., Hagemann, S., Kuhry, P., Lafleur, P.M., Lee, H. and Mazhitova, G., 2008. Vulnerability of permafrost carbon to climate change: Implications for the global carbon cycle. *BioScience*, *58*(8), pp.701-714.

Schuur, E.A., Druffel, E.R. and Trumbore, S.E. eds., 2016. *Radiocarbon and climate change: Mechanisms, applications and laboratory techniques*. Springer.

Segarra, K.E.A., Schubotz, F., Samarkin, V., Yoshinaga, M.Y., Hinrichs, K.U. and Joye, S.B., 2015. High rates of anaerobic methane oxidation in freshwater wetlands reduce potential atmospheric methane emissions. *Nature Communications*, *6*(1), pp.1-8.

Sepulveda-Jauregui, A., Walter Anthony, K.M., Martinez-Cruz, K., Greene, S. and Thalasso, F., 2015. Methane and carbon dioxide emissions from 40 lakes along a north–south latitudinal transect in Alaska. *Biogeosciences*, *12*(11), pp.3197-3223.

Sepulveda-Jauregui, A., Hoyos-Santillan, J., Martinez-Cruz, K., Anthony, K.M.W., Casper, P., Belmonte-Izquierdo, Y. and Thalasso, F., 2018. Eutrophication exacerbates the impact of climate warming on lake methane emission. *Science of the Total Environment*, *636*, pp.411-419.

Serikova, S., Pokrovsky, O.S., Laudon, H., Krickov, I.V., Lim, A.G., Manasypov, R.M. and Karlsson, J., 2019. High carbon emissions from thermokarst lakes of Western Siberia. *Nature Communications*, *10*(1), pp.1-7.

Shipley, B., 2009. Confirmatory path analysis in a generalized multilevel context. *Ecology*, *90*(2), pp.363-368.

Sieczko, A.K., Duc, N.T., Schenk, J., Pajala, G., Rudberg, D., Sawakuchi, H.O. and Bastviken, D., 2020. Diel variability of methane emissions from lakes. *Proceedings of the National Academy of Sciences*, *117*(35), pp.21488-21494.

Silva, G.G.Z., Green, K.T., Dutilh, B.E. and Edwards, R.A., 2016. SUPER-FOCUS: a tool for agile functional analysis of shotgun metagenomic data. *Bioinformatics*, *32*(3), pp.354-361.

Sivan, O., Adler, M., Pearson, A., Gelman, F., Bar-Or, I., John, S.G. and Eckert, W., 2011. Geochemical evidence for iron-mediated anaerobic oxidation of methane. *Limnology and Oceanography*, *56*(4), pp.1536-1544.

Smith, E.M. and Prairie, Y.T., 2004. Bacterial metabolism and growth efficiency in lakes: the importance of phosphorus availability. *Limnology and Oceanography*, *49*(1), pp.137-147.

Smith, K.B., C.E. Smith, S.F. Forest, and A.J. Richard. 2007. A Field Guide to the Wetlands of the Boreal Plains Ecozone of Canada. Ducks Unlimited Canada, Western Boreal Office: Edmonton, Alberta. Pp. 98.

Smith, S.V., 1985. Physical, chemical and biological characteristics* of CO2 gas flux across the air-water interface. *Plant, Cell & Environment*, *8*(6), pp.387-398.

Sobek, S., Tranvik, L.J. and Cole, J.J., 2005. Temperature independence of carbon dioxide supersaturation in global lakes. *Global Biogeochemical Cycles*, *19*(2).

Spahni, R., Wania, R., Neef, L., Weele, M.V., Pison, I., Bousquet, P., Frankenberg, C., Foster, P.N., Joos, F., Prentice, I.C. and Velthoven, P.V., 2011. Constraining global methane emissions and uptake by ecosystems. *Biogeosciences*, 8(6), pp.1643-1665.

St Pierre, K.A., Danielsen, B.K., Hermesdorf, L., D'Imperio, L., Iversen, L.L. and Elberling, B., 2019. Drivers of net methane uptake across Greenlandic dry heath tundra landscapes. *Soil Biology and Biochemistry*, *138*, p.107605.

Stanley, E.H., Casson, N.J., Christel, S.T., Crawford, J.T., Loken, L.C. and Oliver, S.K., 2016. The ecology of methane in streams and rivers: patterns, controls, and global significance. *Ecological Monographs*, *86*(2), pp.146-171.

St-Jean G, Kieser WE, Crann CA, Murseli S. 2017. Semi-automated equipment for CO2 purification and graphitization at the A.E. Lalonde AMS Laboratory (Canada).

Strauss, J., Schirrmeister, L., Grosse, G., Fortier, D., Hugelius, G., Knoblauch, C., Romanovsky, V., Schädel, C., von Deimling, T.S., Schuur, E.A. and Shmelev, D., 2017. Deep Yedoma permafrost: A synthesis of depositional characteristics and carbon vulnerability. *Earth-Science Reviews*, *172*, pp.75-86.

Ström, L. and Christensen, T.R., 2007. Below ground carbon turnover and greenhouse gas exchanges in a sub-arctic wetland. *Soil Biology and Biochemistry*, *39*(7), pp.1689-1698.

Ström, L., Mastepanov, M. and Christensen, T.R., 2005. Species-specific effects of vascular plants on carbon turnover and methane emissions from wetlands. *Biogeochemistry*, *75*(1), pp.65-82.

Ström, L., Tagesson, T., Mastepanov, M. and Christensen, T.R., 2012. Presence of Eriophorum scheuchzeri enhances substrate availability and methane emission in an Arctic wetland. *Soil Biology and Biochemistry*, *45*, pp.61-70.

Stuiver, M. and Polach, H.A., 1977. Discussion reporting of 14C data. Radiocarbon, 19(3), pp.355-363.

Tan, Z., Zhuang, Q., Henze, D.K., Frankenberg, C., Dlugokencky, E., Sweeney, C., Turner, A.J., Sasakawa, M. and Machida, T., 2016. Inverse modeling of pan-Arctic methane emissions at high spatial resolution: what can we learn from assimilating satellite retrievals and using different process-based wetland and lake biogeochemical models?. *Atmospheric Chemistry and Physics*, *16*(19), pp.12649-12666.

Tanentzap, A., Burd, K., Kuhn, M.A., Estop-Aragonés, C., Tank, S., & Olefeldt, D. In Review. Aged soils contribute little to contemporary carbon cycling downstream of thawing permafrost peatlands. In Review. *Global Change Biology*.

Tank, S.E., Lesack, L.F. and Hesslein, R.H., 2009. Northern delta lakes as summertime CO 2 absorbers within the arctic landscape. *Ecosystems*, *12*(1), pp.144-157.

Tank, S.E., Vonk, J.E., Walvoord, M.A., McClelland, J.W., Laurion, I. and Abbott, B.W., 2020. Landscape matters: Predicting the biogeochemical effects of permafrost thaw on aquatic networks with a state factor approach. *Permafrost and Periglacial Processes*, *31*(3), pp.358-370.

Terentieva, I.E., Glagolev, M.V., Lapshina, E.D., Sabrekov, A.F. and Maksyutov, S., 2016. Mapping of West Siberian taiga wetland complexes using Landsat imagery: implications for methane emissions. *Biogeosciences*, *13*(16), pp.4615-4626.

Thompson, R.L., Nisbet, E.G., Pisso, I., Stohl, A., Blake, D., Dlugokencky, E.J., Helmig, D. and White, J.W.C., 2018. Variability in atmospheric methane from fossil fuel and microbial sources over the last three decades. *Geophysical Research Letters*, *45*(20), pp.11-499.

Thornton, B.F., Wik, M. and Crill, P.M., 2015. Climate-forced changes in available energy and methane bubbling from subarctic lakes. *Geophysical Research Letters*, *42*(6), pp.1936-1942.

Thornton, B.F., Wik, M. and Crill, P.M., 2016. Double-counting challenges the accuracy of high-latitude methane inventories. *Geophysical Research Letters*, *43*(24), pp.12-569.

Toohey, R.C., Herman-Mercer, N.M., Schuster, P.F., Mutter, E.A. and Koch, J.C., 2016. Multidecadal increases in the Yukon River Basin of chemical fluxes as indicators of changing flowpaths, groundwater, and permafrost. *Geophysical Research Letters*, *43*(23), pp.12-120.

Tranvik, L.J., Downing, J.A., Cotner, J.B., Loiselle, S.A., Striegl, R.G., Ballatore, T.J., Dillon, P., Finlay, K., Fortino, K., Knoll, L.B. and Kortelainen, P.L., 2009. Lakes and reservoirs as regulators of carbon cycling and climate. *Limnology and Oceanography*, *54*(6part2), pp.2298-2314.

Treat, C.C. and Jones, M.C., 2018. Near-surface permafrost aggradation in Northern Hemisphere peatlands shows regional and global trends during the past 6000 years. *The Holocene*, *28*(6), pp.998-1010.

Treat, C.C., Bloom, A.A. and Marushchak, M.E., 2018. Nongrowing season methane emissions–a significant component of annual emissions across northern ecosystems. *Global change biology*, *24*(8), pp.3331-3343.

Turetsky, M.R., Abbott, B.W., Jones, M.C., Walter Anthony, K., Olefeldt, D., Schuur, E.A., Grosse, G., Kuhry, P., Hugelius, G., Koven, C. and Lawrence, D.M., 2020. Carbon release through abrupt permafrost thaw. *Nature Geoscience*, *13*(2), pp.138-143.

Turetsky, M.R., Wieder, R.K. and Vitt, D.H., 2002. Boreal peatland C fluxes under varying permafrost regimes. *Soil Biology and Biochemistry*, *34*(7), pp.907-912.

Turetsky, M.R., Abbott, B.W., Jones, M.C., Walter Anthony, K., Olefeldt, D., Schuur, E.A., Grosse, G., Kuhry, P., Hugelius, G., Koven, C. and Lawrence, D.M., 2020. Carbon release through abrupt permafrost thaw. *Nature Geoscience*, *13*(2), pp.138-143.

Turetsky, M.R., Kotowska, A., Bubier, J., Dise, N.B., Crill, P., Hornibrook, E.R., Minkkinen, K., Moore, T.R., Myers-Smith, I.H., Nykänen, H. and Olefeldt, D., 2014. A synthesis of methane

emissions from 71 northern, temperate, and subtropical wetlands. *Global Change Biology*, *20*(7), pp.2183-2197.

Van der Molen, M.K., Huissteden, J.V., Parmentier, F.J.W., Petrescu, A.M.R., Dolman, A.J., Maximov, T.C., Kononov, A.V., Karsanaev, S.V. and Suzdalov, D.A., 2007. The growing season greenhouse gas balance of a continental tundra site in the Indigirka lowlands, NE Siberia. *Biogeosciences*, *4*(6), pp.985-1003.

van Grinsven, S., Sinninghe Damsté, J.S., Abdala Asbun, A., Engelmann, J.C., Harrison, J. and Villanueva, L., 2020. Methane oxidation in anoxic lake water stimulated by nitrate and sulfate addition. *Environmental Microbiology*, *22*(2), pp.766-782.

Van Huissteden, J., Maximov, T.C. and Dolman, A.J., 2005. High methane flux from an arctic floodplain (Indigirka lowlands, eastern Siberia). *Journal of Geophysical Research: Biogeosciences*, *110*(G2).

Virtanen, R., Oksanen, L., Oksanen, T., Cohen, J., Forbes, B.C., Johansen, B., Käyhkö, J., Olofsson, J., Pulliainen, J. and Tømmervik, H., 2016. Where do the treeless tundra areas of northern highlands fit in the global biome system: toward an ecologically natural subdivision of the tundra biome. *Ecology and Evolution*, *6*(1), pp.143-158.

Virtanen, T. and Ek, M., 2014. The fragmented nature of tundra landscape. *International Journal of Applied Earth Observation and Geoinformation*, *27*, pp.4-12.

Vitt, D.H., Halsey, L.A. and Zoltai, S.C., 2000. The changing landscape of Canada's western boreal forest: the current dynamics of permafrost. *Canadian Journal of Forest Research*, *30*(2), pp.283-287.

von Fischer, J.C., Rhew, R.C., Ames, G.M., Fosdick, B.K. and von Fischer, P.E., 2010. Vegetation height and other controls of spatial variability in methane emissions from the Arctic coastal tundra at Barrow, Alaska. *Journal of Geophysical Research: Biogeosciences*, *115*(G4).

Wagner, D., Kobabe, S., Pfeiffer, E.M. and Hubberten, H.W., 2003. Microbial controls on methane fluxes from a polygonal tundra of the Lena Delta, Siberia. *Permafrost and Periglacial processes*, *14*(2), pp.173-185.

Walter, K.M., Zimov, S.A., Chanton, J.P., Verbyla, D. and Chapin, F.S., 2006. Methane bubbling from Siberian thaw lakes as a positive feedback to climate warming. *Nature*, *443*(7107), pp.71-75.

Walter Anthony, K.M., Vas, D.A., Brosius, L., Chapin III, F.S., Zimov, S.A. and Zhuang, Q., 2010. Estimating methane emissions from northern lakes using ice-bubble surveys. *Limnology and Oceanography: Methods*, *8*(11), pp.592-609.

Walter Anthony, K.M., Daanen, R., Anthony, P., von Deimling, T.S., Ping, C.L., Chanton, J.P. and Grosse, G., 2016. Methane emissions proportional to permafrost carbon thawed in Arctic lakes since the 1950s. *Nature Geoscience*, *9*(9), pp.679-682.

Walter Anthony, K.M., von Deimling, T.S., Nitze, I., Frolking, S., Emond, A., Daanen, R., Anthony, P., Lindgren, P., Jones, B. and Grosse, G., 2018. 21st-century modeled permafrost

carbon emissions accelerated by abrupt thaw beneath lakes. *Nature communications*, *9*(1), pp.1-11.

Walter Anthony, K.M., Lindgren, P., Hanke, P., Engram, M., Anthony, P., Daanen, R.P., Bondurant, A., Liljedahl, A.K., Lenz, J., Grosse, G. and Jones, B.M., 2021. Decadal-scale hotspot methane ebullition within lakes following abrupt permafrost thaw. Environmental Research Letters, 16(3), p.035010.

Walvoord, M.A., Voss, C.I. and Wellman, T.P., 2012. Influence of permafrost distribution on groundwater flow in the context of climate-driven permafrost thaw: Example from Yukon Flats Basin, Alaska, United States. *Water Resources Research*, *48*(7).

Walvoord, M.A. and Kurylyk, B.L., 2016. Hydrologic impacts of thawing permafrost—A review. *Vadose Zone Journal*, *15*(6).

Watson, A., Stephen, K.D., Nedwell, D.B. and Arah, J.R., 1997. Oxidation of methane in peat: kinetics of CH4 and O2 removal and the role of plant roots. *Soil Biology and Biochemistry*, *29*(8), pp.1257-1267.

Watts, J.D., Kimball, J.S., Bartsch, A. and McDonald, K.C., 2014. Surface water inundation in the boreal-Arctic: potential impacts on regional methane emissions. *Environmental Research Letters*, *9*(7), p.075001.

Wauthy, M., Rautio, M., Christoffersen, K.S., Forsström, L., Laurion, I., Mariash, H.L., Peura, S. and Vincent, W.F., 2018. Increasing dominance of terrigenous organic matter in circumpolar freshwaters due to permafrost thaw. *Limnology and Oceanography Letters*, *3*(3), pp.186-198.

Weishaar, J.L., Aiken, G.R., Bergamaschi, B.A., Fram, M.S., Fujii, R. and Mopper, K., 2003. Evaluation of specific ultraviolet absorbance as an indicator of the chemical composition and reactivity of dissolved organic carbon. *Environmental science & technology*, *37*(20), pp.4702-4708.

Wessel, P. and Smith, W.H., 1996. A global, self-consistent, hierarchical, high-resolution shoreline database. *Journal of Geophysical Research: Solid Earth*, *101*(B4), pp.8741-8743.

Weyhenmeyer, G.A., Livingstone, D.M., Meili, M., Jensen, O., Benson, B. and Magnuson, J.J., 2011. Large geographical differences in the sensitivity of ice-covered lakes and rivers in the Northern Hemisphere to temperature changes. *Global Change Biology*, 17(1), pp.268-275.

Weyhenmeyer, G.A., Kosten, S., Wallin, M.B., Tranvik, L.J., Jeppesen, E. and Roland, F., 2015. Significant fraction of CO 2 emissions from boreal lakes derived from hydrologic inorganic carbon inputs. *Nature Geoscience*, *8*(12), pp.933-936.

Whalen, S.C., 2005. Biogeochemistry of methane exchange between natural wetlands and the atmosphere. *Environmental Engineering Science*, *22*(1), pp.73-94.

Wik, M., Thornton, B.F., Bastviken, D., MacIntyre, S., Varner, R.K. and Crill, P.M., 2014. Energy input is primary controller of methane bubbling in subarctic lakes. *Geophysical Research Letters*, *41*(2), pp.555-560.

Wik, M., Crill, P.M., Varner, R.K. and Bastviken, D., 2013. Multiyear measurements of ebullitive methane flux from three subarctic lakes. *Journal of Geophysical Research: Biogeosciences*, *118*(3), pp.1307-1321.

Wik, M., Johnson, J.E., Crill, P.M., DeStasio, J.P., Erickson, L., Halloran, M.J., Fahnestock, M.F., Crawford, M.K., Phillips, S.C. and Varner, R.K., 2018. Sediment characteristics and methane ebullition in three subarctic lakes. *Journal of Geophysical Research: Biogeosciences*, *123*(8), pp.2399-2411.

Wik, M., Thornton, B.F., Bastviken, D., Uhlbäck, J. and Crill, P.M., 2016. Biased sampling of methane release from northern lakes: A problem for extrapolation. *Geophysical Research Letters*, *43*(3), pp.1256-1262.

Wik, M., Thornton, B.F., Bastviken, D., Uhlbäck, J. and Crill, P.M., 2016b. Biased sampling of methane release from northern lakes: A problem for extrapolation. *Geophysical Research Letters*, *43*(3), pp.1256-1262.

Wik, M., Varner, R.K., Anthony, K.W., MacIntyre, S. and Bastviken, D., 2016. Climate-sensitive northern lakes and ponds are critical components of methane release. *Nature Geoscience*, *9*(2), pp.99-105.

Wood, M.E., Macrae, M.L., Strack, M., Price, J.S., Osko, T.J. and Petrone, R.M., 2016. Spatial variation in nutrient dynamics among five different peatland types in the Alberta oil sands region. *Ecohydrology*, *9*(4), pp.688-699.

Woodcroft, B.J., Singleton, C.M., Boyd, J.A., Evans, P.N., Emerson, J.B., Zayed, A.A., Hoelzle, R.D., Lamberton, T.O., McCalley, C.K., Hodgkins, S.B. and Wilson, R.M., 2018. Genome-centric view of carbon processing in thawing permafrost. *Nature*, *560*(7716), pp.49-54.

Yu, Z.G., Göttlicher, J., Steininger, R. and Knorr, K.H., 2016. Organic sulfur and organic matter redox processes contribute to electron flow in anoxic incubations of peat. *Environmental Chemistry*, 13(5), pp.816-825.

Yvon-Durocher, G., Allen, A.P., Bastviken, D., Conrad, R., Gudasz, C., St-Pierre, A., Thanh-Duc, N. and Del Giorgio, P.A., 2014. Methane fluxes show consistent temperature dependence across microbial to ecosystem scales. Nature, 507(7493), pp.488-491.

Yvon-Durocher, G., Montoya, J. M., Woodward, G., Jones, J. I. & Trimmer, M. 2011. Warming increases the proportion of primary production emitted as methane from freshwater mesocosms. *Global Change Biology*, 17, pp. 1225–1234.

Zhu, X., Zhuang, Q., Qin, Z., Glagolev, M. and Song, L., 2013. Estimating wetland methane emissions from the northern high latitudes from 1990 to 2009 using artificial neural networks. *Global Biogeochemical Cycles*, *27*(2), pp.592-604.

Zoltai, S.C., 1993. Cyclic development of permafrost in the peatlands of northwestern Alberta, Canada. *Arctic and Alpine Research*, *25*(3), pp.240-246.

Zona, D., Gioli, B., Commane, R., Lindaas, J., Wofsy, S.C., Miller, C.E., Dinardo, S.J., Dengel, S., Sweeney, C., Karion, A. and Chang, R.Y.W., 2016. Cold season emissions dominate the

Arctic tundra methane budget. *Proceedings of the National Academy of Sciences*, *113*(1), pp.40-45.

Appendices

A.1. Supporting information for Chapter 1.

There is no supporting information for Chapter 1.

A.2. Supporting information for Chapter 2.

All data for Chapter 2 are available at the Arctic Data Center: https://doi.org/10.18739/A27H1DN5S.

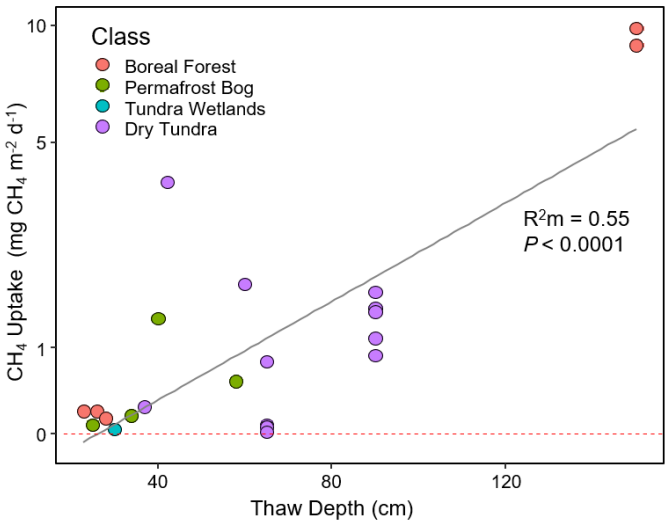

Figure A.2. 1. Correlation between thaw depth and CH_4 uptake. Positive numbers represent net uptake from the atmosphere. Colors represented different ecosystem classes. Neutral (i.e. zero) fluxes were not included in the regression analyses.

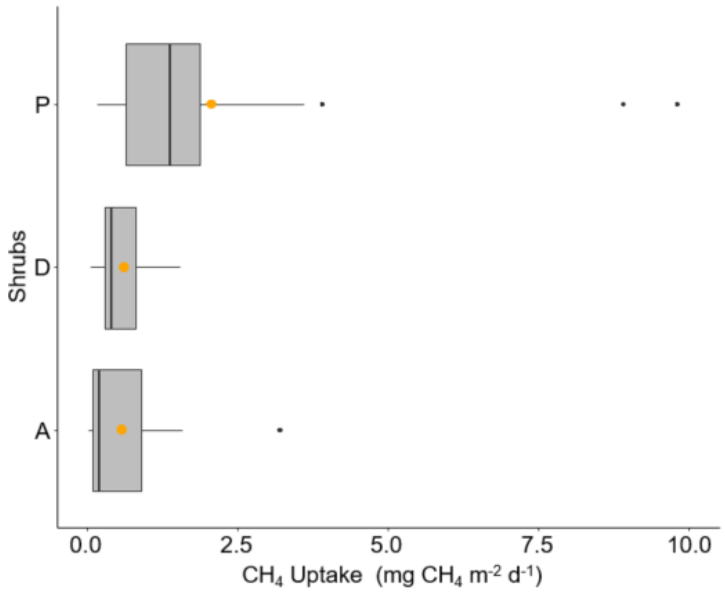

Figure A.2. 2. Boxplots of CH_4 uptake as a factor of shrub cover. Positive numbers represent net uptake from the atmosphere. Orange dots represent mean uptake within a given category. P = Present; D = Dominant; A = Absent. Neutral fluxes (i.e. zero) were not included in the boxplots.

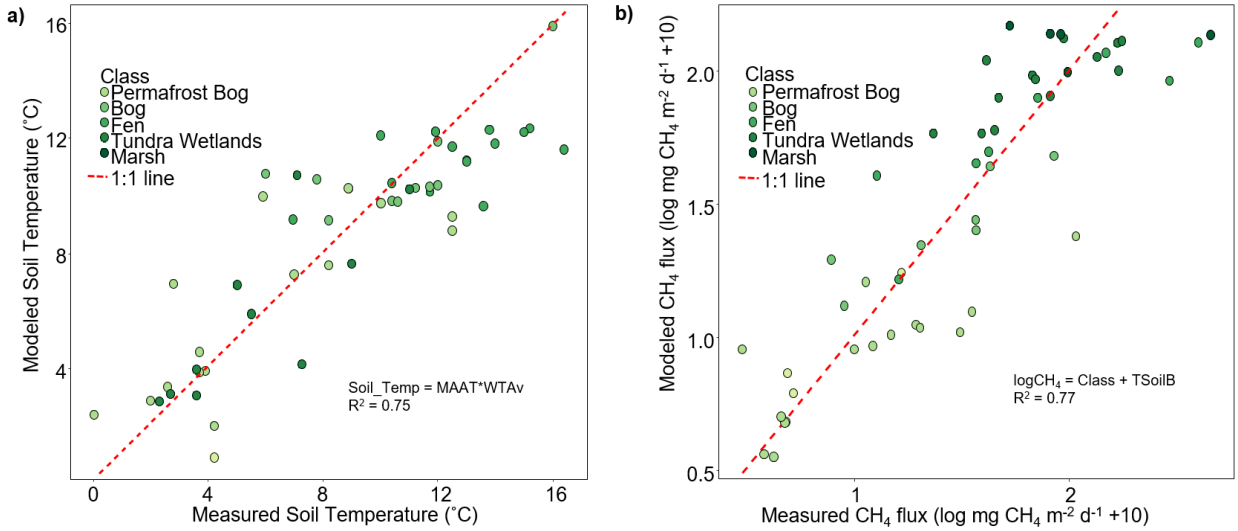

Figure A.2. 3. Model cross-validation output for a) soil temperature and b) wetland CH_4 fluxes.

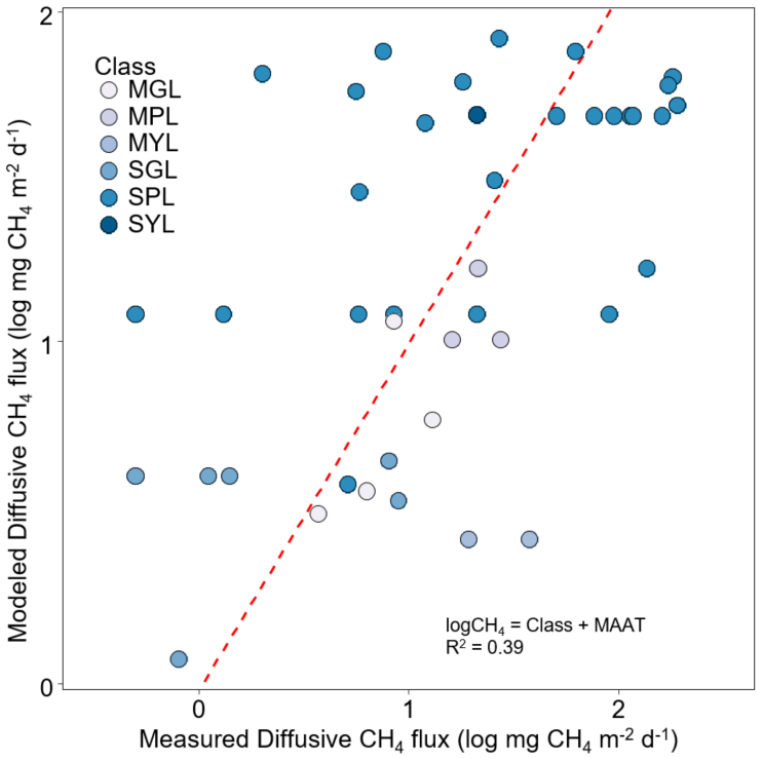

Figure A.2. 4. Model cross-validation output for aquatic diffusive CH_4 fluxes. LAL = Large Lakes. MGL = Midsize Glacial Lakes. MPL = Midsize Peatland Lakes. MYL = Midsize Yedoma Lakes. SGL = Small Glacial Lakes. SPL = Small Peatland Lakes. SYL = Small Yedoma Lakes.

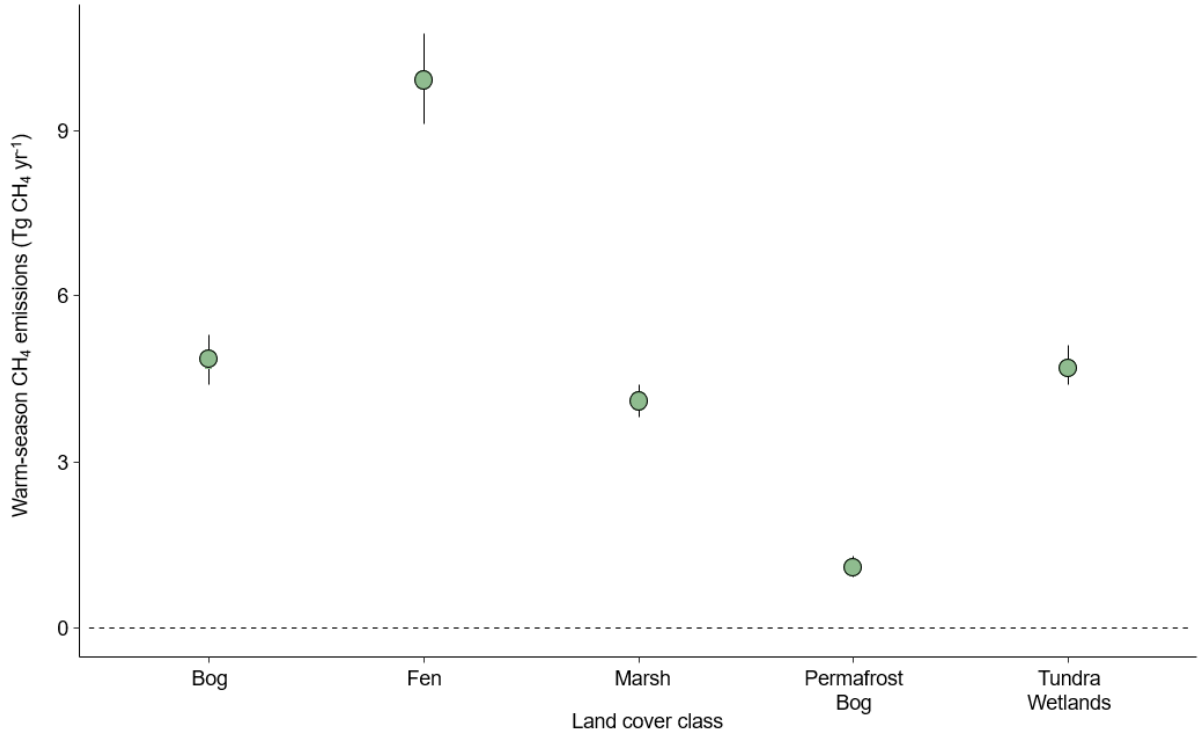

Figure A.2. 5. Warm-season emissions for each wetland class and their associated model uncertainty (does not include the uncertainty from individual class areas).

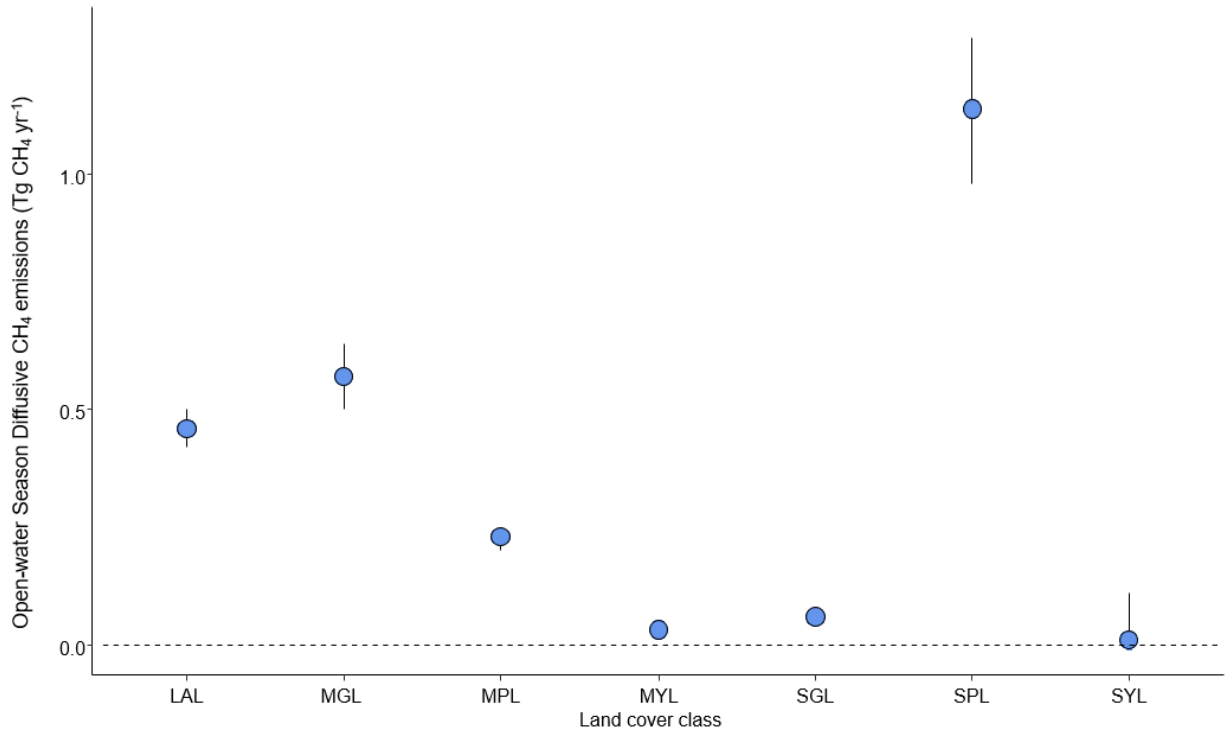

Figure A.2. 6. Ice-free season diffusive emissions for each aquatic class and their associated model uncertainty (does not include the uncertainty from class areas). LAL = Large Lakes. MGL = Midsize Glacial Lakes. MPL = Midsize Peatland Lakes. MYL = Midsize Yedoma Lakes. SGL = Small Glacial Lakes. SPL = Small Peatland Lakes. SYL = Small Yedoma Lakes.

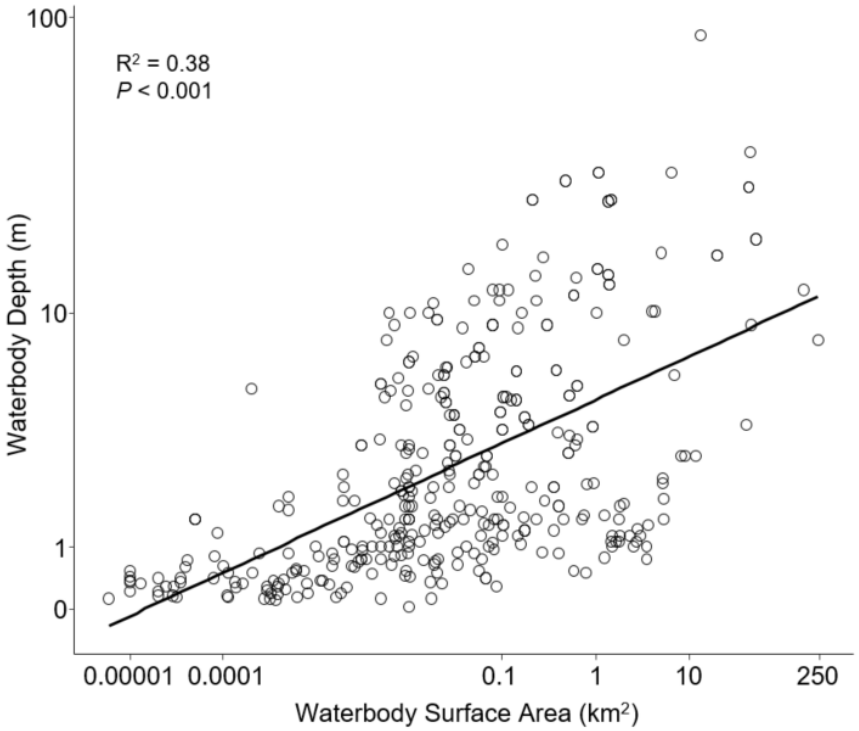

Figure A.2. 7. Relationship between waterbody surface area and water column depth.

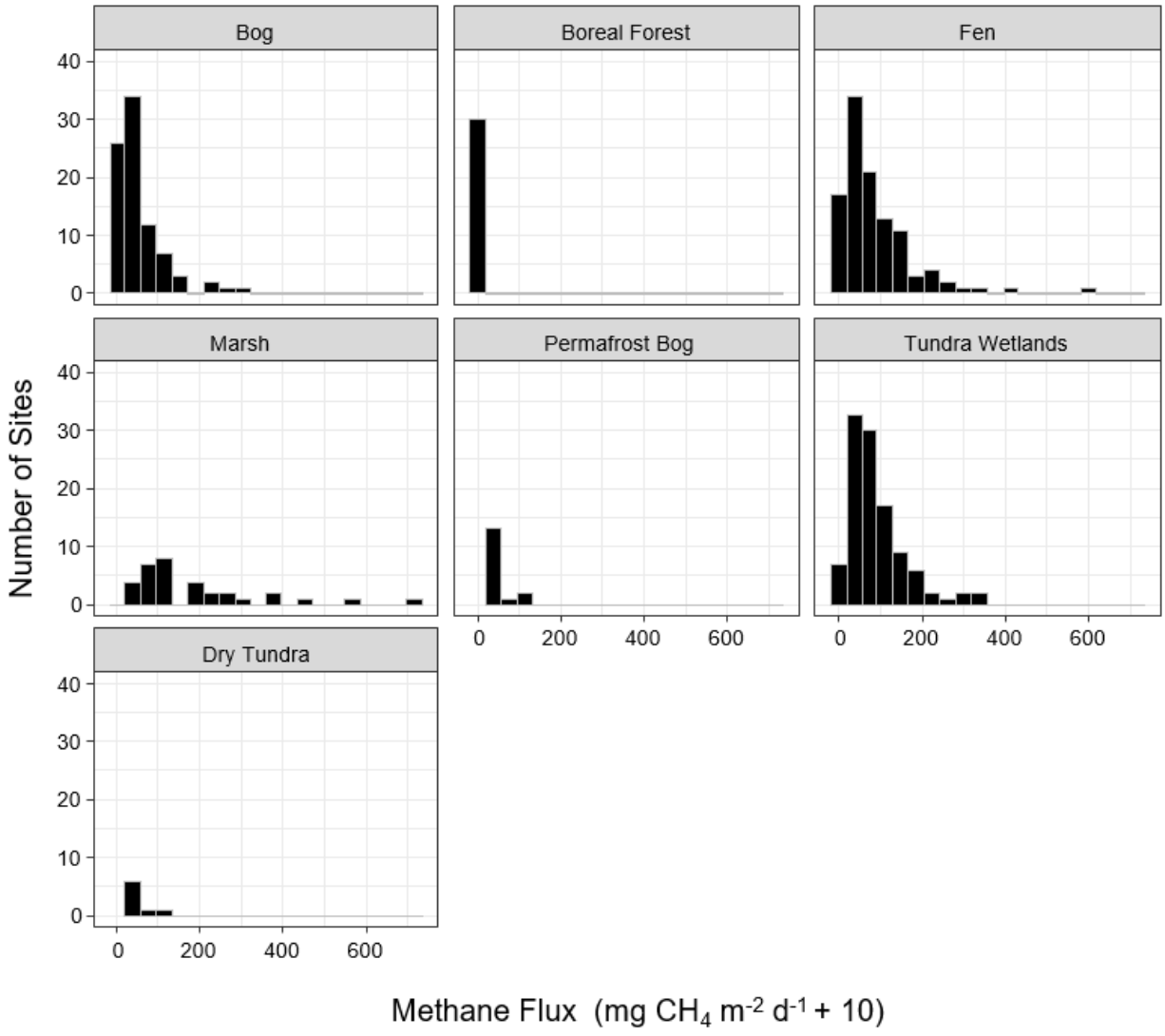

Figure A.2. 8. Non-transformed flux frequencies across the terrestrial land cover classes. A constant of 10 was added to include CH_4 uptake.

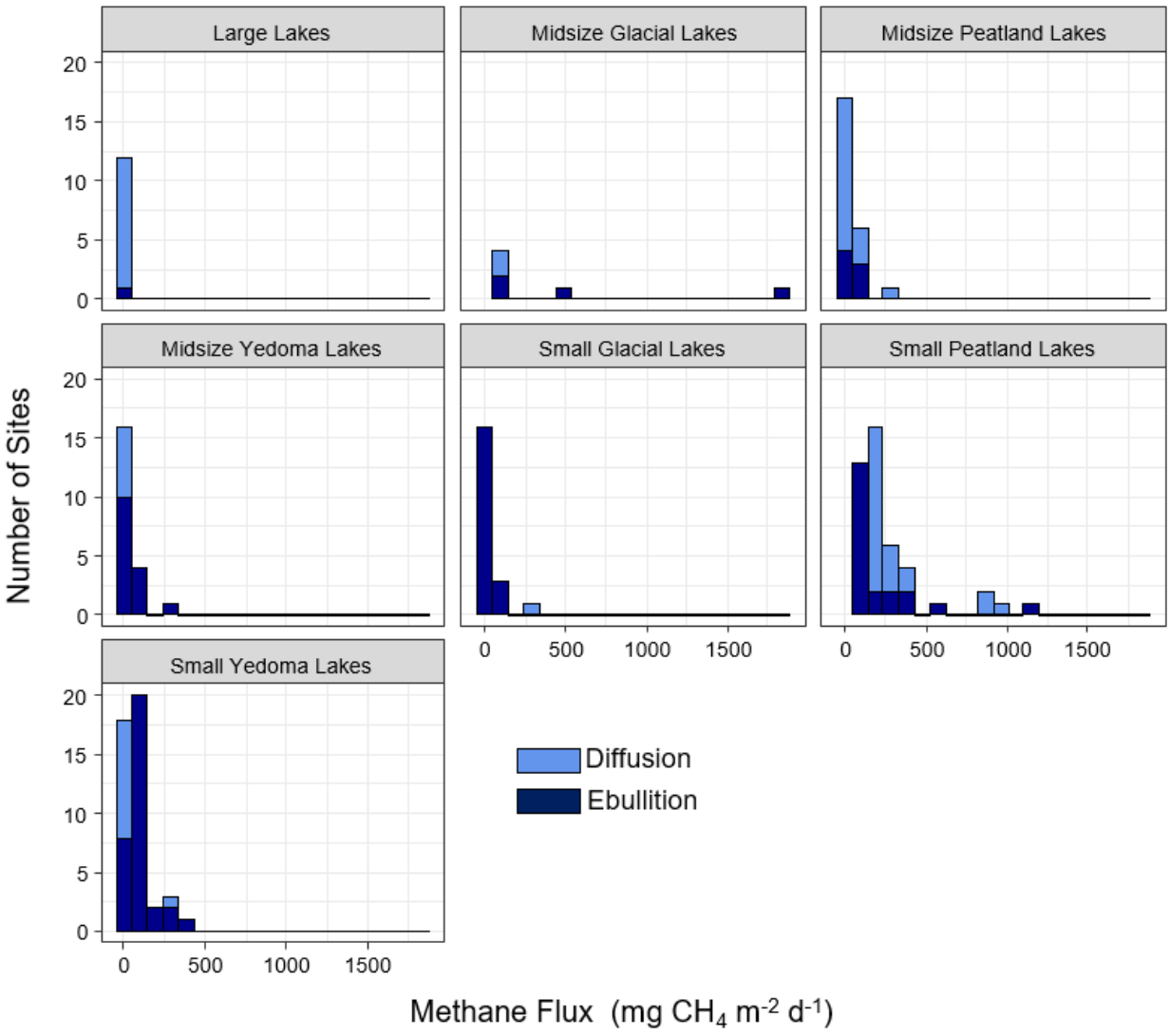

Figure A.2. 9. Non-transformed flux frequencies across the aquatic land cover classes.

Table A.2. 1. Temperature sensitivities of CH_4 fluxes (Q_{10} values) across terrestrial and aquatic ecosystem classes. Individual classes without Q_{10} values did not have significant relationships with temperature when analyzed on their own or did not have a large enough sample size (minimum n = 15).

Class or group of classes	Q10
All terrestrial class	2.88
"Wet" terrestrial classes (Marshes, Tundra Wetlands, Fens, Bogs)	2.82
"Dry" terrestrial classes (Dry Tundra and Boreal Forest, Permafrost Bogs)	3.71
Marshes	-
Tundra Wetlands	2.57
Fens	1.99
Bogs	3.39
Permafrost Bogs	-
Dry Tundra	2.63
Boreal Forest	-
All aquatic classes diffusion	4.27
All peatland lakes diffusion	2.63
All yedoma lakes diffusion	3.89
All glacial lakes diffusion	-
All aquatic class ebullition	2.40

Table A.2. 2. Model selection for terrestrial CH_4 emissions. "Site" represents the best model using site-level predictor variables (biophysical variables measured directly by the authors). "Region" represents the best model using predictor variables that can be attributed across larger spatial scales and extracted from gridded or mapped products. Tests with "site and region" represent the model models that include both site level and regional level predictors. The null model includes only the random effect of SiteID. The best models for each test represented here were picked through forward model selection. K = number of fixed terms the model, AICc = size-corrected Akaike information criterion, DeltaAICc = change in AICc between a given model and the best model, AICcwt = AICc weights indicating the probability a given model is the most parsimonious model in the group of models tested, R^2m = marginal R^2 for the fixed terms for mixed models. R^2c = conditional R^2 for fixed and random terms for mixed effects models. See main text for explanation of fixed effects short names. Non-significant fixed terms that were tested include MAAT, MAP, Permafrost Zone, Permafrost Presence or Absence, and Biome. TsoilB = soil temperature at 5-25 cm. WTAv – average water table position. Sedge = graminoid cover.

Variable modeled	Test	Fixed effect	K	AICc	DeltaAICc	AICcwt	R^2m/R^2c
Terrestrial Log.CH4.Flux (n=206)	Site*region	TsoilB*Class+ WTAv*Class + Sedge	25	98.87	0		0.73/0.83
	Site + region	TsoilB + WTAv+ Sedge + Class	13	99.70	0.84		0.69/0.81
	Site	TsoilB + WTAv+ Sedge	7	131.20	32.34		0.54/0.78
	Region	Class	9	172.77	73.91		0.55/0.71
	Null	-	3	275.8	176.92		0/0.72

Table A.2. 3. Model selection for aquatic diffusive CH_4 emissions. "Site" represents the best model using site-level predictor variables (biophysical variables measured directly by the authors). "Region" represents the best model using predictor variables that can be attributed across larger spatial scales and extracted from gridded or mapped products. Tests with "site and region" represent the model models that include both site level and regional level predictors. The null model was run as follows lm(log.CH4.flux) ~1. The best models for each test represented here were picked through forward model selection. K = number of fixed terms the model, AICc = size-corrected Akaike information criterion, DeltaAICc = change in AICc between a given model and the best model, AICcwt = AICc weights indicating the probability a given model is the most parsimonious model in the group of models tested, R^2m = marginal R^2 for the fixed terms for mixed models. R^2c = conditional R^2 for fixed and random terms for mixed effects models. See main text for explanation of predictor variable short names. Non-significant predictor terms that were tested include MAP, Permafrost Zone, DOC, Biome, waterbody depth, and Class). SA = waterbody surface area. TYPE = overarching lake type by lake genesis. TEMP = measured water temperature. GRID_T = gridded mean annual temperature. LAT = latitude.

Variable modeled	Test	Predictor variable	K	AICc	DeltaAICc	AICcwt	Adj R^2
Aquatic diffusion Log.CH4.Flux (n=149)	Site*Region	log10(SA)*TYPE + TEMP	8	162.5	0	0.79	0.41
	Site	log10(SA) + TEMP	4	165.8	3.3	0.94	0.36
	Site + Region	log10(SA) + TEMP + GRID_T	7	167.5	5.0	1.0	0.38
	Region	GRID_T + TYPE + LAT	6	201.7	39.2	1.0	0.35
	Null	-	3	215.1	52.6	1.0	-

Table A.2. 4. Joint analysis of terrestrial and aquatic warm-season/ice-free emissions. The best models for each test represented here were picked through forward model selection. K = number of fixed terms the model, AICc = size-corrected Akaike information criterion, DeltaAICc = change in AICc between a given model and the best model, AICcwt = AICc weights indicating the probability a given model is the most parsimonious model in the group of models tested, R^2m = marginal R^2 for the fixed terms for mixed models. GRID_P = gridded mean annual precipitation. GRID_T = gridded mean annual temperature.

Variable modeled	Fixed effect	K	AICc	DeltaAICc	AICcwt	R^2m
Log.CH4.Flux (n=793)	Class + GRID_T	17	959.8	0	0.64	0.47
	Class + GRID_T + Biome	18	961.6	1.83	0.25	0.47
	Class + Grid_T + Permafrost Zone	21	963.3	3.53	0.11	0.47
	Class + GRID_P + Permafrost Zone	21	977.3	17.5	0	0.46
	Class + GRID_P	17	979.5	19.7	0	0.44
	Class + Permafrost Zone	20	994.4	34.7	0	0.46
	Class	16	996.4	36.6	0	44
	Null	3	1276.7	316.9	0	-

A.3. Supporting information for Chapter 3

Data used in Chapter 3 are available at the University of Alberta Libraries' Dataverse network (https://doi.org/10.7939/DVN/LF4WDG).

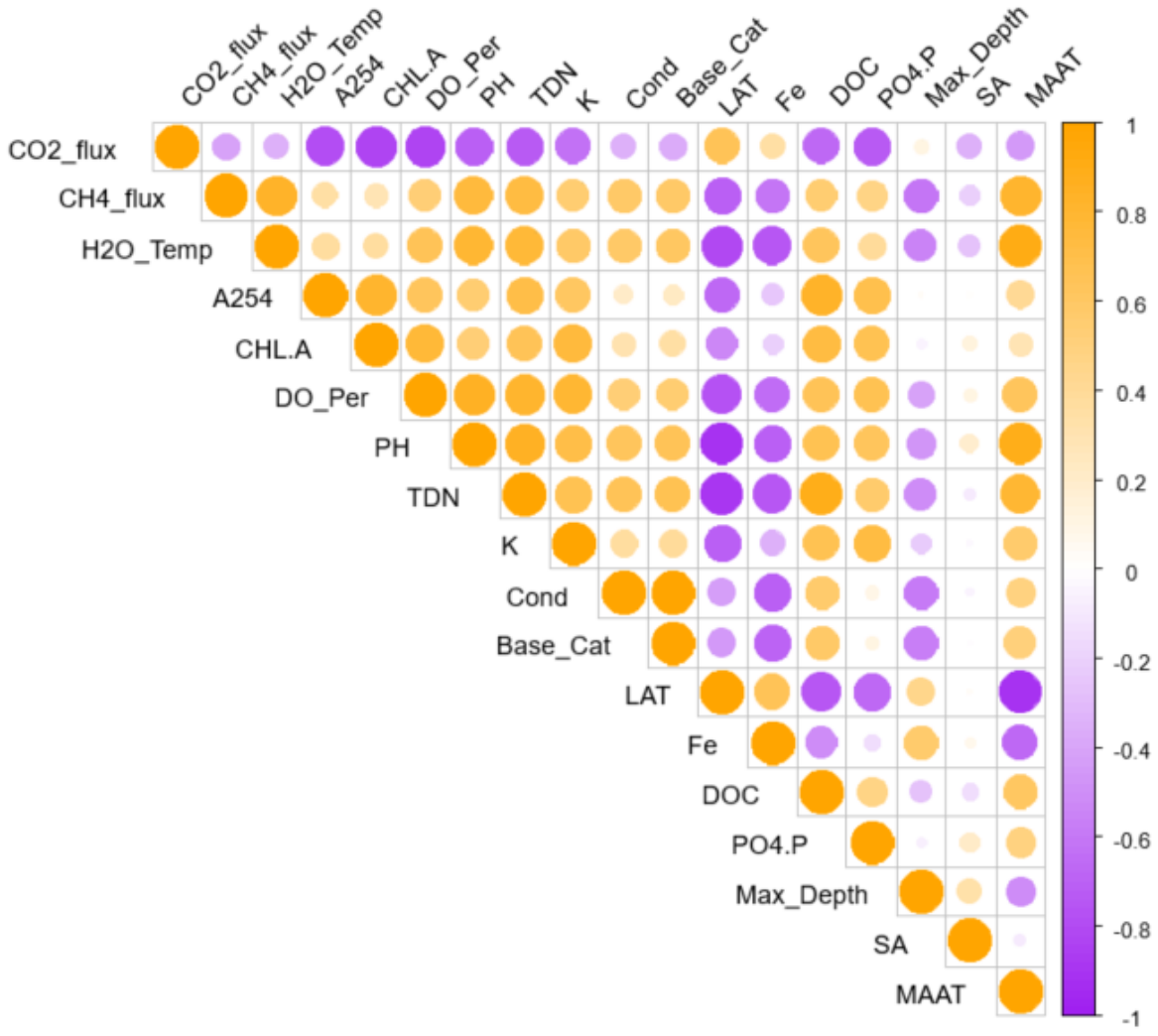

Figure A.3. 1. Correlation matrices for lake variables overaged over the whole sampling period. Variables include average diffusive carbon dioxide flux (CO2_flux), average diffusive methane flux (CH4_flux), water temperature (H2O_Temp), absorbance at 254 nm (A254), chlorophyll *a* (CHL.A), percent dissolved oxygen (DO_Per), PH, total dissolved nitrogen (TDN), potassium (K), specific conductivity (Cond), base cations ($Na^+ + Ca^{2+} + Mg^{2+}$; Base_Cat), latitude (LAT), total dissolved iron (Fe), dissolved organic carbon (DOC), dissolved phosphate (PO4.P), max lake depth (Max_Depth), lake surface area (SA), mean annual air temperature (MAAT).

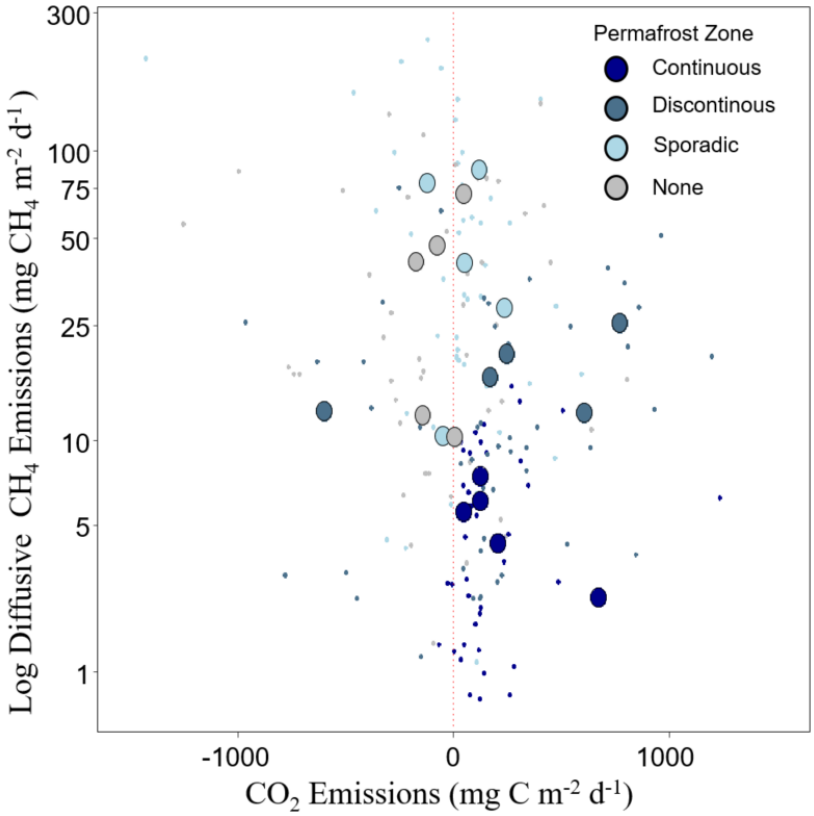

Figure A.3. 2. Average daytime log CO_2 emissions vs average daytime log diffusive CH_4 emissions (large circles). Small dots represent individual daytime measurements. CO_2 points on the left of the red line represent net uptake from the atmosphere. Methane emissions have not been corrected for diel variation.

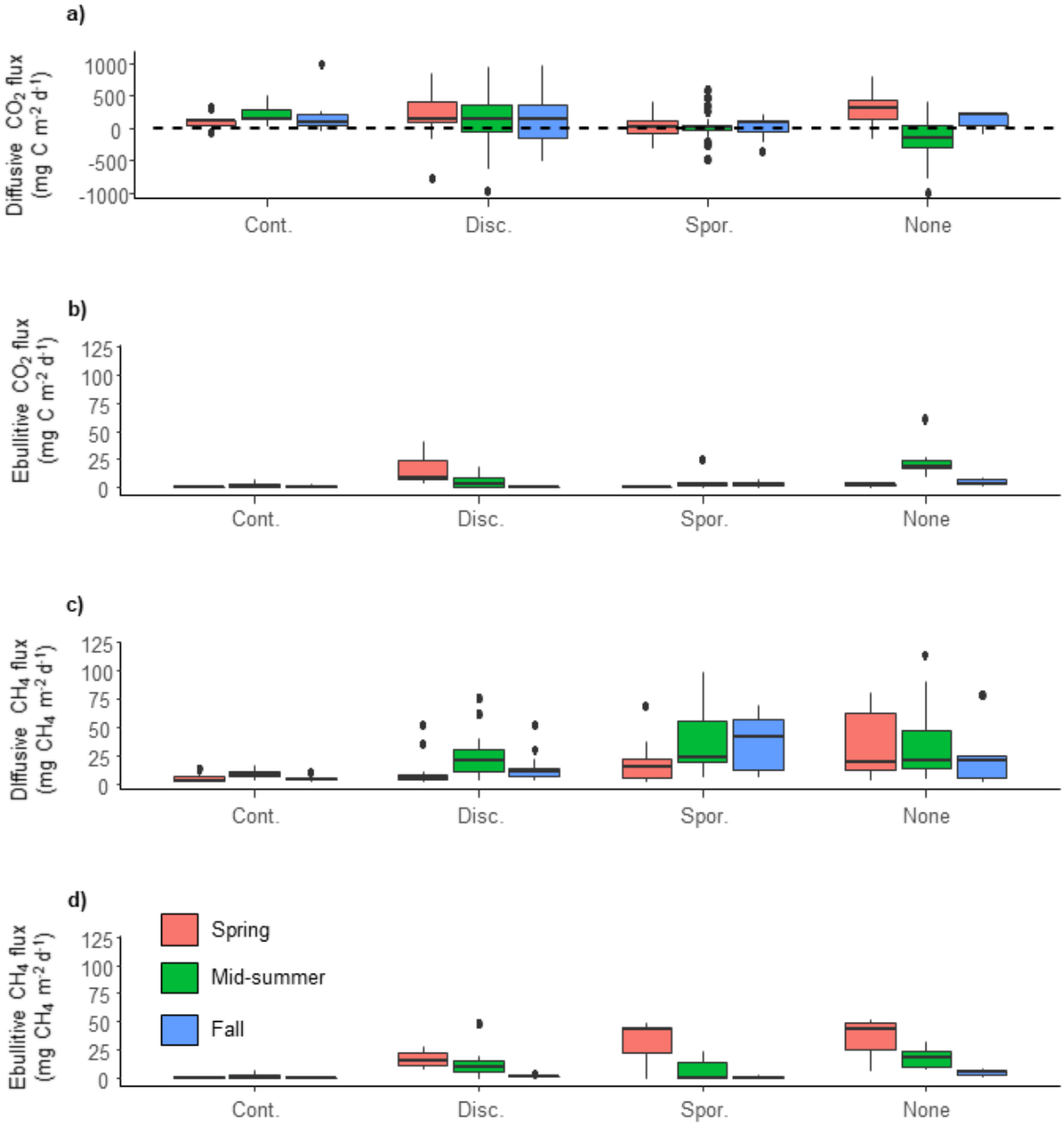

Figure A.3. 3. Seasonal emission patterns. a) Daytime CO_2 exchange. b) Daytime diffusive CH_4 emissions and c) daytime ebullitive CH_4 emissions. Measurements were performed during the daytime between 8:00 and 18:00. Methane emissions have not been corrected for diel variation. Note the different units for CH_4 and CO_2 fluxes and the different y-axis scales.

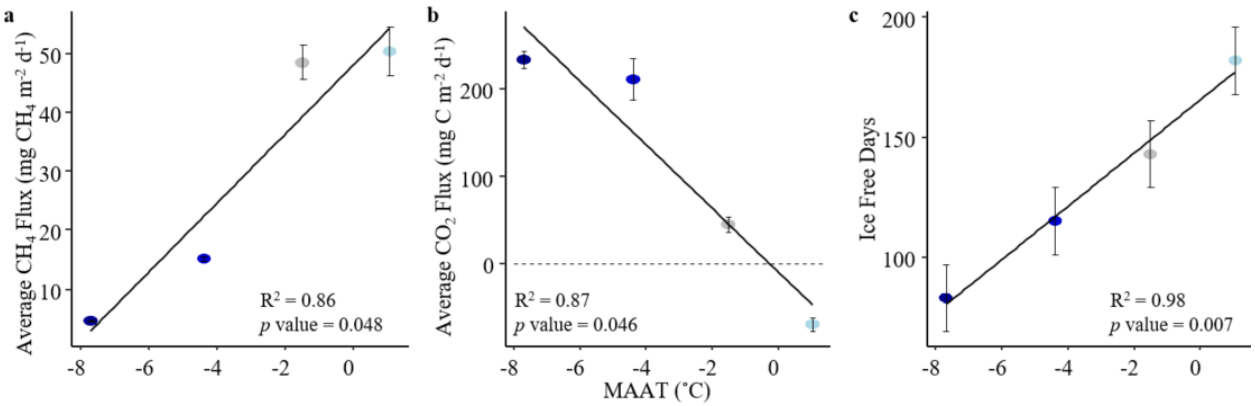

Figure A.3. 4. Linear models used for scaling. (a) Average 24-hour CH_4 emissions (corrected for diel changes; Sieczko et al. 2020) for each permafrost zone verse mean annual air temperature (MAAT). (b) Average daytime CO_2 emissions and mean annual air temperature. (c) The relationship between the number of ice-free days and mean annual temperature in each region. The points represent the mean of the average flux for each of the five lakes over the study period in each permafrost zone. Error bars in a and b represent standard deviation between the five lakes while the error bars in c represent the largest variation in ice-cover days overserved over the 3 years (+/- 14 days).

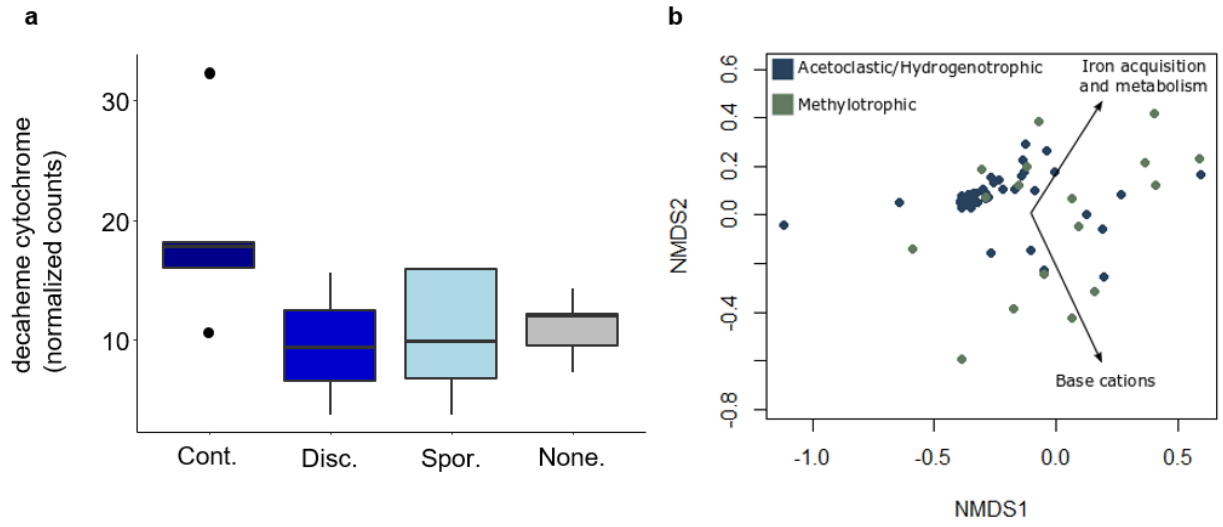

Figure A.3. 5. Decaheme cytochrome abundances and methanogenesis enzymes. A) Normalised abundance of iron reduction markers MtrA and MtrD (decaheme cytochromes) and homologues within each permafrost zone. Cont. = Continuous. Disc. = Discontinuous. Spor. = Sporadic. B) Methanogenesis enzymes shift with both iron acquisition and metabolism genes and aquatic base cation concentrations. I visualized methanogenesis enzyme composition with a non-metric multidimensional scaling (NMDS) ordination fitted with 2 axes (stress = 0.04). Environmental variables were superimposed using the envfit() function in the vegan package (Oksanen et al, 2019). Points are individual enzymes classed under Subsystem 3 function: Methanogenesis in SEED and have been coloured according to whether they were associated with methylotrophic or other forms of methanogenesis. The green methylotrophic enzyme points fall along the iron acquisition/metabolism and base cations vector (arrows). The blue acetoclastic/hydrogentrophic points cluster away from the vectors towards the 0.0 axes markers. This indicates that methylotrophic enzymes are correlated with iron acquisition and metabolism and base cations, suggesting that communities shift from acetoclastic/hydrogenotrophic methanogenesis to methylotophic methanogenesis in the presence of high iron concentrations.

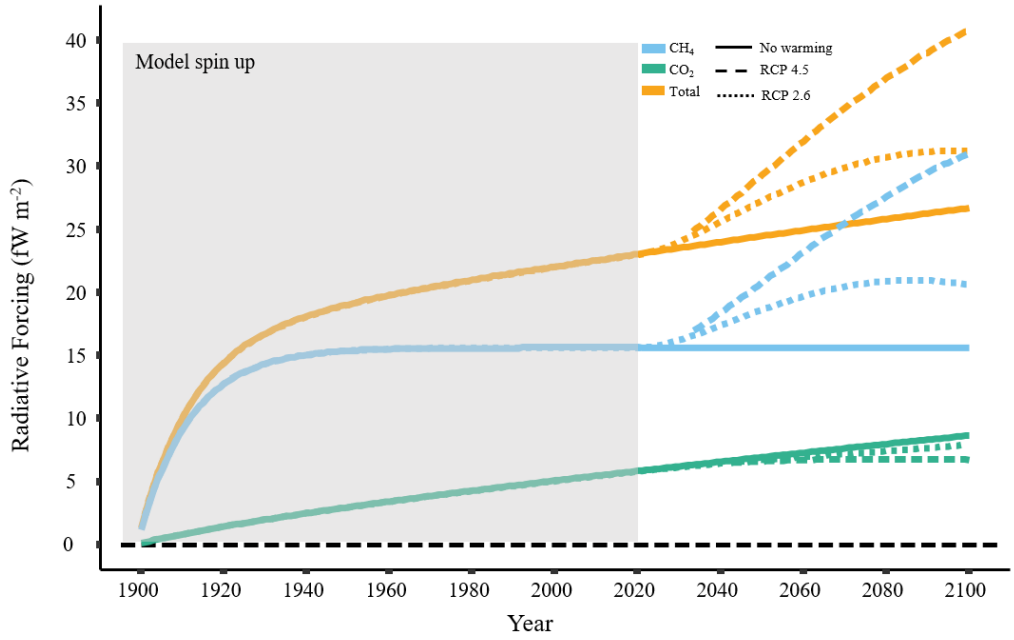

Figure A.3. 6. Simple model spin up for the radiative forcing model. Emission rates were held constant between 1900 and 2020 to arrive at a relative baseline for 2020 and the changes in emissions thereafter. The figure in the main text was referenced to the year 2020 and reflects the relative changes in radiative forcing from the year 2020 on. Radiative forcing units are per m^{-2} lake area. fW = 10^{-15} Watts.

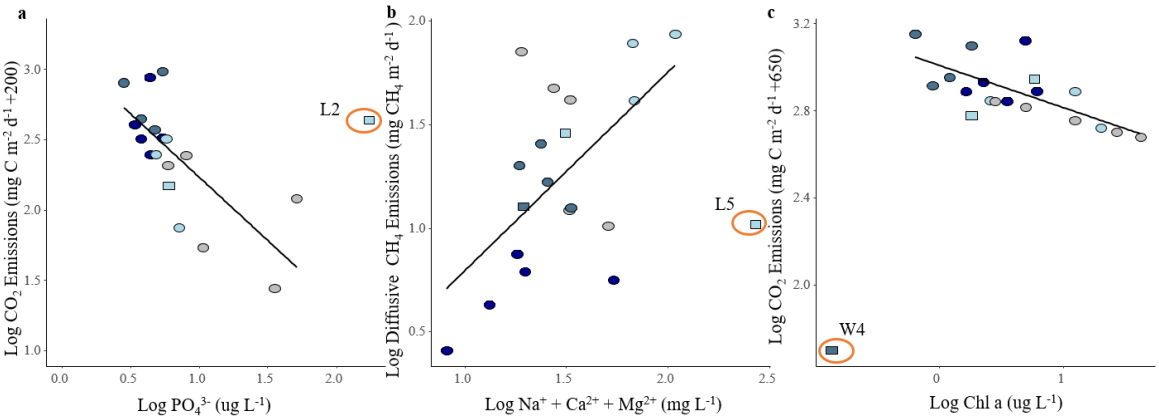

Figure A.3. 7. Outlier lakes. a) Log phosphate (PO_4^{3-}) vs log CO_2 emissions plus 200 (lake averages from the entire sampling period) which highlights L2 (sporadic zone) as an outlier with high phosphate concentrations. High nutrient concentrations in this lake may be linked to the presence of a beaver. b) Log base cations ($Na^+ + Ca^{2+} + Mg^{2+}$) vs log daytime CH_4 emissions (sampling period averages) which highlights L5 (sporadic zone) as an outlier with high base cation concentrations. High ion concentrations in this lake likely indicate this lake receives direct input from a groundwater spring. c) Log Chl*a* vs log CO_2 emissions plus 650 (whole period averages) which highlights W4 (discontinuous zone) as an outlier with extreme CO_2 uptake unrelated to Chl*a* concentration. Note that W4 is not shown in panel a because it is out of the range of the frame.

Table A.3. 1. Climatic and peat characteristics of each study site in the study region.

Location	[+]Ave. Annual Temp (C)	[+]Precipitation (mm)	[*]Permafrost zone	Approximate peat depth (m)
Utikuma (U)	1.6	386	None	2
Lutose (L)	-1.0	372	Sporadic	4-5
Wrigley (W)	-4.1	388	Discontinuous	2-3
Fort McPherson (F)	-7.3	298	Continuous	2

[+]*Government of Canada* [*]*Cryospheric Information Network*

Table A.3. 2. Differences in daytime emissions between the four permafrost zones using mixed model ANOVAs.

Response	Factor	df	P-value	Group	n	Level
Log Diffusive methane	Permafrost Zone	4	1.086e-10	Continuous		A
				Discontinuous		B
				Sporadic		C
				None		C
Log Ebullitive methane	Permafrost Zone	4	0.0002	Continuous		A
				Discontinuous		B
				Sporadic		AC
				None		BC
Diffusive carbon dioxide	Permafrost Zone	4	0.27	Continuous		-
				Discontinuous		-
				Sporadic		-
				None		-

Table A.3. 3. Non-parametric post-hoc test for seasonal differences in CH_4 and CO_2 emissions. E = early season (May or early June). M = mid-season (June-early August). L = Late august through September.

Response	Zone	Pair	Estimate	SE	df	P-value
Log diffusive methane	Continuous	**E~M**	**-1.11**	**0.288**	**164**	**0.009**
		E~L	0.058	0.313	167	1
		M~L	**-1.17**	**0.313**	**167**	**0.013**
	Discontinuous	**E~M**	**-1.17**	**0.281**	**164**	**0.0029**
		E~L	-0.586	0.294	164	0.69
		M~L	-0.584	0.249	164	0.44
	Sporadic	**E~M**	**-1.03**	**0.290**	**164**	**0.0236**
		E~L	-0.64	0.339	164	0.76
		M~L	-0.38	0.270	164	0.95
	None	E~M	-0.301	0.298	164	0.99
		E~L	0.43	0.441	164	0.99
		M~L	-0.74	0.379	164	0.72
Log ebullitive methane	Continuous	E~M	0.62	0.668	30	0.99
		E~L	-0.03	0.668	30	1
		M~L	-0.65	0.668	30	0.99
	Discontinuous	E~M	1.15	0.501	30	0.49
		E~L	**2.18**	**0.578**	**30**	**0.028**
		M~L	-1.03	0.501	30	0.65
	Sporadic	E~M	1.58	0.578	30	0.25
		E~L	1.86	0.668	30	0.23
		M~L	-0.27	0.578	30	1
	None	E~M	0.36	0.555	30	0.99
		E~L	1.68	0.668	30	0.36
		M~L	-1.32	0.555	30	0.44
Diffusive carbon dioxide	Continuous	E~M	-187.16	155	163	0.98
		E~L	-208.30	155	163	0.97
		M~L	21.14	155	163	1
	Discontinuous	E~M	275.30	153	163	0.81
		E~L	134.62	159	163	0.99
		M~L	140.68	135	163	0.99
	Sporadic	E~M	-313.04	165	167	0.76
		E~L	-353.81	194	167	0.80
		M~L	40.76	151	163	1
	None	E~M	**547.70**	**161**	**164**	**0.038**
		E~L	213.85	238	163	0.99
		M~L	333.85	204	163	0.89

Table A.3. 4. Physical and chemical characteristics averaged over the entire sampling period for each lake. F = Fort Simpson. W = Wrigley. L = Lutose. U = Ursa. C = Continuous. D = Discontinuous. S = Sporadic/isolated. N = no permafrost. Depth = max lake depth. Area = lake surface area. CH_4_eb = daytime CH_4 ebullition flux. CH4_dif = daytime diffusive CH_4 flux. CO2_flux = daytime diffusive carbon dioxide flux. Negative values represent uptake. [Fe] = dissolved iron in the lake surface waters. mrcA = a) methyl coenzyme A reductase abundance and methanotrophy marker. pmoA = particulate methane monooxygenase. mmoX = methane monooxygenase subunit-A. Silva reads can be found by following the data availability links provided.

Lake ID	Perm Zone	Lat (dec)	Lon (dec)	Depth (m)	Area (ha)	CH_4_eb (mg CH_4 m^{-2} d^{-1})	CH_4_dif (mg CH_4 m^{-2} d^{-1})	CO_2_flux (mg C m^{-2} d^{-1})	[Fe] (mg L^{-1})	mrcA	pmoA	mmoX abund
F1	C	67.47346	-134.69	1.2	5.8	3.2	7.5	124.4	0.47	292	32	13
F2	C	67.45098	-134.762	2.5	0.95	-	4.3	203.7	0.66	158	8	4
F3	C	67.47738	-134.705	>3	0.55	0.4	2.6	672.8	0.82	109	15	6
F4	C	67.3705	-134.856	1.5	2	-	5.6	44.7	0.10	29	8	5
F5	C	67.35743	-134.83	2	8.9	0.3	6.1	120.4	0.21	51	39	21
W1	D	63.15164	-123.25	3	4.2	4.3	16.7	170.4	0.19	-	-	-
W2	D	63.15134	-123.254	1.1	1	9.8	20.0	244.3	0.19	353	22	21
W3	D	63.14579	-123.25	0.8	0.5	-	25.6	768.2	0.43	153	33	7
W4	D	63.16055	-123.271	1.75	12	36.6	12.7	-600.1	0.03	402	17	3
W5	D	62.87401	-123.163	1.5	3.8	-	12.6	603.1	0.05	156	27	10
L1	S	59.48023	-117.183	1	0.4	22.4	78.3	-125.5	0.06	149	24	12
L2	S	59.44539	-117.268	2.5	2.7	12.2	28.8	234.9	1.85	138	52	50
L3	S	59.22571	-117.463	1.2	9.2	-	41.3	48.7	0.07	209	23	5
L4	S	59.48396	-117.181	0.8	0.3	-	86.4	118.2	0.09	386	29	12
L5	S	59.35342	-117.315	0.75	1.9	0.3	10.4	-51.9	0.06	9	1	1
U1	N	55.98267	-115.193	2	10.1	15.6	41.9	-172.5	0.20	295	10	7
U2	N	56.01082	-115.366	0.8	0.3	11.8	71.7	43.1	0.04	341	40	23
U3	N	56.00957	-115.353	1.5	8.2	-	12.2	-146.2	0.12	192	42	23
U4	N	56.07421	-115.477	0.85	0.7	-	10.3	5.8	0.06	219	29	5
U5	N	56.02335	-115.375	1.5	2.9	17.8	47.4	-79.7	0.11	157	142	41

Supporting information for Chapter 4.

Data used in Chapter 4 are available at the University of Alberta Dataverse (https://doi.org/10.7939/DVN/WUDIRK).

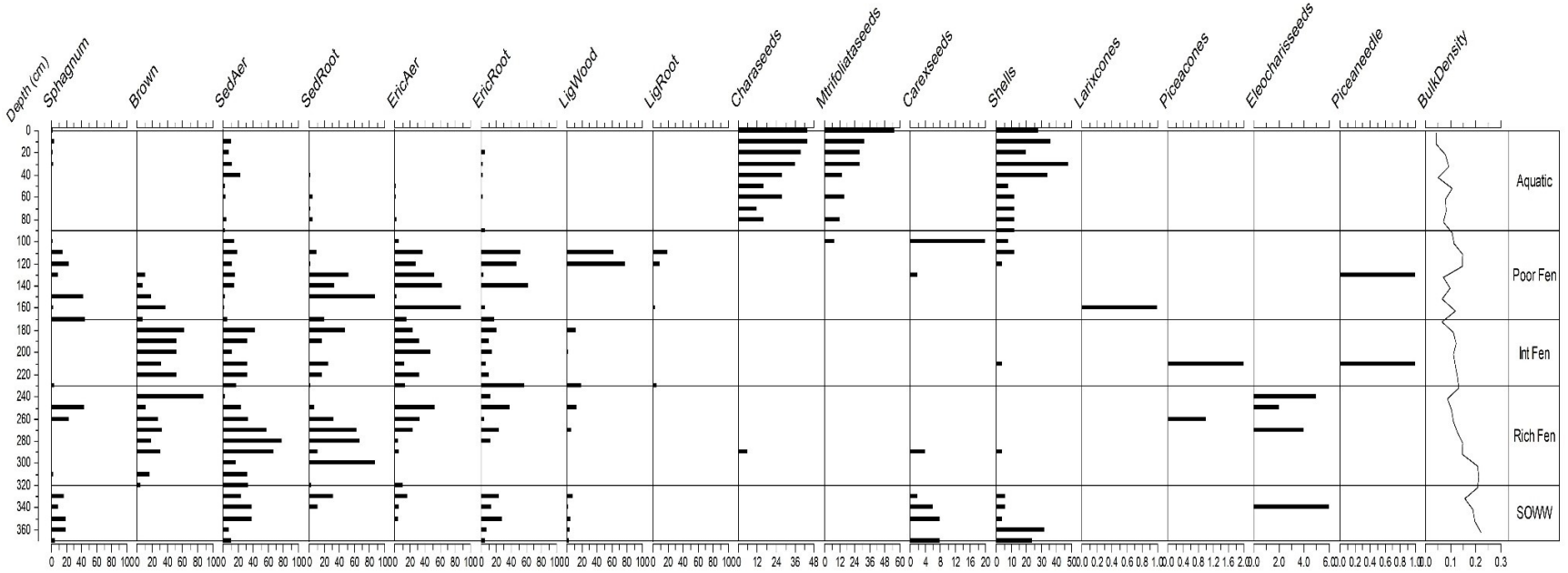

Figure A.4. 1. Stratigraphic diagram based on macrofossil analysis of the core from the center of Eli Lake. Sphagnum to LigRoot expressed as a relative percentage; items expressed as the number found per sample; bulk density expressed as gcm^{-3}. Transitions and zones are determined by shifts in vegetation composition and density. Stages of development classified as shallow open water wetland (SOWW)/marsh, fen with internal shifts from rich to poor, and current aquatic (i.e. limnic). Int Fen = intermediate fen. Aer = above-ground vegetation parts. Root = below-ground vegetation parts. Sed = *sedge spp.* Eric = *Ericaceous spp.* Lig = Unidentified wood. Carex = *carex spp.* Larix = *larix laricina*. Chara = *Chara spp.* Picea = *Picea mariana.* Eleocharis = *Eleocharis spp.* Mtrifoliata = *Meyanthus Trifoliata.*

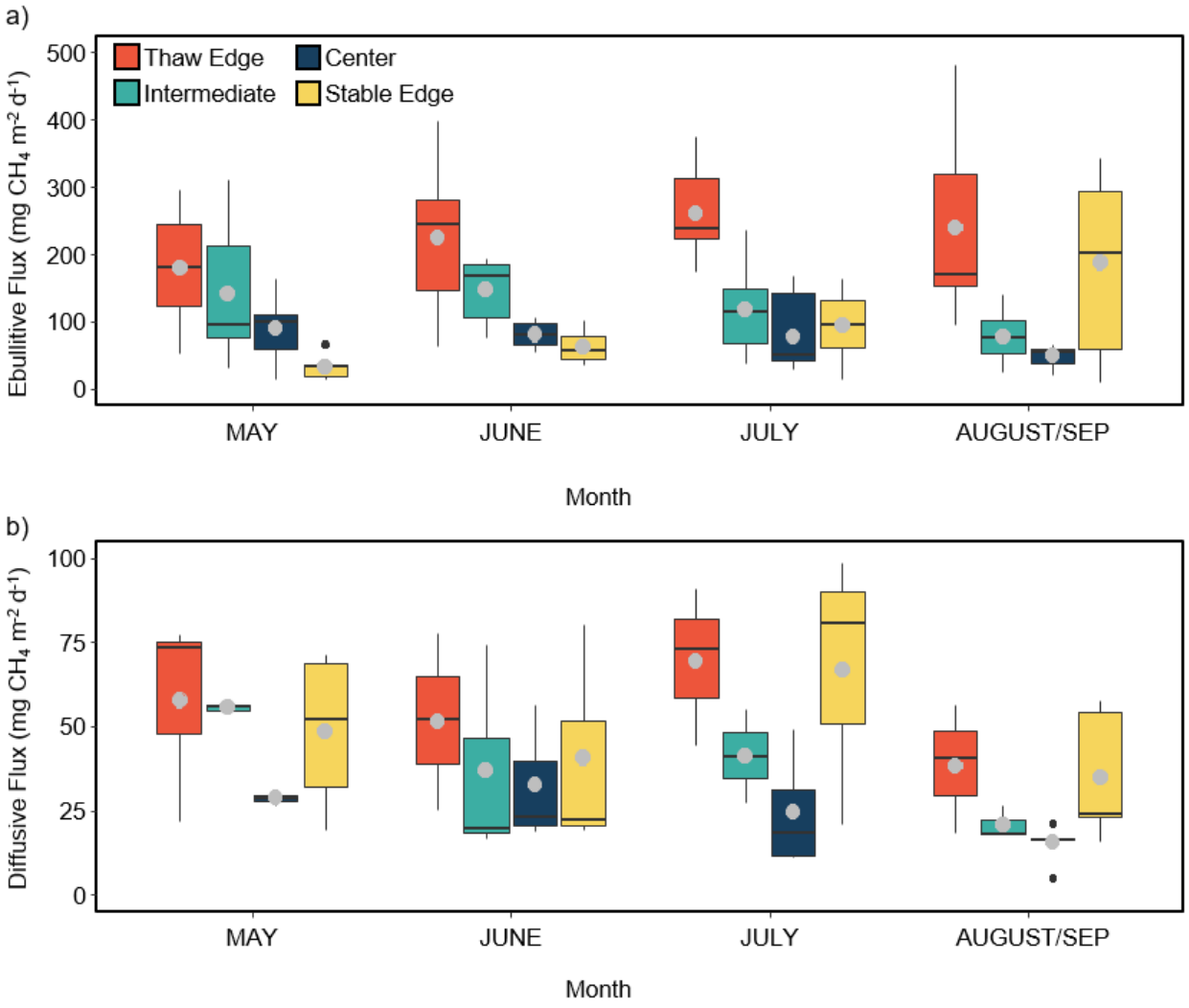

Figure A.4. 2. Monthly patterns in a) ebullitive CH_4 fluxes and b) diffusive CH_4 fluxes. Sep = September.

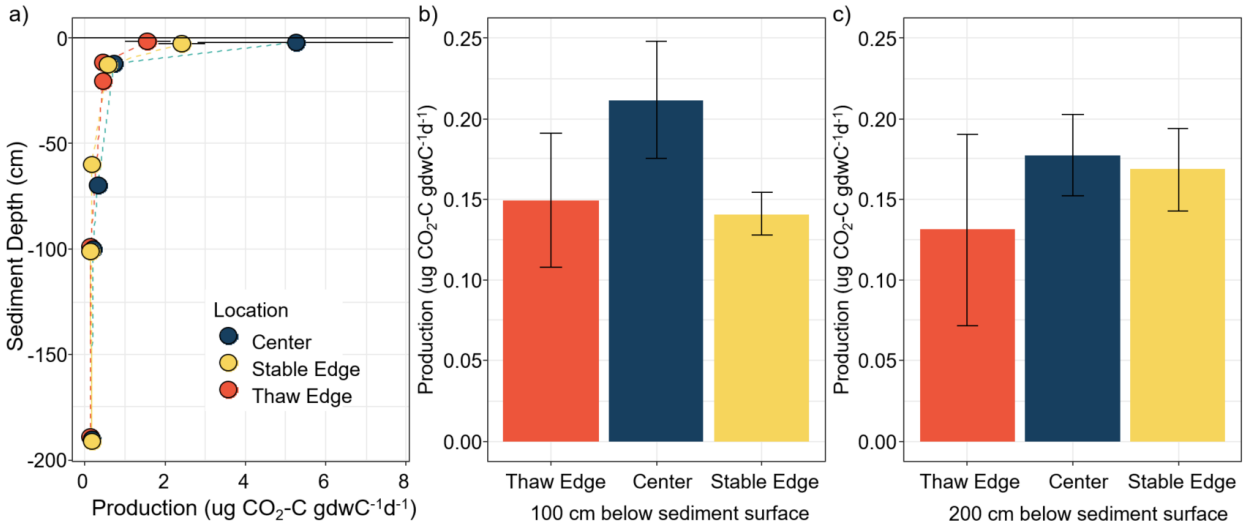

Figure A.4. 3. Potential production rates of CO_2 in the sediments. a) Depth profile of production rates. b) Production rates at 100 cm sediment depths. c) Production rates at 200 cm sediment depths. Error bars represent one standard deviation.

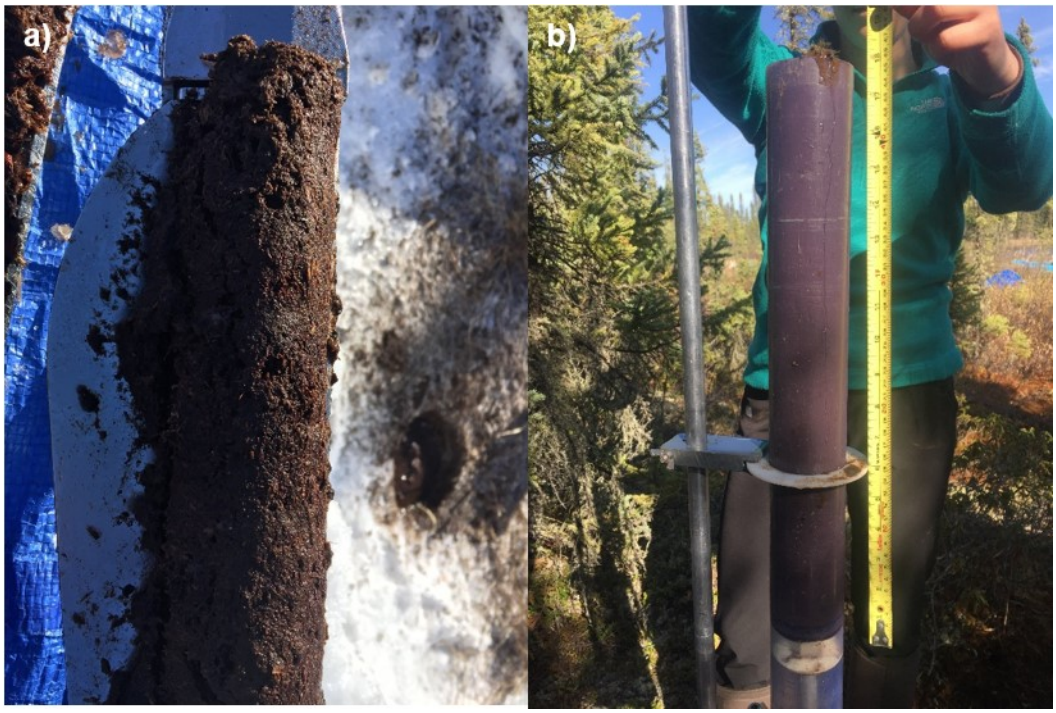

Figure A.4. 4. Examples of the different lake sediment types. a) Compact and less humified peat sediment from deeper sediment depths and b) highly humified, loose limnic sediments from the surface.

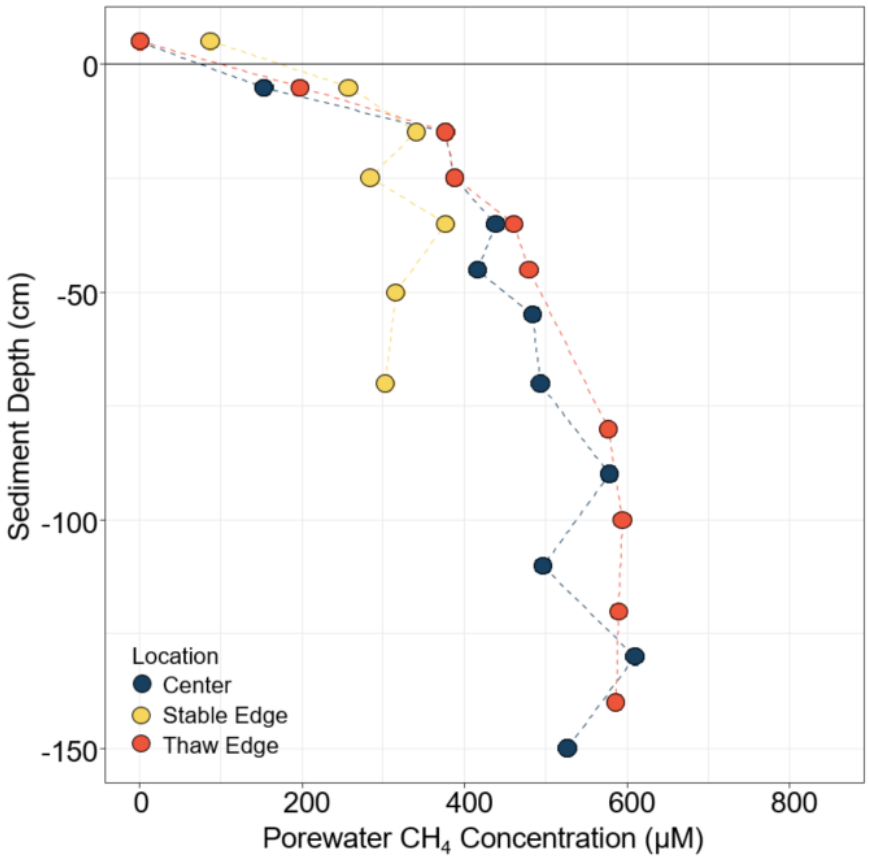

Figure A.4. 5. Porewater CH_4 concentrations from the MLP samplers deployed in 2017.

Table A.4. 1. Sampling timeframe. TE= Thaw Edge, M = Intermediate, C = Center, SE = Stable Edge. Note- in 2017 only Cl^- and SO_4^{2-} were measured.

Measurement	2017												2018						2019		
	5/20	5/24	6/2	6/18	6/20	7/2	7/3	7/18	8/1	8/3	8/18	9/12	5/19	5/21	7/3	7/5	8/12	8/16	6/22	8/30	9/1
Concentration/CH_4 Diffusive flux	TE, M, C, SE	TE, M, C, SE	TE, M, C, SE	TE, M, C, SE	TE, M, C, SE	TE, M, C, SE	TE, M, C, SE	TE, M, C, SE	TE, M, C, SE	TE, M, C, SE	M, C, SE	M, C, SE	TE, C, SE	TE, C, SE	TE, C, SE	TE, C, SE	TE, C, SE	TE, C, SE			
Ebullitive flux		TE, M, C, SE	TE, M, C, SE	TE, M, C, SE		TE, M, C, SE		TE, M, C, SE	TE, M, C, SE		TE, M, C, SE	TE, M, C, SE		TE, M, C, SE		TE, M, C, SE		TE, M, C, SE			
Bubble concentrations		TE, M, C, SE		TE, M, C, SE		TE, M, C, SE		TE, M, C, SE			TE, M, C, SE	TE, M, C, SE		TE, M, C, SE		TE, M, C, SE		TE, M, C, SE			
Chamber flux	TE, M, C, SE	TE, M, C, SE	TE, M, C, SE	TE, M, C, SE	TE, M, C, SE	TE, M, C, SE	TE, M, C, SE	TE, M, C, SE	TE, M, C, SE	TE, M, C, SE	TE, M, C, SE	TE, M, C, SE									
DOC		C		C		C					C	C		C		C		C	C	C	C
IONS		C		C		C					C	C		C		C		C	C	C	C
YSI	TE, M, C, SE	TE, M, C, SE	TE, M, C, SE	TE, M, C, SE	TE, M, C, SE	TE, M, C, SE	TE, M, C, SE	TE, M, C, SE	TE, M, C, SE	TE, M, C, SE	M, C, SE	M, C, SE	TE, M, C, SE	TE, M, C, SE	TE, M, C, SE	TE, M, C, SE	TE, M, C, SE	TE, M, C, SE	TE, SE	TE, SE	TE, SE
Sediment Temps	TE, C	TE, C	TE, C	TE, C	TE, C	TE, C	TE, C	TE, C	TE, C	TE, C	TE, C	TE, C									
Chl*a*														C		C		C	C	C	C
Sediment CH_4 Concentrations								TE, C, SE			TE, C, SE					TE, C, SE		TE, C, SE			
Diffusive CO_2 flux													TE, SE	TE, SE	TE, SE	TE, SE	TE, SE	TE, SE	TE, SE	TE, SE	TE, SE

Table A.4. 2. Radiocarbon analysis of sediment CH_4 and CO_2 bubbles. TE = Thaw edge. SE = Stable edge. C = Center.

Publication Code	Sample Identifier	Gas	%Modern	%Modern 1 σ error	Radiocarbon Age (years BP)	Radiocarbon Age 1 σ uncertainty	CO_2 volume (ml)	$\delta^{13}C$-VPDB‰
SUERC-90522	ELI.2018-08-16-TE-a CH4	CH4	85.95	0.38	1,216	35	4.84	-63.2
SUERC-90523	ELI.2018-08-16-TE-b CH4	CH4	87.97	0.41	1,029	37	7.17	-62.4
SUERC-90524	ELI.2018-07-05-TE CH4	CH4	84.14	0.39	1,388	37	8.41	-63.7
SUERC-90528	ELI.2018-08-16-C-a CH4	CH4	98.00	0.45	162	37	6.34	-67.4
SUERC-90529	ELI.2018-08-16-C-b CH4	CH4	99.49	0.46	41	37	6.64	-65.0
SUERC-90530	ELI.2018-07-05-C CH4	CH4	100.28	0.46	n/a	n/a	3.64	-60.3
SUERC-90531	ELI.2018-08-16-SE-a CH4	CH4	100.17	0.46	n/a	n/a	11.98	-64.6
SUERC-90532	ELI.2018-08-16-SE-b CH4	CH4	101.74	0.47	n/a	n/a	6.50	-67.1
SUERC-90533	ELI.2018-07-05-SE CH4	CH4	100.64	0.46	n/a	n/a	9.37	-65.0
UCIAMS-225376	ELI.2018-08-16-TE-b CO2	CO2	83.8182	1.71	1420	170	0.11	n/a
UCIAMS-225377	ELI.2018-08-16-SE-a CO2	CO2	99.3905	0.78	50	70	0.19	n/a
UCIAMS-225378	ELI.2018-08-16-SE-b CO2	CO2	100.1327	0.89	n/a	n/a	0.16	n/a
UCIAMS-225379	ELI.2018-07-05-SE CO2	CO2	99.362	0.71	50	60	0.21	n/a

Table A.4. 3. Linear mixed model output for CH_4 fluxes as a factor of lake location. Levels with different letters indicate significant differences among the lake locations.

Response	Factor	df	X square	P-value	Zone	Level
Log Ebullitive CH_4 flux	Zone	3	25.78	1.06e-05	Thaw Edge	A
					Intermediate	B
					Center	B
					Stable Edge	B
Log Diffusive CH_4 flux	Zone	3	23.69	2.9e-05	Thaw Edge	A
					Intermediate	B
					Center	AB
					Stable Edge	A
Log CH_4 Chamber flux	Zone	3	8.64	0.034	Thaw Edge	AB
					Intermediate	B
					Center	AC
					Stable Edge	AB

Table A.4. 4. Linear mixed model output for CH_4 fluxes and bubble concentrations across the entire lake extent as a factor of sampling month. Levels with different letters indicate significant differences in fluxes between months.

Response	Factor	df	X square	P-value	Month	Level
Log Ebullitive CH_4 flux	Month	3	2.55	0.46	May	-
					June	-
					July	-
					August/Sep	-
Log Diffusive methane flux	Month	3	4.12	0.25	May	-
					June	-
					July	-
					August/Sep	-
Log Chamber flux	Month	4	28.02	3.6e-06	May	AC
					June	AB
					July	B
					August/Sep	C
CH_4 bubble concentration	Month	4	12.18	0.007	May	A
					June	AB
					July	B
					August/Sep	AB

Table A.4. 5. Linear mixed model output for CH_4 fluxes within each lake location as a factor of sampling month. Levels with different letters indicate significant differences in fluxes between months.

Response	Location	Factor	df	X square	P-value	Month	Level
Log Ebullitive CH_4 flux	Thaw edge	Month	3	2.42	0.49	-	-
	Mid			4.98	0.17	-	-
	Center			4.43	0.22	-	-
	Stable Edge			7.7	0.05	-	-
Log Diffusive CH_4 flux	Thaw edge	Month	3	2.28	0.52	-	-
	Mid			3.47	0.32	-	-
	Center			6.65	0.08	-	-
	Stable Edge			2.00	0.57	-	-
Log CH_4 Chamber flux	Thaw edge	Month	3	6.86	0.08	May	ABC
	Mid			**10.21**	**0.02**	June	ABC
	Center			5.36	0.15	July	AB
	Stable Edge			8.53	0.05	August/Sep	AC

Table A.4. 6. Linear mixed model output for ebullitive CO_2 fluxes and bubble concentrations across the entire lake extent as a factor of lake location and sampling month. Levels with different letters indicate significant differences in fluxes between locations and months.

Response	Factor	df	X square	P-value	Zone	Level
Log Ebullitive CO_2 flux	Zone	3	21.38	8.77e-05	Thaw Edge	A
					Intermediate	A
					Center	B
					Stable Edge	A
Log Ebullitive CO_2 flux	Month	3	18.78	0.0003	May	A
					June	AB
					July	B
					August/Sep	B
CO_2 bubble concentrations	Zone	3	8.97	0.030	Thaw Edge	AB
					Intermediate	AB
					Center	B
					Stable Edge	A
CO_2 bubble concentrations	Month	3	18.78		May	A
					June	AC
					July	BC
					August/Sep	BC

Table A.4. 7. Output from Kendall's correlation tests. Correlations were classified as weak (± 0.1-0.30), moderate (± 0.3-0.5), or strong (± > 0.5). See text for short name definitions. Bolded lines represent significant correlations.

Response	Predictor	z/t-value	P-value	Tau	Strength
Ebullitive CH_4 flux	Air pressure	0.71 (Z)	0.48	0.08	weak
	PAR	0.37 (Z)	0.71	0.05	weak
	Water Temp	1.24(Z)	0.21	0.15	weak
	DO	380 (T)	0.08	0.21	weak
	Conductivity	280 (T)	0.35	-0.11	weak
	pH	0.22 (Z)	0.83	0.03	weak
Diffusive CH_4 flux	Air pressure	-2.92 (Z)	**0.003**	**-0.28**	**weak**
	PAR	0.47 (Z)	0.63	0.05	weak
	Water Temp	3.07 (Z)	**0.002**	**0.30**	**moderate**
	DO (mg L-1)	1.63 (Z)	0.10	0.15	weak
	Conductivity	-2.00 (Z)	0.044	-0.19	weak
	pH	-2.1 (Z)	0.035	-0.20	weak
Chamber CH_4 flux	Air pressure	1.08 (Z)	0.28	0.12	weak
	PAR	**3.84** (Z)	**0.0001**	**0.46**	**moderate**
	Water Temp	-0.08 (Z)	0.93	-0.009	weak
	DO		0.65	-0.05	weak
	Conductivity	0.15 (Z)	0.88	0.017	weak
	pH	1.86 (Z)	0.06	0.21	weak
Ebullitive CO_2 flux	Air pressure	1.13 (Z)	0.26	0.15	weak
	PAR	0.96 (Z)	0.34	0.13	weak
	Water Temp	0.34 (Z)	0.74	0.04	weak
	DO	225 (T)	0.81	-0.03	weak
	Conductivity	253 (T	0.49	0.09	weak
	pH	-1.63 (Z)	0.10	-0.21	weak
Diffusive CO_2 flux	Air pressure	-0.05 (Z)	0.96	-0.01	weak
	PAR	-	-	-	-
	Water Temp	42 (T)	0.75	-0.08	weak
	DO	44 (T)	0.91	-0.03	weak
	Conductivity	**0.35 (Z)**	**0.08**	**0.35**	**moderate**
	pH	0.25 (Z)	0.23	0.25	weak

Table A.4. 8. Comparison of average water chemistry characteristics across peatland ponds and lakes. DOC = dissolved organic carbon. Cond = conductivity.

Study	Location	Average surface area (m^2)	DOC (mg L^{-1})	pH	Cond ($\mu S\ cm^{-1}$)
Matveev et al. 2016	Eastern Canada	500	11	< 6.6	50
Kuhn et al. 2018	Northern Sweden	50	40	5	55
This study	Western Canada	5000	44	7.5	359

Table A.4. 9. 2018 and 2019 diffusive CO_2 fluxes and associated water chemistry variables. CO_2_D_flux = diffusive CO_2 flux. Water Temp = Water Temperature. DOC = Dissolved Organic Carbon. TN = Dissolved Total Nitrogen. Cond = Conductivity.

Location	Date	CO_2_D_flux (mg CH_4 m^{-2} d^{-1})	Water Temp (C)	DOC (mg L^{-1})	TN (mg L^{-1})	pH	Cond (µS cm^{-1})	PO_4^{3-}-P (mg L^{-1})	SO_4^{2-}-S (mg L^{-1})	NH_4^{+}-N (mg L^{-1})	Chl*a* (µg L^{-1})
Stable	5/19/2018	-	21.2	-	-	8.05	293.3	-	-	-	-
Thaw	5/19/2018	51.76345559	22.4	-	-	7.35	294.2	-	-	-	-
Stable	5/20/2018	-47.26600321	21.4	36.18	1.36	7.76	315.8	7.75	33.46	0.00076	13.53
Thaw	5/20/2018	-280.200476	21.5	-	-	7.3	316.6	-	-	-	-
Stable	7/3/2018	-56.32148194	20.6	-	-	7.58	268	-	-	-	-
Thaw	7/3/2018	-424.783864	22	-	-	7.6	270.1	-	-	-	-
Stable	7/5/2018	-271.9256918	20.7	44.68	1.74	7.97	283.4	4.90	26.27	0.01252	2.54
Thaw	7/5/2018	-21.9318614	20.3	-	-	7.86	287.8	-	-	-	-
Stable	8/12/2018	43.98261481	24.1	-	-	8.05	441.5	-	-	-	-
Thaw	8/12/2018	48.31038795	20.5	-	-	7.83	369.5	-	-	-	-
Stable	8/16/2018	17.16547536	23.3	56.62	2.10	8.66	446.9	9.93	60.66	0.00306	11.55
Thaw	8/16/2018	150.4107731	22.3	-	-	8.28	441.5	-	-	-	-
Stable	6/22/2019	-460.2119681	16	52.25	2.63	8	450	6.67	18.21	1.44	2.1
Thaw	6/22/2019	-119.6040459	20	-	-	8	450	-	-	-	-
Stable	8/30/2019	128.1548701	15.1	62.81	2.97	8.15	500	6.47	19.12	2.75286	-
Thaw	8/30/2019	86.88422612	15.3	-	-	8.24	505.4	-	-	-	-
Stable	9/1/2019	-357.6733975	18	-	-	9.09	499.6	-	-	-	60
Thaw	9/1/2019	-197.7140003	21.2	-	-	-	-	-	-	-	-